Chemical Strategies for Antigen-Selective Targeting of Autoreactive B Cells

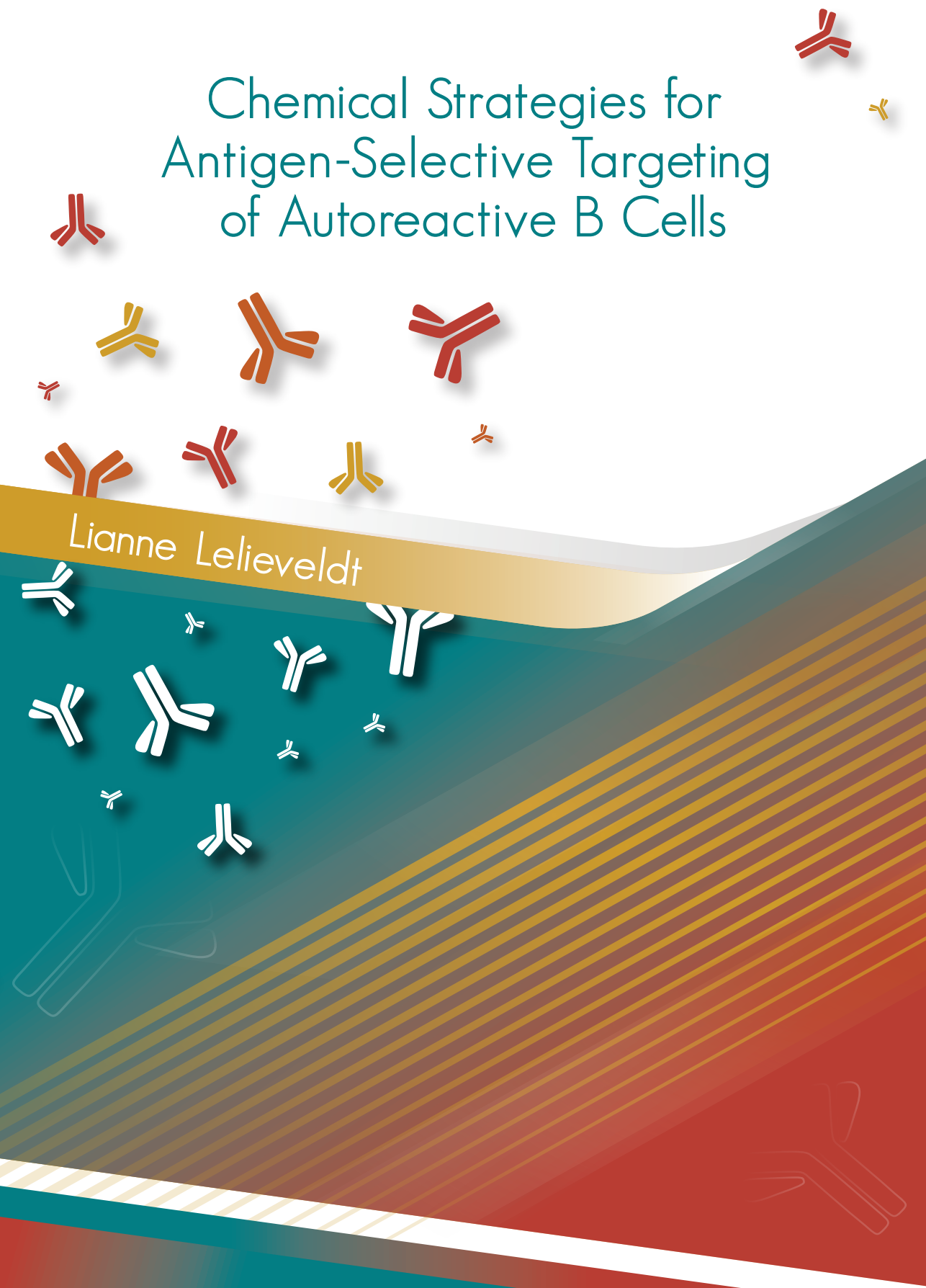

Lianne Lelieveldt

Chemical Strategies for Antigen-Selective Targeting of Autoreactive B Cells

Lianne Lelieveldt

Research presented in this thesis was financially supported by Netherlands Organisation for Scientific Research (NWO) gravity program the 'Institute for Chemical Immunology' NWO-024.002.009.

Cover Evie Lelieveldt

ISBN 978-94-93118-13-3
Press Ipskamp Printing, Enschede

Chemical Strategies for Antigen-Selective Targeting of Autoreactive B Cells

Proefschrift

ter verkrijging van de graad van doctor
aan de Radboud Universiteit Nijmegen
op gezag van de rector magnificus prof. dr. J.H.J.M. van Krieken,
volgens besluit van het college van decanen
in het openbaar te verdedigen op woensdag 8 mei 2019
om 14.30 uur precies

door

Lianne Petronella Wilhelmina Margaretha Lelieveldt

geboren op 6 januari 1990

te Nijmegen

Promotoren

Prof. dr. Ger J.M. Pruijn
Prof. dr. Floris P.J.T. Rutjes

Copromotor

Dr. Kimberly M. Bonger

Manuscriptscommissie

Prof. dr. Daniela A. Wilson
Prof. dr. ir. Jan C.M. van Hest (Technische Universiteit Eindhoven)
Dr. Sander I. van Kasteren (Universiteit Leiden)

Paranimfen

Dr. Lise Schoonen
Bastiaan C. Buddingh'

Voor mijn Lieve Oma's

Table of content

List of Abbreviations

2-PCA	2-pyridinecarboxyaldehyde
ACPA	anti-citrullinated proteins antibodies
ADCC	antibody-dependent cellular cytotoxicity
ADEPT	antibody-directed enzyme prodrug strategy
AM	affinity matrix
Anti-CarP	anti-carbamylated antibodies
APC	allophycocyanin
AT	allergen toxin
B7AP	B7 antisense peptide
BCR	B cell receptor
BPI	bi-functional peptide inhibitor
Ca	carbamylated
CCP	cyclic citrullinated peptide
CD	cluster of differentiation
CDC	complement dependent cytotoxicity
CNBz	carboxynitrobenzyl
CR1	complement receptor 1
CuAAC	Copper-catalyzed Azide−Alkyne Cycloaddition
DC	dendritic cell
DMARDs	disease-modifying antirheumatic drugs
DNP	2, 4- dinitrophenyl
ds	double-stranded
DT	diphtheria toxin
EAE	experimental autoimmune encephalomyelitis
ELISA	enzyme-linked immunosorbent assay
ETA'	aeruginosa exotoxin A
FACS	fluorescence-activated cell sorting
Fc	fragment crystallizable
FO	follicilar
GAD	glutamic acid decarboxylase
HA	hyaluronic acid
HLA	human leukocyte antigen
ICAM	intercellular adhesion molecule-1
IDAC	I-Domain-Antigen Conjugate
IFN	interferon
Ig	immunoglobulin
IL	interleukin
IS	immune synapse
ITIM	immunoreceptor tyrosine-based inhibitory motif
LABL	ICAM-1 blocking peptide
LFA-1	lymphocyte function-associated antigen-1
LTα	lymphotoxin
MA	methacrylated
MAC	membrane-attack complex
MAP	mitogen-activated protein
MHC	major histocompatibility complex

MMAE	monomethyl aurtistatin E
MOG	myelin oligodendrocyte glycoprotein
MS	multiple sclerosis
MVN	multivalent BPIs
MZ	marginal zone
NOD	non-obese diabetes
NP	nitrophenol
NTR	nitroreductase
OVA	ovalbumin
PA	polyacrylamide
PAB	*para*-aminobenzylcarbamate
PAD	peptidylarginine deiminase
PIC	poly-isocyano polypeptide
PIP_3	phosphatidylinositol 3,4,5-trisphosphate
PLGA	poly(lactic-*co*-glycolic acid)
PLP	myelin proteolipid protein
PR 3	proteinase 3
RA	rheumatoid arthritis
RAPA	rapamycin
RF	rheumatoid factor
r.t.	room temperature
Rt	Retention time
SAgA	multivalent soluble antigen array
SA-ZAP	streptavidin-saporin
SHIP	SH2-containing inositol polyphosphate 5-phosphatase
SHP-1	SH2-domain-containing tyrosine phosphatase
Siglec	sialic acid-binding immunoglobulin-like lectin
SLE	systemic lupus erythematosus
SPAAC	strain-promoted alkyne-azide cycloaddition
SMAC	supramolecular activation cluster
STALS	Siglec-engaging tolerance-inducing antigenic liposome
T1D	type 1 diabetes
TCR	T cell receptor
TFA	trifluoroacetic acid
TT	tetanus toxoid
TTC	tetanus toxoid fragment C
WG	Wegener's granulomatosis
ZAP	saporin

Chapter 1

Antigen-Selective B Cell-Targeting in Autoimmune Diseases

Lianne Lelieveldt*, Wilke Castelijns*, Kimberly Bonger. *Manuscript submitted*
*authors contributed equally

Abstract

The ability of the immune system to discriminate between 'self' and 'non-self' is critical to ensure proper immune responses towards foreign substances while simultaneously maintaining self-tolerance. Defects in immunological tolerance to self-components are a characteristic for autoimmune diseases, which affect numerous people worldwide. In recent years, the role of B cells in the pathogenesis of several autoimmune diseases, such as rheumatoid arthritis (RA), systemic lupus erythematosus (SLE) and multiple sclerosis (MS), has become increasingly apparent. Current B cell-directed therapies mainly induce general immune suppression by either inhibiting or eliminating the complete B cell compartment, leaving patients at increased risk of infection. Hence, the need for more selective B cell therapies that solely target pathogenic autoreactive B cells has driven the development of new therapeutic strategies. In this introductory Chapter we provide an overview of approaches in the development of antigen-selective immunotherapies selectively targeting B cells. At the end of this Chapter, we will focus on B cell-selective targeting strategies in rheumatoid arthritis, concluding with the outline of this thesis.

1.1 Introduction

One of the cornerstones of the immune system is its ability to discriminate between 'self' and 'non-self'. This ability ensures the stimulation of proper immune responses towards foreign substances while simultaneously maintaining tolerance towards self-components.[1,2] Here we will provide an introduction on autoimmunity and the involvement of B cells.

B cell development and autoimmunity. B cells are highly specialized cells, functioning in the recognition of antigens by binding to cell-surface immunoglobulins, leading to differentiation into plasma cells to produce and secrete antibodies to that specific antigen.[1, 2] Each B cell expresses immunoglobulins to one specific antigen. Additionally, B cells can present antigens (they are also classified as antigen-presenting cells (APCs)) and secrete cytokines.

B cells develop from hematopoietic stem cells originating in the bone marrow (Figure 1). These cells differentiate into multipotent progenitor cells and common lymphoid cells, from which B cells are derived in several stages.[3] During these stages, gene expression patterns are changing as are the immunoglobulin heavy and light chain gene rearrangements. Before migrating to the periphery, B cells undergo two types of selection; positive selection, in which the B cell receptor (BCR) is tested to recognize a ligand (antigen independent), and negative selection, in which the BCR is tested against self-antigens.[4] The process of negative selection is of great essence for central tolerance. Autoreactive B cells which have failed the negative selection can be rescued, eliminated or functionally inactivated by various regulatory mechanisms (Figure 1),[5] including receptor-editing, apoptosis, suppression by regulatory cells and limitations of survival and growth factors, which when defective can lead to a breakdown in tolerance and the development of autoimmune diseases.[6] The loss of tolerance is a complex process that involves genetic components (*e.g.* in human leukocyte antigen alleles), most likely combined with environmental events (*e.g.* an infection).[7]

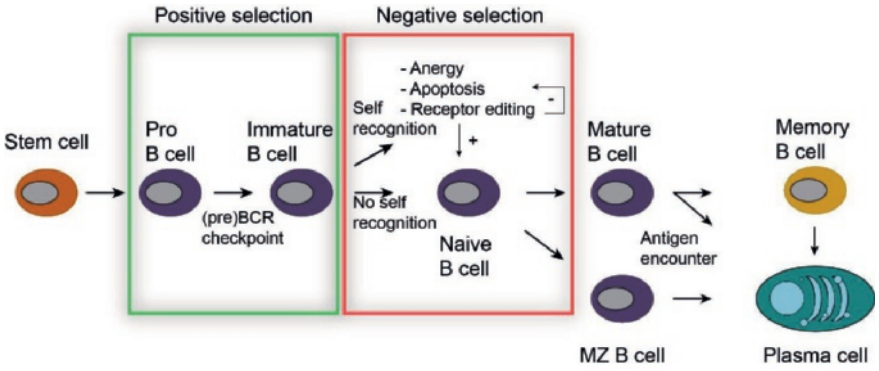

Figure 1. B cell development. Two important checkpoints are implemented to prevent useless or autoreactive B cells to move into the periphery. Positive selection includes the checkpoint for the pre-B cell receptor (heavy chain rearrangement) and the checkpoint for the BCR, after light chain rearrangement. Negative selection includes testing the specificity for self-antigens.

After the negative selection process, the B cells migrate into the spleen and differentiate either into follicular (FO) B cells or marginal zone (MZ) B cells. Next, the B cells enter the circulation and

bind a specific antigen in lymphoid tissue resulting in mature B cells and differentiation into plasma cells.[8-10] The immunoglobulin genes of FO B cells undergo extensive somatic hypermutation and isotope switching in germinal centers (GCs), which emerges in the secretion of different classes of high-affinity antibodies.[11] MZ B cells are able to generate antibodies through both T cell-independent and T cell-dependent pathways.[12]

Autoreactive B cells with low-affinity BCRs can escape negative selection and differentiate into plasma cells.[13] The escaped autoreactive B cells can drive autoimmunity via multiple mechanisms. One example is via the formation of immune complexes in combination with self-antigens. These immune complexes can initiate host effector functions via Fc-mediated activation of the complement (soluble proteolytic proteins) cascade.[14] An antibody-independent function of activated B cells has been revealed by their ability to secrete pro-inflammatory cytokines, such as IL-6, IFN-γ, and LTα, in a similar fashion as T cells.[15] B cell-derived cytokine release can contribute substantially to ongoing autoimmune responses, by regulation of T cell function and inflammation.[1] The function of B cells as antigen-presenting cells is also important, because it provides activating and deactivating signals to $CD4^+$ T cells. To do this, B cells express besides major histocompatibility complex (MHC) proteins co-stimulatory molecules such as B7 and CD40.[16] When self-epitopes are presented on MHC class-II, T cells will be activated, expand and fulfill their effector functions. B cells contribute to a number of autoimmune disorders by producing autoantibodies. The production of autoantibodies is suggested to be similar in nature to protective antibodies.[17] Recognition of the self-antigen bound by MHC class-II by T cells, co-stimulatory molecules and the excreted cytokines will activate B cells to differentiate into plasma cells and produce the autoantibodies. Binding of these autoantibodies to tissues or cells will elicit an inflammatory response and complement will be activated. This can trigger the destruction of these tissues and cells by *e.g.* the formation of the membrane-attack complex. Alternatively, the cells coated with antibody and complement can be cleared by phagocytes, using either Fc receptors or complement receptors. The destruction mechanism of these tissues will be briefly discussed.

Immunological cell-killing strategies. There are different mechanisms by which the immune system induces cell death. One of these mechanisms is antibody-dependent cellular cytotoxicity (ADCC) in which an effector cell actively lyses a target cell (Figure 2A). These effector cells recognize the target cells because they are coated with antibodies (a process which is called opsonization).[16] Although natural killer (NK) cells are the most common cells to clear target cells, also eosinophils can mediate ADCC.[18] NK cells express FcγRIII, which can bind to the Fc tail of the antibody-opsonized cell and induce cell death.[19]

Alternatively, the complement system is involved in the elimination of cells. The complement can coat the surface of bacteria or extracellular virus particles (also called opsonization) which makes them more easily phagocytosed. Besides the elimination of bacterial pathogens, the complement is also capable to initiate the elimination of eukaryotic cells. This occurs by the formation of a membrane-attack complex (MAC), which is initiated by protein C5b. This protein forms a complex with proteins C6, C7 and C8. Next, C7 and C8 expose their hydrophobic sites and can subsequently be inserted into the membrane. This induces the polymerization of multiple (up to 16) molecules of C9, resulting in a transmembrane channel which disrupts the plasma membrane and will kill the cell (Figure 2B).[16] This mechanism is called complement-dependent cytotoxicity (CDC).

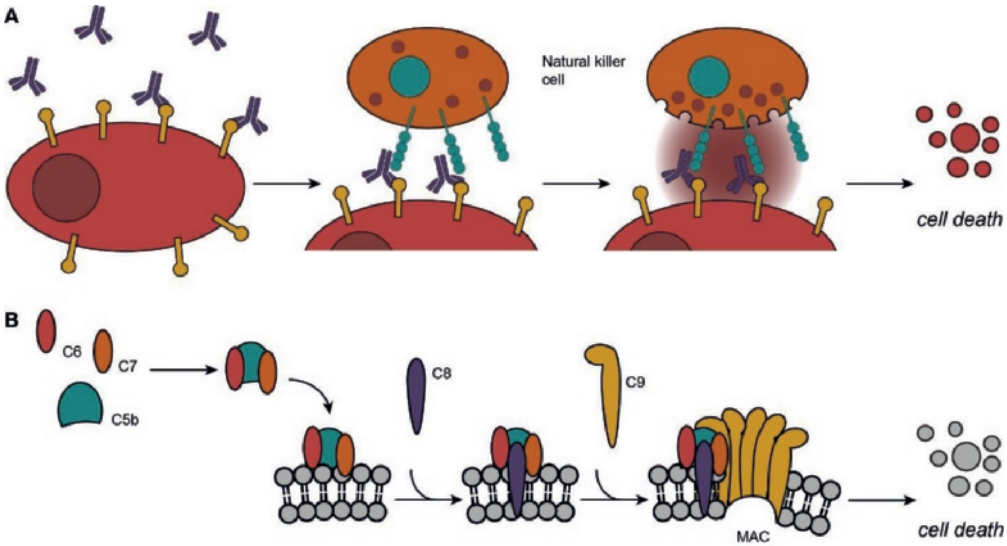

Figure 2. Immunological cell-killing mechanisms. A) Schematic representation of ADCC. Antibodies bind to an antigen of the target cells' membrane. A natural killer cell can bind to the Fc part of the antibody and induce apoptosis; B) Schematic representation of CDC and MAC formation. Protein C5b binds to C6 and C7. C8 is recruited and binds to the membrane. Polymerization of C9 results in the MAC complex and perforates the cell membrane which induces apoptosis.

B cells are considered to play a key role in the pathophysiology of many autoimmune diseases and hence the targeting of these mechanisms can be beneficial in disease treatment. In this Chapter, we will highlight the importance of the selective targeting of B cells. The aforementioned immunological cell killing strategies can be used for this purpose, but also other strategies will be described. We will review the antigen-selective targeting of B cells as well as the use of antigen conjugates to target the BCR directly.

1.2 Targeting of Autoreactive B Cells

Much research has been performed to elucidate the involvement of autoreactive B cells in autoimmune diseases.[20] There is considerable interest in the use of monoclonal antibodies directed against B-cell surface antigens, such as CD20, CD22, CD19 and CD52, as potential therapeutic treatment. Monoclonal antibodies to these targets have been investigated for their effectiveness in several autoimmune diseases, such as RA, SLE and MS.[10] Indirect targeting strategies include blocking of cytokine-signaling as well as intrinsic B cell-activating pathways (such as proteasome inhibition). Cytokines provide B cells with signals necessary to maintain their growth and differentiation. Deprivation of these signals, for instance by the anti-BAFF antibody belimumab,[21] affects the function and survival of B cells. Finally, the agents bortezomib[22] and abatacept[23] – intrinsic proteasome- and co-stimulation inhibitors, respectively – have been clinically approved in the treatment of certain autoimmune disorders.

All these therapies have one thing in common, their targeting of general B cell markers and properties. No distinction is made between protective and autoreactive B cells, resulting in the loss

of also protective B cells and hence immune deficiency for infectious agents.[24] The possibility to target specific autoreactive B cells by using the corresponding autoantigen is gaining interest. This way of targeting pathogenic B cells might prevent autoimmune responses without the undesired adverse effect of targeting all B cells.

Targeting of SIGLEC-G and CD22. Siglecs (sialic acid-binding immunoglobulin-like lectins) are transmembrane proteins and members of the immunoglobulin superfamily.[25-31] With their extracellular ligand binding domain they specifically recognize endogenous sialic acids attached to glycoproteins on the cell surface. Multiple Siglecs have been identified, but the only Siglecs expressed on B cell surfaces are CD22 and Siglec-G.[25, 26] The latter is expressed on mouse B-lymphocytes and its human orthologue with high sequence homology is Siglec-10.[32, 33] These Siglecs function as inhibitory co-receptors, when activated they inhibit the BCR signal and promote tolerance in B cells (Figure 3).[34, 35]

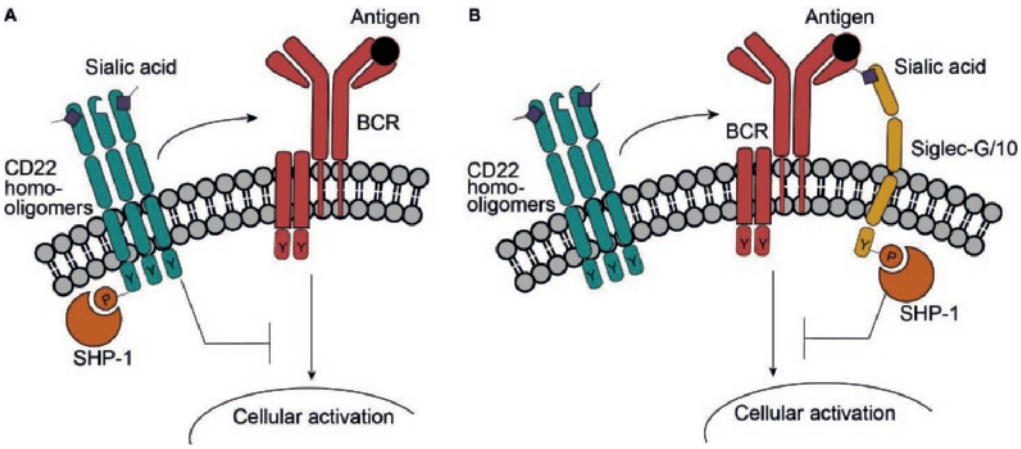

Figure 3. Influence of CD22 and Siglec-G/10 on BCR signaling in B cells. A) CD22 homo-oligomers were formed by intermolecular sialic acid interactions. Upon BCR activation by antigen binding, CD22 homo-oligomers are recruited towards the BCR, promoting phosphorylation of intracellular ITIM domains on CD22. SHP-1 recognizes and binds phosphorylated ITIMs, resulting in dampening of calcium signaling; B) A conclusive mechanism for inhibition by Siglec-G/10 is not known. Studies suggest that direct binding of Siglec-G to sialic acids on the BCR promotes recruitment of Siglecs (CD22) after antigen stimulation. Both phosphorylated Siglec-G and Siglec-10 are bound by SHP-1, resulting in suppression of calcium signaling.

The cytoplasmic signaling domain of all three Siglecs carries an immunoreceptor tyrosine-based inhibitory motif (ITIM); CD22 even contains several of these motifs.[33, 36] These motifs on CD22, containing conserved tyrosine residues, are rapidly phosphorylated by the tyrosine kinase Lyn upon antigen mediated BCR crosslinking.[37] Then SH2-domain-containing tyrosine phosphatase (SHP-1) is recruited towards phosphorylated ITIMs and becomes activated.[38] Subsequently, SHP-1 dephosphorylates positive activators in the BCR signaling pathway, thereby reducing calcium levels, which are the key triggering signals for B cell development and regulation of effector functions, in the cell.[39-41] For Siglec-G and Siglec-10 similar SHP-1-dependent inhibition

mechanisms of BCR signaling have been suggested.[33, 35] Notably, CD22 is the prominent inhibitory co-receptor on B2 cells (conventional B cells, like FO and MZ B cells, developed as described in Section 1.1),[42] while Siglec-G/10 functions seem to be restricted to the subset of B1 cells (minority subset of B cells developed in the prenatal period).[35]

Importantly, CD22 in resting B cells is most prominently bound to sialic acids on other, neighboring CD22 receptors,[43] through which the Siglecs are apparently 'masked'.[44] This so-called *cis*-ligand-binding activity leads to the formation of homo-oligomers of CD22 on the cell surface.[43] These oligomers are recruited to the BCR when antigens are bound,[45] most likely by protein-protein interactions.[46] The proximity of CD22 to the BCR seems essential for the inhibitory function of the Siglec,[46] as association of CD22 and BCR promotes phosphorylation of the ITIMs.[37] Notably, it has been shown that disruption of CD22 *cis*-ligand-binding results in a stronger association of CD22 with the BCR, stronger phosphorylation of ITIMs and an impaired BCR-induced Ca^{2+} response.[45, 47, 48] Additionally, engagement of CD22 in *trans*-interactions with sialic acids on other cells, seems to enforce ligation of the Siglecs to the BCR and suppresses BCR signaling.[49] Co-expression of self-antigen and sialic acids on target cells thereby promotes tolerance towards the respective antigens.[50] The role of competition between both mechanisms – *cis*- and *trans*-interactions – is not fully understood and remains to be elucidated.[51, 52] Furthermore, much less is known about the activating mechanism of Siglec-G.[52] It has recently been shown that Siglec-G is already associated with the BCR in resting B cells.[53] Siglec-G has been suggested to directly bind to sialic acids on the BCR. Supposedly, this interaction can be further increased upon BCR activation.[53]

Siglecs are constitutively active on B cells in order to maintain control over immunity and tolerance.[51, 54] Both CD22-deficient[34, 55, 56] and Siglec-G-deficient[35] mice do not develop autoimmune disease. However, CD22 x Siglec-G double-deficient mice do show an SLE-like phenotype and develop glomerulonephritis.[57] This clearly demonstrates a complementary role for Siglec-G and CD22 in preventing immunity towards self-antigens. CD22 and Siglec-G are expressed during all stages of B cell development.[25] Hence, these are potential B cell targets for inhibition of the BCR-mediated response in autoimmune diseases.

Kelm *et al.*[58] were the first to show that binding of a ligand to the lectin domain of CD22 has a direct influence on the intracellular inhibitory domain.[58] They showed, using synthetic sialosides as inhibitors for the lectin domain of CD22, that tyrosine-phosphorylation of CD22 and SHP-1 recruitment was decreased similar to CD22-deficient B cells. In addition, *trans*-ligand interactions have been reported to strongly dampen B cell activation when the target cell, displaying the antigen, co-expresses sialoglycoconjugates.[50] Courtney *et al.*[59] and Duong *et al.*[60] firstly employed this relationship and synthetically designed multivalent carriers, with self-antigens as well as CD22 or Siglec-G ligands, to dampen autoantigen specific B cells. Courtney *et al.*[59] used ring-opening metathesis polymerization (ROMP) to generate polymers bearing the antigen 2,4-dinitrophenyl (DNP), a sialic acid-terminated trisaccharide – a CD22 ligand –, or both recognition elements. The density and valency of both homopolymers and copolymers was chosen to elicit BCR binding and signaling.[61] Monitoring the intracellular Ca^{2+} ion concentration in living cells showed that stimulation with polymers substituted with only DNP antigens caused a fast rise in calcium concentration, whereas polymers substituted with only CD22 ligands had no effect. The substituted copolymer, with both CD22 ligand and DNP antigens, did not evoke a calcium response, indicating an inhibiting effect by the CD22 ligands. In additional experiments the authors showed that co-expression of both recognition elements on polymers is essential to block B cell-

activation. As a result, the co-cluster of the BCR and CD22 on the B cell surface suggests that *trans*-ligand interactions of CD22 diminish the calcium signal. Alternatively, Duong *et al.*[60] conjugated multiple nitrophenol (NP) haptens, T cell-independent type 2 antigens, and glycan ligands for both CD22 and Siglec-G to a polyacrylamide (PA) polymer. They also prepared corresponding carriers with glycans lacking a sialic acid residue (NP-PA). As anticipated, robust *in vivo* generation of NP-specific plasma cells as well as antibodies against NP were observed in mice immunized with NP-PA. Copolymers with Siglec ligands dramatically reduced plasma cell and antibody counts, indicating that co-presentation of Siglec ligands prevents the immunogenic response to selective antigens. Remarkably, mice injected with high affinity Siglec ligands attached to NP antigens even established antigen-selective tolerance for about a month, as challenges with non-sialylated antigen conjugates afterwards failed to evoke an antibody response. However, when an adjuvant was administered simultaneously with the injection, full tolerance was not observed. This raised doubt as to whether this approach would be effective towards T cell-dependent antigens, since a second stimulating signal from T helper cells could counteract dampening by CD22.

In order to reduce the drawback of previous antigen conjugates, Macauley *et al.*[62] designed liposomal nanoparticles as carriers for protein antigens and CD22 ligands. *In vivo* use of these particles has been validated and robust methods exist for conjugation of peptides and glycans to lipids for incorporation in the lipid bilayer of liposomes.[63-65] Accordingly, the authors constructed Siglec-engaging tolerance-inducing antigenic liposomes (STALs) displaying both a protein antigen and CD22 ligands (Figure 4). Siglec ligands with a 200-fold higher affinity than natural ligands were used, as was the T cell-independent antigen NP. Immunization of mice with STALs showed a dramatically lower anti-NP response than with immunogenic liposomes, and upon two subsequent challenges the mice did not evoke a response at all. Tolerance to NP was induced CD22-dependently. Also STALs with multiple different T cell-dependent antigens proved to induce a tolerogenic effect, showing significantly lower antigen-selective antibody response upon subsequent challenges with corresponding antigens. Noteworthy, it was shown that the mechanism of tolerance induction appears to be intrinsic to depletion of antigen-reactive B cells, by CD22 dependent apoptosis,[62] in which the pro-apoptotic factor BIM appeared to play a critical role.[66] Moreover, this effect on viability was even shown in human naive and memory B cells *in vitro*, suggesting that STALs may additionally be beneficial for suppression of a memory B cell response. Tolerance induction was mainly obtained via CD22 inhibitory effects, due to ligand specificity. Since an independent role for Siglec-G had not been demonstrated before, Pfrengle *et al.*[67] developed a high-affinity ligand with specificity for Siglec-G. Comparable results were obtained in experiments conducted with STALs bearing these Siglec-G ligands. Inhibition of BCR signaling and a reduction in the number of living B cells was observed upon enforced ligation of Siglec-G with the BCR, not only in B1 cells, but surprisingly also in splenic B2 cells. Therefore, it will be of specific interest to determine the manner in which Siglec-G and CD22 act cooperatively in preventing immunogenic reactivity towards autoantigens.

The tolerogenic effect of STALs was further improved by encapsulation of an immunosuppressive agent in the lipid membrane, which had previously been shown successful in poly(lactic-*co*-glycolic acid) (PLGA) nanoparticles for tolerance induction in various immunological compartments.[68, 69] Pang *et al.*[70] constructed STALs with encapsulated rapamycin (RAPA), a natural compound which prevents B and T cell proliferation by blocking IL-2 and IL-15 signaling, and is used to prevent the rejection of organ transplants.[71]

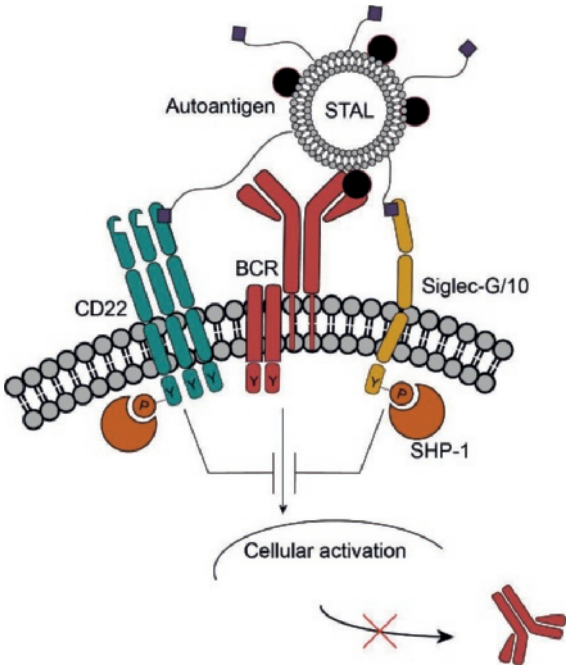

Figure 4. The influence of STALs on BCR signaling in autoimmune B cells. STALs display autoantigens on their membrane surface. Upon interaction of antigen with the BCR, Siglec-G/10 and CD22 are recruited towards activated BCR. Both Siglecs recognize and bind sialic acid ligands present on STALs, forming *trans*-interactions, resulting in suppressed calcium signaling. The B cell becomes tolerant towards the specific auto-antigen presented by STALs and might undergo apoptotic cell death.

The STALs with RAPA showed enhanced antigen-selective tolerance upon *in vivo* immunization in naive mice, compared to STALs without RAPA. To investigate the tolerogenic effect of STALs with RAPA on the memory B cell response *in vivo*, antigen-sensitized mice were immunized accordingly. Neither STALs nor STALs with RAPA were able to completely prevent a memory B cell response towards soluble ovalbumin (OVA) antigens, although a significant reduction of anti-OVA antibodies was observed in the STALs with RAPA group compared to control mice. The authors hypothesized that the lack of complete tolerance induction is the result of relatively low doses of RAPA.[70] In conclusion, these findings demonstrate the potential of STALs as an antigen-selective tolerogenic platform, possibly combined with immunomodulatory agents, in treatment of autoimmune diseases. As CD22 and Siglec-G are displayed on the cell surface of all B cells and have distinct, yet overlapping, affinities for their sialylated glycan ligands, they prove to be suitable B cell targets in achieving antigen-selective B cell tolerance. Recently, a human CD22 transgenic mouse model, showing similar CD22-dependent effects on BCR signaling and tolerance, has been developed.[72] This might be a new valuable model to assess mechanisms of action and future optimization of CD22 targeted therapies in a preclinical setting.

Targeting of ICAM. For a humoral immune response against T cell-dependent antigens, additional stimulation by T helper cells is critical to evoke full B cell activation and differentiation, as binding of the BCR to a single protein antigen is insufficient.[73] Peptide epitopes are presented

on MHC class-II complexes on the surface of B cells after uptake and processing of antigens that bind the BCR. Then $CD4^+$ T helper cells can engage and the T cell receptor (TCR) will specifically recognize and interact with the MHC class II-peptide complex. Subsequent activation of T cells requires additional co-stimulatory signals, which can be provided by intercellular adhesion molecule-1 (ICAM-1/CD45), among others.[73] This is the major receptor for lymphocyte function-associated antigen-1 (LFA-1), an integrin found on T cells.[74] Interaction of LFA-1 with ICAM-1 on APCs is essential for stabilization of cell-cell interactions and induction of a pro-inflammatory response, as well as for transmigration of leukocytes into tissue, since ICAM-1 is also present on endothelial cells.[74, 75]

This adhesion interaction also provides co-stimulation in the immunological synapse (IS) formed between T cells and other APCs, such as dendritic cells (DCs) and macrophages.[76] The mature IS is defined by supramolecular activation clusters (SMACs),[77-79] the center of which is enriched for TCR-peptide-MHC complexes (signal-1), while the outer ring contains the adhesion molecules LFA-1/ICAM-1 (signal-2) (Figures 5A, B). Adhesion molecules first localize in the center of SMACs, whereas the engaged TCRs form a peripheral ring, translocation and segregation follow to form the mature IS. Importantly, in case the co-stimulation by the adhesion ligand ICAM-1 is lacking, T cell-activation is reduced and this might even induce selective tolerance towards the peptides presented. Besides, evidence shows that these adhesion molecules play an important role in the pathogenesis and progression of autoimmune diseases.[74, 80] Formation of the IS between APCs and either $CD4^+$ helper or $CD8^+$ cytotoxic T cells is a critical step in the activation of antigen-selective T cells and subsequent immune responses, as well as B cell-activation and humoral immunity towards T cell-dependent antigens. Hence, the LFA-1/ICAM-1 interaction is a potential target in inducing antigen-selective tolerance in autoimmune diseases.

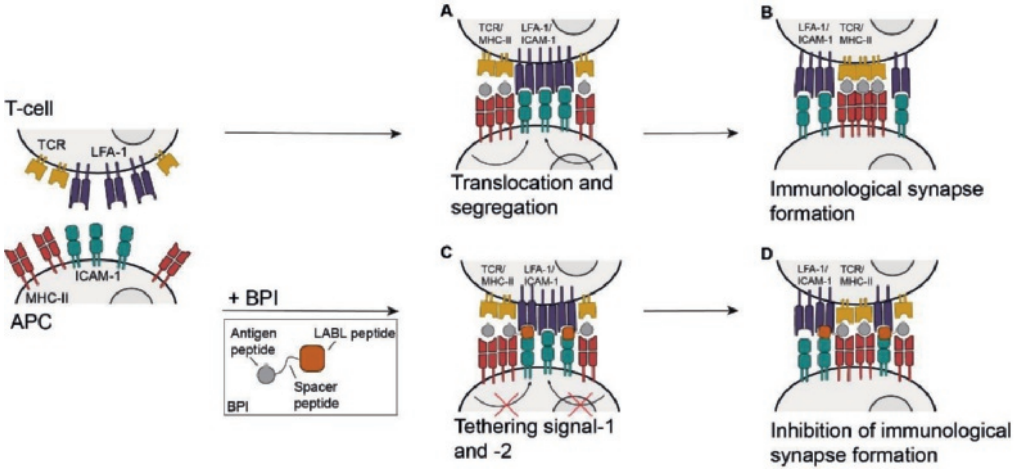

Figure 5. The proposed mechanism of BPI action in preventing formation of the immunological synapse. A) The initial stage of IS formation shows interaction of LFA-1/ICAM-1 at the center and TCR/MHC-antigen complexes at the outer ring; B) Both pairs are transmigrated and segregated to form the mature IS; C) In the presence of BPI, antigen peptide will bind to MHC class-II complexes while LABL peptide will bind ICAM-1 on APCs, forming a bridge in between and partly preventing T cell and APC interactions; D) Since transmigration and segregation are unable to occur properly, the mature IS cannot be formed.

Targeting of ICAM-1 was first employed by the development of a bifunctional peptide inhibitor (BPI). Kobayashi *et al.*[81] developed a spacer peptide conjugated to an antigen epitope peptide as well as an ICAM-1 binding peptide. In this study they used the epitope peptide $PLP_{139–151}$,[82] derived from the self-antigen myelin proteolipid protein (PLP), which is an important antigenic protein in the pathogenesis of MS. The previously discovered ICAM-1 blocking peptide (LABL)[83, 84] was attached on the other end of the peptide spacer. LABL has been shown to block T cell adhesion to epithelial cells by binding ICAM-1.[83-86] The authors hypothesized that the PLP peptide conjugated to LABL simultaneously binds MHC class-II, the antigen can bind to empty active MHC-II,[87, 88] and ICAM-1 on APCs (Figures 5C, D). By forming a bridge between the target molecules, the BPI disables the translocation and segregation of both receptors, which is needed to form the mature IS.[81] Another possible mechanism is inhibition of signal clustering by steric hindrance when either solely PLP binds MHC class-II or only LABL binds ICAM-1, alternatively a combination of all mechanisms is suggested. Notably, if only LABL binds ICAM-1, this would not be an antigen specific strategy. Altogether, this should result in inhibition of T cell-activation and suppression of an autoimmune response towards PLP. The therapeutic activity of PLP-PBI was evaluated in mice induced with experimental autoimmune encephalomyelitis (EAE), which is a model for human MS.

Disease progression and severity were significantly reduced in an antigen-selective manner. Additional experiments suggest that the unique structure of the BPI is important for its suppressing activity and that suppression of EAE is the result of induced regulatory T cells. This approach was also applied to treat type 1 diabetes (T1D) by using the diabetes-associated antigen glutamic acid decarboxylase (GAD).[89, 90] A BPI bearing GAD peptide was employed to test its suppressing activity on T1D, by injection in non-obese diabetes (NOD) mice, a model for human T1D.[91] Positive effects on the suppression of insulitis and disease progression were observed.

Multiple follow-up studies have been reported in order to improve BPI efficacy for future treatment of MS patients.[92-97] Firstly, optimization of PLP-BPI led to newly synthesized derivatives showing more effective suppression of disease severity and morbidity *in vivo* in EAE mice, prior to and after onset of the disease.[92] To reduce the number of treatment injections, a vaccine-like approach was applied.[93, 94] A colloidal gel was prepared consisting of PLGA nanoparticles coated with either positively or negatively charged polysaccharides. Controlled-release of the BPI from the colloidal gel was obtained and suppression of EAE in mice by a one-time injection was comparable with the effect of three injections from previous BPIs.[93, 94] Furthermore, multivalent BPIs (MVB)[96] were developed to address the problem of epitope spreading, a process by which autoimmunity extends to multiple different self-epitopes, that occurs in later stages of the disease.[98]

Targeting B7[99, 100] co-stimulators on APCs instead of ICAM-1, using novel BPIs displaying B7 antisense peptide (B7AP), has also shown to be effective.[97] The B7 receptor is expressed on APCs and can either bind to CD28 to activate naive T cells, or can bind to CTLA-4 on activated T cells to downregulate the activation and proliferation. Stewart *et al.* showed by synthesizing a BPI-containing B7AP with a MS antigenic peptide, that EAE was suppressed in an animal model.[97] Finally, since the short half-life of BPI *in vivo* appeared to be a potential problem,[101] novel BPIs were synthesized in which the two peptides were fused via a fragment crystallizable (Fc) region of a human IgG1 antibody. This proof-of-concept has shown that preparation of such a BPI-Fc fusion is possible and that it still functions to protect mice against EAE.[95]

With respect to previously mentioned epitope spreading in later stages of MS, I-Domain-Antigen Conjugates (IDACs) were developed.[102, 103] The I-domain binds to ICAM and is similar to the

binding region in LFA-1,[104] hence the I-domain is comparable to the LABL peptide. Antigenic peptides are conjugated to the I-domain to form IDACs. Multivalent BPIs display two antigenic peptides, whereas IDACs enable the conjugation of multiple protein epitopes. The authors hypothesized that when the I-domain of IDAC binds ICAM-1 on the surface of APCs, antigen peptides can simultaneously bind MHC class-II molecules. Since IDACs can present multiple different peptides to APCs, they might inhibit antigen-selective T cell activation for several different T cell subsets simultaneously and prevent epitope spreading in MS. To proof the concept, IDACs were prepared by conjugation of several PLP peptides. The multivalent IDACs proved effective in suppressing EAE in mice.[102, 103] Besides, it was shown that delivery of antigenic peptides by the I-domain resulted in immunotolerance when mice were treated both in a prophylactic and vaccine-like manner.[103] The potential of IDACs in prevention of antigenic spreading is yet to be determined.

Similarly, Berkland *et al.*[105] developed so-called multivalent soluble antigen arrays (SAgA), a hyaluronic acid (HA) polymer conjugated with multiple PLP and LABL peptides ($SAgA_{PLP:LABL}$) (Figure 6). HA is a natural glycosaminoglycan that is characterized by highly flexible and water soluble behavior.[106, 107] It has recently been reported that controlling the molecular weight of HA facilitates specific lymphatic uptake of the polymers.[108] Before ligation of the peptides, they were end-functionalized with hydroxylamine,[109-111] which allowed for easy grafting onto the polymers by a one-pot, single-step oxime addition.[105] The different peptides were successfully attached approximately in the desired 1:1 ratio. Simultaneous delivery of both PLP antigens and ICAM-1 ligands (LABL) on the HA graft polymers significantly suppressed EAE disease in mice, compared to multiple controls, such as a mixture of the free components; PLP, LABL and HA.[105] These *in vivo* effects were further investigated by comparing $SAgA_{PLP:LABL}$ with a 1:1 mixture of HA polymer displaying either PLP antigen (HA_{PLP}) or LABL peptide (HA_{LABL}) (Figure 6).[112]

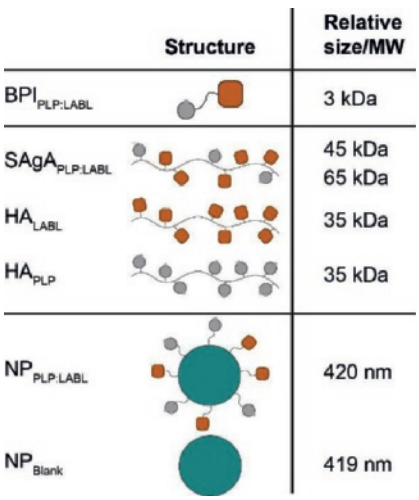

Figure 6. Schematic overview of the various scaffolds used to antigen-selectively target B cells. All scaffolds display both the antigenic peptide PLP and the ICAM-1 ligand LABL. The bifunctional peptide inhibitor ($BPI_{PLP:LABL}$) displays only one entity of both peptides, whereas multivalent soluble antigen arrays ($SAgA_{PLP:LABL}$) and PLGA nanoparticles ($NP_{PLP:LABL}$) are conjugated with a number of both peptides. Linear HA polymers are also depicted with either solely PLP peptides (HA_{PLP}) or only LABL (HA_{LABL}).[115]

Interestingly, clinical data proved that similar *in vivo* protection against EAE was obtained. However, when splenocytes isolated from EAE mice were similarly treated *ex vivo*, cytokine expression profiles appeared to be very different, suggesting that exact mechanisms of protection and the role of co-delivery should be further elucidated.[112] In addition, SAgA carriers were also equipped with both PLP autoantigen and one of the three different B7-binding peptides which specifically targets the B7 co-stimulatory receptor.[113] As binding peptides, either one of the two inhibitory CD28 mimic peptides or a stimulating peptide mimic of CTLA-4 was used. Surprisingly, all three independent SAgAs were found to inhibit disease progression. Berkland *et al.* hypothesized, based on previous reports,[114] that the CTLA-4 mimic is inhibitory instead of stimulatory due to the dampening of T cell inactivation and hence overstimulation of T-cells. This mechanism is therefore possibly inducing anergy.[113]

Various consecutive studies investigated the effect of the physical characteristics of the different scaffolds on their inhibitory potency,[115-117] the preferred routes of administration[118, 119] and the potential mechanism leading to tolerance induction.[35, 39] Sestak *et al.*[115] compared clinical effects of BPIs, 45 kDa SAgA, 65 kDa SAgA and PLGA nanoparticles, all displaying PLP and LABL peptides (Figure 6). They observed that the soluble, small scaffolds – BPI and SAgA – were the most effective treatments, compared to large, insoluble nanoparticles. Overall, the SAgA with a size of 45 kDa showed the best clinical results with respect to disease onset and the maintenance of murine weight.[115] Finally, Hartwell *et al.*[120] used human Raji B cells, B lymphocytes of a Burkitt's lymphoma patient and which harbor the Epstein–Barr virus,[121] as a model for APCs to investigate specificity and binding mode of SAgAs *in vitro.* By competitive dissociation studies using flow cytometry they showed that the addition of antigen-peptides increased an antigen-selective response. The authors hypothesized that PLP peptides on SAgA would bind either MHC class-II complexes or the BCR on the cellular surface of B cells. Also, it has been shown that engagement and clustering of the BCR with an inhibitory co-receptor can cause reduction in IgM-stimulated signaling in the Raji B cells. Furthermore, IgM blocking experiments suggest that the BCR is a target for $SAgA_{PLP:LABL}$. Altogether, they have shown that $SAgA_{PLP:LABL}$ binding dampens BCR-mediated signaling.[120] Replacement of the hydrolyzable oxime bonds between the peptides and the HA scaffold by a hydrolytically stable linkage using a Cu-catalyzed Azide−Alkyne Cycloaddition (CuAAC), greatly enhanced binding avidity as well as calcium flux signaling inhibition.[116] Continuous BCR engagement and clustering was observed *in vitro*, which pointed to a likely therapeutic cellular mechanism in which the click-conjugated $SAgA_{PLP:LABL}$ induces B cell anergy. Lastly, *in vivo* efficacy against EAE was vastly enhanced compared to previous hydrolyzable $SAgA_{PLP:LABL}$, demonstrating its promising potential in the treatment of autoimmune diseases, MS in particular.[116]

In conclusion, BPIs, IDACs and SAgAs have all been proven successful in preventing EAE disease symptoms in mice, and therefore are considered as potential therapeutic strategies in the treatment of MS patients. Currently, the biggest challenge is to elucidate the mechanism by which these peptide carriers effect autoimmune responses and the individual contributions of the antigenic peptide and LABL therein. It has become evident that co-delivery of an auto-antigenic peptide and a secondary signal is critical. The ICAM-1 binding peptide LABL has proven to be an effective secondary signal. Whether this signal prevents the adhesion of APCs with T cells via blocking of the ICAM-1/LFA-1 interaction, or solely functions to support the engagement of the peptide carriers onto the cellular surface of APCs, is yet uncertain. As for interactions of the conjugated autoantigen with APCs, different mechanisms are proposed for different peptide

carriers. Autoantigens on BPIs are considered to interact with MHC class-II complexes on APCs. However, antigenic peptides are usually loaded onto MHC class-II complexes within APCs before being presented on the cellular surface.[122] Also, unloaded MHC complexes are often unstable and in particular abundantly present on immature DCs.[123] Besides, evidence of the mechanism involving MHC class-II has not been provided by the authors to date. Nevertheless, BPIs may exert their function *in vivo* by alteration of the fate of naive T cells. As T cells normally gain an inflammatory phenotype, such as differentiation into $CD4^+$ helper or $CD8^+$ cytotoxic T cells, BPI mediation leads to an increase in the presence of suppressor or regulatory phenotypes. In this case, BPIs might also inhibit an antigen-selective humoral immune response towards T cell-dependent antigens. On the contrary, autoantigens on SAgAs have been suggested to engage and cluster the BCRs on B cells, reducing BCR-mediated signaling. Considering this mechanism, the multivalency of the linear polymers benefits effective receptor clustering. If this is true, it could affect B cell activation towards both T cell-dependent and T cell-independent antigens. Moreover, the *in vivo* effect of $SAgA_{PLP:LABL}$ may completely be a result of B cell-targeting via the BCR, as the possible interaction with MHC class-II remains to be determined. Therefore, SAgA polymers might even specifically target B cells. Altogether, BPI, IDAC and SAgA scaffolds targeting ICAM-1 hold great promise to promote antigen-selective immune tolerance in autoimmune disease.

FcγRIIb. FcγRIIb (CD32) is an inhibitory immunoglobulin G (IgG) co-receptor on B lymphocytes, which is the only IgG Fc-recognizing receptor present on the B cell extracellular surface.[124, 125] IgG immune complexes represent the inhibitory-ligand of this receptor,[125] which were already recognized as such more than 30 years ago.[126] The single-chain FcγRIIb protein holds an ITIM on its cytoplasmic domain, of which the tyrosine residue gets phosphorylated upon co-ligation of the receptor with the BCR.[127, 128] Co-ligation occurs when IgG-antigen complexes interact simultaneously with the BCR and the FcγRIIb receptor.[125] The receptor can effectuate its inhibitory effect via three separable pathways, resulting in either inhibition of both calcium-signaling and cellular proliferation – via ITIM-dependent mechanisms[129-131] – or in induction of apoptosis – via an ITIM-independent mechanism.[132] Calcium-signaling as well as B cell proliferation are reduced via downstream-signaling starting with recruitment of SH2-containing inositol polyphosphate 5-phosphatase (SHIP) to phosphorylated ITIM motifs. SHIP hydrolyzes the membrane phosphatidylinositol 3,4,5-trisphosphate (PIP_3), eventually preventing the influx of extracellular calcium and thereby inhibiting BCR signaling.[133, 134] Recruitment and activation of $p62^{dok}$ and subsequent inactivation of mitogen-activated protein (MAP) kinases leads to arrest of the BCR-triggered proliferation of B cells (Figure 7A).[135, 136] This inhibitory function is of importance in the downregulation of a B cell response. The inhibitory FcγRIIb receptor has been implicated in the development of autoimmune disease, as FcγRIIb deficient mice showed imbalanced immune responses, increased antibody production to both T cell-dependent and T cell-independent antigens, as well as developmental autoimmune pathology.[137-139]

Recently, a novel method using chimeric molecules has been designed to mimic this physiological inhibitory mechanism in order to develop an immune inhibitory therapy targeting B cells in an antigen-selective manner. Tchorbanov *et al.*[140] and Mihaylova *et al.*[141] almost simultaneously reported on the first chimeric molecules mimicking the IgG-containing immune complexes. These chimeric molecules were hypothesized to be able to crosslink the BCR and the FcγRIIb receptor, thereby suppressing an on-going antibody response to the autoantigen of interest (Figure 7B). The authors constructed the chimeric molecules by conjugation of either a DNA-mimicking peptide[140]

or a histone-1 peptide[141] to rat monoclonal anti-mouse FcγRIIb antibody. These antigens were of interest since IgG autoantibodies targeting double-stranded (ds) DNA[142] or histones[143] are characteristic in SLE pathogenesis. Silencing of the ds-DNA- or histone-1-specific B-lymphocytes *in vitro* and *in vivo* in lupus-prone MRL*/lpr* mice[144] resulted in apoptosis of the corresponding B lymphocytes and a reduced number of ds-DNA or histone-1 antibody levels. Nevertheless, constant antibody levels were observed in sick, old mice, probably since pre-existing long-lived antibody secreting plasma cells were unaffected by this treatment. B lymphocytes and antibody levels with other antigen specificities were not affected. Additionally, the progression of lupus disease symptoms were delayed in both young and old mice,[140, 141] although prolonged overall survival of old mice was only observed when treated with the chimeric construct bearing the ds-DNA mimicking peptide.[140] Interestingly, chimeric histone-1 conjugates also partly suppressed the production of ds-DNA antibodies, which might be the result of 'tolerance-spreading', according to the authors.[141]

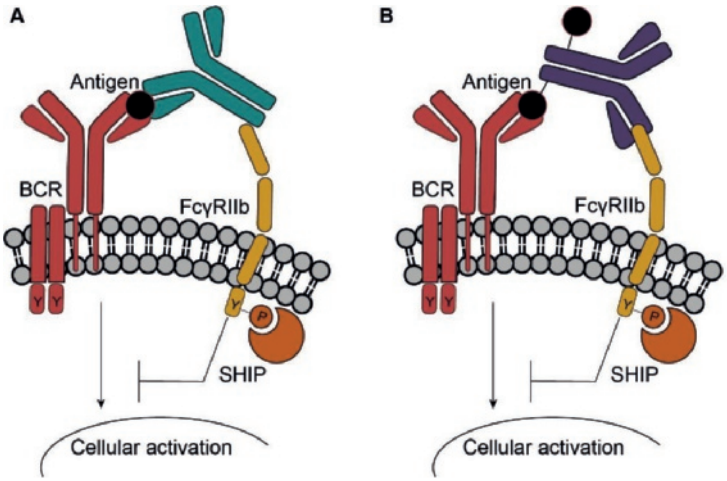

Figure 7. Mechanism and inhibition of FcγRIIb. A) FcγRIIb recognizes the Fc tail of IgG molecules and the IgG-antigen complex can interact simultaneously with this receptor and the BCR to inhibit B cell activity; B) By synthesizing a chimeric construct in which an autoantigen is conjugated to a FcγRIIb-specific monoclonal antibody, simultaneous binding was achieved and selective B cells were inactivated. Co-crosslinking of the respective inhibitory receptor with the antigen-selective BCR on disease-associated autoreactive B cells provided B cell tolerance.

A limitation of this approach was the appearance of an immunogenic response towards the chimeric construct, the rat anti-mouse FcγRIIb antibody in particular, as a result of anti-chimeric immunoglobulin antibody production. To circumvent the immunogenic response towards the chimeric construct, mouse IgG2a, which is able to bind the FcγRIIb receptor, was used as the antibody backbone. Tri-specific chimeric constructs were created, targeting simultaneously the FcγRIIb receptor, the co-inhibitory receptor CD22, and the BCR.[145] This induced two independent inhibitory pathways, effectively suppressing both IgG and IgM anti-DNA antibody levels in lupus prone mice. Despite the use of mouse IgG2a antibodies, the mice still produced antibodies to the mouse antibody scaffold after 15 weeks.[145] To address the resistance of long-lived plasma cells to

this chimeric approach, the treatment was combined with partial plasma cell depletion by simultaneous administration of bortezomib.[146] This combination therapy significantly showed beneficial effects with respect to disease appearance and survival. Similar chimeric conjugates were also employed to target nicotinic acetylcholine receptor-reactive B cells in myasthenia gravis disease, successful antigen-selective depletion of B cells has been shown *in vitro*[147] and *in vivo*.[148] To further decrease an immunogenic response Gesheva *et al.*[149] generated a chimeric gene-engineered DNA molecule, encoding a ds-DNA-like peptide and a single-chain variable fragment (scFv) of the FcγRIIb-specific antibody. The immunogenic Fc fragment was lacking in the corresponding fusion protein, reducing a chimeric immune response in lupus prone mice.[149]

In conclusion, the FcγRIIb is an interesting target for B cell inhibition and the antigen-combined strategies have proven beneficial *in vitro* and *in vivo*. Moreover, in contrast to CD20, FcγRIIb is expressed on plasma cells and may control their activity as well.[150]

Complement receptor 1. Complement receptor 1 (CR1, CD35) represents another interesting target to deliver an inhibitory signal to a selective subset of B cells.[151] This receptor induces cleavage and hence complement activation of C3b into iC3b and C3d. This naturally causes the binding of the pathogen to CR2 and the BCR, resulting in B cell activation. It has been shown that the CR1 can also have an inhibitory function by binding to C3b to prevent overreaction towards an opsonized pathogen.[151] This results in suppression of BCR signaling as well as the dampening of proliferation and differentiation of activated B cells (Figure 8A).[152] Although the expression of CR1 on B lymphocytes in SLE and RA patients is markedly reduced,[153] its inhibitory capacity has been demonstrated to be maintained on B cells from RA patients.[154] Voynova *et al.*[155] created chimeric constructs carrying ds-DNA-mimicking peptide and monoclonal anti-CR1 antibody, aiming to selectively silence autoreactive B cells from SLE patients (Figure 8B).

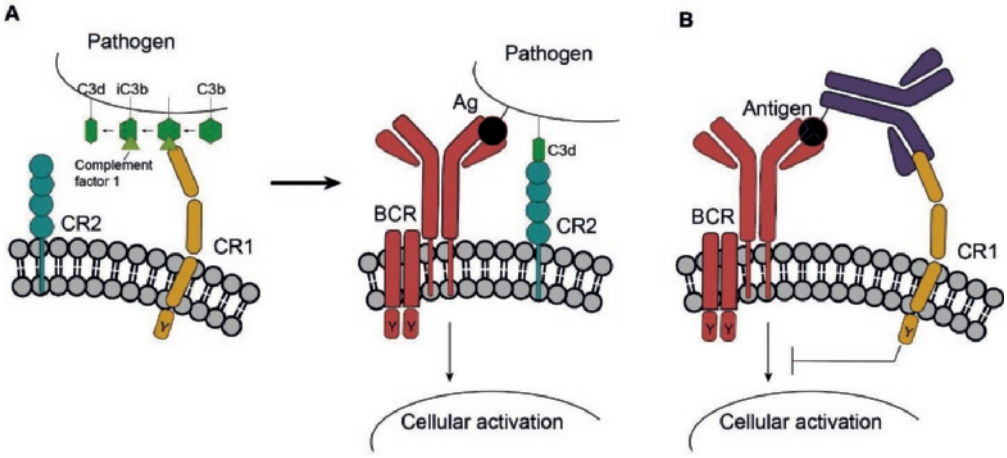

Figure 8. Complement receptor 1. A) Schematic representation of the function of CR1. When CR1 binds to C3b fragments, it makes them susceptible to cleavage by complement factor I (green triangle). Cleavage results in C3d, which can bind to the CR2 component of the B cell co-receptor; B) Suggested strategy to target CR1, which showed to also have an inhibitory function to the BCR.

By employing this strategy, similar as to the FcγRIIb receptor targeting approach, they showed that crosslinking of CR1 with cell surface BCR also effectively provides an inhibitory signal. The peptide chimera reduced the number of anti-dsDNA antibody secreting cells in a culture of lupus patients' PBMCs.[155] This effect has also been demonstrated in humanized SCID mice, transferred with lymphocytes from lupus patients, where it resulted in re-established autoreactive B cell tolerance and prevented the appearance of disease symptoms.[156] In conclusion, the CR1 receptors, which provide negative feedback regulation to activated B cells in natural context, are promising targets in delivering inhibitory signals to autoreactive B cells.[157-159]

The use of antigen-drug conjugates to target autoreactive B cells. Besides using autoantigens combined with inhibitory signals to induce antigen-selective inhibition as described above, autoantigens can also be conjugated directly to a cytotoxic molecule. Since BCRs internalize after the binding to an antigen, the toxin can be specifically delivered to the B cells recognizing the autoantigen.[160]

A truncated form of *Pseudomonas aeruginosa* exotoxin A (ETA') has been used as highly potent toxin conjugated to target and eliminate allergen-specific B cells. ETA' halts protein synthesis in target cells by inhibition of elongation factor 2, a protein involved in translational elongation in the ribosome. Without polypeptide elongation, protein synthesis is stalled. Stöcker *et al.*[161] fused this toxin to epitopes of the Ph1 p 5b allergen specific for timothy grass pollen. They showed that this allergen toxin (AT) was internalized and resulted in antigen-selective cell death *in vitro* (Figure 9A). They predicted that depletion of allergen-specific B cell populations will finally reduce the number of corresponding IgE-producing B cells. A similar approach using diphtheria toxin (DT) and an OVA-DT antigen proved to be effective for OVA-induced allergy in mice. The authors observed selective killing of B cells bearing OVA-specific IgE and decreasing levels of OVA-specific IgE.[162] These methods might be relevant as a therapeutic approach to allergies.

The effectivity of ETA' fusion proteins was demonstrated on human memory B cells as well. The tetanus toxoid fragment C (TTC) was used as a model antigen since it is relatively easy to obtain TT-expressing B cells from human PBMCs. Using a TTC-ETA' fusion construct, an antigen-selective depletion was shown in TTC-reactive human memory B cells from TT-vaccinated donors.[163]

Nachreiner *et al.*[164] focused on the autoreactive B cells producing antibodies targeting the central nervous system in MS. These specific antibodies have a strong demyelinating potential. This damage impairs the conduction of signals in the affected nerves and results in deficiency in for example sensation and movement. The recognition antigen, an extracellular Ig-like domain of human myelin oligodendrocyte glycoprotein (MOG), was fused to ETA' and tested in a MOG-sensitive murine hybridoma cell line or on freshly isolated splenocytes from mice with high numbers of MOG-expressing B cells and high levels of MOG antibodies (TH mice). The authors showed that the chimeric immunotoxin targeted MOG-reactive B-lymphocytes by binding to the appropriate receptors selectively, which led to apoptosis of the target cells.

The ETA' toxin is derived from bacteria, hence these fusion toxins have the disadvantage of high immunogenicity.[165] Therefore, Zochner *et al.*[166] conjugated the C_H2 and C_H3 domains of the human IgG1 heavy chain to MOG (MOG-Fc) (Figure 9B). The Ig isotype chosen for this conjugate functions well for antibody-dependent cellular cytotoxicity and complement-dependent cytotoxicity by effector cells. The advantage of using the C_H2 and C_H3 domains is that two MOG antigens can be attached which increases the avidity. The toxicity of this MOG-Fc was achieved

by binding of MOG to the specific B cell and crosslinking thereof with effector cells. The co-incubation *in vitro* of target cells with human PBMCs showed the complete elimination of target cells. TH mice were used for *in vivo* testing and the authors showed significant depletion of MOG-expressing B cells both *ex vivo* and *in vivo*, even though the MOG reactive antibody titer is high. They showed that not only the number of MOG-expressing B cells was reduced, but that also the serum titer of anti-MOG was decreased.

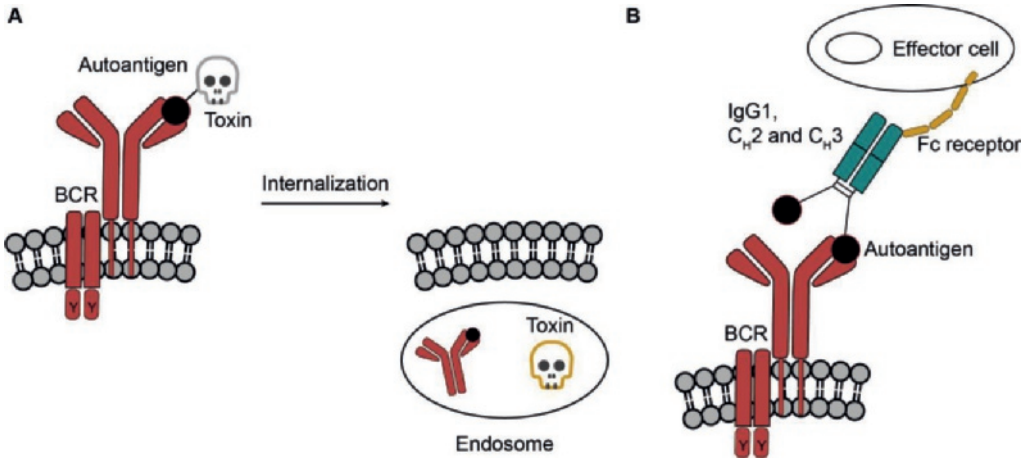

Figure 9. Antigen-toxin conjugation. A) An autoantigen can be fused with a toxin which is active inside the cell. After BCR internalization, elimination of the cell takes place; B) If an autoantigen is fused to a Fc part of IgG1, effector cells are needed for the antibody dependent cellular cytotoxicity.

Alternatively, Reiners *et al.*[167] produced a fusion protein containing a toxin and the mutated and inactive antigen proteinase 3 (PR3). PR3 is a neutrophil and monocyte-derived neutral serine protease. This antigen is the main target of anti-neutrophil cytoplasmic autoantibodies which are present in Wegener's granulomatosis (WG). WG is a rare disease and is a form of vasculitis. The importance of autoreactive B cells in this disease has been established. The toxin fused to PR3 was the ribonuclease angiogenin, a human toxin with low immunogenicity. Using FACS analysis, the authors showed that autoantigen-selective cell death was induced for the WG cell line while a control cell line was unaffected.[167]

Targeting of CD138 and CD44. Autoantibodies are often drivers of consistent autoimmune pathology and chronic inflammation.[20, 168-172] After activation, B cells differentiate into either short-lived plasmablasts or long-lived plasma cells, amongst others.[172-174] The major function of both B cell subsets is to consistently produce and secrete antibodies. Plasmablasts represent a direct result of B cell activity and circulate through the peripheral blood, being consistently regenerated after B cell activation.[175, 176] On the contrary, long-lived plasma cells arise from pre-existing plasmablasts upon a secondary immune response towards a specific antigen. They migrate to and reside in survival niches within the bone marrow or inflamed tissue, and persistently secrete high-affinity antibodies for years, perhaps even decades.[174, 177] They are able to secrete antibodies independently of antigen recognition as well as B or T cell help,[178-180] providing maintenance of humoral memory in response to infection and vaccination.[175, 181] In autoimmune disease, autoreactive long-lived

memory plasma cells have been implicated in disease pathology[173, 182] and constitute a major therapeutic challenge.[172, 173] While short-lived plasmablasts are indirectly addressed via B cell-targeted therapies, long-lived plasma cells are invulnerable to conventional immunosuppression methods as well as regular B and T cell-targeted therapies,[172, 183] as they do not display BCRs and other B cell markers on their extracellular surface.[12] Antigen-selective depletion of long-lived memory plasma cells would be a valuable addition to the treatment spectrum to achieve B cell tolerance to autoantigens.

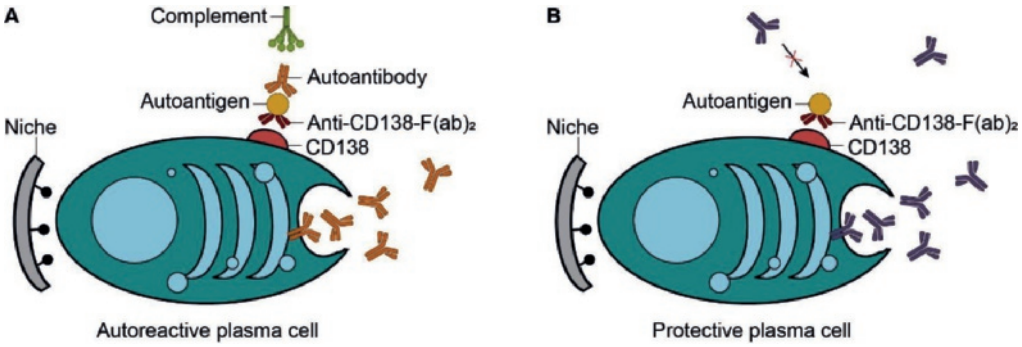

Figure 10. Depletion of autoreactive memory plasma cells by novel affinity matrix (AM) technology. A) CD138 of autoreactive plasma cells are coated with anti-CD138 $F(ab)_2$ fragments conjugated to an autoantigen. Secreted autoantibodies are captured by the AM and the cells are targets for complement-dependent lysis; B) Protective plasma cells are similarly coated with anti-CD138 $F(ab)_2$ fragments conjugated to an autoantigen, since they also express CD138 proteins. Secreted protective antibodies will not recognize nor bind the autoantigen on the AM. Protective plasma cells will not be lysed.

A potential approach to distinguish the autoreactive from protective long-lived plasma cells is based on the antibodies that the cells secrete. This methodology was originally shown to be effective by Köhler *et al*,[184, 185] who showed that coating of a hybridoma cell line with their respective antigen, led to the attachment of its secreted antibodies onto the cell surface. As a result, the complement system was activated and the hybridoma cells were killed by complement-mediated lysis.[184, 185] This novel strategy was later employed in a similar fashion to enable analysis and isolation of live hybridoma cells and T lymphocytes.[186] The cells of interest were coated with a specific affinity matrix (AM), by using a construct containing both an antibody and a high-affinity ligand of the secreted molecule. The antibody specifically binds a molecular target on the extracellular surface of the secreting cells, after which the high-affinity ligands bind the secreted molecules.[186] Then this AM technology was utilized to specifically target autoreactive long-lived plasma cells in mice, by targeting CD138 or CD44, both surface markers on plasma cells (Figure 10).[187] Anti-CD138 and anti-CD44 $F(ab)_2$ fragments were conjugated to antigens of interest, in this study either ovalbumin or the acetylcholine receptor was used. In principle, all plasma cells will be coated with the AM, however, the matrix will only capture any antigen-selective antibodies if those are secreted by the cell. Subsequently the cells will undergo complement-mediated lysis. This technique was successfully applied to deplete autoreactive long-lived plasma cells from a murine model of experimental autoimmune myasthenia gravis *ex vivo*. In addition, by testing the AM technology with a mixture of different antibody secreting plasma cells, the matrix significantly

showed a high level of specificity for the antigen used in the matrix.[187] Lastly, preliminary experiments in mice suggested the *in vivo* therapeutic potential.[172]

In conclusion, this strategy might be an elegant approach to antigen-selectively target and deplete autoreactive long-lived memory plasma cells involved in autoimmune disease pathogenesis, while keeping the protective humoral memory untouched.[172] Potential limitations of this approach *in vivo* might be the presence of circulating autoantibodies, which could bind the AM of protective plasma cells.[172] Besides, clinical translation of this approach may prove difficult when various autoantibodies are involved in disease pathology.[168] Also, the effect of the AM on the surface of protective plasma cells has to be investigated.

1.3 Targeting of ACPA-Specific Autoreactive B Cells in Rheumatoid Arthritis

One of the most frequently occurring autoimmune diseases is rheumatoid arthritis. Although the complete mechanism of this disease remains to be elucidated, autoantibodies are known to sustain inflammation. The B cells producing these antibodies are therefore a relevant target to treat RA.

Rheumatoid arthritis. Rheumatoid arthritis is an autoimmune disease affecting ~1% of the Western population, with women outnumbering men by three to one. This autoimmune disease involves inflammation, which eventually leads to the destruction of joints and cartilage. RA is hallmarked by the presence of anti-citrullinated protein antibodies (ACPA) and/or rheumatoid factor (antibodies targeting the Fc region of human IgG, RF) in 50-80% of the patients. Although the exact mechanism is not fully understood, it is known that genetic and environmental factors affect the risk for RA.

Antibodies to citrullinated proteins are sustaining the destructive inflammation. Protein citrullination is a posttranslational modification, in which an arginine is converted into a citrulline by a calcium-dependent enzyme called peptidylarginine deiminase (PAD).[188] Within the cell, PADs reside mostly in an inactive state as the minimal calcium concentration for PAD activity is 10^{-5} mol/L while the intracellular concentration is 10^{-7} mol/L. Upon cell death, the integrity of the plasma membrane is lost, allowing extracellular calcium (concentration 10^{-3} mol/L) to enter the cell and activate the PADs. Alternatively, PADs might leak out of the cell and become activated extracellularly. The conversion of arginine to citrulline results in the loss of a positive charge (Figure 11A), which might affect protein folding or protein-protein interactions. Activation of PADs and citrullination of proteins is a general process in inflammation; however, RA patients develop an immune response to these citrullinated proteins. B cells that produce ACPA are thought to be the key factor for the chronicity of the inflammation.[189] ACPA can be detected up to several years before the onset of the disease.[190] In addition, ACPA are correlated to the severity of the disease and are therefore an interesting marker to predict the development of the disease.[191]

ACPA recognize citrullinated vimentin on osteoclast precursor cells,[192] which stimulate TNF production and differentiate to bone-resorbing osteoclasts. Osteoclasts express high levels of PAD type 2, which in turn increases local citrullination, including vimentin on the precursor cells. This initial bone loss may initiate recruitment of B and T cells by the bone marrow adjacent to the joint. The synovitis leads to the production of proinflammatory cytokines which in turn stimulates osteoclastogenesis, aided by T-helper cells,[193] and subsequently enhances bone erosion (Figure 11B). Hence, established RA is marked by bone erosion combined with inflamed tissue.[194]

Since these ACPA-producing B cells are known to be pathogenic and ACPA are highly disease-specific biomarkers that are associated with joint destruction, B-cell depletion strategies like Rituximab (targeting CD20) are effective.[195] This treatment destroys B cells through the mechanism of ADCC. However, the lack of specificity causes serious side-effects due to the concomitant loss of protective memory cells. Therefore, new strategies in which only autoreactive B cells are targeted are of great interest.

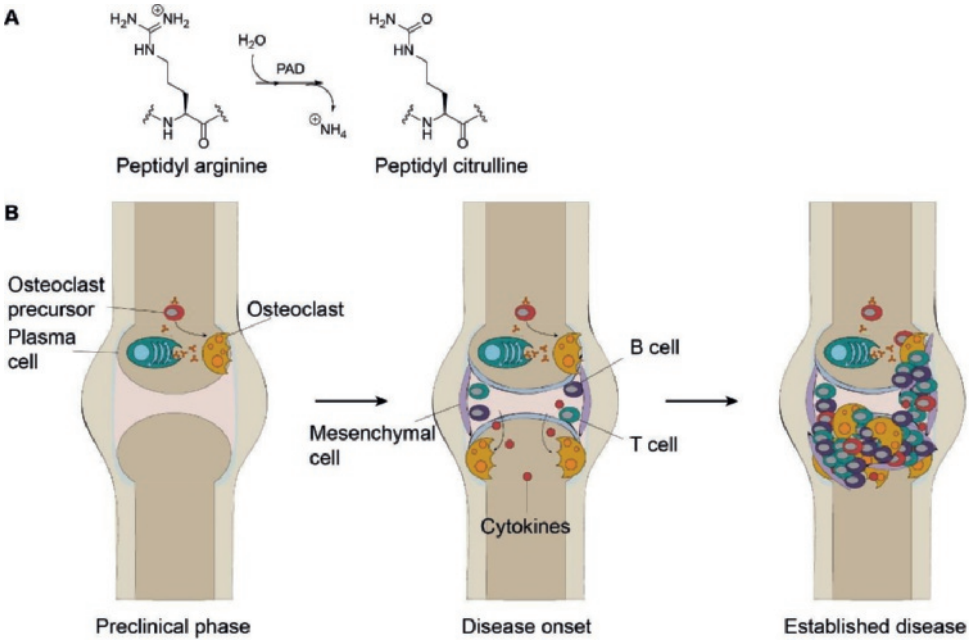

Figure 11. Development of RA. A) The guanidinium functional group from a peptidyl-arginine is converted into an ureido moiety by PADs, creating a peptidyl-citrulline; B) Schematic representation of the postulated different stages of disease onset. Bone resorbing osteoclasts differentiate from their precursor cells due to TNF production stimulated by surface ACPA binding on for example citrullinated vimentin. Immune cells are attracted and inflammation is initiated. Expanding cells establish a chronic inflammation and bone and cartilage degradation is sustained.

B cell receptor targeting. Autoreactive B cells from RA patients have been selectively detected and depleted *in vitro* by targeting the BCR.[6, 196] The majority of RA patients express ACPA that are disease-specific biomarkers and associated with disease pathogenesis.[197] In order to study ACPA-expressing B cells, Kerkman *et al.*[198] developed autoantigen tetramers as tool to isolate them from the peripheral blood of RA patients (Figure 12A). The tetramers were constructed by conjugation of biotinylated cyclic citrullinated peptide 2 (CCP2) to streptavidin, labeled with a fluorescent dye. These conjugates allowed the detection and selection of *ex vivo* ACPA-producing B cells.[198]

Pozsgay *et al.*[196] employed an analogous technique to selectively target and deplete citrullinated protein-specific B cells from ACPA-positive RA patients (Figure 12B). They synthesized PLGA nanoparticles displaying multiple copies of β60-74Cit peptide, the major epitope of citrullinated fibrinogen,[199, 200] as well as a complement-activating lytic peptide derived from gp120 of HIV-1.[201] By using these bifunctional nanoparticles, the authors showed that they could significantly reduce

the β60-74Cit specific ACPA production. They were able to specifically deplete citrullinated protein-specific B cells in *ex vivo* cultures of patient's blood. Lysis of β60-74Cit epitope-specific autoreactive B cells was selectively induced via complement-dependent cytotoxicity, achieved by the formation of the complement membrane attack complex, C5b-9. Both ACPA and ACPA-producing B cells were effectively reduced.[196]

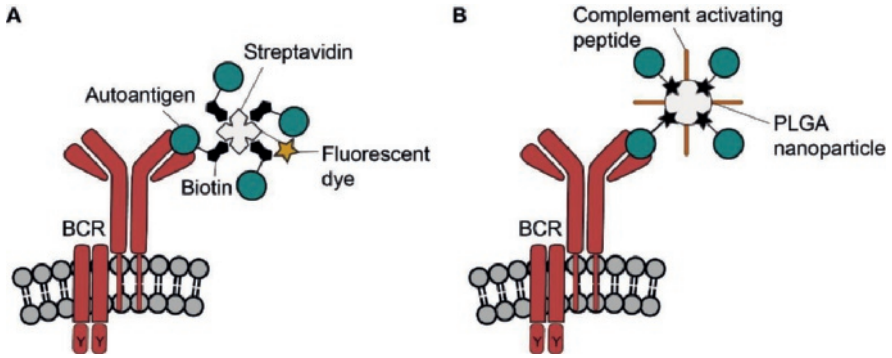

Figure 12. Detection, isolation and depletion of autoreactive B cells by targeting of the BCR. A) Biotinylated citrullinated peptides (blue circles) are conjugated to fluorescently labeled streptavidin. Antigen-selective targeting of B cells via the BCR enables detection and isolation of B cells of interest; B) Multiple citrullinated peptides as well as complement-activating peptides are conjugated to a PLGA nanoparticle. Antigen-selective targeting of autoreactive B cells using this peptide combination induced the formation of the complement membrane attack complex and hence depletion of these B cells.

In conclusion, this strategy is an elegant approach to target and deplete autoreactive B cells in an antigen-selective manner.[196] Protective B cells would remain untouched, while the B cells involved in autoimmune disease pathogenesis can be depleted. On a critical note, the BCR is well-known to internalize when bound to an antigen.[202] An interesting question is whether the BCR is internalized when bound by the PLGA nanoparticles, and whether the nanoparticles are internalized when bound to the receptor. If this happens, it would probably affect the efficacy of the treatment strategy. The possibility of BCR internalization is not discussed by the authors.[196] However, this internalization also gives new possibilities, such as antigen-selective internalization of cytotoxic molecules. Moreover, since the β60-74Cit peptide is not the only epitope targeted by ACPA in RA patients, clinical translation of this treatment method should involve simultaneous administration of a number of different lytic nanoparticles, displaying various autoantigenic epitopes.[196] Although this approach has only been applied in *in vitro* studies so far, it holds potential in the development of antigen-selective B cell-targeted therapies by targeting the BCR on autoreactive B cells.

1.4 Conclusions and Outlook

Current B cell-directed therapies mainly induce immune suppression by either inhibiting or eliminating the complete B cell compartment, leaving patients at increased risk of infection.[2] Ideally, therapeutics would only target autoreactive B cells involved in disease pathogenesis, while leaving healthy B cells intact. Although antigen-selective immunotherapies targeting the B cell

compartment have only emerged during recent years, many promising approaches have been developed. The display of autoantigen peptides is important for B cell specificity and efficacy of targeted therapies. Therefore, the identification of autoantigens and respective epitopes involved in disease pathology remains an important issue.[2] For RA, much research has been performed on the autoantigens already.[203] To improve targeting strategies described here, reduction of autoantigen clearance by free circulating autoantibodies could be beneficial. Not much is known about the possible interference of autoantibodies with the strategies reviewed in this Chapter. However, the ACPA serum titer of RA patients can be as high as 10-200 μg/mL.[204] To improve B cell binding in these strategies, we suggest that circumventing autoantibody-mediated clearance of the autoantigen could be beneficial. Also, the possibilities to target B cells via their BCR are limited and hence this is the focus of this thesis; strategies to target and eliminate autoreactive B cells while circumventing the clearance by circulating autoantibodies.

1.5 Outline of this Thesis

The goal of the work described in this thesis is to improve antigen-selective B cell targeting and thereby creating specificity of autoreactive B cells over autoantibodies. We envision that by caging of an autoantigen-conjugate binding to both autoreactive B cells and autoantibodies can be circumvented. We envision that selective activation in close proximity of a B cell, by using B cell-specific markers, can result in optimal binding of the antigen conjugate with the autoreactive B cell instead of the autoantibody.

In the studies described in **Chapter 2** we explore the possibility to cage a cyclic citrullinated peptide (CCP) with a carboxynitrobenzyl group and the subsequent removal using the enzyme nitroreductase. In **Chapter 3** we describe a chemical approach to selectively activate the autoantigen, by using an iminosydnone click-to-release reaction. In **Chapter 4** we describe the development of a new click-to-release reaction, using phenylvinyl boronic acids (VBA), and we utilized this reaction to cage a lymphocyte-specific toxin. In the studies described in **Chapter 5** we explore the use poly(isocyanopeptides) (PICs) as alternative multivalent scaffold for the frequently used streptavidin. In **Chapter 6** we describe the discovery of a new synthetic antigen peptide, which can bind to anti-carbamylated antibodies (anti-CarP).

1.6 References

1. Yanaba, K.; Bouaziz, J. D.; Matsushita, T.; Magro, C. M.; St. Clair, E. W.; Tedder, T. F. B-lymphocyte contributions to human autoimmune disease. *Immunol. Rev.* **2008,** *223*, (1), 284-299.
2. Shlomchik, M. J.; Madaio, M. P.; Ni, D.; Trounstein, M.; Huszar, D. The role of B cells in lpr/lpr-induced autoimmunity. *J. Exp. Med.* **1994,** *180*, (4), 1295-1306.
3. Kondo, M. Lymphoid and myeloid lineage commitment in multipotent hematopoietic progenitors. *Immunol. Rev.* **2010,** *238*, (1), 37-46.
4. Mårtensson, I.-L.; Almqvist, N.; Grimsholm, O.; Bernardi, A. I. The pre-B cell receptor checkpoint. *FEBS Lett.* **2010,** *584*, (12), 2572-2579.
5. Goodnow, C. C.; Sprent, J.; de St Groth, B. F.; Vinuesa, C. G. Cellular and genetic mechanisms of self tolerance and autoimmunity. *Nature* **2005,** *435*, (7042), 590.
6. Pozsgay, J.; Szekanecz, Z.; Sármay, G. Antigen-selective immunotherapies in rheumatic diseases. *Nat. Rev. Rheumatol.* **2017,** *13*, (9), 525-537.
7. Rosenblum, M. D.; Remedios, K. A.; Abbas, A. K. Mechanisms of human autoimmunity. *J. Clin. Invest.* **2015,** *125*, (6), 2228-2233.
8. Browning, J. L. B cells move to centre stage: novel opportunities for autoimmune disease treatment. *Nat. Rev. Drug Discov.* **2006,** *5*, (7), 564-576.
9. Edwards, J. C.; Cambridge, G. B-cell targeting in rheumatoid arthritis and other autoimmune diseases. *Nat. Rev. Immunol.* **2006,** *6*, (5), 394-403.
10. Dörner, T.; Radbruch, A.; Burmester, G. R. B-cell-directed therapies for autoimmune disease. *Nat. Rev. Rheumatol.* **2009,** *5*, (8), 433-441.
11. Klein, U.; Dalla-Favera, R. Germinal centres: role in B-cell physiology and malignancy. *Nat. Rev. Immunol.* **2008,** *8*, (1), 22-33.
12. Hoffman, W.; Lakkis, F. G.; Chalasani, G. B cells, antibodies, and more. *Clin. J. Am. Soc. Nephrol.* **2016,** *11*, (1), 137-154.
13. Hiepe, F.; Dörner, T.; Hauser, A. E.; Hoyer, B. F.; Mei, H.; Radbruch, A. Long-lived autoreactive plasma cells drive persistent autoimmune inflammation. *Nat. Rev. Rheumatol.* **2011,** *7*, 170-178.
14. Townsend, M. J.; Monroe, J. G.; Chan, A. C. B-cell targeted therapies in human autoimmune diseases: an updated perspective. *Immunol. Rev.* **2010,** *237*, (1), 264-283.
15. Pistoia, V. Production of cytokines by human B cells in health and disease. *Immunol. today* **1997,** *18*, (7), 343-350.
16. Parham, P., *The immune system*. 3 ed.; Garland Science: 2009.
17. Davidson, A.; Manheimer-Lory, A.; Aranow, C.; Shefner, R. Possible mechanisms of autoantibody production. *Biomed. Pharmacother.* **1989,** *43*, (8), 563-570.
18. Capron, M.; Kazatchkine, M. D.; Fischer, E.; Joseph, M.; Butterworth, A. E.; Kusnierz, J. P.; Prin, L.; Papin, J. P.; Capron, A. Functional role of the alpha-chain of complement receptor type 3 in human eosinophil-dependent antibody-mediated cytotoxicity against schistosomes. *J. Immunol.* **1987,** *139*, (6), 2059-2065.
19. Wang, W.; Erbe, A. K.; Hank, J. A.; Morris, Z. S.; Sondel, P. M. NK Cell-Mediated Antibody-Dependent Cellular Cytotoxicity in Cancer Immunotherapy. *Front. Immunol.* **2015,** *6*, 368-368.
20. Suurmond, J.; Diamond, B. Autoantibodies in systemic autoimmune diseases: specificity and pathogenicity. *J. Clin. Invest.* **2015,** *125*, (6), 2194-2202.
21. Ding, C. Belimumab, an anti-BLyS human monoclonal antibody for potential treatment of inflammatory autoimmune diseases. *Expert Opin. Biol. Ther.* **2008,** *8*, (11), 1805-1814.
22. Neubert, K.; Meister, S.; Moser, K.; Weisel, F.; Maseda, D.; Amann, K.; Wiethe, C.; Winkler, T. H.; Kalden, J. R.; Manz, R. A. The proteasome inhibitor bortezomib depletes plasma cells and protects mice with lupus-like disease from nephritis. *Nat. Med.* **2008,** *14*, (7), 748-755.
23. Genovese, M. C.; Becker, J.-C.; Schiff, M.; Luggen, M.; Sherrer, Y.; Kremer, J.; Birbara, C.; Box, J.; Natarajan, K.; Nuamah, I. Abatacept for rheumatoid arthritis refractory to tumor necrosis factor α inhibition. *N. Engl. J. Med.* **2005,** *353*, (11), 1114-1123.
24. Kaplan, B.; Kopyltsova, Y.; Khokhar, A.; Lam, F.; Bonagura, V. Rituximab and immune deficiency: case series and review of the literature. *J. Allergy Clin. Immunol. Pract.* **2014,** *2*, (5), 594-600.
25. Crocker, P. R.; Paulson, J. C.; Varki, A. Siglecs and their roles in the immune system. *Nat. Rev. Immunol.* **2007,** *7*, (4), 255-266.

26. Nitschke, L. CD22 and Siglec-G: B-cell inhibitory receptors with distinct functions. *Immunol. Rev.* **2009,** *230*, (1), 128-143.
27. Varki, A.; Angata, T. Siglecs—the major subfamily of I-type lectins. *Glycobiology* **2005,** *16*, (1), 1R-27R.
28. Crocker, P. R. Siglecs: sialic-acid-binding immunoglobulin-like lectins in cell–cell interactions and signalling. *Curr. Opin. Struct. Biol.* **2002,** *12*, (5), 609-615.
29. Kelm, S.; Pelz, A.; Schauer, R.; Filbin, M. T.; Tang, S.; de Bellard, M.-E.; Schnaar, R. L.; Mahoney, J. A.; Hartnell, A.; Bradfield, P. Sialoadhesin, myelin-associated glycoprotein and CD22 define a new family of sialic acid-dependent adhesion molecules of the immunoglobulin superfamily. *Curr. Biol.* **1994,** *4*, (11), 965-972.
30. Angata, T.; Brinkman-Van der Linden, E. C. M. I-type lectins. *Biochim. Biophys. Acta Gen. Subj.* **2002,** *1572*, (2-3), 294-316.
31. Powell, L. D.; Varki, A. I-type lectins. *Biol. Chem.* **1995,** *270*, (24), 14243-14246.
32. Munday, J.; Sheena, K.; Jian, N.; Cornish, A. L.; Zhang, J. Q.; Nicoll, G.; Floyd, H.; Mattei, M.-G.; Moore, P.; Ding, L. Identification, characterization and leucocyte expression of Siglec-10, a novel human sialic acid-binding receptor. *Biochem. J.* **2001,** *355*, (2), 489-497.
33. Whitney, G.; Wang, S.; Chang, H.; Cheng, K. Y.; Lu, P.; Zhou, X. D.; Yang, W. P.; McKinnon, M.; Longphre, M. A new siglec family member, siglec-10, is expressed in cells of the immune system and has signaling properties similar to CD33. *Eur. J. Biochem.* **2001,** *268*, (23), 6083-6096.
34. Nitschke, L.; Carsetti, R.; Ocker, B.; Köhler, G.; Lamers, M. C. CD22 is a negative regulator of B-cell receptor signalling. *Curr. Biol.* **1997,** *7*, (2), 133-143.
35. Hoffmann, A.; Kerr, S.; Jellusova, J.; Zhang, J.; Weisel, F.; Wellmann, U.; Winkler, T. H.; Kneitz, B.; Crocker, P. R.; Nitschke, L. Siglec-G is a B1 cell–inhibitory receptor that controls expansion and calcium signaling of the B1 cell population. *Nat. Immunol.* **2007,** *8*, (7), 695-704.
36. Otipoby, K. L.; Draves, K. E.; Clark, E. A. CD22 regulates B cell receptor-mediated signals via two domains that independently recruit Grb2 and SHP-1. *J. Biol. Chem.* **2001,** *276*, (47), 44315-44322.
37. Doody, G. M.; Justement, L. B.; Delibrias, C. C.; Matthews, R. J.; Lin, J.; Thomas, M. L.; Fearon, D. T. A role in B cell activation for CD22 and the protein tyrosine phosphatase SHP. *Science* **1995,** *269*, (5221), 242-244.
38. Blasioli, J.; Paust, S.; Thomas, M. L. Definition of the sites of interaction between the protein tyrosine phosphatase SHP-1 and CD22. *J. Biol. Chem.* **1999,** *274*, (4), 2303-2307.
39. Chen, J.; McLean, P. A.; Neel, B. G.; Okunade, G.; Shull, G. E.; Wortis, H. H. CD22 attenuates calcium signaling by potentiating plasma membrane calcium-ATPase activity. *Nat. Immunol.* **2004,** *5*, (6), 651-657.
40. Gerlach, J.; Ghosh, S.; Jumaa, H.; Reth, M.; Wienands, J.; Chan, A. C.; Nitschke, L. B cell defects in SLP65/BLNK-deficient mice can be partially corrected by the absence of CD22, an inhibitory coreceptor for BCR signaling. *Eur. J. Immunol.* **2003,** *33*, (12), 3418-3426.
41. Fujimoto, M.; Bradney, A. P.; Poe, J. C.; Steeber, D. A.; Tedder, T. F. Modulation of B lymphocyte antigen receptor signal transduction by a CD19/CD22 regulatory loop. *Immunity* **1999,** *11*, (2), 191-200.
42. Lajaunias, F.; Nitschke, L.; Moll, T.; Martinez-Soria, E.; Semac, I.; Chicheportiche, Y.; Parkhouse, R. M. E.; Izui, S. Differentially regulated expression and function of CD22 in activated B-1 and B-2 lymphocytes. *J. Immunol.* **2002,** *168*, (12), 6078-6083.
43. Han, S.; Collins, B. E.; Bengtson, P.; Paulson, J. C. Homomultimeric complexes of CD22 in B cells revealed by protein-glycan cross-linking. *Nat. Chem. Biol.* **2005,** *1*, (2), 93-97.
44. Razi, N.; Varki, A. Masking and unmasking of the sialic acid-binding lectin activity of CD22 (Siglec-2) on B lymphocytes. *Proc. Natl. Acad. Sci.* **1998,** *95*, (13), 7469-7474.
45. Müller, J.; Obermeier, I.; Wöhner, M.; Brandl, C.; Mrotzek, S.; Angermüller, S.; Maity, P. C.; Reth, M.; Nitschke, L. CD22 ligand-binding and signaling domains reciprocally regulate B-cell Ca2+ signaling. *Proc. Natl. Acad. Sci.* **2013,** *110*, (30), 12402-12407.
46. Zhang, M.; Varki, A. Cell surface sialic acids do not affect primary CD22 interactions with CD45 and surface IgM nor the rate of constitutive CD22 endocytosis. *Glycobiology* **2004,** *14*, (11), 939-949.
47. Collins, B. E.; Smith, B. A.; Bengtson, P.; Paulson, J. C. Ablation of CD22 in ligand-deficient mice restores B cell receptor signaling. *Nat. Immunol.* **2006,** *7*, (2), 199-206.

48. Grewal, P. K.; Boton, M.; Ramirez, K.; Collins, B. E.; Saito, A.; Green, R. S.; Ohtsubo, K.; Chui, D.; Marth, J. D. ST6Gal-I restrains CD22-dependent antigen receptor endocytosis and Shp-1 recruitment in normal and pathogenic immune signaling. *Mol. Cell Biol.* **2006,** *26*, (13), 4970-4981.
49. Collins, B. E.; Blixt, O.; DeSieno, A. R.; Bovin, N.; Marth, J. D.; Paulson, J. C. Masking of CD22 by cis ligands does not prevent redistribution of CD22 to sites of cell contact. *Proc. Natl. Acad. Sci.* **2004,** *101*, (16), 6104-6109.
50. Lanoue, A.; Batista, F. D.; Stewart, M.; Neuberger, M. S. Interaction of CD22 with α2, 6-linked sialoglycoconjugates: innate recognition of self to dampen B cell autoreactivity? *Eur. J. Immunol* **2002,** *32*, (2), 348-355.
51. Müller, J.; Nitschke, L. The role of CD22 and Siglec-G in B-cell tolerance and autoimmune disease. *Nat. Rev. Rheumatol.* **2014,** *10*, (7), 422-428.
52. Nitschke, L. CD22 and Siglec-G regulate inhibition of B-cell signaling by sialic acid ligand binding and control B-cell tolerance. *Glycobiology* **2014,** *24*, (9), 807-817.
53. Hutzler, S.; Özgör, L.; Naito-Matsui, Y.; Kläsener, K.; Winkler, T. H.; Reth, M.; Nitschke, L. The ligand-binding domain of Siglec-G is crucial for its selective inhibitory function on B1 cells. *J. Immunol.* **2014**, 1-10.
54. Paulson, J. C.; Macauley, M. S.; Kawasaki, N. Siglecs as sensors of self in innate and adaptive immune responses. *Ann. N. Y. Acad. Sci.* **2012,** *1253*, (1), 37-48.
55. Otipoby, K. L.; Andersson, K. B.; Draves, K. E.; Klaus, S. J.; Farr, A. G.; Kerner, J. D.; Perlmutter, R. M.; Law, C.-L.; Clark, E. A. CD22 regulates thymus-independent responses and the lifespan of B cells. *Nature* **1996,** *384*, (6610), 634-637.
56. Sato, S.; Miller, A. S.; Inaoki, M.; Bock, C. B.; Jansen, P. J.; Tang, M. L.; Tedder, T. F. CD22 is both a positive and negative regulator of B lymphocyte antigen receptor signal transduction: altered signaling in CD22-deficient mice. *Immunity* **1996,** *5*, (6), 551-562.
57. Jellusova, J.; Wellmann, U.; Amann, K.; Winkler, T. H.; Nitschke, L. CD22× Siglec-G double-deficient mice have massively increased B1 cell numbers and develop systemic autoimmunity. *J. Immunol.* **2010**, 1-10.
58. Kelm, S.; Gerlach, J.; Brossmer, R.; Danzer, C.-P.; Nitschke, L. The ligand-binding domain of CD22 is needed for inhibition of the B cell receptor signal, as demonstrated by a novel human CD22-specific inhibitor compound. *J. Exp. Med.* **2002,** *195*, (9), 1207-1213.
59. Courtney, A. H.; Puffer, E. B.; Pontrello, J. K.; Yang, Z.-Q.; Kiessling, L. L. Sialylated multivalent antigens engage CD22 in trans and inhibit B cell activation. *Proc. Natl. Acad. Sci.* **2009,** *106*, 2500-2505.
60. Duong, B. H.; Tian, H.; Ota, T.; Completo, G.; Han, S.; Vela, J. L.; Ota, M.; Kubitz, M.; Bovin, N.; Paulson, J. C. Decoration of T-independent antigen with ligands for CD22 and Siglec-G can suppress immunity and induce B cell tolerance in vivo. *J. Exp. Med.* **2010,** *207*, (1), 173-187.
61. Puffer, E. B.; Pontrello, J. K.; Hollenbeck, J. J.; Kink, J. A.; Kiessling, L. L. Activating B cell signaling with defined multivalent ligands. *ACS Chem. Biol.* **2007,** *2*, (4), 252-262.
62. Macauley, M. S.; Pfrengle, F.; Rademacher, C.; Nycholat, C. M.; Gale, A. J.; von Drygalski, A.; Paulson, J. C. Antigenic liposomes displaying CD22 ligands induce antigen-selective B cell apoptosis. *J. Clin. Invest.* **2013,** *123*, (7), 3074-3083.
63. Shek, P. N. v.; Heath, T. D. Immune response mediated by liposome-associated protein antigens. III. Immunogenicity of bovine serum albumin covalently coupled to vesicle surface. *Immunology* **1983,** *50*, (1), 101-106.
64. Loughrey, H. C.; Choi, L. S.; Cullis, P. R.; Bally, M. B. Optimized procedures for the coupling of proteins to liposomes. *J. Immunol. Methods* **1990,** *132*, (1), 25-35.
65. Chen, W. C.; Completo, G. C.; Sigal, D. S.; Crocker, P. R.; Saven, A.; Paulson, J. C. In vivo targeting of B-cell lymphoma with glycan ligands of CD22. *Blood* **2010**, 1-26.
66. Macauley, M. S.; Paulson, J. C. Siglecs induce tolerance to cell surface antigens by BIM-dependent deletion of the antigen-reactive B cells. *J. Immunol.* **2014**, 1-10.
67. Pfrengle, F.; Macauley, M. S.; Kawasaki, N.; Paulson, J. C. Copresentation of antigen and ligands of Siglec-G induces B cell tolerance independent of CD22. *J. Immunol.* **2013**, 1300921.
68. Maldonado, R. A.; LaMothe, R. A.; Ferrari, J. D.; Zhang, A.-H.; Rossi, R. J.; Kolte, P. N.; Griset, A. P.; O'Neil, C.; Altreuter, D. H.; Browning, E. Polymeric synthetic nanoparticles for the induction of antigen-selective immunological tolerance. *Proc. Natl. Acad. Sci.* **2015,** *112*, (2), E156-E165.

69. Kishimoto, T. K.; Ferrari, J. D.; LaMothe, R. A.; Kolte, P. N.; Griset, A. P.; O'Neil, C.; Chan, V.; Browning, E.; Chalishazar, A.; Kuhlman, W. Improving the efficacy and safety of biologic drugs with tolerogenic nanoparticles. *Nat. Nanotechnol.* **2016,** *11*, (10), 890-899.
70. Pang, L.; Macauley, M. S.; Arlian, B. M.; Nycholat, C. M.; Paulson, J. C. Encapsulating an Immunosuppressant Enhances Tolerance Induction by Siglec-Engaging Tolerogenic Liposomes. *Chembiochem* **2017,** *18*, (13), 1226-1233.
71. Mukherjee, S.; Mukherjee, U. A comprehensive review of immunosuppression used for liver transplantation. *J. Transplant.* **2009,** *2009*, 1-20.
72. Bednar, K. J.; Shanina, E.; Ballet, R.; Connors, E. P.; Duan, S.; Juan, J.; Arlian, B. M.; Kulis, M. D.; Butcher, E. C.; Fung-Leung, W.-P. Human CD22 inhibits murine B cell receptor activation in a human CD22 transgenic mouse model. *J. Immunol.* **2017**, 1-13.
73. Parker, D. C. T cell-dependent B cell activation. *Annu. Rev. Immunol.* **1993,** *11*, (1), 331-360.
74. Yusuf-Makagiansar, H.; Anderson, M. E.; Yakovleva, T. V.; Murray, J. S.; Siahaan, T. J. Inhibition of LFA-1/ICAM-1 and VLA-4/VCAM-1 as a therapeutic approach to inflammation and autoimmune diseases. *Med. Res. Rev.* **2002,** *22*, (2), 146-167.
75. Long, E. O. ICAM-1: getting a grip on leukocyte adhesion. *J. immunol.* **2011,** *186*, (9), 5021-5023.
76. Bromley, S. K.; Burack, W. R.; Johnson, K. G.; Somersalo, K.; Sims, T. N.; Sumen, C.; Davis, M. M.; Shaw, A. S.; Allen, P. M.; Dustin, M. L. The immunological synapse. *Annu. Rev. Immunol.* **2001,** *19*, (1), 375-396.
77. Grakoui, A.; Bromley, S. K.; Sumen, C.; Davis, M. M.; Shaw, A. S.; Allen, P. M.; Dustin, M. L. The immunological synapse: a molecular machine controlling T cell activation. *Science* **1999,** *285*, (5425), 221-227.
78. Monks, C. R. F.; Freiberg, B. A.; Kupfer, H.; Sciaky, N.; Kupfer, A. Three-dimensional segregation of supramolecular activation clusters in T cells. *Nature* **1998,** *395*, (6697), 82-86.
79. Wülfing, C.; Davis, M. M. A receptor/cytoskeletal movement triggered by costimulation during T cell activation. *Science* **1998,** *282*, (5397), 2266-2269.
80. Furuzawa-Carballeda, J.; Alcocer-Varela, J. Interleukin-8, interleukin-10, intercellular adhesion molecule-1 and vascular cell adhesion molecule-1 expression levels are higher in synovial tissue from patients with rheumatoid arthritis than in osteoarthritis. *Scand. J. Immunol.* **1999,** *50*, (2), 215-222.
81. Kobayashi, N.; Kobayashi, H.; Gu, L.; Malefyt, T.; Siahaan, T. J. Antigen-selective suppression of experimental autoimmune encephalomyelitis by a novel bifunctional peptide inhibitor. *J. Pharmacol. Exp. Ther.* **2007,** *322*, (2), 879-886.
82. Tuohy, V. K.; Lu, Z.; Sobel, R. A.; Laursen, R. A.; Lees, M. B. Identification of an encephalitogenic determinant of myelin proteolipid protein for SJL mice. *J. Immunol.* **1989,** *142*, (5), 1523-1527.
83. Yusuf-Makagiansar, H.; Makagiansar, I. T.; Hu, Y.; Siahaan, T. J. Synergistic inhibitory activity of α- and β-LFA-1 peptides on LFA-1/ICAM-1 interaction. *Peptides* **2001,** *22*, (12), 1955-1962.
84. Yusuf-Makagiansar, H.; Makagiansar, I. T.; Siahaan, T. J. Inhibition of the adherence of T-lymphocytes to epithelial cells by a cyclic peptide derived from inserted domain of lymphocyte function-associated antigen-1. *Inflammation* **2001,** *25*, (3), 203-214.
85. Yusuf-Makagiansar, H.; Siahaan, T. J. Binding and internalization of an LFA-1-derived cyclic peptide by ICAM receptors on activated lymphocyte: a potential ligand for drug targeting to ICAM-1-expressing cells. *Pharm. Res.* **2001,** *18*, (3), 329-335.
86. Huang, M.; Matthews, K.; Siahaan, T. J.; Kevil, C. G. αL-Integrin I domain cyclic peptide antagonist selectively inhibits T cell adhesion to pancreatic islet microvascular endothelium. *Am. J. Physiol. Gastrointest. Liver Physiol.* **2005,** *288*, (1), G67-G73.
87. Santambrogio, L.; Sato, A. K.; Fischer, F. R.; Dorf, M. E.; Stern, L. J. Abundant empty class II MHC molecules on the surface of immature dendritic cells. *Proc. Natl. Acad. Sci.* **1999,** *96*, (26), 15050-15055.
88. Vacchino, J. F.; McConnell, H. M. Peptide binding to active class II MHC protein on the cell surface. *J. Immunol.* **2001,** *166*, (11), 6680-6685.
89. Mackay, I. R.; Rowley, M. J. Autoimmune epitopes: autoepitopes. *Autoimmun. Rev.* **2004,** *3*, (7-8), 487-492.
90. Reijonen, H.; Mallone, R.; Heninger, A.-K.; Laughlin, E. M.; Kochik, S. A.; Falk, B.; Kwok, W. W.; Greenbaum, C.; Nepom, G. T. GAD65-specific CD4+ T-cells with high antigen avidity are prevalent in peripheral blood of patients with type 1 diabetes. *Diabetes* **2004,** *53*, (8), 1987-1994.

91. Murray, J. S.; Oney, S.; Page, J. E.; Kratochvil-Stava, A.; Hu, Y.; Makagiansar, I. T.; Brown, J. C.; Kobayashi, N.; Siahaan, T. J. Suppression of type 1 diabetes in NOD mice by bifunctional peptide inhibitor: modulation of the immunological synapse formation. *Chem. Biol. Drug Des.* **2007,** *70*, (3), 227-236.
92. Kobayashi, N.; Kiptoo, P.; Kobayashi, H.; Ridwan, R.; Brocke, S.; Siahaan, T. J. Prophylactic and therapeutic suppression of experimental autoimmune encephalomyelitis by a novel bifunctional peptide inhibitor. *Clin. Immunol.* **2008,** *129*, (1), 69-79.
93. Badawi, A. H.; Kiptoo, P.; Wang, W.-T.; Choi, I.-Y.; Lee, P.; Vines, C. M.; Siahaan, T. J. Suppression of EAE and prevention of blood–brain barrier breakdown after vaccination with novel bifunctional peptide inhibitor. *Neuropharmacology* **2012,** *62*, (4), 1874-1881.
94. Büyüktimkin, B.; Wang, Q.; Kiptoo, P.; Stewart, J. M.; Berkland, C.; Siahaan, T. J. Vaccine-like controlled-release delivery of an immunomodulating peptide to treat experimental autoimmune encephalomyelitis. *Mol. Pharm.* **2012,** *9*, (4), 979-985.
95. White, D. R.; Khedri, Z.; Kiptoo, P.; Siahaan, T. J.; Tolbert, T. J. Synthesis of a Bifunctional Peptide Inhibitor–IgG1 Fc Fusion That Suppresses Experimental Autoimmune Encephalomyelitis. *Bioconjug. Chem.* **2017,** *28*, (7), 1867-1877.
96. Badawi, A. H.; Siahaan, T. J. Suppression of MOG-and PLP-induced experimental autoimmune encephalomyelitis using a novel multivalent bifunctional peptide inhibitor. *J. Neuroimmunol.* **2013,** *263*, (1-2), 20-27.
97. Stewart, J.; Badawi, A. H.; Kiptoo, P.; Siahaan, T. J. A vaccine-like administration of PLP-PEG-B7AP and MOG-PEG-B7AP to control EAE in relapse-remission and chronic progressive animal models of multiple sclerosis: Bifunctional peptide inhibitors as peptide-based therapeutic vaccines. *Chim. Oggi Chem. Today Oligos Pept.* **2015,** *33*, (2), 41-48.
98. Vanderlugt, C. J.; Miller, S. D. Epitope spreading. *Curr. Opin. Immunol.* **1996,** *8*, (6), 831-836.
99. Koulova, L.; Clark, E. A.; Shu, G.; Dupont, B. The CD28 ligand B7/BB1 provides costimulatory signal for alloactivation of CD4+ T cells. *J. Exp. Med.* **1991,** *173*, (3), 759-762.
100. Dubey, C.; Croft, M.; Swain, S. L. Costimulatory requirements of naive CD4+ T cells. ICAM-1 or B7-1 can costimulate naive CD4 T cell activation but both are required for optimum response. *J. Immunol.* **1995,** *155*, (1), 45-57.
101. Ridwan, R.; Kiptoo, P.; Kobayashi, N.; Weir, S.; Hughes, M.; Williams, T.; Soegianto, R.; Siahaan, T. J. Antigen-selective suppression of experimental autoimmune encephalomyelitis by a novel bifunctional peptide inhibitor: structure optimization and pharmacokinetics. *J. Pharmacol. Exp. Ther.* **2010,** *332*, (3), 1136-1145.
102. Manikwar, P.; Büyüktimkin, B.; Kiptoo, P.; Badawi, A. H.; Galeva, N. A.; Williams, T. D.; Siahaan, T. J. I-domain-antigen conjugate (IDAC) for delivering antigenic peptides to APC: synthesis, characterization, and in vivo EAE suppression. *Bioconjug. Chem.* **2012,** *23*, (3), 509-517.
103. Büyüktimkin, B.; Manikwar, P.; Kiptoo, P. K.; Badawi, A. H.; Stewart Jr, J. M.; Siahaan, T. J. Vaccinelike and prophylactic treatments of EAE with novel I-domain antigen conjugates (IDAC): targeting multiple antigenic peptides to APC. *Mol. Pharm.* **2013,** *10*, (1), 297-306.
104. Shimaoka, M.; Xiao, T.; Liu, J.-H.; Yang, Y.; Dong, Y.; Jun, C.-D.; McCormack, A.; Zhang, R.; Joachimiak, A.; Takagi, J. Structures of the αL I domain and its complex with ICAM-1 reveal a shape-shifting pathway for integrin regulation. *Cell* **2003,** *112*, (1), 99-111.
105. Sestak, J.; Mullins, M.; Northrup, L.; Thati, S.; Forrest, M. L.; Siahaan, T. J.; Berkland, C. Single-step grafting of aminooxy-peptides to hyaluronan: a simple approach to multifunctional therapeutics for experimental autoimmune encephalomyelitis. *J. Control. Release* **2013,** *168*, (3), 334-340.
106. Fraser, J. R. E.; Laurent, T. C.; Laurent, U. B. G. Hyaluronan: its nature, distribution, functions and turnover. *J. Intern. Med.* **1997,** *242*, (1), 27-33.
107. Necas, J.; Bartosikova, L.; Brauner, P.; Kolar, J. Hyaluronic acid (hyaluronan): a review. *Vet. Med.* **2008,** *53*, (8), 397-411.
108. Bagby, T. R.; Cai, S.; Duan, S.; Thati, S.; Aires, D. J.; Forrest, L. Impact of molecular weight on lymphatic drainage of a biopolymer-based imaging agent. *Pharmaceutics* **2012,** *4*, (2), 276-295.
109. Ossipov, D. A.; Piskounova, S.; Varghese, O. P.; Hilborn, J. n. Functionalization of hyaluronic acid with chemoselective groups via a disulfide-based protection strategy for in situ formation of mechanically stable hydrogels. *Biomacromolecules* **2010,** *11*, (9), 2247-2254.
110. Novoa-Carballal, R.; Müller, A. H. E. Synthesis of polysaccharide-b-PEG block copolymers by oxime click. *ChemComm* **2012,** *48*, (31), 3781-3783.

111. Gajewiak, J.; Cai, S.; Shu, X. Z.; Prestwich, G. D. Aminooxy pluronics: synthesis and preparation of glycosaminoglycan adducts. *Biomacromolecules* **2006,** *7*, (6), 1781-1789.
112. Sestak, J. O.; Sullivan, B. P.; Thati, S.; Northrup, L.; Hartwell, B.; Antunez, L.; Forrest, M. L.; Vines, C. M.; Siahaan, T. J.; Berkland, C. Codelivery of antigen and an immune cell adhesion inhibitor is necessary for efficacy of soluble antigen arrays in experimental autoimmune encephalomyelitis. *Mol. Ther. Methods Clin. Dev.* **2014,** *1*, 14008-14016.
113. Northrup, L.; Sestak, J. O.; Sullivan, B. P.; Thati, S.; Hartwell, B. L.; Siahaan, T. J.; Vines, C. M.; Berkland, C. Co-delivery of autoantigen and b7 pathway modulators suppresses experimental autoimmune encephalomyelitis. *AAPS J.* **2014,** *16*, (6), 1204-1213.
114. Yamamoto, T.; Hattori, M.; Yoshida, T. Induction of T-cell activation or anergy determined by the combination of intensity and duration of T-cell receptor stimulation, and sequential induction in an individual cell. *Immunology* **2007,** *121*, (3), 383-391.
115. Sestak, J. O.; Fakhari, A.; Badawi, A. H.; Siahaan, T. J.; Berkland, C. Structure, size, and solubility of antigen arrays determines efficacy in experimental autoimmune encephalomyelitis. *AAPS J.* **2014,** *16*, (6), 1185-1193.
116. Hartwell, B. L.; Pickens, C. J.; Leon, M.; Berkland, C. Multivalent Soluble Antigen Arrays Exhibit High Avidity Binding and Modulation of B Cell Receptor-Mediated Signaling to Drive Efficacy against Experimental Autoimmune Encephalomyelitis. *Biomacromolecules* **2017,** *18*, (6), 1893-1907.
117. Hartwell, B. L.; Smalter Hall, A.; Swafford, D.; Sullivan, B. P.; Garza, A.; Sestak, J. O.; Northrup, L.; Berkland, C. Molecular Dynamics of Multivalent Soluble Antigen Arrays Support a Two-Signal Co-delivery Mechanism in the Treatment of Experimental Autoimmune Encephalomyelitis. *Mol. Pharm.* **2016,** *13*, (2), 330-343.
118. Thati, S.; Kuehl, C.; Hartwell, B.; Sestak, J.; Siahaan, T.; Forrest, M. L.; Berkland, C. Routes of administration and dose optimization of soluble antigen arrays in mice with experimental autoimmune encephalomyelitis. *J. Pharm. Sci.* **2015,** *104*, (2), 714-721.
119. Kuehl, C.; Thati, S.; Sullivan, B.; Sestak, J.; Thompson, M.; Siahaan, T.; Berkland, C. Pulmonary administration of soluble antigen arrays is superior to antigen in treatment of experimental autoimmune encephalomyelitis. *J. Pharm. Sci.* **2017,** *106*, (11), 3293-3302.
120. Hartwell, B. L.; Martinez-Becerra, F. J.; Chen, J.; Shinogle, H.; Sarnowski, M.; Moore, D. S.; Berkland, C. Antigen-selective Binding of Multivalent Soluble Antigen Arrays Induces Receptor Clustering and Impedes B Cell Receptor Mediated Signaling. *Biomacromolecules* **2016,** *17*, (3), 710-722.
121. Karpova, M. B.; Schoumans, J.; Ernberg, I.; Henter, J. I.; Nordenskjöld, M.; Fadeel, B. Raji revisited: cytogenetics of the original Burkitt's lymphoma cell line. *Leukemia* **2005,** *19*, (1), 159-161.
122. Gosselin, E. J.; Tony, H.-P.; Parker, D. C. Characterization of antigen processing and presentation by resting B lymphocytes. *J. Immunol.* **1988,** *140*, (5), 1408-1413.
123. Wieczorek, M.; Abualrous, E. T.; Sticht, J.; Álvaro-Benito, M.; Stolzenberg, S.; Noé, F.; Freund, C. Major Histocompatibility Complex (MHC) Class I and MHC Class II Proteins: Conformational Plasticity in Antigen Presentation. *Front. Immunol.* **2017,** *8*, 1-16.
124. Ravetch, J. V.; Kinet, J.-P. Fc receptors. *Annu. Rev. Immunol.* **1991,** *9*, (1), 457-492.
125. Ravetch, J. V.; Lanier, L. L. Immune inhibitory receptors. *Science* **2000,** *290*, (5489), 84-89.
126. Chan, P.; Sinclair, N. S. Regulation of the immune response: V. An analysis of the function of the Fc portion of antibody in suppression of an immune response with respect to interaction with components of the lymphoid system. *Immunology* **1971,** *21*, (6), 967-981.
127. Amigorena, S.; Bonnerot, C.; Choquet, D.; Hunziker, W.; Guillet, J.; Webster, P.; Sautes, C.; Mellman, I.; Fridman, W. H. Cytoplasmic domain heterogeneity and functions of IgG Fc receptors in B lymphocytes. *Science* **1992,** *256*, (5065), 1808-1812.
128. Muta, T.; Kurosaki, T.; Misulovin, Z.; Sanchez, M.; Nussenzweig, M. C.; Ravetch, J. V. A 13-amino-acid motif in the cytoplasmic domain of FcγRIIB modulates B-cell receptor signalling. *Nature* **1994,** *368*, (6466), 70-73.
129. Daëron, M.; Latour, S.; Malbec, O.; Espinosa, E.; Pina, P.; Pasmans, S.; Fridman, W. H. The same tyrosine-based inhibition motif, in the intra-cytoplasmic domain of FcγRIIB, regulates negatively BCR-, TCR-, and FcR-dependent cell activation. *Immunity* **1995,** *3*, (5), 635-646.
130. Ono, M.; Bolland, S.; Tempst, P.; Ravetch, J. V. Role of the inositol phosphatase SHIP in negative regulation of the immune system by the receptor FeγRIIB. *Nature* **1996,** *383*, (6597), 263-266.

131. Malbec, O.; Fong, D. C.; Turner, M.; Tybulewicz, V. L. J.; Cambier, J. C.; Fridman, W. H.; Daëron, M. Fcε receptor I-associated lyn-dependent phosphorylation of Fcγ receptor IIB during negative regulation of mast cell activation. *J. Immunol.* **1998,** *160*, (4), 1647-1658.
132. Pearse, R. N.; Kawabe, T.; Bolland, S.; Guinamard, R.; Kurosaki, T.; Ravetch, J. V. SHIP recruitment attenuates FcγRIIB-induced B cell apoptosis. *Immunity* **1999,** *10*, (6), 753-760.
133. Scharenberg, A. M.; El-Hillal, O.; Fruman, D. A.; Beitz, L. O.; Li, Z.; Lin, S.; Gout, I.; Cantley, L. C.; Rawlings, D. J.; Kinet, J. P. Phosphatidylinositol-3, 4, 5-trisphosphate (PtdIns-3, 4, 5-P3)/Tec kinase-dependent calcium signaling pathway: a target for SHIP-mediated inhibitory signals. *EMBO J.* **1998,** *17*, (7), 1961-1972.
134. Bolland, S.; Pearse, R. N.; Kurosaki, T.; Ravetch, J. V. SHIP modulates immune receptor responses by regulating membrane association of Btk. *Immunity* **1998,** *8*, (4), 509-516.
135. Tamir, I.; Stolpa, J. C.; Helgason, C. D.; Nakamura, K.; Bruhns, P.; Daeron, M.; Cambier, J. C. The RasGAP-binding protein p62dok is a mediator of inhibitory FcγRIIB signals in B cells. *Immunity* **2000,** *12*, (3), 347-358.
136. Yamanashi, Y.; Tamura, T.; Kanamori, T.; Yamane, H.; Nariuchi, H.; Yamamoto, T.; Baltimore, D. Role of the rasGAP-associated docking protein p62 dok in negative regulation of B cell receptor-mediated signaling. *Genes Dev.* **2000,** *14*, (1), 11-16.
137. Takai, T.; Ono, M.; Hikida, M.; Ohmori, H.; Ravetch, J. V. Augmented humoral and anaphylactic responses in FcγRII-deficient mice. *Nature* **1996,** *379*, (6563), 346-349.
138. Bolland, S.; Ravetch, J. V. Spontaneous autoimmune disease in FcγRIIB-deficient mice results from strain-specific epistasis. *Immunity* **2000,** *13*, (2), 277-285.
139. Hamaguchi, Y.; Xiu, Y.; Komura, K.; Nimmerjahn, F.; Tedder, T. F. Antibody isotype-specific engagement of Fcγ receptors regulates B lymphocyte depletion during CD20 immunotherapy. *J. Exp. Med.* **2006,** *203*, (3), 743-753.
140. Tchorbanov, A. I.; Voynova, E. N.; Mihaylova, N. M.; Todorov, T. A.; Nikolova, M.; Yomtova, V. M.; Chiang, B. L.; Vassilev, T. L. Selective silencing of DNA-specific B lymphocytes delays lupus activity in MRL/lpr mice. *Eur. J. Biochem.* **2007,** *37*, (12), 3587-3596.
141. Mihaylova, N.; Voynova, E.; Tchorbanov, A.; Nikolova, M.; Michova, A.; Todorov, T.; Srebreva, L.; Taskov, H.; Vassilev, T. Selective silencing of disease-associated B-lymphocytes by chimeric molecules targeting their FcγIIb receptor. *Int. Immunol.* **2007,** *20*, (2), 165-175.
142. Kotzin, B. L. Systemic lupus erythematosus. *Cell* **1996,** *20*, 303-306.
143. Schett, G.; Smolen, J.; Zimmermann, C.; Hiesberger, H.; Hoefler, E.; Fournel, S.; Muller, S.; Rubin, R.; Steiner, G. The autoimmune response to chromatin antigens in systemic lupus erythematosus: autoantibodies against histone H1 are a highly specific marker for SLE associated with increased disease activity. *Lupus* **2002,** *11*, (11), 704-715.
144. Liu, J.; Karypis, G.; Hippen, K. L.; Vegoe, A. L.; Ruiz, P.; Gilkeson, G. S.; Behrens, T. W. Genomic view of systemic autoimmunity in MRLlpr mice. *Genes Immun.* **2006,** *7*, (2), 156-168.
145. Mihaylova, N.; Voynova, E.; Tchorbanov, A.; Dolashka-Angelova, P.; Bayry, J.; Devreese, B.; Kaveri, S.; Vassilev, T. Simultaneous engagement of FcγIIb and CD22 inhibitory receptors silences targeted B cells and suppresses autoimmune disease activity. *Mol. Immunol.* **2009,** *47*, (1), 123-130.
146. Nikolova-Ganeva, K. A.; Gesheva, V. V.; Todorov, T. A.; Voll, R. E.; Vassilev, T. L. Targeted silencing of DNA-specific B cells combined with partial plasma cell depletion displays additive effects on delaying disease onset in lupus-prone mice. *Clin. Exp. Immunol.* **2013,** *174*, (2), 221-228.
147. Chang, T.; Lin, H.; Gao, J.; Li, W.; Xu, J.; Sun, C. J.; Li, H.; Li, F. F.; Song, Y.; Ye, J. Selective recognition and elimination of nicotinic acetylcholine receptor-reactive B cells by a recombinant fusion protein AChR-Fc in myasthenia gravis in vitro. *J. Neuroimmunol.* **2010,** *227*, (1-2), 35-43.
148. Homma, M.; Uzawa, A.; Tanaka, H.; Kawaguchi, N.; Kanai, T.; Nakajima, K.; Narita, M.; Hara, Y.; Maruyama, H.; Ogawa, Y. A Novel Fusion Protein, AChR-Fc, Ameliorates Myasthenia Gravis by Neutralizing Antiacetylcholine Receptor Antibodies and Suppressing Acetylcholine Receptor-Reactive B Cells. *Neurotherapeutics* **2017,** *14*, (1), 191-198.
149. Gesheva, V.; Szekeres, Z.; Mihaylova, N.; Dimitrova, I.; Nikolova, M.; Erdei, A.; Prechl, J.; Tchorbanov, A. Generation of gene-engineered chimeric DNA molecules for specific therapy of autoimmune diseases. *Hum. Gene Ther. Methods* **2012,** *23*, (6), 357-365.

150. Xiang, Z.; Cutler, A. J.; Brownlie, R. J.; Fairfax, K.; Lawlor, K. E.; Severinson, E.; Walker, E. U.; Manz, R. A.; Tarlinton, D. M.; Smith, K. G. FcγRIIb controls bone marrow plasma cell persistence and apoptosis. *Nat. Immunol.* **2007,** *8*, (4), 419-429.
151. Kremlitzka, M.; Mácsik-Valent, B.; Polgár, A.; Kiss, E.; Poór, G.; Erdei, A. Complement receptor type 1 suppresses human B cell functions in SLE patients. *J. Immunol. Res.* **2016,** *2016*, 1-10.
152. Józsi, M.; Prechl, J.; Bajtay, Z.; Erdei, A. Complement receptor type 1 (CD35) mediates inhibitory signals in human B lymphocytes. *J. Immunol.* **2002,** *168*, (6), 2782-2788.
153. Isaák, A.; Gergely Jr, P.; Szekeres, Z.; Prechl, J.; Poór, G.; Erdei, A.; Gergely, J. Physiological up-regulation of inhibitory receptors FcγRII and CR1 on memory B cells is lacking in SLE patients. *Int. Immunol.* **2008,** *20*, (2), 185-192.
154. Kremlitzka, M.; Polgár, A.; Fülöp, L.; Kiss, E.; Poór, G.; Erdei, A. Complement receptor type 1 (CR1, CD35) is a potent inhibitor of B-cell functions in rheumatoid arthritis patients. *Int. Immunol.* **2012,** *25*, (1), 25-33.
155. Voynova, E.; Tchorbanov, A.; Prechl, J.; Nikolova, M.; Baleva, M.; Erdei, A.; Vassilev, T. An antibody-based construct carrying DNA-mimotope and targeting CR1 (CD35) selectively suppresses human autoreactive B-lymphocytes. *Immunol. Lett.* **2008,** *116*, (2), 168-173.
156. Kerekov, N. S.; Mihaylova, N. M.; Grozdev, I.; Todorov, T. A.; Nikolova, M.; Baleva, M.; Nikolova, M.; Prechl, J.; Erdei, A.; Tchorbanov, A. I. Elimination of autoreactive B cells in humanized SCID mouse model of SLE. *Eur. J. Immunol.* **2011,** *41*, (11), 3301-3311.
157. Nikolova, K.; Mihaylova, N.; Voynova, E.; Kerekov, N.; Gesheva, V.; Prechl, J.; Nikolova, M.; Tchorbanov, A. Re-establishing tolerance to DNA in humanized and murine models of SLE. *Autoimmun. Rev.* **2010,** *9*, (7), 499-502.
158. Nikolova, K. A.; Mihaylova, N. M.; Voynova, E. N.; Tchorbanov, A. I.; Voll, R. E.; Vassilev, T. L. Selective silencing of autoreactive B lymphocytes—Following the Nature's way. *Autoimmun. Rev.* **2010,** *9*, (11), 775-779.
159. Mihaylova, N.; Tchorbanov, A. New Biotechnologycal Approaches for Immunotherapy of Autoimmune Diseases. *Biotechnol. Biotec. Eq.* **2011,** *25*, (1), 24-29.
160. Lanzavecchia, A. Receptor-mediated antigen uptake and its effect on antigen presentation to class II-restricted T lymphocytes. *Annu. Rev. Immunol.* **1990,** *8*, (1), 773-793.
161. Stöcker, M.; Klockenbring, T.; Huhn, M.; Nachreiner, T.; Wicklein, D.; Petersen, A.; Bauer, R.; Goerlich, R.; Fischer, R.; Barth, S. Antigen-selective targeting and elimination of EBV-transformed B cells by allergen toxins. *J. Allergy Clin. Immunol.* **2005,** *116*, (4), 910-915.
162. Lee, B. K.; Yoo, J. E.; Jang, Y. S.; Kim, J. Y.; Hong, C. S.; Ro, J. Y. Allergen-specific immunosuppression by ovalbumin fused with diphtheria toxin in mice sensitized with albumins of different origin. *Clin. Exp. Allergy* **2004,** *34*, (10), 1642-1648.
163. Klose, D.; Saunders, U.; Barth, S.; Fischer, R.; Jacobi, A. M.; Nachreiner, T. Novel fusion proteins for the antigen-selective staining and elimination of B cell receptor-positive cell populations demonstrated by a tetanus toxoid fragment C (TTC) model antigen. *BMC biotechnol.* **2016,** *16*, (1), 18-28.
164. Nachreiner, T.; Kampmeier, F.; Thepen, T.; Fischer, R.; Barth, S.; Stöcker, M. Depletion of autoreactive B-lymphocytes by a recombinant myelin oligodendrocyte glycoprotein-based immunotoxin. *J. Neuroimmunol.* **2008,** *195*, (1-2), 28-35.
165. Kreitman, R. J. Immunotoxins in cancer therapy. *Curr. Opin. Immunol.* **1999,** *11*, (5), 570-578.
166. Zocher, M.; Baeuerle, P. A.; Dreier, T.; Iglesias, A. Specific depletion of autoreactive B lymphocytes by a recombinant fusion protein in vitro and in vivo. *Int. Immunol.* **2003,** *15*, (7), 789-796.
167. Reiners, K. S.; Hansen, H. P.; Krüssmann, A.; Schön, G.; Csernok, E.; Gross, W. L.; Engert, A.; Von Strandmann, E. P. Selective killing of B-cell hybridomas targeting proteinase 3, Wegener's autoantigen. *Immunology* **2004,** *112*, (2), 228-236.
168. Hoyer, B. F.; Radbruch, A. Protective and pathogenic memory plasma cells. *Immunol. Lett.* **2017,** *189*, 10-12.
169. Hahn, B. H. Antibodies to DNA. *N. Engl. J. Med.* **1998,** *338*, (19), 1359-1368.
170. Couser, W. G.; Johnson, R. J. The etiology of glomerulonephritis: roles of infection and autoimmunity. *Kidney Int.* **2014,** *86*, (5), 905-914.
171. Kurts, C.; Panzer, U.; Anders, H.-J.; Rees, A. J. The immune system and kidney disease: basic concepts and clinical implications. *Nat. Rev. Immunol.* **2013,** *13*, (10), 738-753.

172. Hiepe, F.; Radbruch, A. Plasma cells as an innovative target in autoimmune disease with renal manifestations. *Nat. Rev. Nephrol.* **2016,** *12*, (4), 232-240.
173. Hiepe, F.; Dörner, T.; Hauser, A. E.; Hoyer, B. F.; Mei, H.; Radbruch, A. Long-lived autoreactive plasma cells drive persistent autoimmune inflammation. *Nat. Rev. Rheumatol.* **2011,** *7*, (3), 170-178.
174. Radbruch, A.; Muehlinghaus, G.; Luger, E. O.; Inamine, A.; Smith, K. G. C.; Dörner, T.; Hiepe, F. Competence and competition: the challenge of becoming a long-lived plasma cell. *Nat. Rev. Immunol.* **2006,** *6*, (10), 741-750.
175. Manz, R. A.; Hauser, A. E.; Hiepe, F.; Radbruch, A. Maintenance of serum antibody levels. *Annu. Rev. Immunol.* **2005,** *23*, 367-386.
176. Odendahl, M.; Jacobi, A.; Hansen, A.; Feist, E.; Hiepe, F.; Burmester, G. R.; Lipsky, P. E.; Radbruch, A.; Dörner, T. Disturbed peripheral B lymphocyte homeostasis in systemic lupus erythematosus. *J. Immunol.* **2000,** *165*, (10), 5970-5979.
177. Nutt, S. L.; Hodgkin, P. D.; Tarlinton, D. M.; Corcoran, L. M. The generation of antibody-secreting plasma cells. *Nat. Rev. Immunol.* **2015,** *15*, (3), 160-171.
178. Ahuja, A.; Anderson, S. M.; Khalil, A.; Shlomchik, M. J. Maintenance of the plasma cell pool is independent of memory B cells. *Proc. Natl. Acad. Sci.* **2008,** *105*, (12), 4802-4807.
179. DiLillo, D. J.; Hamaguchi, Y.; Ueda, Y.; Yang, K.; Uchida, J.; Haas, K. M.; Kelsoe, G.; Tedder, T. F. Maintenance of long-lived plasma cells and serological memory despite mature and memory B cell depletion during CD20 immunotherapy in mice. *J. Immunol.* **2008,** *180*, (1), 361-371.
180. Manz, R. A.; Löhning, M.; Cassese, G.; Thiel, A.; Radbruch, A. Survival of long-lived plasma cells is independent of antigen. *Int. Immunol.* **1998,** *10*, (11), 1703-1711.
181. Höfer, T.; Muehlinghaus, G.; Moser, K.; Yoshida, T.; E. Mei, H.; Hebel, K.; Hauser, A.; Hoyer, B.; O. Luger, E.; Dörner, T. Adaptation of humoral memory. *Immunol. Rev.* **2006,** *211*, (1), 295-302.
182. Cheng, Q.; Mumtaz, I. M.; Khodadadi, L.; Radbruch, A.; Hoyer, B. F.; Hiepe, F. Autoantibodies from long-lived 'memory'plasma cells of NZB/W mice drive immune complex nephritis. *Ann. Rheum. Dis.* **2013**, 2011-2017.
183. Mumtaz, I. M.; Hoyer, B. F.; Panne, D.; Moser, K.; Winter, O.; Cheng, Q. Y.; Yoshida, T.; Burmester, G.-R.; Radbruch, A.; Manz, R. A. Bone marrow of NZB/W mice is the major site for plasma cells resistant to dexamethasone and cyclophosphamide: implications for the treatment of autoimmunity. *J. Autoimmun.* **2012,** *39*, (3), 180-188.
184. Köhler, G.; Shulman, M. J. Immunoglobulin M mutants. *Eur. J. Immunol* **1980,** *10*, (6), 467-476.
185. Köhler, G.; Potash, M. J.; Lehrach, H.; Shulman, M. J. Deletions in immunoglobulin mu chains. *EMBO J.* **1982,** *1*, (5), 555-563.
186. Manz, R.; Assenmacher, M.; Pflüger, E.; Miltenyi, S.; Radbruch, A. Analysis and sorting of live cells according to secreted molecules, relocated to a cell-surface affinity matrix. *Proc. Natl. Acad. Sci.* **1995,** *92*, (6), 1921-1925.
187. Taddeo, A.; Gerl, V.; Hoyer, B. F.; Chang, H. D.; Kohler, S.; Schaffert, H.; Thiel, A.; Radbruch, A.; Hiepe, F. Selection and depletion of plasma cells based on the specificity of the secreted antibody. *Eur. J. Immunol.* **2015,** *45*, (1), 317-319.
188. Hensen, S. M. M.; Pruijn, G. J. M. Methods for the detection of peptidylarginine deiminase (PAD) activity and protein citrullination. *Mol. Cell Proteomics* **2014,** *13*, (2), 388-396.
189. Nakken, B.; Munthe, L. A.; Konttinen, Y. T.; Sandberg, A. K.; Szekanecz, Z.; Alex, P.; Szodoray, P. B-cells and their targeting in rheumatoid arthritis — Current concepts and future perspectives. *Autoimmun. Rev.* **2011,** *11*, (1), 28-34.
190. Jilani, A. A.; Mackworth-Young, C. G. The role of citrullinated protein antibodies in predicting erosive disease in rheumatoid arthritis: a systematic literature review and meta-analysis. *J. Int. Rheum.* **2015,** *2015*, (2015), 1-8.
191. Van Gaalen, F. A.; Linn-Rasker, S. P.; Van Venrooij, W. J.; De Jong, B. A.; Breedveld, F. C.; Verweij, C. L.; Toes, R. E. M.; Huizinga, T. W. J. Autoantibodies to cyclic citrullinated peptides predict progression to rheumatoid arthritis in patients with undifferentiated arthritis: a prospective cohort study. *Arthritis Rheum.* **2004,** *50*, (3), 709-715.
192. Harre, U.; Georgess, D.; Bang, H.; Bozec, A.; Axmann, R.; Ossipova, E.; Jakobsson, P.-J.; Baum, W.; Nimmerjahn, F.; Szarka, E. Induction of osteoclastogenesis and bone loss by human autoantibodies against citrullinated vimentin. *J. Clin. Invest.* **2012,** *122*, (5), 1791-1802.

193. Sato, K.; Suematsu, A.; Okamoto, K.; Yamaguchi, A.; Morishita, Y.; Kadono, Y.; Tanaka, S.; Kodama, T.; Akira, S.; Iwakura, Y. Th17 functions as an osteoclastogenic helper T cell subset that links T cell activation and bone destruction. *J. Exp. Med.* **2006,** *203*, (12), 2673-2682.
194. Schett, G.; Gravallese, E. Bone erosion in rheumatoid arthritis: mechanisms, diagnosis and treatment. *Nat. Rev. Rheumatol.* **2012,** *8*, 656-664.
195. Edwards, J. C. W.; Szczepański, L.; Szechiński, J.; Filipowicz-Sosnowska, A.; Emery, P.; Close, D. R.; Stevens, R. M.; Shaw, T. Efficacy of B-cell–targeted therapy with rituximab in patients with rheumatoid arthritis. *N. Engl. J. Med.* **2004,** *350*, (25), 2572-2581.
196. Pozsgay, J.; Babos, F.; Uray, K.; Magyar, A.; Gyulai, G.; Kiss, É.; Nagy, G.; Rojkovich, B.; Hudecz, F.; Sármay, G. In vitro eradication of citrullinated protein specific B-lymphocytes of rheumatoid arthritis patients by targeted bifunctional nanoparticles. *Arthritis Res. Ther.* **2016,** *18*, (1), 15.
197. Willemze, A.; Trouw, L. A.; Toes, R. E. M.; Huizinga, T. W. J. The influence of ACPA status and characteristics on the course of RA. *Nat. Rev. Rheumatol.* **2012,** *8*, (3), 144-152.
198. Kerkman, P. F.; Fabre, E.; van der Voort, E. I.; Zaldumbide, A.; Rombouts, Y.; Rispens, T.; Wolbink, G.; Hoeben, R. C.; Spits, H.; Baeten, D. L. Identification and characterisation of citrullinated antigen-selective B cells in peripheral blood of patients with rheumatoid arthritis. *Ann. Rheum. Dis.* **2015,** *75*, (6), 1170-1176.
199. Cornillet, M.; Sebbag, M.; Verrouil, E.; Magyar, A.; Babos, F.; Ruyssen-Witrand, A.; Hudecz, F.; Cantagrel, A.; Serre, G.; Nogueira, L. The fibrin-derived citrullinated peptide β60–74Cit60, 72, 74 bears the major ACPA epitope recognised by the rheumatoid arthritis-specific anticitrullinated fibrinogen autoantibodies and anti-CCP2 antibodies. *Ann. Rheum. Dis.* **2014,** *73*, 1246-1252.
200. Sebbag, M.; Moinard, N.; Auger, I.; Clavel, C.; Arnaud, J.; Nogueira, L.; Roudier, J.; Serre, G. Epitopes of human fibrin recognized by the rheumatoid arthritis-specific autoantibodies to citrullinated proteins. *Eur. J. Immunol.* **2006,** *36*, (8), 2250-2263.
201. Susal, C.; Kirschfink, M.; Kropelin, M.; Daniel, V.; Opelz, G. Identification of complement activation sites in human immunodeficiency virus type-1 glycoprotein gp120. *Blood* **1996,** *87*, (6), 2329-2336.
202. Stoddart, A.; Dykstra, M. L.; Brown, B. K.; Song, W.; Pierce, S. K.; Brodsky, F. M. Lipid rafts unite signaling cascades with clathrin to regulate BCR internalization. *Immunity* **2002,** *17*, (4), 451-462.
203. Auger, I.; Balandraud, N.; Rak, J.; Lambert, N.; Martin, M.; Roudier, J. New autoantigens in rheumatoid arthritis (RA): screening 8268 protein arrays with sera from patients with RA. *Ann. Rheum. Dis.* **2009,** *68*, (4), 591-594.
204. Willemze, A.; Shi, J.; Mulder, M.; Stoeken-Rijsbergen, G.; Drijfhout, J. W.; Huizinga, T. W. J.; Trouw, L. A.; Toes, R. E. M. The concentration of anticitrullinated protein antibodies in serum and synovial fluid in relation to total immunoglobulin concentrations. *Ann. Rheum. Dis.* **2013,** *72*, 1059-1063.

Chapter 2

Sequential Prodrug Strategy to Target and Eliminate ACPA-Selective Autoreactive B Cells

This Chapter has been published as:
Lianne Lelieveldt, Hendy Kristyanto, Ger Pruijn, Hans Ulrich Scherer, René Toes, Kimberly Bonger, *Molecular Pharmaceutics*, **2018**, *15*, (12), 5565-5573.

Abstract

Autoreactive B cells are thought to play a pivotal role in many autoimmune diseases. Rheumatoid arthritis (RA) is an autoimmune disease affecting ~1% of the Western population and is hallmarked by the presence of anti-citrullinated proteins antibodies (ACPA) produced by autoreactive B cells. We intend to develop a method to target and selectively eliminate these autoreactive B cells using a sequential antigen prodrug targeting strategy. As ACPA-expressing B cells are thought to play essential roles in RA-disease pathogenesis, we used this B cell response as a prototype to analyze the feasibility to generate a construct consisting of a biologically silenced, *i.e.* caged, antigen connected to a cytotoxic prodrug. Caging of the antigen is considered relevant as it is anticipated that circulating autoantibodies will otherwise clear the antigen-prodrug before it can reach the target cell. The antigen-prodrug can only bind to the autoantigen-specific B cell receptor (BCR) upon enzymatic removal of the caging group in close proximity of the B cell surface. BCR binding ultimately induces antigen-selective cytotoxicity after internalization of the antigen. We have synthesized a cyclic citrullinated peptide (CCP) antigen suitable for BCR binding, and demonstrated that binding by ACPA was impaired upon introduction of a carboxy-*p*-nitrobenzyl (CNBz) caging group at the side chain of the citrulline residue. Enzymatic reduction of the CNBz moiety by nitroreductase fully restored citrulline-selective recognition by both ACPA and ACPA-expressing B cells and showed targeted cell death of CCP-recognizing B cells only. These results mark an important step towards antigen-selective B cell targeting in general and more specifically in RA, as successful caging and activation of citrullinated antigens forms the basis for subsequent use of such construct as a prodrug in the context of autoimmune diseases.

2.1 Introduction

Many autoimmune diseases are characterized by the presence of antibodies that are directed to self-antigens.[1] The importance of autoreactive B cells in autoimmunity is well recognized, however, the exact mechanisms of their involvement have not been fully established. Rheumatoid arthritis (RA) is an inflammatory autoimmune disease that is characterized by chronic synovitis and erosive destruction of articular cartilage and bone. RA affects 0.5-1% of adults in the developed world.[2] Of these patients, 70-80% harbor anti-citrullinated protein antibodies (ACPA).[3]

Protein citrullination, the process in which a peptidylarginine is enzymatically converted into a peptidylcitrulline by peptidylarginine deiminase (PAD), is a posttranslational modification commonly observed in inflammation.[4] Antibodies directed to citrullinated proteins can be detected several years before the onset of RA, are associated with severity of the disease and are therefore an interesting marker to predict the development of RA.[5] Cyclic citrullinated peptides (CCPs) are often used as a test substrate for the detection of ACPA.[6]

Depletion of CD20-expressing B cells (*e.g.* using rituximab) is effective in treating RA.[7] The therapeutic effect is greater in ACPA-positive RA patients than in the ACPA-negative counterpart.[8] These observations suggest that autoreactive ACPA-expressing B cells may play central roles in driving and maintaining the inflammatory processes in RA. As CD20-expression by B cells is not restricted to the autoreactive B cell compartment, depletion of the entire CD20-positive population by rituximab leads to immune deficiency against infectious agents.[9] Hence, a strategy to specifically deplete autoreactive B cells is of great interest. For example, the use of an autoantigen-toxin conjugate that selectively targets the BCR can be beneficial.

So far, researchers have used autoantigens as part of selective targeting strategies for autoreactive B cells (outlined in more detail in Chapter 1). For example, Reiners and coworkers showed that by using proteinase 3, an autoantigen in Wegener's granulomatosis, conjugated to an angiogenin toxin, proteinase 3-selective B cell hybridomas could be selectively targeted.[10] Similar approaches using alternative toxins have also been described for the selective targeting of B cells involved in multiple sclerosis[11, 12] or B cells producing antibodies against a tetanus toxoid fragment.[13] However, since specific B cells can differentiate into plasma cells excreting the same immunoglobulin, antigen-conjugates might be cleared by these free circulating autoantibodies. Especially since the ACPA serum titer of RA patients can be as high as 10-200 μg/mL.[14] To improve B cell binding in these strategies, we suggest that circumventing autoantibody-mediated clearance of the autoantigen could be beneficial.

Here, we aimed to develop a sequential antigen-prodrug targeting strategy using the RA-selective autoimmune response as example, where a specific citrullinated peptide (CP) is conjugated to a cytotoxic entity (Figure 1). As a CP is able to bind to ACPA-expressing B cells and to soluble, free-circulating ACPA, we introduced a protecting group to circumvent undesired antigen binding to soluble ACPA upon administration. We envisioned that the exposure of the citrullinated epitope of the antigen can be locally restored to ensure high concentrations of the antigen-drug conjugate in close proximity of ACPA-expressing B cells (Figure 1). Antigen binding via the specific B cell receptor followed by internalization of the toxin conjugate should subsequently result in selective ACPA-positive B cell death.

We based our approach on the concept of an antibody-directed enzyme prodrug therapy (ADEPT) as our ultimate goal for the activation of a CP. This strategy has been explored extensively for local activation of cytotoxic prodrugs for tumor treatment.[15] In an ADEPT strategy,

an enzyme is conjugated to a targeting antibody after which a nontoxic prodrug is administered. The prodrug is then locally activated by the enzyme, releasing the toxin specifically at the directed site. Several enzymes have been explored for this strategy including alkaline phosphatase,[16] beta-lactamase[17] and carboxypeptidase G2.[18]

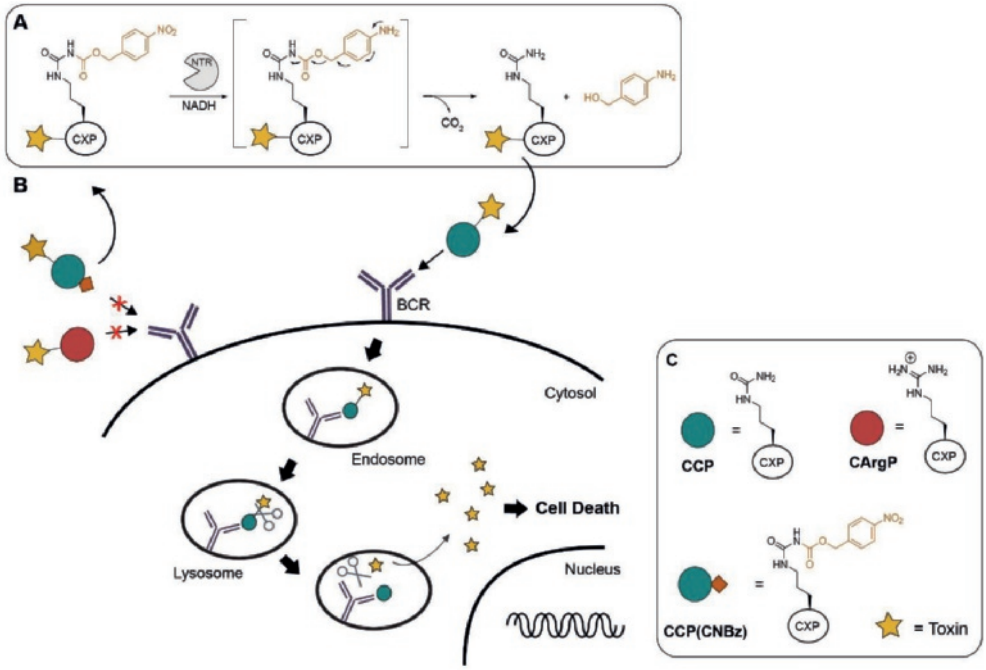

Figure 1. Schematic representation of the sequential prodrug strategy. A) Antigen activation mechanism. NTR reduction of the aromatic nitro group to the (hydroxyl)amine and subsequent 1,6-elimination; in future applications, enzymatic reduction will have to be included in an ADEPT strategy so that antigen activation takes place locally, in the vicinity of the BCR; B) CArgP and CCP(CNBz) will not bind to the BCR. After reduction with NTR, the activated CCP-toxin can selectively bind the BCR followed by BCR-mediated internalization and initiation of cell death; C) Schematic representation of the CXP (with X being different amino acids) peptides used. CCP contains citrulline, CArgP contains arginine and CCP(CNBz) contains the carboxynitrobenzyl caged citrulline. Together with the toxin, this shows the proposed structure of the sequential antigen-prodrug.

In our studies, we focused on using nitroreductase (NTR), which reduces an aromatic nitro group into an amine (or hydroxylamine).[19] This enzyme has been explored before in ADEPT strategies, where a potent cytotoxic drug was liberated *in vivo* upon reduction of the aromatic nitro group.[20, 21] In this and other studies, a nitrobenzyl alcohol protecting group was used as self-immolative linker upon reduction.[22-24] We therefore envisioned that a carboxy-*p*-nitrobenzyl (CNBz) would serve as a good protecting group for citrulline and that reduction by NTR would initiate 1,6-elimination and CO_2 release, resulting in a free ureido group at the citrulline side chain (Figure 1A). In our study, we used NTR as a proof of concept for selective activation of a prototype autoantigen, acting on the assumption that this concept can in the future be implemented into an ADEPT strategy.

2.2 Results and Discussion

Autoantigen selection. We started our studies by exploring different possible autoantigens for the ACPA-expressing immortalized B cells and their monoclonal antibodies used as model system. These B cells were previously isolated from an ACPA-positive RA patient and transduced with BCL-XL, BCL-6 and GFP genes resulting in ACPA-secreting and -expressing, GFP-positive immortalized B cell line.[25]

We selected a set of known peptide epitopes and evaluated binding to ACPA for future use as prodrug antigen for ACPA-expressing B cells.[26-28] Figure 2 shows the results from an ELISA experiment with nine different peptides, tested against the monoclonal ACPA. Fibronectin and cyclic citrullinated peptide-1 (CCP1) showed to be the best hits in this assay. We selected a CCP1 analogue (CCP), a well-known ACPA antigen,[29, 30] as initial antigen for our conjugate assembly, since this peptide epitope contains only one citrulline, whereas fibronectin does have two sides of citrullination.

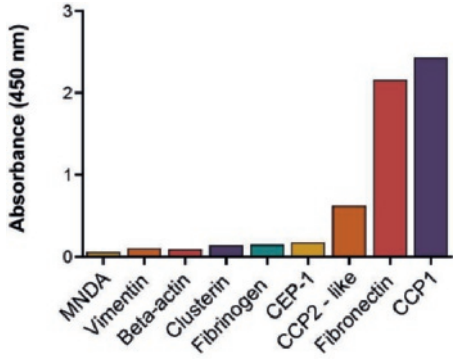

Figure 2. ELISA screening of different peptide epitopes for monoclonal ACPA produced by immortalized B cells which were used as a model system. Both fibronectin and CCP1 gave high signals.

Synthesis of (caged) citrullinated antigens. We next explored a synthetic strategy to generate a caged cyclic citrullinated peptide antigen. As the citrulline residue is key for recognition by ACPA and citrulline-directed BCRs, we envisioned that the urea moiety of the citrulline residue itself would be the best position to introduce the CNBz caging group. The incorporation of CO_2 as a driving force in antigen activation can be advantageous, however, only a few reactions with ureas to produce N-(carbamoyl)carbamates have been reported in literature.[31, 32]

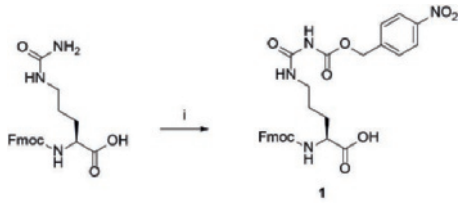

Scheme 1. Citrulline caging with carboxy-*p*-nitrobenzyl. i) *p*-Nitrobenzyl chloroformate, THF, 19 h, 40 °C, 77% yield based on recovered starting material.

Citrulline caging was finally achieved by reacting Fmoc-citrulline with *para*-nitrobenzyl chloroformate in THF in reasonable yield after recovery of the unreacted starting material (Scheme 1). The carboxy-*p*-nitrobenzyl caged Fmoc-citrulline (**1**) proved very stable towards 20% piperidine as well as TFA and could thus be used in standard peptide synthesis to produce the full CCP antigen.

CCP is recognized by 37-62% of ACPA-positive sera,[29] whereas the arginine containing variant of the peptide (CArgP) does not have affinity for ACPA and can therefore serve as a negative control. We synthesized CXP peptides (with X being different amino acids) using standard Fmoc solid phase peptide synthesis with arginine (**2**, CArgP) as the negative control, citrulline (**3**, CCP) as the positive control and caged citrulline **1** (**4**, CCP(CNBz)) (Figure 3A). A biotin moiety was installed at the single free amine functionality on resin for further experimental evaluation. The CXP peptides were covalently cyclized by first reacting the N-terminus with chloroacetic anhydride followed by deprotection of the full peptide and substitution of the chloride by the internal cysteine.

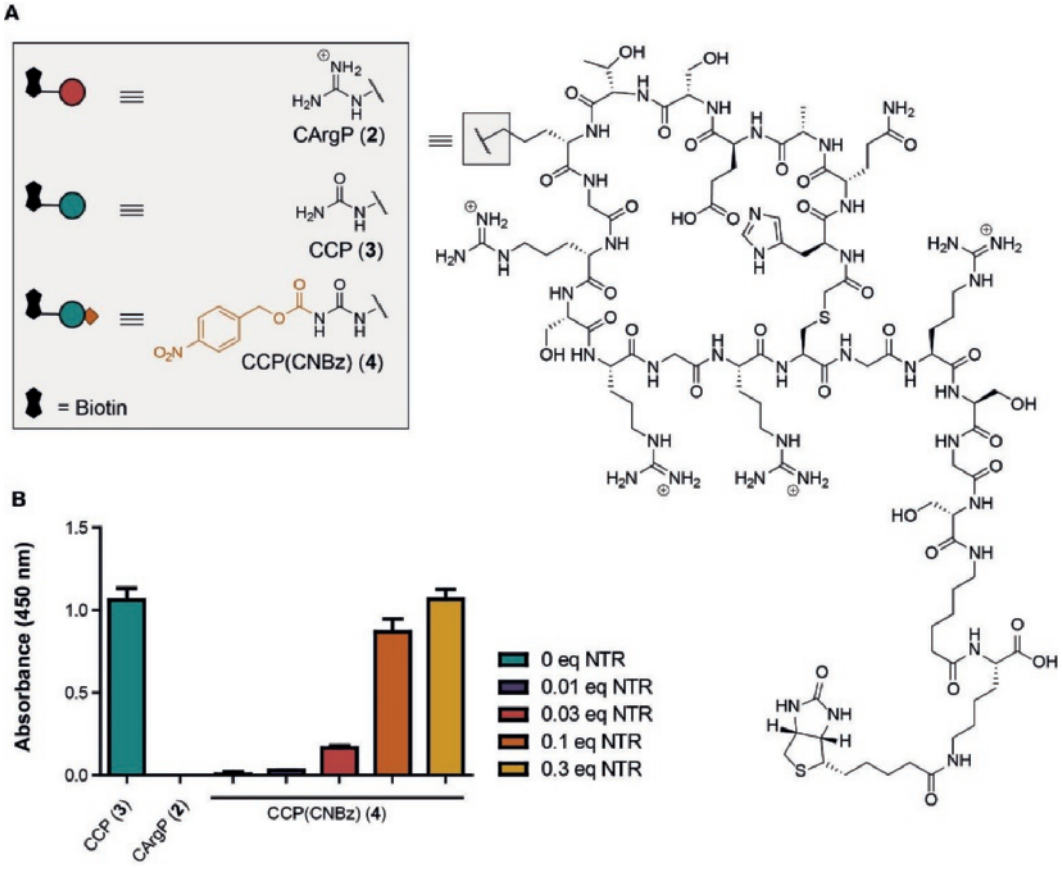

Figure 3. ACPA binding to caged CCP and the activation using NTR. A) Structures of CArgP (**2**), CCP (**3**) and the CNBz caged CCP (**4**). Biotin was used for conjugation purposes; B) CCP ELISA using caged antigens detected by monoclonal ACPA. 1 h incubation of the caged peptide with different NTR concentrations fully restored ACPA binding. Experiment was performed twice in triplicate.

This covalently cyclized CCP variant (CCP) showed slightly higher affinity to monoclonal ACPA compared to original CCP1 which is cyclized via a thiol-bridge including a second cysteine on our alanine position (Figure SI-1). The CNBz-caged variant of CCP proved to be stable for at least 7 days in acidic to neutral pH (Figure SI-2).

NTR-mediated activation of CCP(CNBz). Having the biotinylated controls and caged CXP antigens **2-4** in hand, we explored the rate of CNBz reduction by NTR. We first established that activation of the CNBz-caged citrulline building block **1** using NTR and NADH as cofactor was fast and full activation was observed within 5 minutes using 0.3 equivalents of NTR (Figure SI-3). Next, we evaluated whether the CNBz caging group retained the CCP antigen from binding to ACPA in an enzyme-linked immunosorbent assay (ELISA) using monoclonal ACPA obtained from the supernatant of ACPA-producing immortalized B cells. Biotinylated and caged peptide **4** as well as control peptides **2** and **3** were coupled to a streptavidin-coated ELISA plate and incubated with monoclonal ACPA-containing supernatant. Reduction of the CNBz group by NTR was performed before coupling of the peptide to the ELISA plate. Figure 3B shows that monoclonal ACPA-recognized CCP, as expected. More importantly, CNBz caging of CCP retained monoclonal ACPA from binding to the level observed for the negative control peptide (CArgP, **2**). Treatment of CCP(CNBz) with NTR and NADH (for 1 h at 37 °C in PBS pH 7.4) showed a concentration-dependent antigen activation, as evidenced by restoration of the binding to the monoclonal ACPA. Full restoration of antigen binding was already achieved within 5 minutes using 0.3 equivalents NTR (Figure SI-4).

As ACPA present in blood of RA-patients are not monoclonal,[33] the recognition of these peptides by patient sera was investigated. We selected sera of five different patients that were highly positive for antibodies to CCP2, the common antigen used for the detection of ACPA in a clinical diagnostic setting. Four of these RA patients were highly positive and one weakly positive for CCP recognition (Figure 4). The CArgP negative control was not bound by patient ACPA, and, similarly, no recognition of CCP(CNBz) antigen was observed. Antigen activation using 0.3 equivalents of NTR resulted in the full recovery of initial binding to the polyclonal ACPA for all five patients showing that both caging and activation of CCP for recognition by patient derived polyclonal ACPA is feasible.

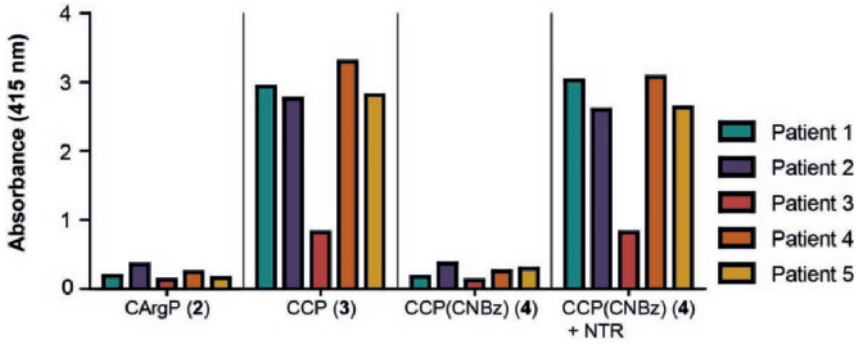

Figure 4. ELISA with the CXP antigens incubated with ACPA-positive patient sera. 0.3 equiv. nitroreductase was used for antigen activation. This experiment was performed in duplicate.

Antigen-dependent selective cellular targeting and toxicity. Application of the sequential antigen prodrug targeting strategy presented here requires efficient antigen activation in the proximity of cells. To this end, biotinylated CXP antigens were conjugated to fluorescently labelled streptavidin tetramers to visualize antigen binding to B cells by flow cytometry.[34] Two B cell clones derived from immortalized ACPA-expressing and anti-tetanus toxoid (TT)-specific B cells were used for this purpose. The antigen specificity of the immortalized B cell clones is shown in Figure SI-5.

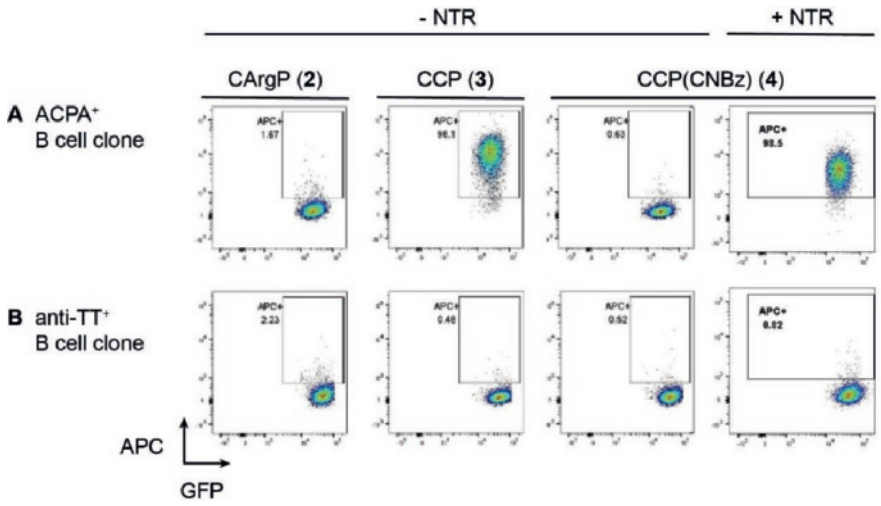

Figure 5. Flow cytometric binding studies of streptavidin-coupled, biotinylated CCP, CArgP, and (activated) CCP(CNBz) to A) an ACPA-expressing B cell clone and B) an anti-TT-specific B cell clone. This experiment was performed in duplicate.

Figure 5A shows staining of CCP-streptavidin-APC conjugates (y-axis) to clonal ACPA-expressing immortalized B cells (GFP-positive, x-axis), indicating binding of CCP-streptavidin tetramers to cell surface BCRs. No binding was observed for the CArgP and CCP(CNBz) antigen variants, demonstrating specificity of the signals observed for CCP. Notably, addition of 0.3 equivalents NTR for 1 hour almost completely recovered antigen-binding to ACPA-expressing B cells (last panel), while no binding was observed to anti-TT-specific control B cell clones (Figure 5B). Together, these data indicate that caging and activation of CCP can be achieved for antigen-specific recognition by both soluble antibodies and surface-expressed B cell receptors.

To demonstrate that we can not only deprotect and restore antigen-recognition by B cells but also achieve selective killing of ACPA-expressing B cells, we next conjugated the biotinylated antigen variants to a streptavidin-saporin conjugate (SA-ZAP).[35, 36] Saporin is a cytotoxic ribosome inhibitor that induces cell death by apoptosis,[37] which has been used in many *in vivo* studies as antibody-drug conjugate and was found to be stable and well-tolerated.[35, 38-41] Equal numbers (1 x 10^4) of ACPA-expressing and anti-TT-specific immortalized B cells were cultured with 0, 0.1, 1, 10 and 100 nM antigen-SA-ZAP conjugates. After 4 days of incubation, a XTT cell viability assay was performed to assess the amount of remaining viable cells. The percentage of living cells was calculated by dividing the optical density value of cells treated with antigen-SA-ZAP by the optical

density of cells treated in parallel with the corresponding antigen-SA complex. Figures 6A and B schematically show the structure of the prodrug and controls, and propose the expected outcome of this experiment, while Figures 6C and D show the percentage of living ACPA-expressing B cells or anti-TT-expressing B cells, respectively, after treatment with SA-ZAP conjugated to CXP either treated or non-treated with NTR.

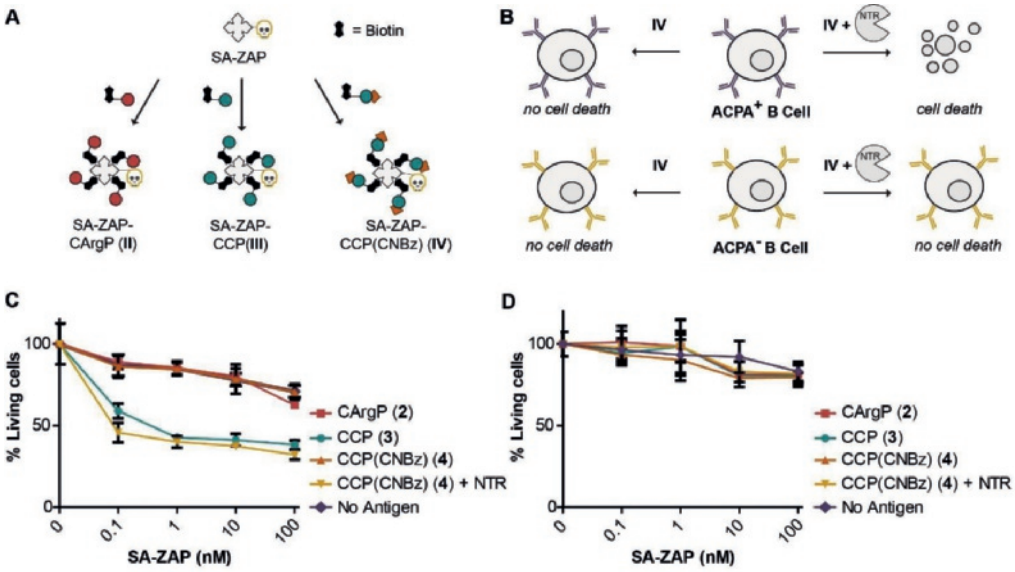

Figure 6. Selective cytotoxicity by caging and activation of CCP. A) Schematic representation of streptavidin-ZAP bound to the CXP peptides; B) schematic representation of the expected toxicity of the different SA-ZAP conjugates to ACPA-expressing B cells. Percentage of living ACPA-expressing B cells (C) and anti-TT-specific B cells (D) after four days of treatment with antigen-toxin conjugates.

The exposure of cells to CCP-SA-ZAP at 1 nM as well as the activated CCP(CNBz) induced death of up to 60% of ACPA-expressing B cells. At this SA-ZAP concentration, 86% of ACPA-expressing B cells survived the treatment when bound to CCP(CNBz), comparable to CArgP-SA-ZAP or SA-ZAP without peptide. Increasing the concentration resulted in more cell death, although increasing cellular toxicity was then also noted for SA-ZAP that was not conjugated to any antigen (Figure 6C). The lack of 100% death of ACPA-expressing B cell clone by either CCP-SA-ZAP or NTR-treated CCP(CNBz)-SA-ZAP could relate to the transfection of these cells with anti-apoptotic genes, which might make them less susceptible to toxic agents than conventional B cells would be.

As the antigen-toxin conjugate, once it is activated by nitroreductase, can bind to both the B cell receptor of ACPA-expressing cells and to secreted ACPA molecules we consider it important that antigen activation eventually occurs in close vicinity to the B cell receptor that we envision to be achieved by an ADEPT approach. Nonetheless, binding of secreted ACPA molecules to the conjugate could lead to the formation of immune complexes. Circulating ACPA-immune complexes have been reported to be capable of stimulating effector cells *in vitro* via binding to Fc receptors.[42] Thus, unwanted Fc receptor-mediated effects such as antibody dependent cellular

cytotoxicity cannot be fully excluded and future *in vivo* studies will have to be performed to evaluate this possibility.

Finally, selectivity of the approach was demonstrated by the lack of toxicity of the conjugates for anti-TT-specific B cells (Figure 6D), and also NTR by itself did not show toxic effects on the B cells used (Figure SI-6). These results indicate that CCP-SA-ZAP and NTR-treated CCP(CNBz)-SA-ZAP can be used for the selective depletion of ACPA-expressing B cells *ex vivo*.

2.3 Conclusions

The therapeutic efficacy of CD20 depletion in the treatment of RA, the risks of long-lasting systemic immunosuppression associated with this treatment, and the high specificity of the ACPA immune response for this disease have fueled efforts aimed at the selective elimination of ACPA-expressing memory B cells as a prospect of targeted therapy in RA. Here, we demonstrate a sequential two-step prodrug strategy to selectively eliminate autoreactive B cells. By exploiting the essential requirement of the citrulline residue in the antigen for recognition by ACPA-BCR and soluble ACPA molecules, we showed that caging this amino acid with CNBz resulted in complete loss of binding to ACPA and ACPA-expressing B cells. Furthermore, the CNBz group could be removed by nitroreductase to restore binding of the antigen. Using this strategy, we selectively induced cell death in immortalized ACPA-expressing B cell clones using an antigen coupled to a streptavidin-toxin, while anti-TT expressing B cells were insensitive to these conjugates.

We expect that antigen activation in close proximity to the B cell membrane, *e.g.* by using NTR, can circumvent binding of antigen to free circulating ACPA, thereby decreasing the risk for rapid clearance of the drug from tissue and the circulation. The CNBz reduction using NTR may be beneficial as elevated levels of reductases are found in hypoxic inflamed tissue.[43] In addition, NTR has been explored previously in ADEPT[21] and enzyme-selective cofactors for *E. coli* NTR are reported circumventing the use of serum-sensitive cofactors such as NAD(P)H.[44]

In conclusion, we show that we can selectively cage and activate CCP, thereby tuning the affinity to ACPA and ACPA-expressing B cells. Using this approach, we expect that it will be possible to circumvent CCP(CNBz) from binding to ACPA and after selective activation by NTR in the proximity of B cells, using a possible ADEPT construct, regain binding to the BCR and thereby the internalization of a cytotoxin. Since not all autoreactive B cells reside in inflamed tissue, but also in lymph nodes, we currently investigate additional approaches for the selective activation of target antigens including click-to-release chemistry (Chapter 3).[45]

In this study, we demonstrated caging and activation of CCP in the context of the citrulline-specific B cell response, and we expect that this modular strategy will be applicable interchangeably for other (auto)antigens as well. The selectivity of the antigen and the possibility to retain binding to circulation ACPA brings us a step closer to the selective elimination of autoreactive B cells for the treatment of patients with ACPA-positive RA.

2.4 Materials and Methods

General methods and materials. Unless stated otherwise, all chemicals were used without further purification. Amino acids were obtained from Bachem (Bubendorf, Switzerland) or Novabiochem (EMD Chemicals, Gibbstown, USA). Solvents were purchased from J.T. Baker,

Biosolve, Fisher Scientific and Merck Millipore and used as received. If no further details are given the reaction was performed under ambient atmosphere and temperature. Analytical thin layer chromatography (TLC) was performed on silica gel-coated plates (Merck, 60 F254) with the indicated solvent mixture, visualization was done using ultraviolet (UV) irradiation (λ = 254 nm) and/or staining with aqueous $KMnO_4$. Purification by column chromatography was carried out using silica gel 60 (Merck, 0.040-0.063 mm). ^{1}H-NMR chemical shifts (δ), recorded on a Bruker 500 MHz Avance III spectrometer equipped with a Prodigy BB cryoprobe, are reported in parts per million (ppm) relative to a residual proton peak of the solvent, δ = 7.26 for $CDCl_3$. ^{13}C-NMR chemical shifts (δ), are reported in parts per million (ppm) relative to $CDCl_3$ (δ = 77.16). Coupling constants are reported as a *J*-value in Hertz (Hz). Low-resolution mass spectra (LRMS) were recorded on Thermo LCQ Advantage Max (ESI). A Thermo Finnigan LCQ Fleet ESI ion-trap mass spectrometer, which is equipped with a Shimadzu HPLC (C18-column, particle size 3 µm, acetonitrile/water gradient 5 - 100%, in 16 minutes and a flow of 0.2 ml/min) and a PDA detector, was used to separate organic compounds and record low-resolution mass spectra. High-resolution mass spectra (HRMS) of small molecules were recorded on a JEOL AccuTOF JMS-T100CS (ESI). Preparative HPLC was performed on a Shimadzu LC-20A Prominence system (Shimadzu, 's-Hertogenbosch, The Netherlands) equipped with a Gemini NX-C18 column, 150 × 21.2 mm, particle size 10 µm (Phenomenex, Utrecht, The Netherlands). Gradient used was acetonitrile/water 5-50%, in 30 minutes and a flow of 6 ml/min. Analytical HPLC measurements were performed on a Shimadzu LC-20A Prominence system (Shimadzu, 's-Hertogenbosch, The Netherlands) equipped with a Gemini NX-C18 column, 150 × 3 mm, particle size 3 µm (Phenomenex, Utrecht, The Netherlands). Gradient used is acetonitrile/water 5 - 100%, in 30 minutes and a flow of 0.4 ml/min. Injected peptides were monitored at 254 nm and 215 nm and the desired peaks were integrated manually using a LabSolutions software package (Shimadzu, 's-Hertogenbosch, The Netherlands).

14-(9*H*-Fluoren-9-yl)-1-(4-nitrophenyl)-3,5,12-trioxo-2,13-dioxa-4,6,11-triazatetradecane-10-carboxylic acid (1). Fmoc-Cit-OH (2.00 g, 5.0 mmol, 1 equiv.) was dissolved in THF (115 ml) and heated to 40 °C. 4-Nitrobenzyl chloroformate (1.63 g, 7.6 mmol, 1.5 equiv.) was dissolved in THF (5 mL) and added to Fmoc-Cit-OH. The reaction mixture was stirred for 19 h. The mixture was concentrated in vacuo and the mixture was purified over silica (2.5-5% MeOH in CH_2Cl_2), yielding a yellow solid product (**1**) (948 mg, 77% after regaining starting material). R_f = 0.49 (5% MeOH in EtOAc). ^{1}H NMR (500 MHz, chloroform-*d*) δ 9.08 (s, 1H), 8.15 (d, *J* = 8.3 Hz, 2H), 7.93 (s, 1H), 7.73 (d, *J* = 7.5 Hz, 2H), 7.63 – 7.52 (m, 2H), 7.43 (d, *J* = 8.1 Hz, 2H), 7.37 (t, *J* = 7.3 Hz, 2H), 7.31 – 7.26 (m, 2H), 5.58 (d, *J* = 6.2 Hz, 1H), 5.17 (s, 2H), 4.43 (s, 1H), 4.39 (d, *J* = 6.6 Hz, 2H), 4.19 (t, *J* = 6.6 Hz, 1H), 3.46 – 3.11 (m, 2H), 1.98 – 1.69 (m, 2H), 1.66 – 1.55 (m, 2H). ^{13}C NMR (126 MHz, chloroform-*d*) δ 176.01, 156.18, 154.74, 153.97, 147.97, 143.75, 142.18, 141.42, 128.40, 127.87, 127.19, 125.19, 123.99, 120.14, 67.07, 66.30, 53.49, 47.32, 39.45, 29.64, 25.51. HRMS (ESI+) m/z calcd for $C_{29}H_{28}N_4NaO_9^+$ $[M+Na]^+$ 599.17485, found: 599.17540.

General peptide synthesis. The first amino acid, Fmoc-Lys(Mtt)-OH, (2 equiv.) was added to the Wang resin with DIPCDI (2 equiv.), HOBt (4 equiv.) and DMAP (2 equiv.) in DMF. The mixture was shaken for 16 h at room temperature. After washing, the Mtt group was cleaved off

using 2% TFA in DCM repeatable for 2 minutes. After washing with DCM and DMF, biotin was coupled using DIPCDI (3.3 equiv.) and HOBt (3.6 equiv.). Upon completion, the resin was flushed three times with DMF and piperidine was then added for 30 min to cleave off the Fmoc protecting group. The resin was subsequently flushed three times with DMF. A mixture of 3 equiv. Fmoc-AA-OH, 3.6 equiv. HOBt and 3.3 equiv. DIPCDI was added to the resin to bind the subsequent amino acid. This reaction was incubated at room temperature. After coupling of the next amino acid, the remaining free amines were capped with acetic anhydride (1 mL) and pyridine (1 mL) in DMF (12 mL). After washing three times with DMF, piperidine was added again and the cycles continued. After the last amino acid, chloroacetic anhydride (5 equiv.) and DIPEA (5 equiv.) were added in DMF and shaken for 45 min. Finally, a mixture of 92.5% TFA, 2.5% H_2O, 2.5% EDT and 2.5% TIPS was made. This mixture was added to the resin and incubated for 3 h at room temperature to cleave off the peptide from the resin and to deprotect the amino acid residues. The peptide was precipitated in diethyl ether, filtered and dried. Kaiser tests were performed to follow the coupling reactions.

General peptide cyclisation. The crude peptides were dissolved in a 50 mM NH_4HCO_3 buffer pH 8.4: MeCN 1:1, at a concentration of 2 mg/mL and stirred for 24 h. MeCN was evaporated and the remaining H_2O was lyophilized. The peptides were purified using preparative reversed-phase HPLC and analyzed using analytical HPLC.

CArgP (2). CArgP was synthesized following the procedures described in the general peptide synthesis. Next, this peptide was cyclized and purified as described in the general cyclisation method. HPLC: Rt. 12.731 min. LCMS (ESI+) m/z calcd for $C_{100}H_{172}N_{42}O_{33}S_2^{2+}$ $[M+2H]^{2+}$ 1277.13, found 1277.56. $C_{100}H_{172}N_{41}O_{34}S_2^{3+}$ $[M+3H]^{3+}$ 851.75, found 852.28. $C_{100}H_{173}N_{41}O_{34}S_2^{4+}$ $[M+4H]^{4+}$ 639.06, found 640.20.

CCP(3). CCP was synthesized following the procedures described in the general peptide synthesis. Next, this peptide was cyclized and purified as described in the general cyclisation method. HPLC: Rt. 12.753 min. LCMS (ESI+) m/z calcd for $C_{100}H_{171}N_{41}O_{34}S_2^{2+}$ $[M+2H]^{2+}$ 1277.61, found 1278.08. $C_{100}H_{172}N_{41}O_{34}S_2^{3+}$ $[M+3H]^{3+}$ 852.07, found 852.68. $C_{100}H_{173}N_{41}O_{34}S_2^{4+}$ $[M+4H]^{4+}$ 639.31, found 641.16.

CCP(CNBz) (4). CCP(CNBz) was synthesized following the procedures described in the general peptide synthesis. Next, this peptide was cyclized and purified as described in the general cyclisation method. HPLC: Rt. 14.854 min. LCMS (ESI+) m/z calcd for $C_{108}H_{176}N_{42}O_{38}S_2^{2+}$ $[M+2H]^{2+}$ 1367.12, found 1367.52. $C_{108}H_{177}N_{42}O_{38}S_2^{3+}$ $[M+3H]^{3+}$ 911.75, found 912.20. $C_{108}H_{178}N_{42}O_{38}S_2^{4+}$ $[M+4H]^{4+}$ 684.06, found 685.20.

CCP(CNBz) stability measurements at various pH. The peptide was dissolved in 1% DMSO / McIlvaine buffer (pH 4-9 at a concentration of 0.2 mg/ml). The reaction was set at 37°C at 600 rpm for 1-7 days. A sample was taken and was measured by LCMS. The area under the curve of the chromatogram shows the percentage of starting material or degradation material (CCP).

Cell culture and monoclonal antibodies. Immortalized B cell clones recognizing CCP and tetanus toxoid (TT) were generated by transducing antigen-specific human memory B cells with

retroviruses encoding BCL-6 and BCL-XL, as previously described.[46, 47] Cells were cultured in Dulbecco's Modified Eagle's Medium (DMEM) supplemented with 8% heat-inactivated fetal calf serum, penicillin/streptomycin (PS, 100 U/ml), 2 mM Glutamax and 1 μg/ml puromycin in the presence of irradiated CD40L-expressing cells and mouse interleukin-21-Fc (mIL21-Fc). These B cell clones maintained the expression of membrane bound ACPA or anti-TT antibody and also secreted antibodies recognizing CCP or TT, respectively. Supernatants of the cell cultures which contained secreted monoclonal antibodies against CCP or TT were harvested after three days of culture.

RA plasma. Peripheral blood was obtained from ACPA-positive RA patients who visited the outpatient clinic of the Department of Rheumatology at Leiden University Medical Centre (LUMC). The patients met the 2010 ACR/EULAR criteria for RA at the time of diagnosis and gave written informed consent to participate in the study. Permission to conduct the study was obtained from the ethical review board of LUMC. Blood plasma was obtained by centrifuging heparin-treated peripheral blood.

ELISA measurements. The ability of the CNBz moiety to protect CCP epitopes from the recognition of both monoclonal and polyclonal ACPA and the capacity of NTR to remove the CNBz group and recover CCP reactivity were assessed by ELISA. All reactants were dissolved in PBS pH = 7.4. 10 μM (1 equiv.) of biotinylated CCP(CNBz) was treated with 3 μM (0.3 equiv.), 1 μM (0.1 equiv.), 0.3 μM (0.03 equiv.) and 0.1 μM (0.01 equiv.) NTR and 50 equiv. NADH (both from Sigma Aldrich) to test the NTR capacity for 1 hour at 37 °C. Next, biotinylated CCP, CArgP, CCP(CNBz) and NTR-pretreated CCP(CNBz) were coupled to streptavidin-coated ELISA plates (C96 Maxisorp Nunc-immuno plate, Thermo-Scientific). Undiluted supernatants of the immortalized B cell clones and 1:50 diluted patient's plasma samples were incubated with the respective antigens; antigen-bound IgG was detected by polyclonal rabbit anti-human IgG HRP (DAKO) and stained with ABTS.H_2O_2 (Sigma-Aldrich) or TMB-UP (Biomerieux). The absorbance of the colorimetric signal was measured with iMark TM Microplate Reader (BioRad) at 415nm or 450nm, resp.

FACS measurements. Biotinylated CCP(CNBz), CCP and CArgP were coupled with APC-labelled streptavidin (Lifetechnologies), as previously described.[48] One equivalent of APC-labelled CCP(CNBz) tetramer was treated with 0.3 equiv. NTR and 50 equiv. NADH for 1 hour at 37 °C in cell cultures containing either ACPA-expressing or anti-TT-expressing immortalized B cells in a 96 well plate. Subsequently, the cells were kept on ice for 30 minutes, washed, resuspended with 1% paraformaldehyde and measured by flow cytometry using BD LSRFortessa (BD Biosciences).

Cell viability assay. Biotinylated CCP, CArgP and CCP(CNBz) were conjugated with streptavidin-saporin (Advanced Targeting systems) in a 4:1 ratio to make peptide-drug conjugates. 1 x 10^4 ACPA-expressing and/or anti-TT-specific B cell clones were cultured with medium, mIL21-Fc and soluble CD40L (from Biolegend) in the presence of 0, 0.1, 1, 10, 100 nM peptide-drug conjugates in a 96-well plate. After 4 days, supernatants were collected and XTT labelling and electron-coupling reagents (Roche) were added to the culture according to the manufacturer's protocol and incubated for 6 hours. Cell viability was measured on an iMark TM Microplate Reader (from BioRad).

2.5 References

1. Dörner, T.; Jacobi, A. M.; Lipsky, P. E. B cells in autoimmunity. *Arthritis Res. Ther.* **2009,** *11*, (5), 247-257.
2. Scott, D. L.; Wolfe, F.; Huizinga, T. W. J. Rheumatoid arthritis. *Lancet* **2010,** *376*, (9746), 1094-1108.
3. Vossenaar, E. R.; van Venrooij, W. J. Citrullinated proteins: sparks that may ignite the fire in rheumatoid arthritis. *Arthritis Res. Ther.* **2004,** *6*, (3), 107-111.
4. Valesini, G.; Gerardi, M. C.; Iannuccelli, C.; Pacucci, V. A.; Pendolino, M.; Shoenfeld, Y. Citrullination and autoimmunity. *Autoimmun. rev.* **2015,** *14*, (6), 490-497.
5. Jilani, A. A.; Mackworth-Young, C. G. The role of citrullinated protein antibodies in predicting erosive disease in rheumatoid arthritis: a systematic literature review and meta-analysis. *J. Int. Rheum.* **2015,** *2015*, 1-8.
6. Van Venrooij, W. J.; Van Beers, J. J. B. C.; Pruijn, G. J. M. Anti-CCP antibodies: the past, the present and the future. *Nat. Rev. Rheumatol.* **2011,** *7*, (7), 391-398.
7. Edwards, J. C. W.; Szczepański, L.; Szechiński, J.; Filipowicz-Sosnowska, A.; Emery, P.; Close, D. R.; Stevens, R. M.; Shaw, T. Efficacy of B-cell–targeted therapy with rituximab in patients with rheumatoid arthritis. *N. Engl. J. Med.* **2004,** *350*, (25), 2572-2581.
8. Chatzidionysiou, K.; Lie, E.; Nasonov, E.; Lukina, G.; Hetland, M. L.; Tarp, U.; Gabay, C.; van Riel, P. L. C. M.; Nordström, D. C.; Gomez-Reino, J. Highest clinical effectiveness of rituximab in autoantibody-positive patients with rheumatoid arthritis and in those for whom no more than one previous TNF antagonist has failed: pooled data from 10 European registries. *Ann. Rheum. Dis.* **2011,** *70*, (9), 1575-1580.
9. Kaplan, B.; Kopyltsova, Y.; Khokhar, A.; Lam, F.; Bonagura, V. Rituximab and immune deficiency: case series and review of the literature. *J. Allergy Clin. Immunol. Pract.* **2014,** *2*, (5), 594-600.
10. Reiners, K. S.; Hansen, H. P.; Krüssmann, A.; Schön, G.; Csernok, E.; Gross, W. L.; Engert, A.; von Strandmann, E. P. Selective killing of B-cell hybridomas targeting proteinase 3, Wegener's autoantigen. *Immunology* **2004,** *112*, (2), 228-236.
11. Zocher, M.; Baeuerle, P. A.; Dreier, T.; Iglesias, A. Specific depletion of autoreactive B lymphocytes by a recombinant fusion protein in vitro and in vivo. *Int. Immunol.* **2003,** *15*, (7), 789-796.
12. Nachreiner, T.; Kampmeier, F.; Thepen, T.; Fischer, R.; Barth, S.; Stöcker, M. Depletion of autoreactive B-lymphocytes by a recombinant myelin oligodendrocyte glycoprotein-based immunotoxin. *J. Neuroimmunol.* **2008,** *195*, (1-2), 28-35.
13. Klose, D.; Saunders, U.; Barth, S.; Fischer, R.; Jacobi, A. M.; Nachreiner, T. Novel fusion proteins for the antigen-specific staining and elimination of B cell receptor-positive cell populations demonstrated by a tetanus toxoid fragment C (TTC) model antigen. *BMC biotechnol.* **2016,** *16*, (1), 18.
14. Willemze, A.; Shi, J.; Mulder, M.; Stoeken-Rijsbergen, G.; Drijfhout, J. W.; Huizinga, T. W. J.; Trouw, L. A.; Toes, R. E. M. The concentration of anticitrullinated protein antibodies in serum and synovial fluid in relation to total immunoglobulin concentrations. *Ann. Rheum. Dis.* **2013,** *72*, 1059-1063.
15. Prosser, G. A.; Copp, J. N.; Syddall, S. P.; Williams, E. M.; Smaill, J. B.; Wilson, W. R.; Patterson, A. V.; Ackerley, D. F. Discovery and evaluation of Escherichia coli nitroreductases that activate the anti-cancer prodrug CB1954. *Biochem. Pharmacol.* **2010,** *79*, (5), 678-687.
16. Senter, P. D.; Saulnier, M. G.; Schreiber, G. J.; Hirschberg, D. L.; Brown, J. P.; Hellström, I.; Hellström, K. E. Anti-tumor effects of antibody-alkaline phosphatase conjugates in combination with etoposide phosphate. *Proc. Natl. Acad. Sci.* **1988,** *85*, (13), 4842-4846.
17. Walther, R.; Rautio, J.; Zelikin, A. N. Prodrugs in medicinal chemistry and enzyme prodrug therapies. *Adv. Drug Deliv. Rev.* **2017,** *118*, 65-77.
18. Sharma, S. K.; Bagshawe, K. D. Antibody Directed Enzyme Prodrug Therapy (ADEPT): Trials and tribulations. *Adv. Drug Deliv. Rev.* **2017,** *118*, 2-7.
19. Williams, E. M.; Little, R. F.; Mowday, A. M.; Rich, M. H.; Chan-Hyams, J. V. E.; Copp, J. N.; Smaill, J. B.; Patterson, A. V.; Ackerley, D. F. Nitroreductase gene-directed enzyme prodrug therapy: insights and advances toward clinical utility. *J. Biochem.* **2015,** *471*, (2), 131-153.

20. Mauger, A. B.; Burke, P. J.; Somani, H. H.; Friedlos, F.; Knox, R. J. Self-immolative prodrugs: candidates for antibody-directed enzyme prodrug therapy in conjunction with a nitroreductase enzyme. *J. Med. Chem.* **1994,** *37*, (21), 3452-3458.
21. Dubowchik, G. M.; Walker, M. A. Receptor-mediated and enzyme-dependent targeting of cytotoxic anticancer drugs. *Pharmacol. Ther.* **1999,** *83*, (2), 67-123.
22. Jain, N.; Smith, S. W.; Ghone, S.; Tomczuk, B. Current ADC linker chemistry. *Pharm. Res.* **2015,** *32*, (11), 3526-3540.
23. Hay, M. P.; Wilson, W. R.; Denny, W. A. A novel enediyne prodrug for antibody-directed enzyme prodrug therapy (ADEPT) using E. coli B nitroreductase. *Bioorg. Med. Chem. Lett.* **1995,** *5*, (23), 2829-2834.
24. Xie, X.; Li, X.-M.; Qin, F.; Lin, J.; Zhang, G.; Zhao, J.; Bao, X.; Zhu, R.; Song, H.; Li, X. D. Genetically encoded photoaffinity histone marks. *J. Am. Chem. Soc.* **2017,** *139*, (19), 6522-6525.
25. Kwakkenbos, M. J.; Helden, P. M.; Beaumont, T.; Spits, H. Stable long-term cultures of self-renewing B cells and their applications. *Immunol. Rev.* **2016,** *270*, (1), 65-77.
26. Sebbag, M.; Moinard, N.; Auger, I.; Clavel, C.; Arnaud, J.; Nogueira, L.; Roudier, J.; Serre, G. Epitopes of human fibrin recognized by the rheumatoid arthritis-specific autoantibodies to citrullinated proteins. *Eur. J. Immunol.* **2006,** *36*, (8), 2250-2263.
27. van Venrooij, W. J.; Zendman, A. J. W. Anti-CCP2 antibodies: an overview and perspective of the diagnostic abilities of this serological marker for early rheumatoid arthritis. *Clin. Rev. Allergy Immunol.* **2008,** *34*, (1), 36-39.
28. Lundberg, K.; Kinloch, A.; Fisher, B. A.; Wegner, N.; Wait, R.; Charles, P.; Mikuls, T. R.; Venables, P. J. Antibodies to citrullinated α-enolase peptide 1 are specific for rheumatoid arthritis and cross-react with bacterial enolase. *Arthritis Rheum.* **2008,** *58*, (10), 3009-3019.
29. Schellekens, G. A.; de Jong, B. A. W.; van den Hoogen, F. H. J.; Van de Putte, L. B.; van Venrooij, W. J. Citrulline is an essential constituent of antigenic determinants recognized by rheumatoid arthritis-specific autoantibodies. *J. Clin. Invest.* **1998,** *101*, (1), 273-281.
30. Schellekens, G. A.; Visser, H.; De Jong, B. A. W.; Van Den Hoogen, F. H. J.; Hazes, J. M. W.; Breedveld, F. C.; Van Venrooij, W. J. The diagnostic properties of rheumatoid arthritis antibodies recognizing a cyclic citrullinated peptide. *Arthritis Rheum.* **2000,** *43*, (1), 155-163.
31. Mauguin. *Ann. Chim.* **1911,** *22*, (8), 316.
32. Biltz, J. *Chem. Ber.* **1923,** *56*, 1918.
33. Ioan-Facsinay, A.; el-Bannoudi, H.; Scherer, H. U.; van der Woude, D.; Ménard, H. A.; Lora, M.; Trouw, L. A.; Huizinga, T. W. J.; Toes, R. E. Anti-cyclic citrullinated peptide antibodies are a collection of anti-citrullinated protein antibodies and contain overlapping and non-overlapping reactivities. *Ann. Rheum. Dis.* **2011,** *70*, (1), 188-193.
34. Kerkman, P. F.; Rombouts, Y.; van der Voort, E. I. H.; Trouw, L. A.; Huizinga, T. W. J.; Toes, R. E. M.; Scherer, H. U. Circulating plasmablasts/plasmacells as a source of anticitrullinated protein antibodies in patients with rheumatoid arthritis. *Ann. Rheum. Dis.* **2013,** *72*, (7), 1259-1263.
35. Palchaudhuri, R.; Saez, B.; Hoggatt, J.; Schajnovitz, A.; Sykes, D. B.; Tate, T. A.; Czechowicz, A.; Kfoury, Y.; Ruchika, F. N. U.; Rossi, D. J.; Verdine, G. L.; Mansour, M. K.; Scadden, D. T. Non-genotoxic conditioning for hematopoietic stem cell transplantation using a hematopoietic-cell-specific internalizing immunotoxin. *Nat. Biotechnol.* **2016,** *34*, 738-745.
36. Collins, B. E.; Blixt, O.; Han, S.; Duong, B.; Li, H.; Nathan, J. K.; Bovin, N.; Paulson, J. C. High-affinity ligand probes of CD22 overcome the threshold set by cis ligands to allow for binding, endocytosis, and killing of B cells. *J. Immunol.* **2006,** *177*, (5), 2994-3003.
37. Bergamaschi, G.; Perfetti, V.; Tonon, L.; Novella, A.; Lucotti, C.; Danova, M.; Glennie, M. J.; Merlini, G.; Cazzola, M. Saporin, a ribosome-inactivating protein used to prepare immunotoxins, induces cell death via apoptosis. *Br. J. Haematol.* **1996,** *93*, (4), 789-794.
38. Lee, S. C.; Seo, K. W.; Kim, H. J.; Kang, S. W.; Choi, H.-J.; Kim, A.; Kwon, B. S.; Cho, H. R.; Kwon, B. Depletion of Alloreactive T-Cells by Anti-CD137-Saporin Immunotoxin. *Cell Transplant.* **2015,** *24*, (6), 1167-1181.
39. Alonso, M. N.; Gregorio, J. G.; Davidson, M. G.; Gonzalez, J. C.; Engleman, E. G. Depletion of inflammatory dendritic cells with anti-CD209 conjugated to saporin toxin. *Immunol. Res.* **2014,** *58*, (2-3), 374-377.

40. Kato, J.; Satake, N.; O'Donnell, R. T.; Abuhay, M.; Lewis, C.; Tuscano, J. M. Efficacy of a CD22-targeted antibody-saporin conjugate in a xenograft model of precursor-B cell acute lymphoblastic leukemia. *Leuk. Res,* **2013,** *37*, (1), 83-88.
41. Kuroda, K.; Liu, H.; Kim, S.; Guo, M.; Navarro, V.; Bander, N. H. Saporin toxin-conjugated monoclonal antibody targeting prostate-specific membrane antigen has potent anticancer activity. *Prostate* **2010,** *70*, (12), 1286-1294.
42. England, B. R.; Thiele, G. M.; Mikuls, T. R. Anticitrullinated protein antibodies: origin and role in the pathogenesis of rheumatoid arthritis. *Curr. Opin. Rheumatol.* **2017,** *29*, (1), 57-64.
43. Quiñonez-Flores, C. M.; González-Chávez, S. A.; Pacheco-Tena, C. Hypoxia and its implications in rheumatoid arthritis. *J. Biomed. Sci* **2016,** *23*, (62), 1-9.
44. Friedlos, F.; Knox, R. J. Metabolism of nad(p)h by blood components: Relevance to bioreductively activated prodrugs in a targeted enzyme therapy system. *Biochem. Pharmacol.* **1992,** *44*, (4), 631-635.
45. Versteegen, R. M.; Rossin, R.; ten Hoeve, W.; Janssen, H. M.; Robillard, M. S. Click to Release: Instantaneous Doxorubicin Elimination upon Tetrazine Ligation. *Angew. Chem. Int. Ed.* **2013,** *52*, (52), 14112-14116.
46. Kwakkenbos, M. J.; Diehl, S. A.; Yasuda, E.; Bakker, A. Q.; van Geelen, C. M. M.; Lukens, M. V.; van Bleek, G. M.; Widjojoatmodjo, M. N.; Bogers, W. M. J. M.; Mei, H.; Radbruch, A.; Scheeren, F. A.; Spits, H.; Beaumont, T. Generation of stable monoclonal antibody–producing B cell receptor–positive human memory B cells by genetic programming. *Nat. Med.* **2009,** *16*, 123.
47. Rivellese, F.; Mauro, D.; Nerviani, A.; Pagani, S.; Fossati-Jimack, L.; Messemaker, T.; Kurreeman, F. A. S.; Toes, R. E. M.; Ramming, A.; Rauber, S.; Schett, G.; Jones, G. W.; Jones, S. A.; Rossi, F. W.; de Paulis, A.; Marone, G.; El Shikh, M. E. M.; Humby, F.; Pitzalis, C. Mast cells in early rheumatoid arthritis associate with disease severity and support B cell autoantibody production. *Ann. Rheum. Dis.* **2018,** *77*, (12), 1773-1781.
48. Kerkman, P. F.; Fabre, E.; van der Voort, E. I. H.; Zaldumbide, A.; Rombouts, Y.; Rispens, T.; Wolbink, G.; Hoeben, R. C.; Spits, H.; Baeten, D. L. P.; Huizinga, T. W. J.; Toes, R. E. M.; Scherer, H. U. Identification and characterisation of citrullinated antigen-specific B cells in peripheral blood of patients with rheumatoid arthritis. *Ann. Rheum. Dis.* **2015**.

2.6 Supplementary Figures

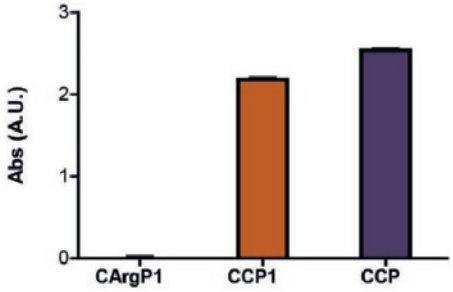

Figure SI-1. ELISA data. CCP is covalently cyclized citrullinated peptide, while CCP1 is the cyclized peptide via sulfide bridges.

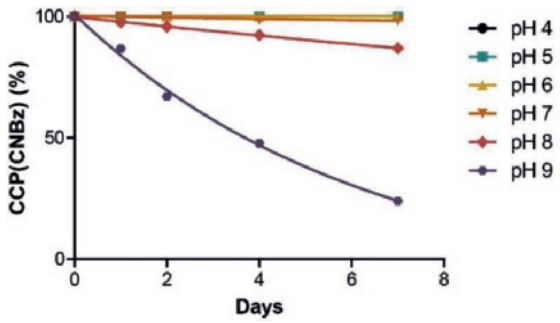

Figure SI-2. The stability of the CNBz linker of the caged CCP in pH 4-9 (McIlvaine buffer) for 1-7 days at 37 °C and 600 rpm. Conversion was measured by LCMS and the percentage was the area under the curve for CCP(CNBz)

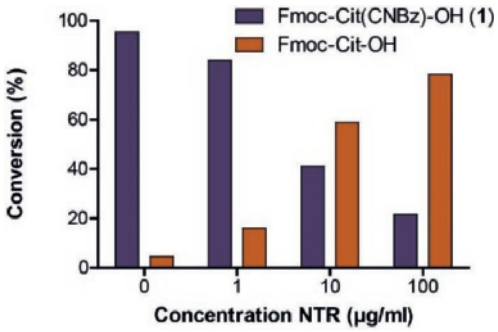

Figure SI-3. Activation of Fmoc-Cit(CNBz)-OH using nitroreductase at t = 5 min. Y-axis represents the percentage of material, either Fmoc-Cit(CNBz)-OH starting material (purple) or Fmoc-Cit-OH, activated product (orange). Different amounts of nitroreductase (concentration on the x-axis) were added and all conditions were measured after 5 minutes. Using 100 µg/ml NTR showed almost complete citrulline activation.

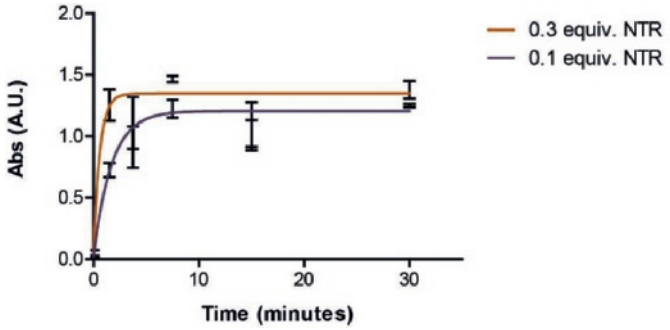

Figure SI-4. Activation of CCP(CNBz) followed over time. The activation using NTR was stopped by adding nicotinic acid (20 equiv. compared to NADH, which was used in a 50 times excess over CCP(CNBz)) at various time points, to replace the NADH necessary for NTR activity. Error bars are standard deviations calculated using GraphPad Prism.

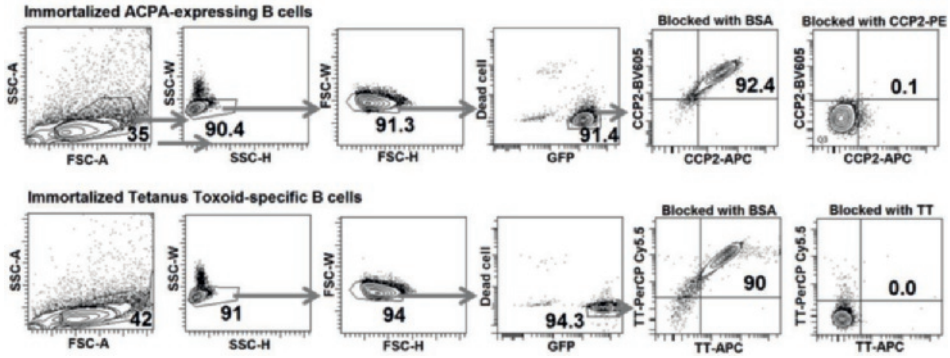

Figure SI-5. Antigen specificity of ACPA-expressing and anti-TT-specific B cell clones. Primary ACPA+ and anti-TT+ MBC were sorted and immortalized using lentiviral transduction with BCL-6 and BCL-XL. The immortalized ACPA-expressing B cell clone stained positive for CCP2-APC- and CCP2-BV605-tetramers and the signal can be blocked by pre-incubation with an excess of CCP2-PE-tetramer. Immortalized anti-TT-specific B cells stained positive for directly labelled TT-APC and TT-PE; the signal can be blocked by pre-incubation with an excess of unlabeled TT.

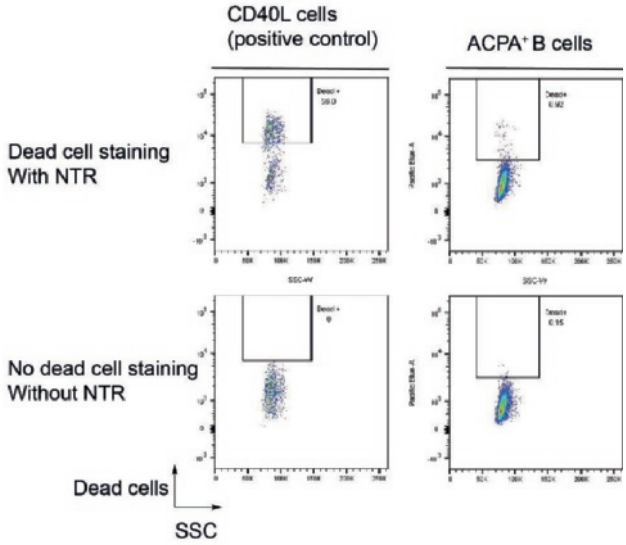

Figure SI-6. Less than one percent of ACPA-expressing B cells was positive for dead cell staining when incubated with NTR at 37 °C for 1 h. As a positive control, over fifty percent of the CD40L cells (cultured with ACPA-expressing cells) stained positive for death cells. This shows that NTR on its own is not toxic for B cells within 1 hour.

Chapter 3

Selective Activation of ACPA Recognition Peptides by Iminosydnone Click-to-Release Reactions

Abstract

Rheumatoid arthritis (RA) is an autoimmune disease affecting ca. 1% of the Western population. Autoantibodies against citrullinated proteins (ACPA) are prevalent in RA patients and eliminating the ACPA-producing B cells would be a promising strategy for the treatment of RA. Here we aim to develop an antigen-drug conjugate which is caged to prevent undesired binding to circulating antibodies. By selective activation of the recognizing antigen at the autoreactive B cell membrane, we envision to enhance B cell receptor (BCR) binding only. After binding and internalization of the BCR, we envisioned that a conjugated toxin, monomethyl auristatin E (MMAE), becomes activated and induces apoptosis in an antigen selective manner. We showed in Chapter 2 that antigen-selective silencing and activation could be achieved using a specific enzyme-substrate combination. While enzymes are promising for activating multiple substrates, it is challenging to find orthogonal and non-immunogenic enzymes that can be used for *in vivo* applications. In this Chapter, we describe the possibility of using an alternative antigen activation strategy based on a so-called click-to-release reaction. We show that iminosydnones (Im) function as a potent caging group for the citrullines in antigen peptides, and that activation and liberation of the autoantigen can be achieved after the cycloaddition with dibenzocyclooctyne (DBCO). We conjugated the cyclic citrullinated peptide (CCP) antigen to MMAE and compared the cytotoxicity with CCP(Im)-MMAE and MMAE alone and observed no difference. As MMAE is a highly potent toxin, this suggests that monovalent antigen binding is not sufficient to induce receptor internalization that is required to induce MMAE-dependent cell death. The use of multivalent systems therefore seems essential for internalization- and antigen-dependent cell death strategies when applied to B cells.

3.1 Introduction

Rheumatoid arthritis (RA) is an autoimmune disease characterized by chronic inflammation of joint tissue and is more prevalent in women than in men.[1] Autoantibodies against citrullinated proteins are the key factor to sustained inflammation. Citrullination is a post-translational modification and results from the conversion of peptidyl arginine by peptidyl arginine deiminase (PAD) enzymes. Although this is a common process, many RA patients develop antibodies against these citrullinated proteins (ACPA). These ACPA are present years before the disease onset and therefore function as a relevant clinical marker to predict the development of RA.[2]

RA treatment is currently directed at decreasing inflammation, preventing joint and organ damage and reducing pain. Nonsteroidal anti-inflammatory drugs are drugs which ease RA symptoms, whereas disease-modifying antirheumatic drugs (DMARDs) such as methotrexate or hydroxychloroquin are drugs that reduces disease progression. These drugs however do no treat the origin of the disease, but are directed at addressing the symptoms.

Approximately 70-80% of RA patients are positive for ACPA, antibodies which are involved in chronic inflammation and cartilage damage. ACPA can bind to osteoclasts precursor cells and help them differentiate into bone-resorbing osteoclasts. These osteoclasts produce PAD enzymes, which are responsible for the citrullination of tissue in joints, especially vimentin.[3] More effector cells are attracted to this site and the inflammation becomes sustained. ACPA stimulate osteoclastogenesis and osteoclasts induce citrulline modifications, so the removal of ACPA can likely decrease bone resorption and cartilage loss. Since ACPA are produced by autoreactive B cells, they are a relevant target for specific RA therapy. Depletion of the entire B cell population by rituximab is beneficial,[4] however, as targeting is not restricted to the autoreactive B cell compartment this treatment leads to severe side effects such as immune deficiency against infectious agents.[5]

In Chapter 2 we described a strategy to target and eliminate autoreactive B cells selectively by using an autoantigen-drug conjugate. Since free circulating ACPA are present in very high concentrations (up to hundreds of μg/mL)[6] these can neutralize the autoantigen. We therefore suggested an approach to physically cage the autoantigen, to prevent binding to circulating ACPA, which can then be enzymatically removed in close proximity of B cells. Although we observed antigen-selective cell death using this approach, the use of an enzymatic activation strategy may be challenging *in vivo*. For example, to circumvent nonselective antigen activation by endogenous enzymes, orthogonal enzyme-substrate pairs are needed, and as these are often derived from other species, they may cause unwanted immune responses. To circumvent the use of enzymes, we here explore the use of a chemical activation strategy, which is bioorthogonal and provides full control of antigen-drug activation.

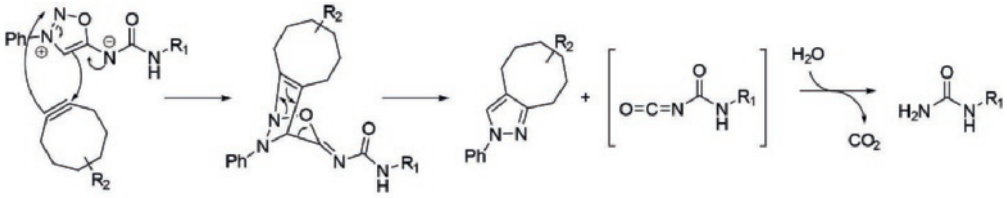

Figure 1. Proposed click-to-release antigen activation mechanism using an iminosydnone and a cyclooctyne.

The interest in so-called bioorthogonal click-to-release reactions for activation of protected (caged) biologically relevant molecules *in vivo* has increased significantly in the last years. Several bioorthogonal bond cleavage reactions have been developed,[7] including the tetrazine ligation with *trans*-cyclooctenes followed by a retro Diels-Alder reaction releasing an amine,[8] and the tetrazine ligation using vinyl ethers releasing an alkoxy moiety.[9, 10]

Very recently, Bernard *et al.* published an article on the use of iminosydnones in a fast-reacting bioorthogonal click-to-release reaction.[11] In this reaction, a cyclooctyne reacts in a [3+2] cycloaddition with an iminosydnone yielding an unstable tricyclic adduct, which rapidly dissociated into a cyclooctane-fused pyrazole and an isocyanate after a retro Diels-Alder reaction (Figure 1). Due to the reaction with water, this isocyanate degrades rapidly into CO_2 and a stable ureido moiety.

In this Chapter we describe the use of an iminosydnone as a caging group for citrulline to mask the binding to ACPA and ACPA-expressing B cells. We hypothesize that with the use of a cyclooctyne, such as DBCO, we can activate the citrulline-containing antigen peptide (cyclic citrullinated peptide, CCP). As suggested in Chapter 2, we aim to employ an antibody-directed targeting strategy, for example directed to CD20, to activate the ACPA antigen in close proximity to the B cell membrane (Figure 2).

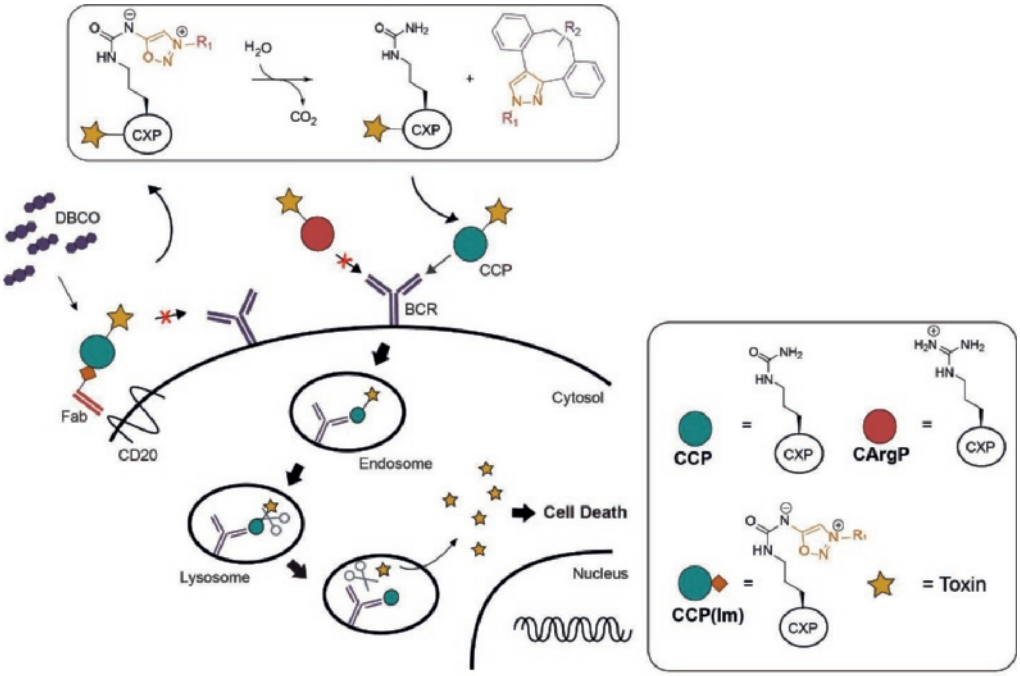

Figure 2. Schematic representation of the caging and activation strategy using iminosydnones. Iminosydnone (Im) functions as a linker between a targeting anti-CD20 Fab fragment and CCP. The caged antigen-drug conjugates do not have affinity for the BCR or ACPA, but after cycloaddition using DBCO the CCP peptide is liberated. After binding of the antigen-drug conjugate to the BCR, it will be internalized, cleaved in the cell and the liberated toxin can induce apoptosis.

To this end, we aim to use a Fab (antigen-binding site-containing) fragment for the targeting of CD20 instead of a full antibody, since Fab fragments are known to be less immunogenic than a full antibody, as the Fc part is lacking.[12] Our final aim is to prepare a conjugate containing both a CD20-targeting Fab fragment and the CCP peptide, linked via a cleavable iminosydnone. The iminosydnone-conjugated antigen is targeted to the B cell membrane and is cleaved upon addition of DBCO. The advantage of this strategy is that a large excess of DBCO can be used to cleave the iminosydnone and liberate the antigen. The antigen subsequently binds to the B cell receptor, which it is then internalized. As our first aim, we tested the approach in unconjugated form. For this, we prepared a CCP antigen that was caged on the citrulline with an iminosydnone moiety and modified on the C-terminus with a potent toxin. For activation purposes DBCO was used, which should lead to internalization and cleavage of the toxin and thereby inducing apoptosis.

3.2 Results and Discussion

Synthesis of Fmoc-Cit(Im)-OH and CCP(Im). We started the synthesis of the caged non-natural amino acid Fmoc-Cit(Im)-OH (**6**) with the preparation of the iminosydnone according to the reported literature procedure.[11] Aniline was reacted under basic conditions and elevated temperature with chloroacetonitrile providing 2-(phenylamino)acetonitrile (**1**) in quantitative yield (Scheme 1). This compound was reacted with isoamyl nitrite and subsequently cyclized with HCl in dioxane to yield sydnone **2**. Next, Fmoc-Orn(Cbz)-OH was converted into a *tert*-butyl ester and the Cbz moiety was removed from the δ-amine using hydrogen and Pd/C. In one pot, the free amine was reacted with triphosgene to create an isocyanate followed by the addition of iminosydnone **2** to form an ureido linkage between ornithine **4** and iminosydnone **2**. After removal of the *tert*-butyl ester of **5** using TFA in DCM, the target caged Fmoc-Cit(Im)-OH (**6**) was obtained and subsequently used in solid phase peptide synthesis (SPPS).

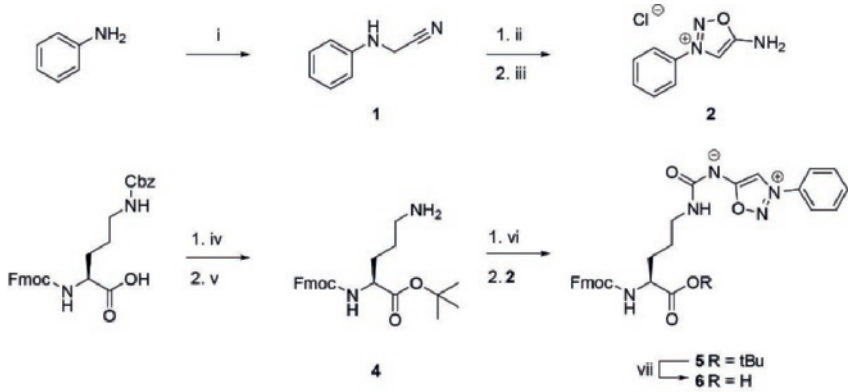

Scheme 1. Synthesis of Fmoc-Orn(Im)-OH (**6**). i) Chloroacetonitrile, acetonitrile, NaI, K_2CO_3, 3 h, reflux, quantitative; ii) amyl nitrite, diethyl ether, 20h, r.t.; iii) 4M HCl in dioxane, 24 h, 32% over two steps; iv) *tert*-butyl 2,2,2-trichloroacetimidate, BF_3 etherate, THF/hexane (1:1), overnight, 0 °C → r.t.; v) Pd/C, H_2, MeOH, 2 h, r.t., 80% over two steps; vi) 1. triphosgene, sat. $NaHCO_3$/DCM (1:1), 10 min, 0 °C. 2. Sydnone **2** was added, 3 h, 0 °C, 28% yield; vii) TFA/DCM (1:1), 2 h, r.t., quant.

We synthesized CCP(Im) (Figure 3A) using standard Fmoc-based SPPS while Fmoc-Cit(Im)-OH (**6**) was treated as a regular amino acid. After completion of the synthesis, chloroacetic anhydride was reacted with the N-terminus prior to cleavage from the resin. The peptide was then covalently cyclized by a substitution reaction of the internal cysteine onto the chloride in a basic solution. Biotin was coupled to the side chain of the C-terminal lysine for enzyme-linked immunosorbent assay (ELISA) purposes (Figure 3A). In a similar fashion, CArgP (**7**) and CCP (**8**) were synthesized as negative and positive control, respectively.

DBCO-mediated activation of CCP(Im). Having the biotinylated caged CCP and control peptides in hand (Figure 3A), we next explored the binding for ACPA with and without the addition of DBCO.

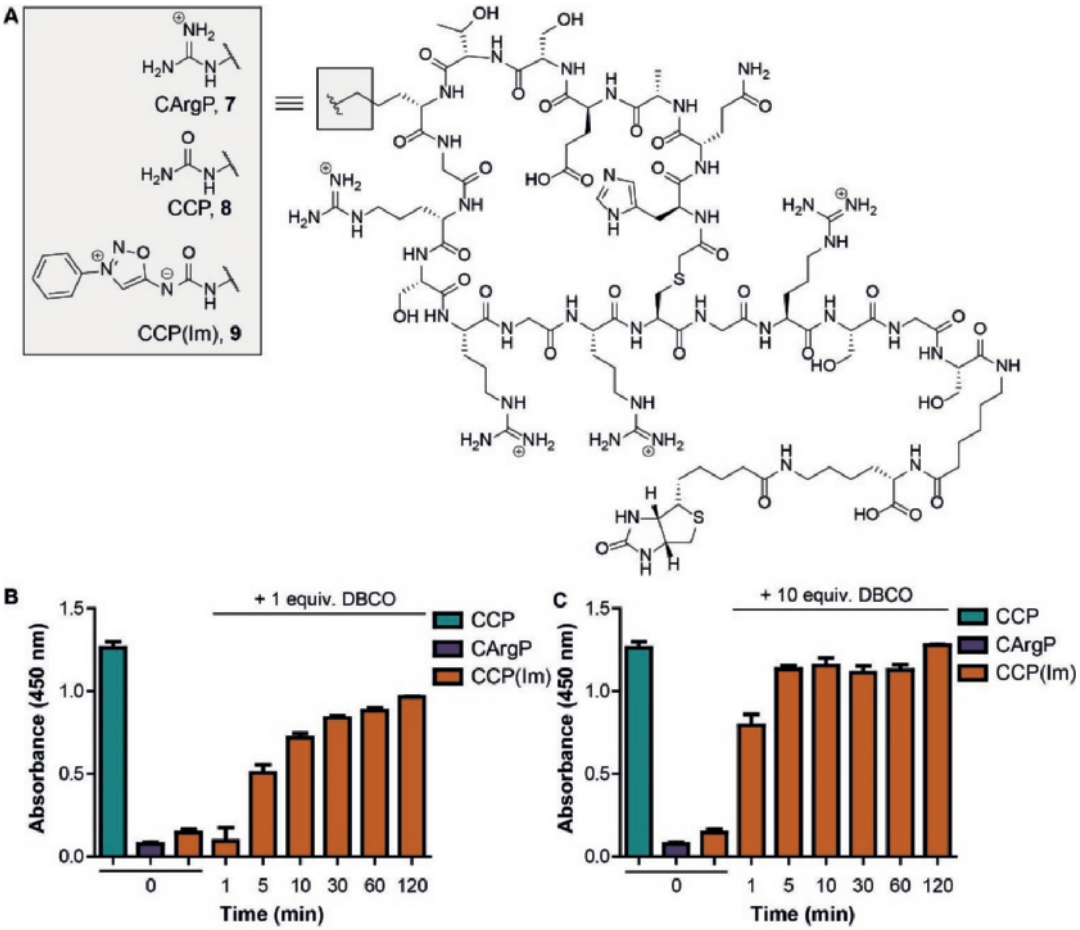

Figure 3. ACPA binding of caged CCP and the activation using DBCO. A) Structures of CArgP (**7**), CCP (**8**) and the iminosydnone-caged CCP (**9**). Biotin is used for conjugation purposes; B, C) ELISA using caged antigens detected by monoclonal ACPA. Incubation of the caged peptide over a time range at 37 °C with B) 1 equiv. DBCO or C) 10 equiv. DBCO. Absorbance at 450 nm.

To evaluate the rate of the iminosydnone cycloaddition, we treated CCP(Im) **9** with 1 equiv. or 10 equiv. of DBCO and measured the conversion over time at 37 °C. At specific time points, an excess benzyl azide (100 equiv. compared to DBCO) was added to quench the DBCO and thereby the reaction with the iminosydnone. The activated or untreated peptides were then added to a streptavidin-coated ELISA plate and incubated with monoclonal ACPA obtained from the supernatant of ACPA-producing immortalized B cells. Next, horseradish peroxidase (HRP)-conjugated secondary antibodies and a HRP substrate were added to provide information on the relative binding efficiency of the different peptides by measuring absorption.

Figure 3B shows the results of the ELISA of CCP(Im) when subjected to 1 and 10 equiv. of DBCO over time. Monoclonal ACPA did not bind CCP(Im) showing a similar absorption level as observed for the negative control peptide (CArgP, **7**). Immobilizing CCP confirmed ACPA binding, as expected. Addition of 1 equiv. of DBCO provided a time-dependent increase in binding within 2 hours at 37 °C, whereas the iminosydnone click-to-release reaction seemed complete after 5-10 minutes when using 10 equiv. of DBCO (Figure 3C).

To validate that the observed binding is specific to the activation by DBCO, we investigated the stability of the iminosydnone caged CCP (**9**) by dissolving the peptide in McIlvaine buffer[13] (a mixture of aqueous Na_2HPO_4 and citric acid) in the range from pH 4 to pH 9. We measured the sample using analytical HPLC up to 7 days, and calculated the area under the curve. Slight degradation was observed at pH 8 and 9, but the iminosydnone-caged CCP (**9**) proved to be stable for at least 7 days in acidic to neutral pH (Figure 4).

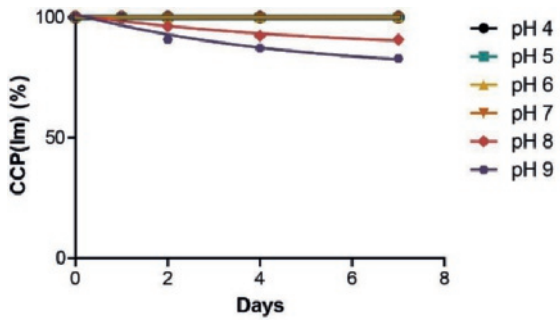

Figure 4. The stability of the iminosydnone caged CCP. Stability was tested in pH 4-9 (McIlvaine buffer) for 1-7 days at 37 °C and 600 rpm. The amount of CCP(Im) was determined by HPLC and was quantified by the area under the curve. The graph shows the relative amount compared to the amount of starting material.

To test whether the caging and activation of CCP(Im) (**9**) also worked in de proximity of B cells, we conjugated the biotinylated CXP antigens (with X being different amino acids) to fluorescently labelled streptavidin tetramers to visualize antigen binding to B cells by flow cytometry.[14] Two B cell clones derived from immortalized ACPA-expressing and anti-tetanus toxoid (TT) specific B cells were used for this purpose. The antigen specificity of the immortalized B cell clones is shown in Chapter 2 (Section 2.6, SI-5). Click-to-release activation was performed for 1 hour at 37 °C prior to the incubation with cells.

Figure 5 shows the data from the flow cytometric binding studies with all different peptide-streptavidin conjugates. Streptavidin contains allophycocyanin (APC) as a fluorophore and hence

binding of the antigen-streptavidin complex will result in a positive APC signal. All cells express also GFP and are therefore always GFP positive. For ACPA-expressing B cells (Figure 5A), no binding for TT is observed as expected, similar to CArgP and CCP(Im). All ACPA-expressing cells become positive for APC when CCP is bound, and this effect is seen for the CCP(Im) preincubated with 5 mM of DBCO (see Figure SI-1 for all DBCO concentrations). This shows that caging and activation of CCP(Im) is effective for ACPA-expressing B cells.

We further demonstrated that binding is specific for ACPA-expressing B cells, as no binding of either CCP or the activated CCP(Im) is observed for anti-TT-expressing B cells (Figure 5B). As expected, these cells are only positive for TT, the cognate antigen for these immortalized B cells.

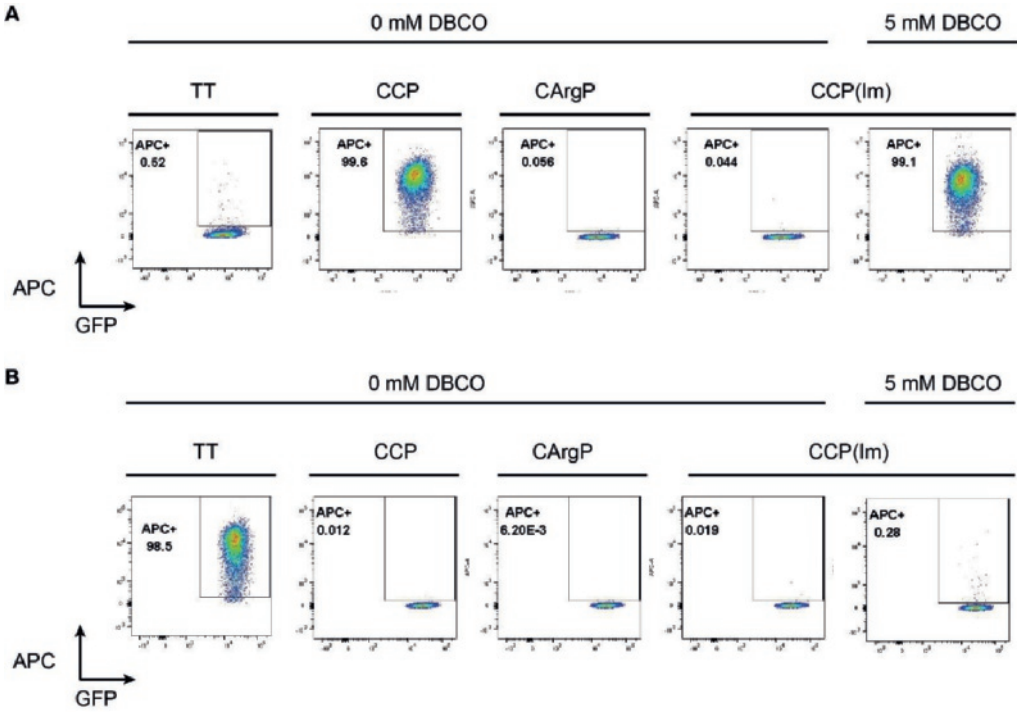

Figure 5. Flow cytometric binding studies of streptavidin-coupled, biotinylated CCP, CArgP, and (activated) CCP(Im) to A) an ACPA-expressing B cell clone and B) an anti-TT-specific B cell clone. Activation of CCP(Im) was performed using 5 mM DBCO for 1 h at 37 °C, before addition to the cells.

Synthesis and activity of MMAE-conjugated ACPA antigens. To show that we can induce selective cell death depending on the antigen used, we next attached a toxin, monomethyl auristatin E (MMAE), to the C-terminal lysine of the peptides. MMAE is a highly potent antimitotic drug, which inhibits cell division by caging the polymerization of tubulin.[15] Due to its potency, MMAE is often used as drug conjugated to monoclonal antibodies (mAb) for selective cell targeting, showing effectiveness in preclinical studies against certain tumors.[16] MMAE is often conjugated to mAb via a maleimide coupling, containing a Val-Cit motif and a cleavable linker (Figure 6). Due to this Val-Cit motif, cathepsin B can cleave this linker inside lysosomes and induce 1,6-elimination of the *para*-aminobenzyl carbamate (PAB) spacer thereby releasing the conjugated cargo.[17, 18]

Here, we aim to exploit the same cleavage mechanism by attaching the commercially available maleimide-functionalized MMAE toxin (maleimide-Val-Cit-PAB-MMAE) to CXP antigens. The binding of this antigen will then induce B cell receptor (BCR) internalization and hence access to cathepsin B to liberate MMAE.

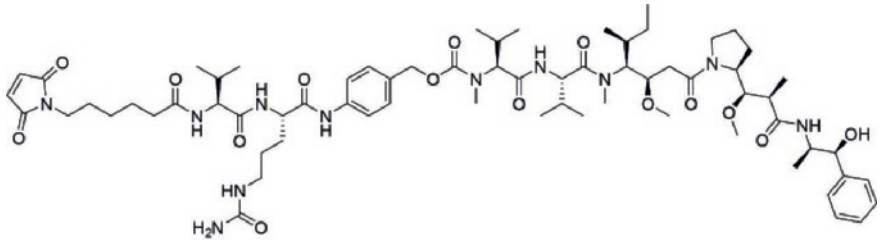

Figure 6. Structure of maleimide-Val-Cit-PAB-MMAE.

Since our CXP antigens do not contain a free thiol group needed for the reaction with a maleimide, we first synthesized a small thiol-containing linker that could be attached to the C-terminal lysine. For this, thioglycolic acid was first protected with a trityl group (compound **10**) and the carboxylic acid was subsequently activated with a hydroxysuccinimide.[19] (**11**, Scheme 2)

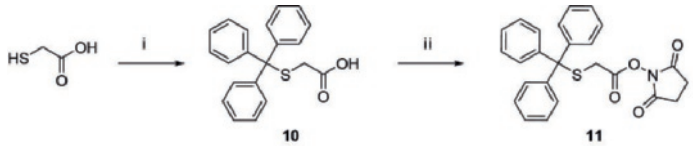

Scheme 2. Reaction scheme for the synthesis of NHS ester **11**.[19] i) Trityl chloride, BF_3 etherate, DCM/AcOH (1:1), 30 min, r.t., 85%; ii) NHS, EDC-HCl, MeCN, 2 h, r.t., 70%.

We synthesized the CXP peptides as described previously, while retaining the C-terminal lysine for further modification. After cleavage from the resin, the peptides were cyclized, purified (antigen peptides **12a-14a**, Figure 7) and subjected to NHS ester **11**. While CArgP was used as a negative control in Chapter 2, we here use CNleP because we observed lower background using this norleucine peptide compared to arginine (see Chapter 5). After reaction with NHS ester **11**, the trityl group was removed using TFA and the peptides were subsequently purified by preparative HPLC (antigen peptides **12b-14b**). Next, the purified peptides were treated for 1 hour with TCEP on resin to reduce potential oxidized cysteines, and finally incubated with maleimide-Val-Cit-PAB-MMAE for 24 hours at room temperature to yield the MMAE-conjugated CXP antigens (antigen peptides **12c-14c**).

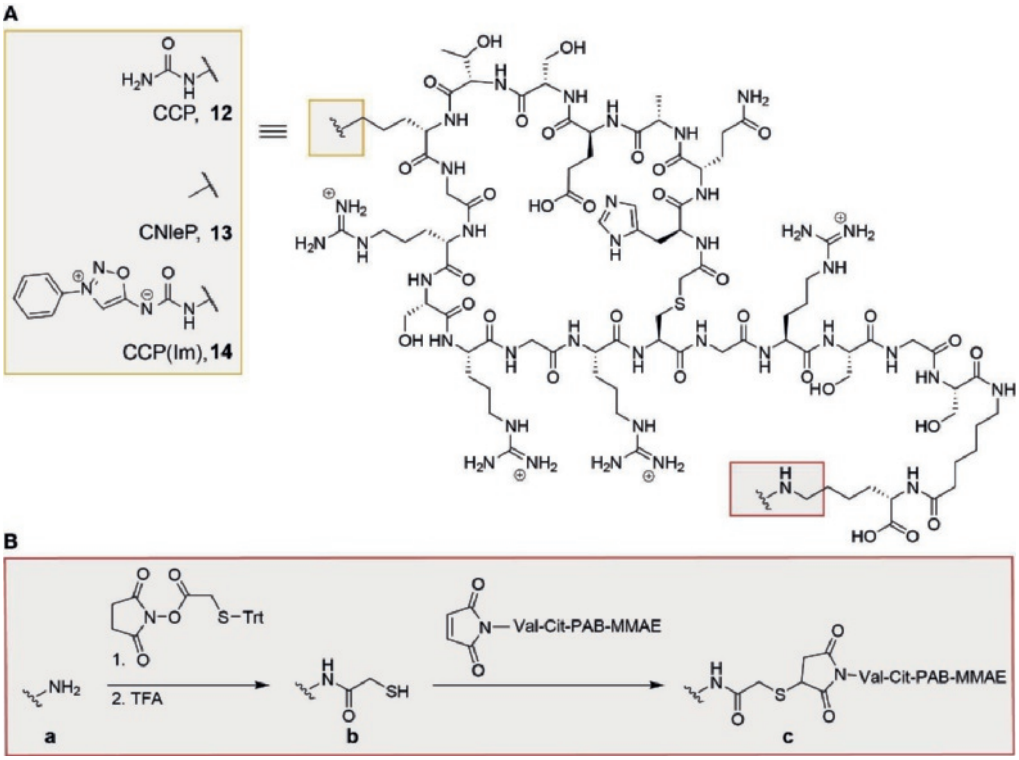

Figure 7. Synthesis of MMAE containing peptides **12-14**. A) The side chains are depicted with CCP as positive control, CNleP as negative control and CCP(Im) as the caged and activatable antigen; B) Schematic representation of the synthesis steps towards the toxin-functionalized antigen peptides. All lysine peptides **12a-14a** were reacted with NHS ester **11**. The trityl linker was removed using TFA to yield thiol-containing peptides **12b-14b** after purification. Treatment with TCEP was performed for 1 hour before the maleimide-Val-Cit-PAB-MMAE was added yielding the final antigen-drug conjugates **12c-14c**.

Antigen-dependent selective cellular targeting and cytotoxicity. Having the antigen-drug conjugates in hand, we examined the cytotoxicity and selective activation of CXP in close proximity of B cells. We first measured the selective cytotoxicity to ACPA- and anti-TT-positive B cells with peptides **12c-14c** and MMAE alone. We mixed the cells with varying CXP-MMAE concentrations and incubated the cells at 37 °C for 3 days before evaluating cell viability in a XTT assay.

Figure 8A shows the dose response curves for all peptide-MMAE conjugates incubated with ACPA-positive B cells. MMAE shows dose-dependent toxicity to ACPA-positive B cells. Unexpectedly, no difference was observed when MMAE was conjugated to CCP (**12c**, positive control) as compared to CNleP (**13c**, negative control). Since MMAE is only toxic after internalization and cleavage of the Val-Cit sequence,[20] we expected a lower cytotoxicity for the CNleP-MMAE conjugate due to the lack of BCR binding. The addition of iminosydnone to CCP (**14c**) also did not affect the cytotoxicity of MMAE. Moreover, all peptide conjugates showed similar cytotoxicity as MMAE alone, meaning that the cytotoxicity is not antigen-dependent, but may be due to unselective uptake of MMAE. A similar result was observed for the anti-TT-positive

B cells (Figure 8B). The results demonstrate that the observed cytotoxicity is independent of the conjugated antigen, which may be due to the monovalent structure of the peptide-MMAE conjugates or to the mechanism of MMAE toxin itself.

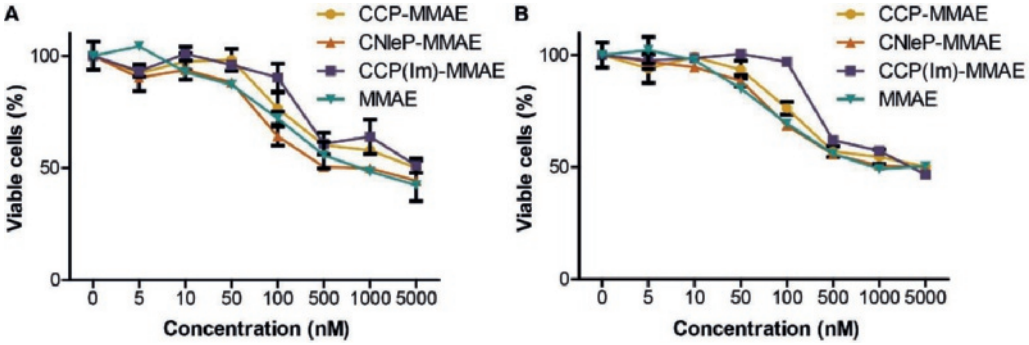

Figure 8. Cytotoxicity assay using antigen-MMAE conjugates for A) ACPA-positive B cells, and B) anti-TT-positive B cells. Different concentrations of peptide-MMAE conjugates were tested for cytotoxicity. MMAE alone was also tested as the control for no antigen-specificity. Cell viability was measured using an XTT assay. MMAE showed to be cytotoxic in a dose-dependent manner, but no difference was observed when any of the antigen peptides was added.

3.3 Conclusions and Outlook

In this Chapter we have shown the synthesis of an iminosydnone-modified citrulline building block and the incorporation of this non-natural amino acid into a peptide. The iminosydnone functioned as a caging group for the citrulline-containing CCP antigen, which was validated by its lack of binding to both ACPA and ACPA-expressing B cells. By the addition of DBCO, we showed that a cycloaddition and subsequent release reaction liberated the CCP antigen. By the use of 10 equiv. of DBCO, the reaction was already complete within 5-10 minutes at 37 °C. After the release of CCP we showed that binding to ACPA and ACPA-expressing B cells was restored, to the same extent as the regular CCP peptide, demonstrating that full activation was achieved using this click-to-release reaction.

We next synthesized a set of antigen peptides conjugated to the MMAE toxin, with the ultimate goal to activate the antigens in close proximity of the B cell membrane for enhanced specificity. However, the cytotoxicity of peptide-MMAE conjugates proved not antigen-selective and similar cytotoxicity was observed for the positive and negative control peptides. It seems that the monovalent antigen binds insufficiently to the BCR or that the BCR was not internalized due to the lack of receptor clustering. The minimum level of BCR signaling required for antigen internalization is still unclear.[21] Although it was shown that inducing BCR clustering is possible using a monovalent peptide in a specific case,[22] possibly more signals are needed in general to overcome a threshold to elicit downstream BCR signaling and BCR clustering.[21] One example to bypass this specificity threshold concerning our autoantigen is by using agents capable of BCR crosslinking. Reagents directed to the constant region of IgG (such as anti-IgG) crosslink the BCR by bringing BCRs in close proximity.[21] Such strategies may be adopted in future studies.

Alternatively the use of a multivalent system (such as streptavidin described in Chapter 2) would induce receptor clustering and selective targeting of the antigen-MMAE conjugates. Hence, we

aim to produce multivalent antigen-MMAE conjugates in the future, to test the DBCO activation in the vicinity of ACPA-positive B cells. Local antigen activation can be achieved when DBCO is localized to the B cell membrane using *e.g.* Fab fragment conjugates. Since more DBCO might be needed locally to deprotect the multimeric CCP(Im), we will also explore the possibility to make a multivalent Fab-DBCO conjugate. Other possibilities to create high local DBCO concentrations may be achieved, for example, by using DBCO-infused polymeric gels.[23, 24] For such a strategy, hydrogels excreting DBCO can be injected locally in the site of inflammation or in lymph nodes, locations where autoreactive B cells are found, to activate antigens (see Chapter 7).

Finally, we are interested in using a single conjugate of the anti-CD20 Fab fragment attached to the iminosydnone caging group on the CCP antigen peptide. When a biotin is attached to the CCP antigen, this conjugate can bind a streptavidin-toxin thereby creating a multivalent dual targeting strategy. We have successfully demonstrated in Chapter 2 that a similar strategy ensures antigen-selective B cell cytotoxicity. By creating such a streptavidin anti-CD20 Fab-CCP conjugate, the Fab fragment and CCP are simultaneously targeted to the B cell membrane allowing selective antigen activation in close proximity of the B cell membrane by using an excess of DBCO (see also Chapter 7).

3.4 Acknowledgements

Mike Smeenk is kindly acknowledged for synthesizing compounds **1-14**. Hendy Kristyanto (Leiden University Medical Centre) is kindly acknowledged for the flow cytometry data and the cytotoxicity study.

3.5 Materials and Methods

For general methods, see the materials and methods section of Chapter 2 (paragraph 2.4).

2-(Phenylamino)acetonitrile (1). To a mixture of aniline (4.56 mL, 50 mmol, 1.0 equiv.) in dry acetonitrile (50 mL) NaI (7.5 g, 50 mmol, 1.0 equiv.), K_2CO_3 (6.9 g, 50 mmol, 1 equiv.) and chloroacetonitrile (3.36 mL, 53 mmol, 1.1 equiv.) were added. This mixture was refluxed under nitrogen for 3 h. The solids were filtered off and the filtrate was partitioned between ethyl acetate/water. The organic layer was separated, washed with brine, dried with $MgSO_4$ and purified on a silica column (30% EtOAc in heptane) yielding compound **1** as a yellow oil (6.46 g, quant.). R_f = 0.42 (30% EtOAc in heptane). ^{1}H-NMR (400 MHz, DMSO-d_6) δ 7.18-7.16 (m, 2H), 6.72-6.69 (m, 3H), 4.24 (s, 2H). ^{13}C-NMR (100 MHz, DMSO-d_6) δ 146.55, 129.03(2C), 118.62, 117.85, 113.00 (2C), 31.42. LRMS (ESI+): m/z calcd for $C_8H_9N_2^+$ $[M+H]^+$ 133.1, found: 133.2. The data corresponds to the reported literature values.[11]

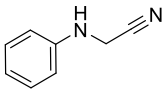

5-Amino-3-phenyl-1,2,3-oxadiazol-3-ium chloride (2). Compound **1** (2.36 g, 20 mmol, 1.0 equiv.) was added to diethyl ether (40 mL). To this mixture, amyl nitrite (4.04 mL, 60 mmol, 3.0 equiv.) was slowly added. This was stirred for 20 h at room temperature. Afterwards, 4M HCl in dioxane (38 mL) was added and stirred for 24 h. The product was obtained via filtration and trituration in methanol

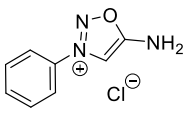

by addition of diethyl ether yielding compound **2** as a salt (1.26 g, 32%). ^{1}H-NMR (400 MHz, DMSO-d_6) δ 10.08 (s, 2H), 8.68 (s, 1H), 8.07-8.05 (m, 2H), 7.84-7.74 (m, 3H). ^{13}C-NMR (100 MHz, DMSO- d_6) δ 169.90, 134.02, 133.28, 130.84 (2C), 123.14 (2C), 102.72. LRMS (ESI+): m/z calcd for $C_8H_8N_3O$ [M-Cl$^-$] 162.1, found: 162.1. The data corresponds to the reported literature values.[11]

Fmoc-Orn(Cbz)-OtBu (3). Fmoc-Orn(Cbz)-OH (1.73 g, 3.7 mmol, 1.0 equiv.) was dissolved in THF/Hexane (30 mL, 1:1). This was cooled down to 0 °C and afterwards *tert*-butyl 2,2,2-trichloroacetimidate (1.32 mL, 7.4 mmol, 2.0 equiv.) was added. This was stirred for 15 min and then BF_3 etherate (228 uL, 1.8 mmol, 0.5 equiv.) was added to the mixture and the reaction was stirred overnight at room temperature. The product was obtained via column chromatography using a gradient of EtOAc in heptane (0% to 40%). R_f = 0.30 (30% EtOAc in heptane). ^{1}H NMR (500 MHz, MeOH-d_4) δ 7.79 (d, J = 7.5 Hz, 2H), 7.67 (t, J = 7.0 Hz, 2H), 7.39 (t, J = 7.4 Hz, 2H), 7.37 – 7.26 (m, 7H), 5.49 (s, 2H), 5.08 (s, 2H), 4.37 (qd, J = 10.6, 7.1 Hz, 2H), 4.22 (t, J = 6.8 Hz, 1H), 4.06 (dd, J = 8.6, 5.0 Hz, 1H), 3.15 (t, J = 6.7 Hz, 2H), 1.89 – 1.61 (m, 2H), 1.59 (d, J = 6.5 Hz, 2H), 1.46 (s, 9H). ^{13}C NMR (126 MHz, MeOH-d_4) δ 171.88, 157.50, 157.19, 143.92, 143.76, 141.18 (2C), 137.01, 128.06 (2C), 127.54 (2C), 127.38 (3C), 126.77 (2C), 124.86 (2C), 119.53 (2C), 81.36, 66.49, 65.96, 54.57, 47.04, 39.92, 28.55, 26.90 (3C), 26.00. HRMS (ESI+) m/z calcd for $C_{32}H_{36}N_2NaO_6^+$ [M+Na]$^+$ 567.24711, found 567.24580.

Fmoc-Orn-OtBu (4). Fmoc-Orn(Cbz)-OtBu was dissolved in methanol (40 mL). To this palladium on activated carbon (40 mg, 0.14 mmol) was added. The flask was then closed and H_2 was bubbled through while stirring till completion. The product was filtrated over celite and obtained via column chromatography in 10% methanol in DCM (1.20 g, 80% yield over two steps). R_f = 0.23 (10% MeOH in DCM). ^{1}H NMR (500 MHz, MeOH-d_4) δ 7.78 (d, J = 7.5 Hz, 2H), 7.66 (t, J = 7.8 Hz, 2H), 7.38 (t, J = 7.4 Hz, 2H), 7.30 (t, J = 7.4 Hz, 2H), 6.25 (s, 1H), 4.89 (s, 2H), 4.42 (dd, J = 10.6, 6.8 Hz, 1H), 4.31 (dd, J = 10.6, 6.8 Hz, 10H), 4.20 (t, J = 6.9 Hz, 1H), 4.06 (t, J = 8.8 Hz, 1H), 2.95 (t, J = 7.1 Hz, 1H), 1.95 – 1.83 (m, 1H), 1.74 (dt, J = 16.6, 8.9 Hz, 3H), 1.46 (s, 9H). ^{13}C NMR (126 MHz, MeOH-d_4) δ 171.36, 157.29, 143.75 (2C), 141.20 (2C), 127.42 (2C), 126.79 (2C), 124.80 (2C), 119.57 (2C), 81.66, 66.59, 54.28, 46.99, 38.92, 28.15, 26.89 (3C), 23.85. HRMS (ESI+) m/z calcd for $C_{24}H_{31}N_2O_4^+$ [M+H]$^+$ 411.228383, found 411.22757. $C_{24}H_{30}N_2NaO_4^+$ [M+Na]$^+$ 433.21033, found 433.20943.

Fmoc-Cit(Im)-OtBu (5). Compound **4** (721 mg, 1.8 mmol, 1.0 equiv.) was dissolved in 8 mL DCM and sat. $NaHCO_3$ (1:1) and cooled down to 0 °C. Whilst stirring vigorously, triphosgene (174 mg, 0.59 mmol, 0.3 equiv.) was added and stirred was continued for 10 minutes. Afterwards, compound **2** (348 mg, 1.8 mmol, 1 equiv.) was added and the reaction was stirred at 0 °C until completion. The reaction was quenched with brine and the compound was purified by column chromatography (60% EtOAc/heptane to 100% EtOAC) to yield compound **5** (290 mg, 28% yield). R_f = 0.30 (100% EtOAc). ^{1}H NMR (500 MHz, MeOH-d_4) δ 8.00 (d, J = 8.1 Hz, 1H), 7.91 (d, J = 7.9 Hz, 1H), 7.83 – 7.61 (m, 6H), 7.34 (dq, J = 35.2, 7.4 Hz, 5H), 4.41 – 4.32 (m, 2H), 4.22 (t, J = 7.0 Hz, 1H), 4.07 (dd, J = 8.6, 4.9 Hz, 1H), 3.47 – 3.35 (m,

1H), 3.23 (t, *J* = 6.9 Hz, 1H), 1.90 – 1.79 (m, 1H), 1.76 – 1.65 (m, 2H), 1.65 – 1.57 (m, 1H), 1.45 (s, 9H) (1 proton missing). ^{13}C-NMR (100 MHz, MeOH-*d*$_4$) 171.98, 157.22, 143.89 (2C), 141.16 (2C), 132.63, 130.09 (2C), 127.36 (2C), 126.65 (2C), 124.85 (2C), 121.72 (2C), 119.43 (2C), 104.99, 81.29, 66.50, 54.64, 47.04, 39.39, 28.60, 26.86 (3C), 26.18 (2 carbons missing). HRMS (ESI+) *m*/*z* calcd for $C_{33}H_{36}N_5O_6^+$ [M+H]$^+$ 598.266560, found 598.26471.

Fmoc-Cit(Im)-OH (6). Compound **5** (500 mg, 0.84 mmol) was dissolved in 5 mL DCM. TFA (5 mL) was slowly added and the resulting solution was stirred for 2 h. The solvents were removed via evaporation and complete removal of TFA was realized by co-evaporation with DCM (3 x). The product was then lyophilized and obtained as a pure dark yellow solid (452 mg, quant.). R_f = 0.40 (5% MeOH, 1% AcOH in DCM). ^{1}H NMR (500 MHz, MeOH-*d*$_4$) δ 8.01 (d, *J* = 7.8 Hz, 1H), 7.84 (t, *J* = 7.0 Hz, 1H), 7.79 – 7.71 (m, 4H), 7.65 (t, *J* = 7.0 Hz, 2H), 7.32 (dt, *J* = 34.3, 7.4 Hz, 5H), 4.33 (dd, *J* = 15.5, 7.2 Hz, 2H), 4.25 – 4.13 (m, 2H), 3.32 (d, *J* = 5.8 Hz, 1H), 3.17 (dq, *J* = 37.1, 7.1 Hz, 1H), 2.01 – 1.88 (m, 1H), 1.81 – 1.62 (m, 2H). (1 proton missing). ^{13}C NMR (126 MHz, MeOH-*d*$_4$) δ 174.27, 157.27, 143.85 (2C), 141.12 (2C), 134.00, 132.99, 130.45 (2C), 127.38 (2C), 126.77 (2C), 124.87 (2C), 122.30 (2C), 119.50 (2C), 106.74, 83.51, 66.72, 53.51, 47.00, 39.44, 28.52, 25.72. (1 carbon missing). HRMS (ESI+) *m*/*z* calcd for $C_{29}H_{28}N_5O_6^+$ [M+H]$^+$ 542.203960, found 542.20316. *m*/*z* calcd for $C_{29}H_{27}N_5NaO_6^+$ [M+Na]$^+$ 620.24850, found 620.24681.

2-(Tritylthio)acetic acid (10). Thioglycolic acid (1.8 mL, 26 mmol, 1 equiv.) was dissolved in DCM/AcOH (1:1, 24 mL) and trityl chloride (7.20 g, 26 mmol, 1 equiv.) was added. BF_3 etherate (2 mL, 13 mmol, 0.5 equiv.) was added dropwise and the reaction was stirred for 30 minutes at room temperature. Afterwards, the volatiles were evaporated and water (10 mL) was added. The product was obtained by extraction with EtOAc (3 x 30 mL), drying with $MgSO_4$ and removing the EtOAc *in vacuo* to yield a white powder (7.29 g, 85%). R_f = 0.36 (10% MeOH in DCM). ^{1}H NMR (400 MHz, chloroform-*d*) δ 7.46 – 7.36 (m, 6H), 7.32 – 7.26 (m, 6H), 7.25 – 7.19 (m, 3H), 3.02 (s, 2H). ^{13}C-NMR(100 MHz, chloroform-*d*) δ 173.05, 145.60(3C), 130.68 (6C), 129.02 (6C), 127.99 (3C), 68.09, 35.69. LRMS (ESI+): cannot be found with ESI. The data corresponds to reported literature values.[19]

2,5-Dioxopyrrolidin-1-yl 2-(tritylthio)acetate (11). Compound **10** (5.00 g, 15 mmol, 1.0 equiv.) was dissolved in acetonitrile (20 mL) and to this *N*-hydroxysuccinimide (1.72 g, 15 mmol, 1.0 equiv.) and EDC-HCl (3.16 g, 17 mmol, 1.1 equiv.) were added. The mixture was stirred for 2 h at room temperature. The mixture was then left at -20 °C for 1 h to form crystal seeds and transferred to the fridge to precipitate overnight. The precipitate was collected to yield a white powder (4.58 g, 70% yield). R_f = 0.50 (50% EtOAc in heptane). ^{1}H NMR (400 MHz, chloroform-*d*) δ 7.43 – 7.39 (m, 6H), 7.34 – 7.28 (m, 6H), 7.26 – 7.21 (m, 3H), 3.18 (s, 2H), 2.80 (s, 4H). ^{13}C-NMR (100 MHz, chloroform-*d*) δ 168.60, 165.08, 143.56 (3C), 129.51 (6C), 128.25 (6C), 127.16 (3C), 68.06, 31.44, 25.56 (2C). LRMS (ESI+): cannot be found with ESI. The data corresponds to the reported literature values.[19]

General peptide synthesis and cyclization method. See the materials and methods section of Chapter 2 (paragraph 2.4).

CArgP-biotin (7). CArgP was synthesized following the procedures described in the general peptide synthesis Section 2.4. Next, this peptide was cyclized and purified as described in the general cyclization method. HPLC: Rt. 12.731 min. LCMS (ESI+) m/z calcd for $C_{100}H_{172}N_{42}O_{33}S_2^{2+}$ $[M+2H]^{2+}$ 1277.13, found 1277.56. $C_{100}H_{172}N_{41}O_{34}S_2^{3+}$ $[M+3H]^{3+}$ 851.75, found 852.28. $C_{100}H_{173}N_{41}O_{34}S_2^{4+}$ $[M+4H]^{4+}$ 639.06, found 640.20.

CCP-biotin (8). CCP was synthesized following the procedures described in the general peptide synthesis Section 2.4. Next, this peptide was cyclized and purified as described in the general cyclization method. HPLC: Rt. 12.753 min. LCMS (ESI+) m/z calcd for $C_{100}H_{171}N_{41}O_{34}S_2^{2+}$ $[M+2H]^{2+}$ 1277.61, found 1278.08. $C_{100}H_{172}N_{41}O_{34}S_2^{3+}$ $[M+3H]^{3+}$ 852.07, found 852.68. $C_{100}H_{173}N_{41}O_{34}S_2^{4+}$ $[M+4H]^{4+}$ 639.31, found 641.16.

CCP(Im)-biotin (9). CCP(Im) was synthesized following the procedures described in the general peptide synthesis Section 2.4. Next, this peptide was cyclized and purified as described in the general cyclization method. HPLC: Rt. 13.867 min. LCMS (ESI+) *m/z* calcd for $C_{108}H_{176}N_{43}O_{35}S_2^{2+}$ $[M+2H]^{2+}$ 1349.63, found 1349.64. $C_{108}H_{177}N_{43}O_{35}S_2^{3+}$ $[M+3H]^{3+}$ 900.09, found 900.20. $C_{108}H_{178}N_{43}O_{35}S_2^{4+}$ $[M+4H]^{4+}$675.32, found 675.72.

CCP-Lys (12a). CCP-Lys was synthesized following the procedures described in the general peptide synthesis Section 2.4. Next, this peptide was cyclized and purified as described in the general cyclization method. HPLC: Rt. 10.209 min. LCMS (ESI+) m/z calcd for $C_{90}H_{157}N_{39}O_{32}S^{2+}$ $[M+2H]^{2+}$ 1164.08, found 1163.00. $C_{90}H_{158}N_{39}O_{32}S^{3+}$ $[M+3H]^{3+}$ 776.39, found 776.92. $C_{90}H_{159}N_{39}O_{32}S^{4+}$ $[M+4H]^{4+}$ 582.54, found 583.00.

CNleP-Lys (13a). CNleP-Lys was synthesized following the procedures described in the general peptide synthesis Section 2.4. Next, this peptide was cyclized and purified as described in the general cyclization method. HPLC: Rt. 12.054 min. LCMS (ESI+) m/z calcd for $C_{90}H_{157}N_{37}O_{31}S^{2+}$ $[M+2H]^{2+}$ 1142.08, found 1142.88. $C_{90}H_{158}N_{37}O_{31}S^{3+}$ $[M+3H]^{3+}$ 761.72, found 762.68. $C_{90}H_{159}N_{37}O_{31}S^{4+}$ $[M+4H]^{4+}$ 571.54, found 573.68.

CCP(Im)-Lys (14a). CCP(Im)-Lys was synthesized following the procedures described in the general peptide synthesis Section 2.4. Next, this peptide was cyclized and purified as described in the general cyclization method. HPLC: Rt. 12.185. LCMS (ESI+) *m/z* calcd for $C_{98}H_{161}N_{41}O_{33}S^{2+}$ $[M+2H]^{2+}$ 1236.83, found 1236.72. $C_{98}H_{162}N_{41}O_{33}S^{3+}$ $[M+3H]^{3+}$ 824.88, found 825.16. $C_{98}H_{163}N_{41}O_{33}S^{4+}$ $[M+4H]^{4+}$ 618.92, found 619.12. $C_{98}H_{164}N_{41}O_{33}S^{5+}$ $[M+5H]^{5+}$ 495.33, found 495.60. $C_{98}H_{165}N_{41}O_{33}S^{6+}$ $[M+6H]^{6+}$ 412.94, found 412.96.

General linker attachment protocol. The peptide (**12a**-**14a**) (1 equiv.) was dissolved in DMF (2 mL) and DIPEA (100 equiv.). To this mixture was added **11** (1 equiv.) in DMF and the resulting mixture was stirred for 2 h. The peptide was then precipitated in diethyl ether, collected and dried. A cleavage mixture of TFA/TIS/EDT/H_2O (92.5:2.5:2.5:2.5) was added and left to shake for 2

h. The peptide was precipitated in diethyl ether, collected and lyophilized. The crude peptide was then purified using preparative HPLC (see Chapter 2 for specifics).

CCP-SH (12b). HPLC: Rt. 12.405. LCMS (ESI+) *m/z* calcd for $C_{92}H_{159}N_{39}O_{33}S_2^{2+}$ $[M+2H]^{2+}$ 1201.82, found 1201.60. $C_{98}H_{162}N_{41}O_{33}S^{3+}$ $[M+3H]^{3+}$ 801.54, found 801.48. $C_{98}H_{163}N_{41}O_{33}S^{4+}$ $[M+4H]^{4+}$ 601.41, found 601.52. $C_{98}H_{164}N_{41}O_{33}S^{5+}$ $[M+5H]^{5+}$ 481.33, found 481.48

CNleP-SH (13b). HPLC: Rt. 13.166. LCMS (ESI+) *m/z* calcd for $C_{92}H_{159}N_{37}O_{32}S_2^{2+}$ $[M+2H]^{2+}$ 1179.76, found 1179.68. $C_{92}H_{160}N_{37}O_{32}S_2^{3+}$ $[M+3H]^{3+}$ 786.84, found 786.84. $C_{92}H_{161}N_{37}O_{32}S_2^{4+}$ $[M+4H]^{4+}$ 590.38, found 590.40. $C_{92}H_{162}N_{37}O_{32}S_2^{5+}$ $[M+5H]^{5+}$ 472.52, found 472.76.

CCP(Im)-SH (14b). HPLC: Rt. 13.719. LCMS (ESI+) *m/z* calcd for $C_{100}H_{163}N_{41}O_{34}S_2^{2+}$ $[M+2H]^{2+}$ 1273.88, found 1273.44. $C_{98}H_{164}N_{41}O_{33}S^{2+}$ $[M+3H]^{3+}$ 849.59, found 849.64. $C_{98}H_{165}N_{41}O_{33}S^{2+}$ $[M+4H]^{4+}$ 637.44, found 637.32. $C_{98}H_{166}N_{41}O_{33}S^{2+}$ $[M+5H]^{5+}$ 510.15, found 510.36.

General maleimide coupling protocol. Peptides **12b**-**14b** were treated with Piercer™ TCEP reducing gel for 1 h at room temperature in milliQ (750 μL). The gel was centrifuged and the supernatant was collected. The gel was washed two times with milliQ (250 μL), and this was combined with the first supernatant. To the peptide solution MC-Val-Cit-PAB-MMAE dissolved in DMSO (10 mM, 0.75 equiv.) was added. The suspension was shaken overnight at room temperature. The peptides were purified using a reversed phase preparative HPLC using an acetonitrile/water gradient (5-100%, 1-45 min).

CCP-MMAE (12c) HPLC: Rt. 19.187. LCMS (ESI+) *m/z* calcd for $C_{160}H_{265}N_{50}O_{48}S_2^{3+}$ $[M+3H]^{3+}$ 1240.43, found 1240.16. $C_{160}H_{266}N_{50}O_{48}S_2^{4+}$ $[M+4H]^{4+}$ 930.57, found 930.48. $C_{160}H_{267}N_{50}O_{48}S_2^{5+}$ $[M+5H]^{5+}$ 744.66, found 744.44.

CNleP-MMAE (13c) HPLC: Rt. 19.018. LCMS (ESI+) *m/z* calcd for $C_{160}H_{265}N_{48}O_{47}S_2^{3+}$ $[M+3H]^{3+}$ 1225.76, found 1225.52. $C_{160}H_{266}N_{48}O_{47}S_2^{4+}$ $[M+4H]^{4+}$ 919.57, found 919.52. $C_{160}H_{267}N_{48}O_{47}S_2^{5+}$ $[M+5H]^{5+}$ 735.85, found 735.60.

CCP(Im)-MMAE (14c) HPLC: Rt. 19.108. LCMS (ESI+) *m/z* calcd for $C_{168}H_{269}N_{52}O_{49}S_2^{3+}$ $[M+3H]^{3+}$ 1288.47, found 1288.16. $C_{168}H_{270}N_{52}O_{49}S_2^{4+}$ $[M+4H]^{4+}$ 966.60, found 966.52. $C_{168}H_{271}N_{52}O_{49}S_2^{5+}$ $[M+5H]^{5+}$ 773.48, found 773.28. $C_{168}H_{272}N_{52}O_{49}S_2^{6+}$ $[M+5H]^{6+}$ 644.74, found 644.52.

CCP(Im) stability measurements at various pH. The peptide was dissolved in 1% DMSO/McIlvaine buffer (pH 4-9 at a concentration of 0.2 mg/mL). Aqueous Na_2HPO_4 was used for pH 9. The reaction was set at 37 °C at 600 rpm for 1-7 days. A sample was taken and measured by HPLC. The area under the curve of the chromatogram shows the percentage of starting material or degradation material (CCP).

ELISA experiments. In general, the CCP(Im)-biotin peptide (**9**) was dissolved in MilliQ with a final concentration of 1.25 mg/mL. The solution was divided in parts of 400 µL and transferred to 6 vials. A DBCO stock solution (10 equiv.) was prepared and a dilution was made to make a second stock solution (1 equiv.). In a similar manner, the benzyl azide stock solutions were made (1000 or 100 equiv.), after which aliquots of 50 µL of the benzyl azide stock solutions were put in small vials.

To the 400 µL peptide solution 100 µL of the DBCO stock solution was added. The reaction was performed at 37 °C. After 0 min, 1 min, 5 min, 10 min, 30 min, 1 h, 2 h, the reaction was quenched by taking 50 µL of sample and adding it to the vial containing the 100 equiv. of benzyl azide (relative to DBCO). The sample was then kept at -20 °C overnight until use in ELISA.

The sample solutions (0.5 mg/mL) and the solutions containing peptides **7**-**9** were then diluted to 10 µg/mL using 0.1% BSA/PBS. The solutions (100 µL) were added to the ELISA plate, coated with streptavidin, and incubated for 1 hour at 37 °C. The plate was washed three times with PBS/0.1% Tween, followed by and incubation step with ACPA-positive or anti-TT-positive serum (100 µL) for 1 hour at 37 °C. The plate was then again washed three times with PBS/0.1% Tween. Afterwards, the wells were incubated with 100 µL of rabbit anti-human-HRP (1:2000 dilution) for 1 hour at 37 °C and washed. Finally, the wells were incubated with 100 µL of a mixture of TMB/UP (1:1) at room temperature for 5 minutes. The coloring reaction was quenched by addition of 100 µL of 2M H_2SO_4. The absorbance was measured at 450 nm.

FACS experiments. The streptavidin-peptide complexes were prepared as described in literature.[25] Briefly, the CXP-biotin peptide derivatives (**7**-**9**) were dissolved in PBS to make a 2 mg/mL stock solution. This solution was further diluted to make 14 µL of 1 mg/mL peptide solution in PBS buffer. In a vial 37.5 µL of Streptavidin-APC solution (S32362, LUMC), 12.5 µL CCP-biotin derivative solution (1 mg/mL) was added and these were incubated overnight at 4 °C.

A Bio-Spin 30 column was resuspended and centrifuged for 2 min at 1000 g twice with the removal of buffer. The column was then placed in a vial and the sample was loaded. The column was centrifuged for 4 minutes at 1000 g to get the APC tetramer samples in vials. These samples were stored at 4 °C.

CCP(Im) tetramers (1 µL, 0.9 µg/mL) were incubated in the dark for 1 hour with 0 µL, 1 µL, 2 µL, 3 µL, 4 µL, 5 µL, 6 µL, 7 µL, 8 µL, 9 µL or 10 µL of a 10 mM DBCO-CO_2H solution (final volume 20 µL). The peptide tetramers were all 1000 times diluted and 30 µL was added to both ACPA-expressing B cells or anti-TT-expressing B cells in a 48 well plate. The cells were put on ice for 30 min. 100 µl of PBA was added per well, the plate was centrifuged and the supernatant discarded. This was repeated once. Then, 100 µl of 1% paraformaldehyde was added and the cell suspensions were transferred to micronic tubes and measured by flow cytometry using BD LSRFortessa (BD Biosciences).

3.6 References

1. Cross, M.; Smith, E.; Hoy, D.; Carmona, L.; Wolfe, F.; Vos, T.; Williams, B.; Gabriel, S.; Lassere, M.; Johns, N. The global burden of rheumatoid arthritis: estimates from the global burden of disease 2010 study. *Ann. Rheum. Dis.* **2014**.
2. Jilani, A. A.; Mackworth-Young, C. G. The role of citrullinated protein antibodies in predicting erosive disease in rheumatoid arthritis: a systematic literature review and meta-analysis. *Int. J. Rheum. Dis.* **2015,** *2015*, 1-8.
3. Schett, G.; Gravallese, E. Bone erosion in rheumatoid arthritis: mechanisms, diagnosis and treatment. *Nat. Rev. Rheumatol.* **2012,** *8*, (11), 656-664.
4. Edwards, J. C. W.; Szczepański, L.; Szechiński, J.; Filipowicz-Sosnowska, A.; Emery, P.; Close, D. R.; Stevens, R. M.; Shaw, T. Efficacy of B-cell–targeted therapy with rituximab in patients with rheumatoid arthritis. *N. Engl. J. Med.* **2004,** *350*, (25), 2572-2581.
5. Kaplan, B.; Kopyltsova, Y.; Khokhar, A.; Lam, F.; Bonagura, V. Rituximab and immune deficiency: case series and review of the literature. *J. Allergy Clin. Immunol. Pract.* **2014,** *2*, (5), 594-600.
6. Willemze, A.; Shi, J.; Mulder, M.; Stoeken-Rijsbergen, G.; Drijfhout, J. W.; Huizinga, T. W. J.; Trouw, L. A.; Toes, R. E. M. The concentration of anticitrullinated protein antibodies in serum and synovial fluid in relation to total immunoglobulin concentrations. *Ann. Rheum. Dis.* **2013,** *72*, 1059-1063.
7. Li, J.; Chen, P. R. Development and application of bond cleavage reactions in bioorthogonal chemistry. *Nat. Chem. Biol.* **2016,** *12*, (3), 129-137.
8. Versteegen, R. M.; Rossin, R.; ten Hoeve, W.; Janssen, H. M.; Robillard, M. S. Click to Release: Instantaneous Doxorubicin Elimination upon Tetrazine Ligation. *Angew. Chem. Int. Ed.* **2013,** *52*, (52), 14112-14116.
9. Jiménez-Moreno, E.; Guo, Z.; Oliveira, B. L.; Albuquerque, I. S.; Kitowski, A.; Guerreiro, A.; Boutureira, O.; Rodrigues, T.; Jiménez-Osés, G.; Bernardes, G. J. L. Vinyl ether/tetrazine pair for the traceless release of alcohols in cells. *Angew. Chem. Int. Ed.* **2017,** *56*, (1), 243-247.
10. Wu, H.; Alexander, S. C.; Jin, S.; Devaraj, N. K. A bioorthogonal near-infrared fluorogenic probe for mRNA detection. *J. Am. Chem. Soc.* **2016,** *138*, (36), 11429-11432.
11. Bernard, S.; Audisio, D.; Riomet, M.; Bregant, S.; Sallustrau, A.; Plougastel, L.; Decuypere, E.; Gabillet, S.; Kumar, R. A.; Elyian, J. Bioorthogonal Click and Release Reaction of Iminosydnones with Cycloalkynes. *Angew. Chem. Int. Ed.* **2017,** *56*, (49), 15612-15616.
12. Nelson, A. L. Antibody fragments: Hope and hype. *mAbs* **2010,** *2*, (1), 77-83.
13. McIlvaine, T. C. A buffer solution for colorimetric comparison. *J. Biol. Chem.* **1921,** *49*, (1), 183-186.
14. Kerkman, P. F.; Rombouts, Y.; van der Voort, E. I. H.; Trouw, L. A.; Huizinga, T. W. J.; Toes, R. E. M.; Scherer, H. U. Circulating plasmablasts/plasmacells as a source of anticitrullinated protein antibodies in patients with rheumatoid arthritis. *Ann. Rheum. Dis.* **2013,** *72*, (7), 1259-1263.
15. Doronina, S. O.; Toki, B. E.; Torgov, M. Y.; Mendelsohn, B. A.; Cerveny, C. G.; Chace, D. F.; DeBlanc, R. L.; Gearing, R. P.; Bovee, T. D.; Siegall, C. B.; Francisco, J. A.; Wahl, A. F.; Meyer, D. L.; Senter, P. D. Development of potent monoclonal antibody auristatin conjugates for cancer therapy. *Nat. Biotechnol.* **2003,** *21*, 778-784.
16. Francisco, J. A.; Cerveny, C. G.; Meyer, D. L.; Mixan, B. J.; Klussman, K.; Chace, D. F.; Rejniak, S. X.; Gordon, K. A.; DeBlanc, R.; Toki, B. E. cAC10-vcMMAE, an anti-CD30–monomethyl auristatin E conjugate with potent and selective antitumor activity. *Blood* **2003,** *102*, (4), 1458-1465.
17. Senter, P. D. Potent antibody drug conjugates for cancer therapy. *Curr. Opin. Chem. Biol.* **2009,** *13*, (3), 235-244.
18. Doronina, S. O.; Bovee, T. D.; Meyer, D. W.; Miyamoto, J. B.; Anderson, M. E.; Morris-Tilden, C. A.; Senter, P. D. Novel Peptide Linkers for Highly Potent Antibody−Auristatin Conjugate. *Bioconjugate Chem.* **2008,** *19*, (10), 1960-1963.
19. Le Gal, J.; Latapie, L.; Gressier, M.; Coulais, Y.; Dartiguenave, M.; Benoist, E. Design and synthesis of a novel family of semi-rigid ligands: versatile compounds for the preparation of 99mTc radiopharmaceuticals. *Org. Biomol. Chem.* **2004,** *2*, (6), 876-883.

20. Gikanga, B.; Adeniji, N. S.; Patapoff, T. W.; Chih, H.-W.; Yi, L. Cathepsin B Cleavage of vcMMAE-Based Antibody–Drug Conjugate Is Not Drug Location or Monoclonal Antibody Carrier Specific. *Bioconjugate Chem.* **2016,** *27*, (4), 1040-1049.
21. Avalos, A. M.; Ploegh, H. L. Early BCR events and antigen capture, processing, and loading on MHC class II on B cells. *Front. Immunol.* **2014,** *5*, (92), 1-5.
22. Avalos, A. M.; Bilate, A. M.; Witte, M. D.; Tai, A. K.; He, J.; Frushicheva, M. P.; Thill, P. D.; Meyer-Wentrup, F.; Theile, C. S.; Chakraborty, A. K.; Zhuang, X.; Ploegh, H. L. Monovalent engagement of the BCR activates ovalbumin-specific transnuclear B cells. *J. Exp. Med.* **2014,** *211*, (2), 365-379.
23. Shih, T.-Y.; Blacklow, S. O.; Li, A. W.; Freedman, B. R.; Bencherif, S.; Koshy, S. T.; Darnell, M. C.; Mooney, D. J. Injectable, Tough Alginate Cryogels as Cancer Vaccines. *Adv. Healthc. Mater.* **2018,** *7*, (10), 1701469.
24. Bencherif, S. A.; Sands, R. W.; Bhatta, D.; Arany, P.; Verbeke, C. S.; Edwards, D. A.; Mooney, D. J. Injectable preformed scaffolds with shape-memory properties. *Proc. Natl. Acad. Sci.* **2012,** *109*, (48), 19590.
25. Kerkman, P. F.; Fabre, E.; van der Voort, E. I. H.; Zaldumbide, A.; Rombouts, Y.; Rispens, T.; Wolbink, G.; Hoeben, R. C.; Spits, H.; Baeten, D. L. P.; Huizinga, T. W. J.; Toes, R. E. M.; Scherer, H. U. Identification and characterisation of citrullinated antigen-specific B cells in peripheral blood of patients with rheumatoid arthritis. *Ann. Rheum. Dis.* **2016,** *75*, (6), 1170-1176.

3.7 Supplementary Figure

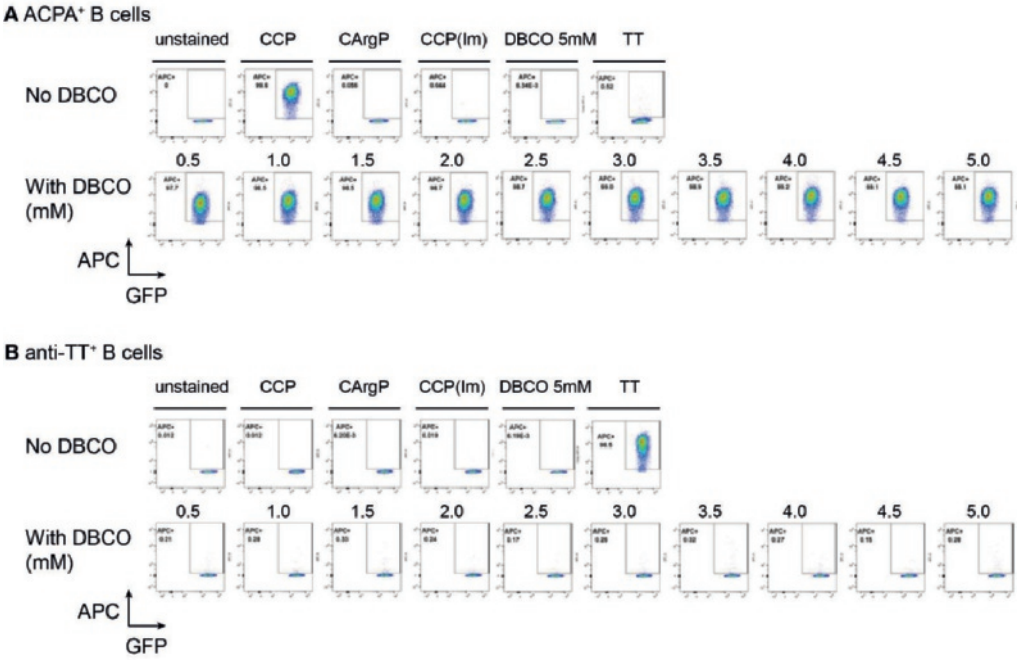

Figure SI-1. Flow cytometric binding studies of streptavidin-coupled, biotinylated CCP, CArgP, and (activated) CCP(Im) to A) an ACPA-expressing B cell clone and B) an anti-TT-specific B cell clone. Activation of CCP(Im) was performed using DBCO for 1 h at 37 °C before addition to the cells.

Chapter 4

Vinylboronic Acid Ligation for Efficient Click-to-Release of a Lymphocyte-Specific Cytotoxic Prodrug

Lianne Lelieveldt, Selma Eising, Abel Wijen, Hendy Kristyanto, Hans Ulrich Scherer, René Toes, Kimberly Bonger. *Manuscript in preparation*

Abstract

Bioorthogonal reactions can be performed selectively in the presence of any biological functional group and are widely used to achieve site-selective chemical modifications of biomolecules. The click-to-release reaction is a variant that has gained much interest over the last few years. The bioorthogonal reaction between tetrazines and *trans*-cyclooctenes or vinyl ethers for example, initiate the release of a small molecule immediately after the cycloaddition. Recently, our group reported that vinyl boronic acids (VBAs) gave exceptionally high reaction rates in the bioorthogonal inverse electron-demand Diels-Alder reaction with pyridyl tetrazines. In the present study, we explore whether VBAs can be used in the click-to-release variant and demonstrate the use with a VBA-protected cladribine prodrug. We show that the cytotoxicity of cladribine is dampened by the attachment of the VBA, and activity can be largely restored upon the reaction with a tetrazine, inducing cell death.

4.1 Introduction

Chemical site-selective protein modifications have become increasingly popular for modification and control over protein functions *in vitro* and in living systems. Over the last few years, more reactions have been developed and used to 'decorate' biomolecules with a desired functionality such as fluorophores, affinity probes or reactive tags. All these reactions have some properties in common; ideally, they must be selective over other functional groups in biomolecules, have fast reaction rates and progress in aqueous media around physiological pH.[1] Reactions such as the Staudinger ligation[2] or the strain-promoted alkyne–azide cycloaddition (SPAAC)[3-4] have been used extensively for modifying purposes. Our group has recently reported a new bioorthogonal reaction based on a vinylboronic acid (VBA) tetrazine ligation. It was shown that by introducing a boronic acid moiety on an alkene, reaction rates of an iEDDA (inverse electron demand Diels-Alder) click reaction were improved several orders of magnitude compared to the non-modified linear alkene.[5] The hydrophilic properties and the small size of VBAs compared to other bioorthogonal reactants make them attractive for the use in biomolecular labeling experiments. VBAs were shown to be biocompatible, non-toxic, and highly stable in aqueous media and cell lysates. Moreover, VBAs can be used orthogonally to the SPAAC reaction for protein modification, making them attractive complements to the bioorthogonal molecular toolbox.[5-7]

While the number of bioorthogonal reactions used *in vivo* is limited due to the need of toxic reagents (*e.g.* copper, in copper (I)-catalyzed alkyne-azide cycloaddition[8-9]) or possible side reactions of the reactants (strained alkenes or alkynes react with cysteines), VBAs appeared useful in cellular experiments. No side reactions with vicinal diols (present in carbohydrates for example) were observed when performing reactions in living cells.[6]

It was shown that the reactivity of VBAs depends on the tetrazine and its substituents. Since the boronic acid coordinates to the pyridyl ring of dipyridyl tetrazine, reaction rates were enhanced in comparison to tetrazines lacking such potent Lewis base.[10] The orthogonal use of this bioorthogonal reaction was shown by using two different tetrazines favoring the reaction with either a VBA or norbornene. This was demonstrated using a subunit-specific proteasome inhibitor conjugated to norbornene and a proteasome inhibitor bearing a VBA. When adding both a phenyl pyrimidyl tetrazine and a dipyridyl tetrazine, containing different fluorophores, it was shown that due to different reaction rates subunit-specific labeling occurred.[7]

The interest in bioorthogonal click-to-release reactions for activation of protected biologically relevant molecules *in vivo* has increased significantly in the last years. Therefore, a significant number of bioorthogonal bond cleavage reactions have been developed.[11] The combination of a tetrazine ligation and a release reaction enables new applications *in vitro* and *in vivo*, such as the activation of prodrugs or fluorogenic compounds. Alkenes bearing a leaving group directly attached to the double bond undergo a subsequent release reaction after the iEDDA, yielding both the leaving group and the pyridazine product.[12] A substituent on the allylic position of the alkene also confers a release reaction, although the amount is dependent on the tautomer and the substituents of the dihydropyridazine product. Positioning the release substituent at the allylic position, though, may be advantageous for the cylcoaddition due to decreased steric hindrance.[12-13]

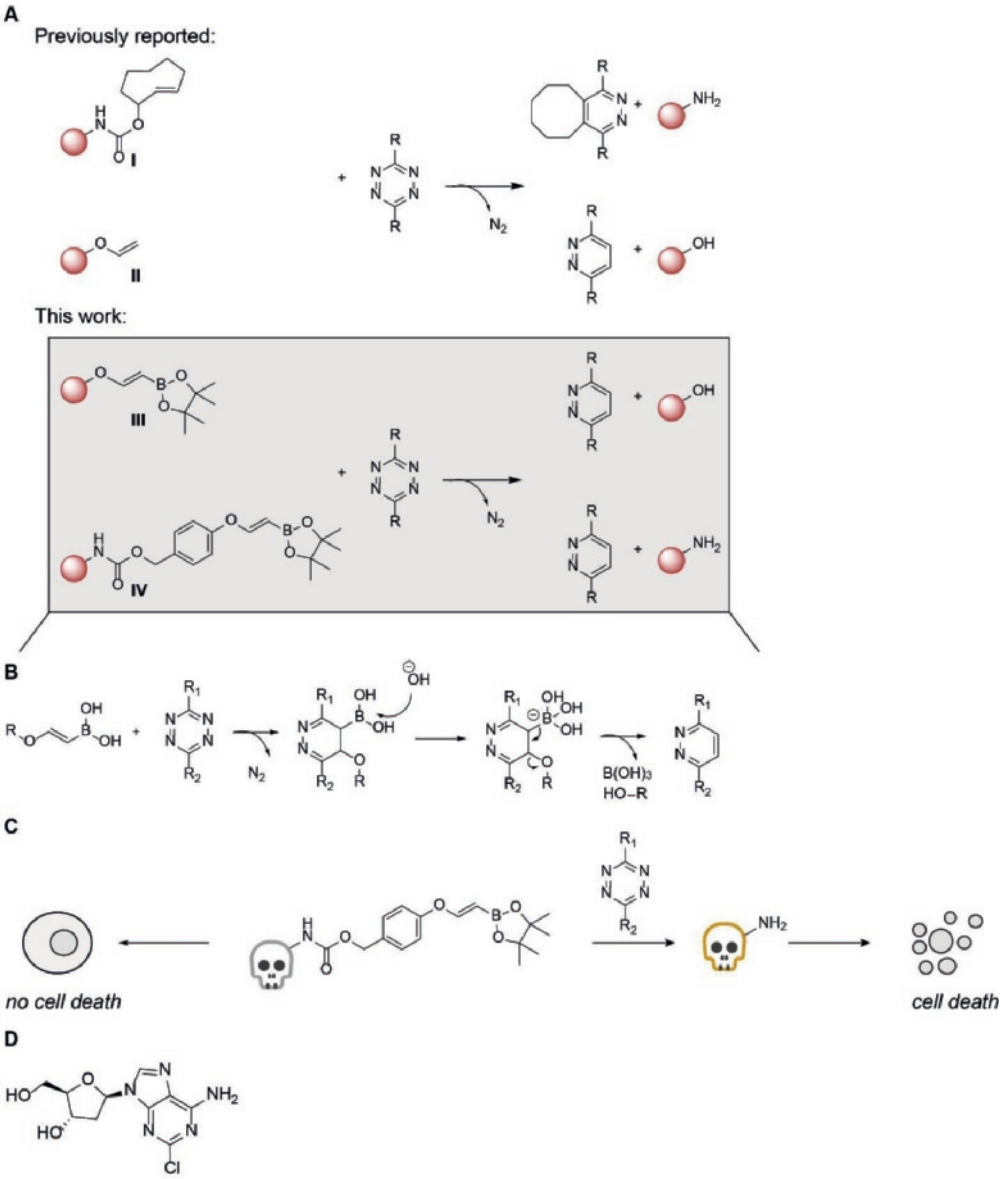

Figure 1. Tetrazine click-to-release reaction. A) Reagents for click-to-release reactions, *trans*-cyclooctene **I**, vinyl ether **II,** vinyl boronic acids **III** and **IV**; B) Proposed click-to-release mechanism, liberating boric acid and a leaving group; C) Schematic overview of click-to-release reaction with cladribine-VBA. Cell death is only expected when the cladribine-VBA is activated by a tetrazine cycloaddition; D) Structure of cladribine.

In 2013, the group of Robillard reported the first bioorthogonal click-to-release reaction based on the reaction of tetrazines with *trans*-cyclooctenes (TCOs) that possess a carbamate substituent at the allylic position (Figure 1A).[14] After the iEDDA of the tetrazine and TCO, the 4,5-dihydropyridazine eliminates the leaving group to liberate both CO_2 and the amine. Unfortunately, part of the dihydropyridazine tautomerizes to the 1,4-dihydropyidazine, which does not lead to a

release reaction. Although this click-to-release process does not give complete elimination, it has been frequently applied in biological systems for activation of prodrugs[15-16] or caged proteins.[17-18] Recently, it was noted that this click-to-release reaction is environmentally sensitive and improvements on both the TCO and tetrazine resulted in ultrafast click-to-release reaction rates and the complete elimination of the leaving group.[19]

In 2016, the groups of Deveraj and Bernardes reported both the bioorthogonal click-to-release reaction of tetrazines and vinyl ethers (Figure 1A).[20-21] These alkenes bear their leaving group directly on the alkene and give therefore full release of the alcohol after the iEDDA. The vinyl ethers appeared stable in aqueous solutions for at least 8 hours and were suitable for applications in living cells. The vinyl ethers have the advantage to be small in size, but have disappointingly low rate constants when reacting with tetrazines.

Since VBAs have proven to be useful in bioorthogonal conjugation, we envisioned that by introducing a boronic acid group on the vinyl ethers, we could increase the rate of these click-to-release reactions. In addition, similar to vinyl ethers,[20-21] we expect that VBA ethers give full release of the alcohol, or amine when linked via a carbamate, after the iEDDA. The proposed iEDDA click-to-release reaction mechanism of boronic acids with tetrazines is shown in Figure 1B. Upon cycloaddition and retro-Diels-Alder reaction liberating N_2, the boric acid and the leaving group, which can be a linked via an alcohol or carbamate, are released.

To proof the applicability of the VBA click-to-release strategy we developed a VBA protected cladribine, which can be released using tetrazine (Figure 1C) in the proximity of cells. Cladribine (2-chlorodeoxyadenosine; 2CdA; Figure 1D) is a purine analogue and resembles deoxyadenosine. Cladribine contains a chlorine atom and is, unlike adenosine, resistant to breakdown by adenosine deaminase. In the cell, cladribine gets activated upon phosphorylation, and is then incorporated into the DNA synthesis pathway, leading to strand breaks in the newly synthesized DNA. The consequence of this is that the cell will go into apoptosis. The high level of deoxycytidine kinase, responsible for the phosphorylation of cladribine, and the low level of 5'-nucleotidase activity in lymphocytes, compared to other cells, results in accumulation of the activated cladribine, specifically in lymphocytes. Therefore, cladribine is already used as a synthetic chemotherapeutic agent in B cell chronic lymphocytic leukemia and multiple sclerosis.[22-24] Lymphocytes also play a major role in disease progression of rheumatoid arthritis (RA), where autoreactive antibodies (such as anti-citrullinated protein antibodies, ACPA) are produced in high numbers by B cell-derived plasma cells. Treatment of RA patients with rituximab, leading to the killing of B-lymphocytes, has been shown to give a therapeutic benefit.[25] Here we show that we can turn cladribine into a prodrug through VBA protection which can be liberated using a VBA-tetrazine click-to-release reaction to selectively target lymphocytes, including autoreactive ACPA-positive B cells.

4.2 Results and Discussion

Synthesis and comparison of vinylboronic acid (6) and vinyl ether (9). Vinyl ethers are relevant for click-to-release reactions due to their relatively small size. However, rather low reaction rates have been observed in reaction with tetrazines.[20] By the introduction of a boronic acid functional group we expect to increase the reaction rates with tetrazines and we expect full release as has been seen for the vinyl ethers.

To make a comparison with the vinyl ethers and later on for the attachment of a toxin, we synthesized VBA **6**, containing the ether moiety, and its primary alkene derivative **9** (Scheme 1).

The synthesis of VBA **6** started with the etherification of 4-hydroxybenzyl alcohol **1** with trichloroethylene and subsequent protection of the primary alcohol. Next, dichlorovinyl ether **3** was treated with *n*-BuLi to eliminate hydrogen chloride and to provide alkynyl ether **4**. Deprotection of the primary alcohol and hydroboration of alkyne **5** with pinacolborane yielded VBA pinacol ester **6**. In our kinetic experiments, we used the pinacol ester as precursor for the free boronic acid as it hydrolyzes quickly in aqueous media (see Figure SI-1). The synthesis of vinyl ether **9** started with 4-hydroxybenzaldehyde (**7**). First, reaction with 1,2-dibromoethane was performed yielding compound **8** and subsequently elimination using *t*-BuOK was carried out. Lastly, $NaBH_4$ was used to reduce the aldehyde to the corresponding benzyl alcohol. All reactions towards the vinyl ether **9** were performed conform a literature procedure.[16]

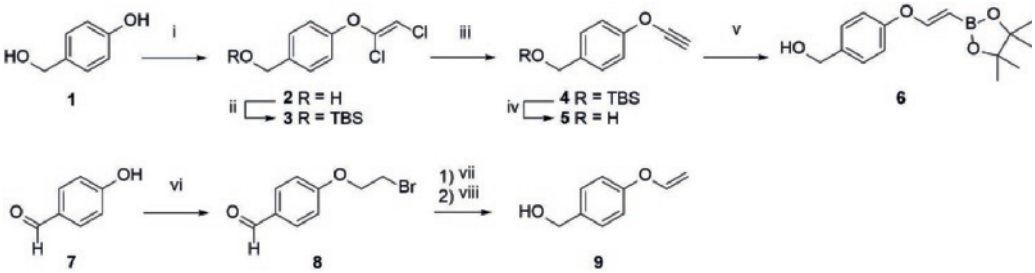

Scheme 1. Synthesis of VBA ether **6** and vinyl ether **9**. i) Trichloroethylene, K_2CO_3, DMF, 70 °C, 16 h, 87%. ii) TBSCl, imidazole, DMF, 2 h, quant. iii) *n*-BuLi, Et_2O, -78 to -40 °C, 87%. iv) TBAF, THF, 0 °C, 91%. v) Pinacolborane, $RuHClCO(PPh_3)_3$, toluene, 50 °C, 16 h, 76%. vi) Dibromoethane, K_2CO_3, MeCN, reflux, 20 h, 79%. vii) *t*-BuOK, DMSO, r.t., 10 min. viii) $NaBH_4$, MeOH, r.t., 1.5 h, 18%.

Having alkenes **6** and **9** in hand, we next examined the second-order rate constants with 3,6-dipyridyl-*s*-tetrazine **10** in 75% MeOH in PBS at a controlled temperature of 20 °C. As we used the pinacol ester as precursor, we incubated ester **6** for 2 h in the solvent mixture to achieve full hydrolysis to the free boronic acid before measuring its k_2 value. Second-order rate constants were obtained by following the decrease of the tetrazine UV absorbance in the visible region (Figure SI-2). The pseudo first-order constant k_{obs} was first determined by plotting the decay of tetrazine absorbance against time (minutes) for five different amounts of excess of alkene. By fitting an exponential nonlinear regression curve, the K_{obs} could be extracted (see also Materials and Methods). Next, the K_{obs} was plotted against the five different alkene concentrations and a linear regression fit gave a linear function, of which the slope corresponded to the k_2 (Figure SI-2). The second-order rate constant for VBA **6** was a 4-fold higher than the rate constant of vinyl ether **9**, clearly indicating a positive effect of the boronic acid on the reactivity of the alkene (Figure 2A).

The observed rate constant of VBA ether **6** was lower than expected as we previously observed rate enhancements of up to 100-fold compared to the unsubstituted alkene derivatives.[5] We hypothesize that the moderate rate enhancement is due to the ether on the vinylic position. Since this alcohol is slightly electron-donating, we assume that the alkene becomes more electron-rich and therefore lowers the Lewis acidity of the boronic acid, which becomes less coordinating to the pyridyl rings of the tetrazine.

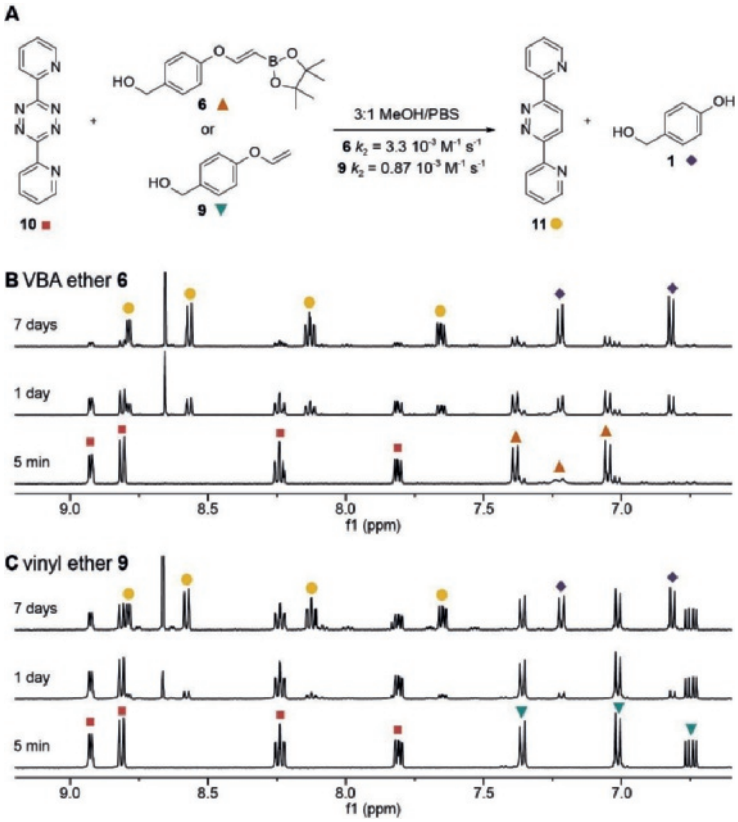

Figure 2. Click-to-release reactions and reaction rates. A) Scheme of the reaction of 3,6-dipyridyl-*s*-tetrazine **10** with VBA ether **6** and vinyl ether **9**. k_2 values were measured in 3:1 MeOH/PBS; B) ^{1}H-NMR study of the reaction between tetrazine **10** (■) and VBA ether **6** (▲) yielding pyridazine **11** (●) and 4-hydroxybenzyl alcohol **1** (♦) in 3:1 CD_3OD/deuterated PBS; C) Same as B, but then the reaction of **10** with vinyl ether **9** (▼).

Next, we looked in more detail into the click-to-release reaction of 3,6-dipyridyl-*s*-tetrazine **10** and alkenes **6** and **9** by ^{1}H NMR in 75% CD_3OD in deuterated PBS over time (Figures 2B, C). A near to complete conversion of VBA ether **6** was observed after 7 days, while vinyl ether **9** gave only around 50% conversion. Both reactions yielded the formation of pyridazine **11** and 4-hydroxybenzyl alcohol **1**, while no intermediates were observed, showing that the release reaction was fast for both vinyl ether **9** as well as VBA ether **6**.

Synthesis of cladribine-VBA as a click-to-release prodrug. To apply the click-to-release reaction with VBA, we next synthesized cladribine-VBA **16**. The VBA is intended to function as a caging group to inactivate cladribine, and upon click-to-release with tetrazine, cladribine would be released and become active again. Figure 3A schematically shows the click-to-release reaction yielding the liberated cladribine toxin.

We commenced the synthesis from VBA alcohol **6** (Scheme 2). Activation of the alcohol using bis(pentafluorophenyl)carbonate and Et_3N as a base was successful to yield VBA **14**. Cladribine

was acetylated using Ac_2O and pyridine to protect the alcohols from reacting with VBA **14**. The acetylated cladribine **13** was deprotonated with NaH to couple with VBA **14**. Deacetylation of cladribine yielded the final compound **16** in which the toxin was linked via a self-cleavable linker[26] to the VBA.

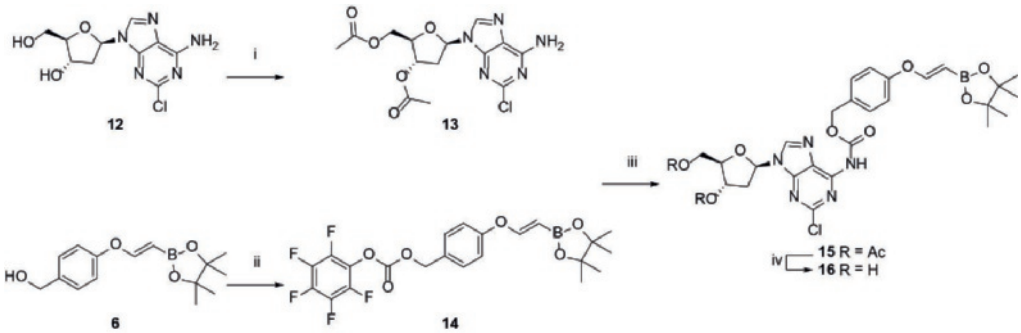

Scheme 2. Synthesis of cladribine-VBA **16**. i) Ac_2O, pyridine, r.t., 1.5 h, quant. ii) Bis(pentafluorophenyl)carbonate, Et_3N, r.t., 1 h, 84%. iii) **11** + **12**, NaH, r.t., 7 h, 42%. iv) NaOMe in MeOH, MeCN, r.t., 1 h, 59% .

To gain an indication of the release rate of cladribine prior to performing click-to-release reactions with cells, we tested the cycloaddition with tetrazine and subsequent release over time in a buffer system. Before reacting VBA **16** with tetrazine **17**, pinacol hydrolysis was performed in PBS at room temperature for 2 hours. Either 1 or 10 equivalents of tetrazine were added and the reaction was followed over time with LCMS. Deprotection in PBS at 37 °C, using 1 equivalent of tetrazine was complete in 24 hours, while using 10 equivalents completion was already achieved within 2 hours (Figure 3B). No intermediate products were observed, indicating that the cleavage of the linker occurs instantaneously after the cycloaddition. While the click-to-release of 4-hydroxybenzyl alcohol **1** took 7 days, the release of cladribine with the same amount of tetrazine was finished in only 24 hours. Protic solvents have been described to accelerate the iEDDA reaction and this effect is even more pronounced when reactions are performed in water.[27] The click-to-release using VBA **6** was achieved after 7 days in 75% MeOH in PBS (this compound is less water soluble than VBA **16**) and after only one day using 1% DMSO in PBS as a solvent for VBA **16**.

As shown in Figure 3A, the addition of tetrazine liberates cladribine upon cycloaddition. In the absence of tetrazine, cladribine is protected and should not be toxic to cells. To test this effect on living cells, we incubated immortalized ACPA-positive B cells, a model cell line for autoreactive B cells in RA, with cladribine-VBA. Cladribine alone was incubated with the cells as a control and showed to be toxic for immortalized B cells in a dose dependent manner (Figure SI-3). The VBA modification on cladribine inactivated the compound, as the observed toxicity was dampened. However, full inactivation was not obtained (Figure 4A). To examine whether this partial toxicity was due to stability issues, we incubated protected cladribine **16** for up to 3 days in PBS at 37 °C. A significant degree of instability was observed for this compound after 3 days, as protodeborylation (17%) and unmodified cladribine (67%) were observed (Figure SI-4).

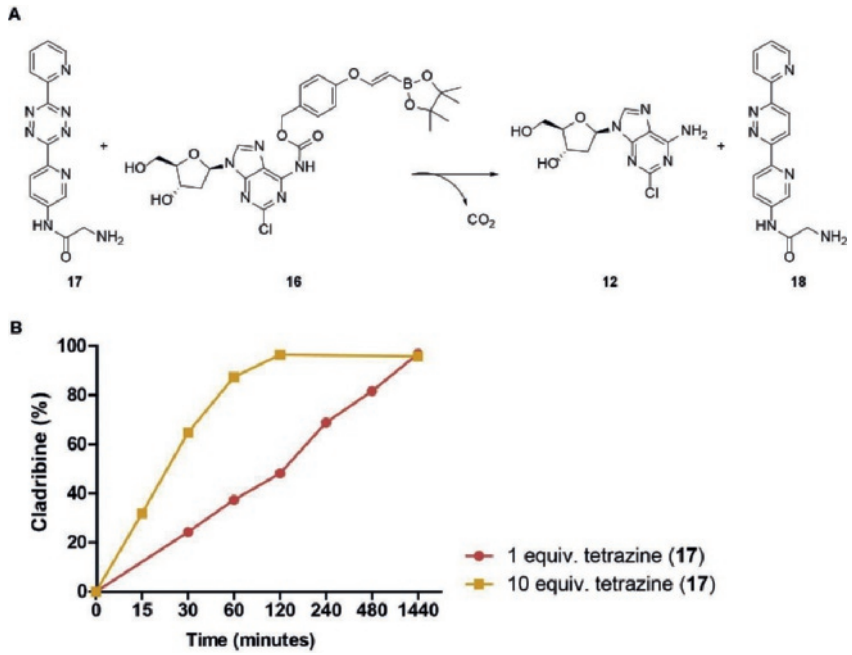

Figure 3. Click-to-release of VBA **16** to yield the free drug cladribine **12**. A) Schematic overview of click-to-release reaction with cladribine-VBA; B) The release of cladribine after the reaction with either 1 (pink) or 10 (yellow) equivalents of tetrazine **17**. The amount of cladribine was determined by LCMS and was quantified by the area under the curve. The graph shows the relative amount compared to the amount of starting material.

Although active cladribine was already observed after 24 h, we continued our studies for activation purposes. We preincubated cladribine-VBA **16** with tetrazine **17** (10 equivalents) for 24 hours before adding the mixture to the cells. After 3 days of incubation, we observed that the toxicity level of tetrazine-activated cladribine was similar to that of cladribine alone (Figure 4A). However, cladribine activation with 10 equivalents of tetrazine in the direct vicinity of cells did not show the anticipated results as shown for the pre-incubated cell cytotoxicity experiment (Figure SI-5). Although significant amounts of cladribine-VBA were liberated compared to the control, only a minority of cells died at 100 nM. This appeared concentration dependent, since the toxicity increased during the experiment with higher concentrations (1 μM). Increasing the amount of tetrazine to 100 equivalents, however, induced toxicity to the same level as observed for cladribine (Figure SI-5). On the other hand, using 100 equivalents of tetrazine without cladribine also induced toxicity, making it impossible to tell whether the cells died because of the liberated cladribine or because of tetrazine toxicity.

As cladribine is more toxic for lymphoid cells (explained above), we tested toxicity on HEK293-TM cells, expressing a transmembrane (TM) domain-containing ACPA receptor. Figure 4B shows that with up to 400 nM of cladribine no toxicity was observed on HEK293-TM cells, while only 13% of the immortalized B cells survived at the same concentration. This shows that cladribine is indeed less toxic for these HEK cells compared to the immortalized B cells. Although deprotection and lymphocyte toxicity of cladribine-VBA were observed over time, hardly any cell death was

seen for HEK cells after 3 days of incubation, indicating a potential therapeutic window using these compounds.

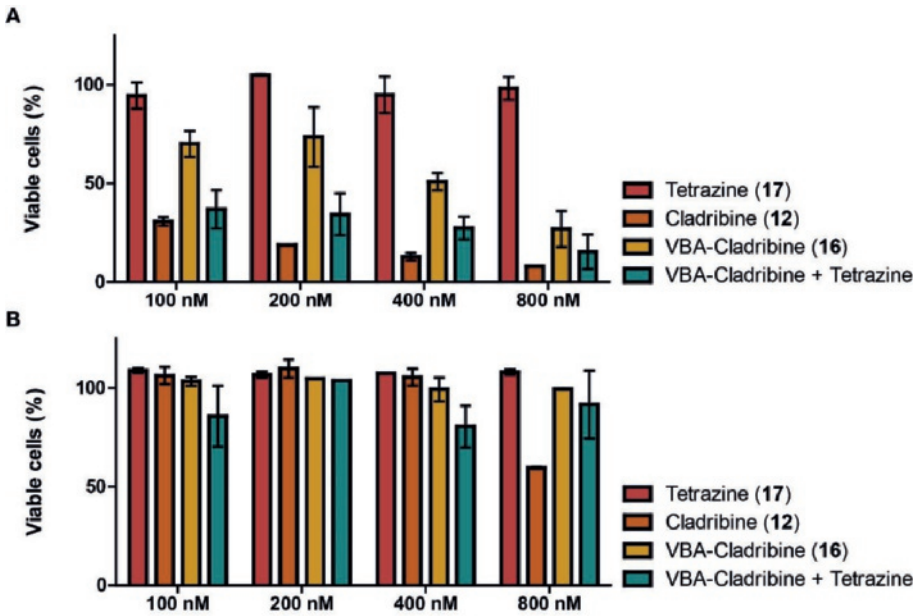

Figure 4. Cytotoxicity of (activated) cladribine-VBA on lymphoid and non-lymphoid cells after 3 days. Cladribine-VBA and tetrazine **17** (10 equiv.) were preincubated for 24h before the addition to the cells. A) Cytotoxicity for autoreactive immortalized B cells, 30,000 cells were used; B) Cytotoxicity for HEK cells expressing ACPA receptors, 10,000 cells were used.

4.3 Conclusion

In this Chapter we have shown that VBAs can be used in click-to-release reactions. The release was instantaneous after the tetrazine cycloaddition as no reaction intermediates were observed by NMR experiments. We assume that the slight electron-donating nature of the ether at the vinylic position reduces the reaction rate as compared to regular VBAs lacking the ether function.

We used the VBA click-to-release strategy on a cytotoxic drug that is initially caged, but released and activated upon reaction with tetrazine. Cladribine-VBA slowly degraded over 3 days so that partial deprotection was observed when cladribine-VBA was incubated, without the addition of tetrazine, with cells. Overall, incubation optimization is required to achieve optimal deprotection of the cladribine-VBA and minimal toxicity of the caged cladribine. Since the used VBA prodrug degrades slowly over time, it is not suited for experiments requiring long incubation times. Exploring other VBA-prodrug linkages or another toxin-VBA conjugate can be beneficial for this purpose and used to dissect the origin of the VBA prodrug instability. Even then, slow degradation of a protected drug does not have to be problematic if prodrug activation and toxicity induction is faster. Hence, it would be interesting to attach a more potent drug which requires a shorter incubation time to induce toxicity, and to further evaluate this strategy as a viable release mechanism.

4.4 Acknowledgements

We thank Selina Thijssen for her pioneering work on this project.

4.5 Materials and Methods

For general methods, see the materials and methods section of Chapter 2 (paragraph 2.4).

***(Z)*-(4-((1,2-Dichlorovinyl)oxy)phenyl)methanol (2)**. 4-Hydroxybenzyl alcohol **1** (2.0 g, 16 mmol, 1.0 equiv.) was dissolved in DMF (16 mL) under ambient atmosphere and K_2CO_3 (2.7 g, 19 mmol, 1.2 equiv.) was added. Next, the mixture was heated at 70 °C and trichloroethylene (1.8 mL, 19 mmol, 1.2 equiv.) was added dropwise. After the mixture was heated at 70 °C overnight, it was cooled down to r.t., H_2O (20 mL) was added and the mixture was extracted with EtOAc (3 × 15 mL). The combined organic layers were washed with brine and dried over Na_2SO_4, and the volatiles were removed under reduced pressure. As there was still water present, the product was resuspended in H_2O and extracted with Et_2O (3 × 15 mL). The combined organic layers were washed with brine and dried over Na_2SO_4. The volatiles were removed under reduced pressure yielding vinyl ether **2** (3.1 g, 87%) as a dark orange oil. R_f = 0.57 (50% EtOAc in heptane). ^{1}H NMR (400 MHz, chloroform-*d*) δ 7.40 – 7.34 (m, 2H), 7.09 – 7.04 (m, 2H), 5.96 (s, 1H), 4.67 (s, 2H). ^{13}C NMR (100 MHz, chloroform-*d*) δ 153.3, 140.0, 137.1, 128.6, 117.2, 103.8, 64.7. GCMS 6.68 min, m/z = 218 (M^+, calcd. for $C_9H_8Cl_2O_2$ = 218, 100%), 107 [$(M\text{-}C_7H_7O)^+$, 55%], 77 [$(M\text{-}C_6H_5)^+$, 85%].

***(Z)-tert*-Butyl((4-((1,2-dichlorovinyl)oxy)benzyl)oxy)dimethylsilane (3)**. Alcohol **2** (2.0 g, 9.1 mmol, 1.0 equiv.) was dissolved in dry DMF (16 mL) and the mixture was cooled to 0 °C. Then, imidazole (750 mg, 11 mmol, 1.2 equiv.) and TBDMSCl (1.7 g, 11 mmol, 1.2 equiv.) were added and the reaction was stirred for 2 h at r.t. The mixture was diluted with Et_2O (20 mL), washed with sat. NH_4Cl and brine and dried over Na_2SO_4. The volatiles were removed under reduced pressure yielding TBDMS ether **8** (3.1 g, quant.) as a slightly yellow oil. R_f = 0.32 (10% EtOAc in heptane). ^{1}H NMR (400 MHz, chloroform-*d*) δ 7.36 – 7.29 (m, 2H), 7.06 – 6.99 (m, 2H), 5.94 (s, 1H), 4.72 (s, 2H), 0.94 (s, 9H), 0.10 (s, 6H). ^{13}C NMR (100 MHz, chloroform-*d*) δ 152.7, 140.2, 137.8, 127.4, 116.9, 103.5, 64.4, 25.9, 18.4, -5.3. GCMS 8.36 min, m/z = 332 (M^+, calcd. for $C_{15}H_{22}Cl_2O_2Si$ = 332, <1%), 275 [$(M\text{-}C_{11}H_{13}O_2Si)^+$, 65%].

***tert*-Butyl((4-(ethynyloxy)benzyl)oxy)dimethylsilane (4)**. Dichlorovinyl ether **3** (2.0 g, 6.0 mmol, 1.0 equiv.) was dissolved in dry Et_2O (50 mL) and *n*-BuLi (15 mL of 1.6 M in hexanes, 23.8 mmol, 4.0 equiv.) was added dropwise to the mixture. The solution was then stirred for 1 h at -78 °C, before the mixture was warmed to -40 °C over the course of 1 h and stirred for another 1 h at -40 °C. Next, the mixture was quenched with H_2O (10 mL) and extracted with Et_2O (3× 15mL). The combined organic layers were washed with sat. NH_4Cl and brine and dried over Na_2SO_4. The volatiles were removed under reduced pressure and the crude product was purified using column chromatography (1% EtOAc in heptane), yielding alkyne **4** (1.4 g, 87%) as a dark brown oil. R_f =

0.33 (1% EtOAc in heptane). ^{1}H NMR (400 MHz, chloroform-*d*) δ 7.35 – 7.29 (m, 2H), 7.26 – 7.23 (m, 2H), 4.71 (s, 2H), 2.07 (s, 1H), 0.94 (s, 9H), 0.09 (s, 6H). ^{13}C NMR (100 MHz, chloroform-*d*) δ 154.5, 137.9, 127.4, 114.7, 84.7, 64.3, 33.2, 25.9, 18.4, -5.2. GCMS 6.71 min, m/z = 262 (M^+, calcd. for $C_{15}H_{22}O_2Si$ = 262, < 1%), 205 [$(M\text{-}C_{11}H_{13}O_2Si)^+$, 100%], 131 [$(M\text{-}C_9H_7O)^+$, 100%], 77 [$(M\text{-}C_6H_5)^+$, 30%].

(4-(Ethynyloxy)phenyl)methanol (5). TBMDS ether **4** (1.0 g, 3.8 mmol, 1.0 equiv.) was dissolved in dry THF (20 mL) and the mixture was cooled to 0 °C. 1 M TBAF in THF (4.2 mL, 4.2 mmol, 1.1 equiv.) was added and the mixture was stirred for 30 mins at 0 °C before the reaction was quenched with H_2O (15 mL). The product was extracted with EtOAc (3 × 15mL) and the combined organic layers were washed with brine and dried over $MgSO_4$. The volatiles were removed under reduced pressure and the crude product was purified using column chromatography (30% EtOAc in heptane), yielding alcohol **5** (506 mg, 91%) as a dark green solid. R_f = 0.3 (30% EtOAc in heptane). ^{1}H NMR (400 MHz, chloroform-*d*) δ 7.40 – 7.36 (m, 2H), 7.30 – 7.27 (m, 2H), 4.68 (s, 2H), 2.10 (s, 1H). ^{13}C NMR (100 MHz, chloroform-*d*) δ 155.0, 137.3, 128.5, 115.1, 84.5, 64.6, 33.5. GCMS 4.64 min, m/z = 148 (M^+, calcd. for $C_9H_8O_2$ = 148, 100%), 77 [$(M\text{-}C_6H_5)^+$, 70%].

***(E)*-(2-(4-(Hydroxymethyl)phenoxy)vinyl)boronic acid pinacol ester (6)**. Alkyne **5** (100 mg, 0.68 mmol, 1.0 equiv.) was dissolved in dry toluene (2 mL) and sparged with N_2 for 10 minutes. Pinacolborane (490 μL, 3.4 mmol, 5.0 equiv.) and $RuHClCO(PPh_3)_3$ (38 mg, 34 μmol, 0.05 equiv.) were added and the mixture was stirred at 50 °C overnight. The mixture was cooled down to r.t. before the volatiles were removed under reduced pressure. The crude product was dissolved in Et_2O (10 mL) and washed with sat. $NaHCO_3$ and brine, and dried over Na_2SO_4. The volatiles were removed under reduced pressure and the crude product was purified using column chromatography (30 to 40% EtOAc in heptane), yielding VBA **6** (141 mg, 76%) as a dark brown oil. R_f = 0.33 (40% EtOAc in heptane). ^{1}H NMR (400 MHz, chloroform-*d*) δ 7.36 – 7.31 (m, 2H), 7.23 (d, J = 13.8 Hz, 1H), 7.07 – 7.02 (m, 2H), 4.88 (d, J = 13.9 Hz, 1H), 4.66 (d, J = 5.7 Hz, 2H), 1.60 (t, J = 5.9 Hz, 1H), 1.27 (s, 12H). ^{13}C NMR (100 MHz, chloroform-*d*) δ 159.4, 136.6, 128.5, 118.4, 83.0, 64.8, 24.7, 21.1. No signal was observed for the carbon attached to boron. GCMS 8.90 min, m/z = 275 (M^+, calcd. for $C_{15}H_{21}BO_4$ = 275, 100%), 77 [$(M\text{-}C_6H_5)^+$, 28%].

4-(2-Bromoethoxy)benzaldehyde (8). 4-Hydroxybenzaldehyde **7** (1.0 g, 8.2 mmol, 1.0 equiv.) was dissolved in MeCN (63 mL) under ambient atmosphere. Dibromoethane (7.1 mL, 82 mmol, 10.0 equiv.) and K_2CO_3 (2.1 g, 14.9 mmol, 1.8 equiv.) were added and the mixture was stirred at 80 °C overnight. The mixture was cooled down to r.t., H_2O (50 mL) was added and the product was extracted with Et_2O (3 × 20 mL). The combined organic layers were washed with brine, dried over $MgSO_4$ and the volatiles were removed under reduced pressure. The crude product was purified using column chromatography (30% EtOAc in heptane), yielding ether **8** (1.5 g, 79%) as a white solid. R_f = 0.38 (30% EtOAc in heptane). ^{1}H NMR (400 MHz, chloroform-*d*) δ 9.90 (s, 1H), 7.92 – 7.81 (m, 2H), 7.06 – 6.98 (m, 2H), 4.38 (t, J = 6.2 Hz, 2H), 3.67 (t, J = 6.2 Hz, 2H). ^{13}C NMR (100 MHz, chloroform-*d*) δ 190.7, 163.0, 132.0, 130.5, 114.9, 68.0, 28.4. GCMS

6.87 min, m/z = 228 (M^+, calcd. for $C_9H_9BrO_2$ = 228.0, 67%), 201 [$(M\text{-}C_8H_8BrO)^+$, 70%], 107 [$(M\text{-}C_2H_4Br)^+$, 5%].

(4-(Vinyloxy)phenyl)methanol (9). Benzaldehyde **8** (400 mg, 1.8 mmol, 1.0 equiv.) was dissolved in dry DMSO (7 mL) and purged with N_2 for 10 minutes. *t*-BuOK (239 mg, 2.1 mmol, 1.2 equiv.) was slowly added in portions and the mixture was stirred for 10 minutes. Then, the mixture was diluted with EtOAc (35 mL) and quenched with ice water (1 mL). The layers were separated and the organic layers was washed with H_2O (3 × 10 mL), brine and dried over $MgSO_4$. The volatiles were removed under reduced pressure and the crude mixture was dissolved in MeOH (20 mL). $NaBH_4$ (132 mg, 3.5 mmol, 2.0 equiv.) was added in portions and the mixture was stirred for 1.5 h. The reaction was quenched with H_2O (20 mL) and the pH was adjusted with 0.1 M HCl until pH = 7. The mixture was extracted with EtOAc (3 × 15 mL), washed with brine and dried over $MgSO_4$. The volatiles were removed and the crude product was purified using column chromatography (20 to 30% EtOAc in heptane) yielding benzyl alcohol **9** (48 mg, 18%) as a colorless oil. R_f = 0.56 (30% EtOAc in heptane). ^{1}H NMR (400 MHz, chloroform-*d*) δ 7.36 – 7.30 (m, 2H), 7.03 – 6.97 (m, 2H), 6.64 (dd, *J* = 13.7, 6.1 Hz, 1H), 4.76 (dd, *J* = 13.7, 1.7 Hz, 1H), 4.65 (d, *J* = 4.2 Hz, 2H), 4.44 (dd, *J* = 6.1, 1.7 Hz, 1H). ^{13}C NMR (100 MHz, chloroform-*d*) δ 156.3, 148.2, 135.7, 128.6, 117.2, 95.2, 64.9. GCMS 4.55 min, m/z = 150 (M^+, calcd. for $C_9H_{10}O_2$ = 150, 100%), 107 [$(M\text{-}C_7H_7O)^+$, 70%], 77 [$(M\text{-}C_6H_5)^+$, 50%].

2-Chloro-2'-deoxy-3',5'-di-O-acetyladenosine (13). Cladribine **12** (25 mg, 88 µmol, 1.0 equiv.) was suspended in acetic anhydride (175 µl) and pyridine (263 µl). The mixture was stired for 1.5 h under N_2. The solvents were evaporated to yield acetylated cladribine **13** as a white solid (33 mg, quant.). R_f = 0.23 (5% MeOH in DCM). ^{1}H NMR (500 MHz, chloroform-*d*) δ 7.97 (s, 1H), 6.41 (dd, *J* = 8.1, 5.8 Hz, 1H), 5.86 (s, 2H), 5.41 – 5.36 (m, 1H), 4.38 (t, *J* = 3.9 Hz, 2H), 4.34 (td, *J* = 4.1, 3.6, 1.9 Hz, 1H), 2.80 (ddd, *J* = 14.4, 8.2, 6.3 Hz, 1H), 2.64 (ddd, *J* = 14.1, 5.8, 2.3 Hz, 1H), 2.14 (s, 3H), 2.11 (s, 3H). ^{13}C NMR (126 MHz, chloroform-*d*) δ 170.37, 170.29, 155.99, 154.35, 150.69, 138.76, 118.90, 84.46, 82.63, 74.39, 63.71, 37.99, 20.94, 20.82. HRMS (ESI+) m/z calcd for $C_{14}H_{17}ClN_5O_5^+$ $[M+H]^+$ 370.09127, found: 370.09182. m/z calcd for $C_{14}H_{16}ClN_5NaO_5^+$ $[M+Na]^+$ 392.07322, found: 392.07377.

***(E)*-(2-(4-(Perfluorophenyl carbonate)phenoxy)vinyl)boronic acid pinacol ester (14)**. Alcohol **6** (100 mg, 0.36 mmol, 1.0 equiv.) was dissolved in DCM (3 mL) under ambient atmosphere. Bis(pentafluorophenyl)carbonate (214 mg, 0.54 mmol, 1.5 equiv.) and Et_3N (252 µl, 1.8 mmol, 5.0 equiv.) were added and the mixture was stirred for 1 h. The volatiles were removed under reduced pressure and the crude product was purified using column chromatography (1 to 5% EtOAc in heptane), yielding VBA **14** (111 mg, 84%) as a colorless oil. R_f = 0.13 (5% EtOAc in heptane). ^{1}H NMR (500 MHz, chloroform-d_3) δ 7.40 (d, *J* = 8.6 Hz, 2H), 7.23 (d, *J* = 13.8 Hz, 1H), 7.08 (d, *J* = 8.6 Hz, 2H), 5.29 (s, 2H), 4.93 (d, *J* = 13.8 Hz, 1H), 1.28 (s, 12H). ^{13}C NMR (126 MHz, chloroform-*d*) δ 158.68, 156.78, 151.26, 142.25, 140.80, 140.20, 138.77, 136.85, 130.46, 130.25, 129.26, 118.41, 83.13, 71.59, 24.72. No signal was observed for the carbon

attached to boron. ^{19}F NMR (471 MHz, chloroform-*d*) δ -152.93 – -153.03 (m), -157.41 (t, *J* = 21.7 Hz), -161.90 – -162.05 (m). ^{11}B NMR (160 MHz, chloroform-*d*) δ 30.59. GCMS 12.91 min, *m/z* = 486 (M^+, $C_{22}H_{20}BF_5O_6$ = 486, 0%), 427 [$(M-C_{19}H_{13}BF_5O_5)^+$, 2%], 259 [$(M-C_{15}H_{20}BO_3)^+$, 50%].

***(E)*-(2-(4-(O-Diacetylated cladribine carbamate)phenoxy)vinyl)boronic acid pinacol ester (15).** 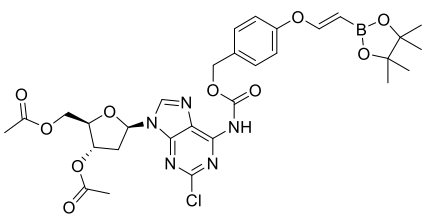 Acetylated cladribine **13** (19 mg, 50 μmol, 1.0 equiv.) was dissolved in DMF (1 ml) and cooled to 0 °C. NaH (2.5 mg, 60 μmol, 1.2 equiv, 60% dispersion in oil) was added. The mixture was stirred for 30 minutes before compound **14** (25 mg, 50 μmol, 1.0 equiv) was added. The reaction was stirred for 7 h and subsequently quenched with H_2O on ice. The water layer was extracted with EtOAc (3 x 5 ml). The combined organic layers were washed with brine and dried over Na_2SO_4. The solvents were removed under reduced pressure. Purification by flash chromatography (50-60% EtOAc in heptane) yielded the desired **15** (14 mg, 42%) as a white oil. R_f = 0.20 (60% EtOAC in heptane). ^{1}H NMR (500 MHz, chloroform-*d*) δ 8.25 (s, 1H), 8.15 (s, 1H), 7.42 (d, *J* = 8.6 Hz, 2H), 7.22 (d, *J* = 13.8 Hz, 1H), 7.05 (d, *J* = 8.6 Hz, 2H), 6.44 (dd, *J* = 8.0, 5.9 Hz, 1H), 5.39 (dt, *J* = 6.1, 2.2 Hz, 1H), 5.26 (s, 2H), 4.90 (d, *J* = 13.8 Hz, 1H), 4.37 (td, *J* = 5.4, 5.0, 2.1 Hz, 3H), 2.80 (ddd, *J* = 14.3, 8.1, 6.3 Hz, 1H), 2.67 (ddd, *J* = 14.2, 5.9, 2.3 Hz, 1H), 2.14 (s, 3H), 2.09 (s, 3H), 1.26 (s, 12H). ^{13}C NMR (126 MHz, chloroform-*d*) δ 170.48, 170.41, 159.09, 156.47, 154.26, 152.54, 150.64, 150.20, 141.18, 130.91, 130.44, 121.53, 118.45, 84.80, 83.21, 82.97, 74.45, 67.82, 63.78, 38.18, 24.88, 21.06, 20.95. No signal was observed for the carbon attached to boron. ^{11}B NMR (160 MHz, $CDCl_3$) δ 22.42. HRMS (ESI+) *m/z* calcd for $C_{30}H_{35}BClN_5NaO_{10}^+$ $[M+Na]^+$ 694.20577, found: 694.20565.

***(E)*-(2-(4-(Cladribine carbamate)phenoxy)vinyl)boronic acid pinacol ester (16).** 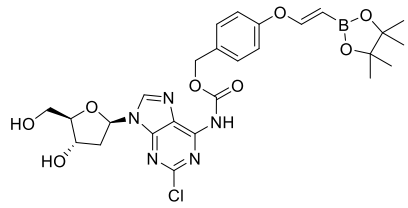 Cladribine-VBA **15** (9.5 mg, 14 μmol, 1.0 equiv) was dissolved in MeCN (500 μL) and NaOMe (7.1 μL, 5M solution in MeOH, 2.5 equiv) was added. After 1 h, the solvents were evaporated and the product was dissolved in 10% H_2O in MeCN to yield pure cladribine-VBA **16** as a yellow solid (5 mg, 59%). R_f = 0.40 (10% MeOH in DCM). ^{1}H NMR (500 MHz, MeOH-d_4) δ 8.03 (s, 1H), 7.26 (d, *J* = 8.6 Hz, 2H), 6.86 (d, *J* = 8.6 Hz, 2H), 6.32 – 6.19 (m, 3H), 5.00 (s, 2H), 4.90 (d, *J* = 13.6 Hz, 1H), 4.46 (dt, *J* = 5.6, 2.7 Hz, 1H), 3.94 (q, *J* = 3.0 Hz, 1H), 3.69 (ddd, *J* = 55.6, 12.3, 3.3 Hz, 2H), 2.72 – 2.62 (m, 1H), 2.31 – 2.24 (m, 1H), 1.10 (s, 12H). ^{13}C NMR (126 MHz, MeOH-d_4) δ 157.77, 153.36, 149.92, 144.80, 139.30, 130.67, 129.13, 115.67, 88.29, 85.47, 74.42, 71.58, 66.04, 62.29, 40.03, 23.62. No signal was observed for the carbon attached to boron. Pinacol is no longer attached, due to the NMR solvent. ^{11}B NMR (160 MHz, MeOH-d_4) δ 4.38. HRMS (ESI+) *m/z* calcd for $C_{26}H_{31}BClN_5NaO_8^+$ $[M+Na]^+$ 610,18519, found: 610,18615.

6-(6-(Pyridin-2-yl)-1,4-dihydro-1,2,4,5-tetrazin-3-yl)pyridine-3-amine (S1).

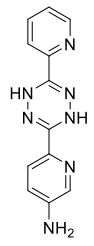

5-Amino-2-pyridinecarbonitrile (1.0 g, 8.39 mmol, 1.0 equiv.) and 2-cyanopyridine (0.87 g, 8.39 mmol, 1.0 equiv.) were heated in hydrazine monohydrate (1.6 mL, 33.57 mmol, 4.0 equiv.) overnight at 90 °C under nitrogen. The solvent was evaporated and the mixture was purified twice using column chromatography, first a column using 40-80% EtOAc in heptane and then 0-5% MeOH in DCM yielding dihydrotetrazine **S1** as a yellow solid (520 mg, 2.05 mmol, 24%). R_f = 0.25 (50% EtOAc in heptane). ^{1}H NMR (400 MHz, DMSO-*d*$_6$) δ 8.70 (s, 1H), 8.65 (s, 1H), 8.62 (ddd, *J* = 4.9, 1.7, 1.0 Hz, 1H), 7.98-7.88 (m, 3H), 7.64 (dd, *J* = 8.6, 0.7 Hz, 1H), 7.51 (ddd, *J* = 7.2, 4.9, 1.5 Hz, 1H), 6.99 (dd, *J* = 8.6, 2.7 Hz, 1H), 5.88 (s, 2H). ^{13}C NMR (100 MHz, DMSO-*d*$_6$) δ 148.6, 147.5, 146.7, 146.64, 146.60, 137.3, 134.2, 134.1, 125.2, 121.8, 120.8, 120.3. LRMS (ESI+) *m*/*z* calcd for $C_{12}H_{12}N_7^+$ $[M+H]^+$ 254.1, found: 254.1. The data agrees with the reported literature values.[28-29]

2-(Boc-amino)-*N*-(6-(6-(pyridine-2-yl)-1,4-dihydro-1,2,4,5-tetrazin-3yl)pyridine-3-yl)acetamide (S2).

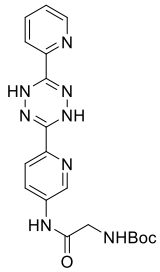

Boc-glycine (622 mg, 3.55 mmol, 2.0 equiv.) was dissolved in dry THF (9 mL) under nitrogen and cooled to 0 °C. *N*-Methylmorpholine (977 µL, 8.88 mmol, 5.0 equiv.) and isobutyl chloroformate (464 µL, 3.55 mmol, 2.0 equiv.) were added and the mixture was stirred for 5 min. Then amine **S1** (450 mg, 1.78 mmol, 1.0 equiv.) was added and the mixture was stirred overnight. Water and EtOAc were added, the layers were separated and the water layer was extracted with EtOAc (2 x). The combined organic layers were washed with sat. $NaHCO_3$ (aq.), dried over Na_2SO_4, and the solvent was removed under reduced pressure. The product was purified using column chromatography (70-100% EtOAc in heptane) yielding amide **S2** as a yellow solid (575 mg, 79%). R_f = 0.37 (70% EtOAc in heptane). ^{1}H NMR (400 MHz, DMSO-*d*$_6$) δ 10.41 (s, 1H), 8.93 (s, 1H), 8.88 (s, 1H), 8.82 (d, *J* = 2.5 Hz, 1H), 8.67-8.57 (m, 1H), 8.15 (dd, *J* = 8.7, 2.5 Hz, 1H), 8.00-7.87 (m, 3H), 7.53 (ddd, *J* = 7.2, 4.9, 1.5 Hz, 1H), 7.13 (t, *J* = 6.1 Hz, 1H), 3.78 (d, *J* = 6.1 Hz, 2H), 1.40 (s, 9H). ^{13}C NMR (100 MHz, DMSO-*d*$_6$) δ 169.2, 155.9, 148.6, 147.3, 146.3, 146.1, 141.3, 138.9, 137.4, 137.0, 126.8, 125.3, 121.4, 121.0, 78.2, 43.8, 28.2. LRMS (ESI+) *m*/*z* calcd for $C_{19}H_{23}N_8O_3^+$ $[M+H]^+$ 411.2, found: 411.1. The data agrees with the reported literature values. [28]

2-(Boc-amino)-*N*-(6-(6-(pyridine-2-yl)-1,2,4,5-tetrazin-3-yl)pyridine-3-yl)acetamide (S3).

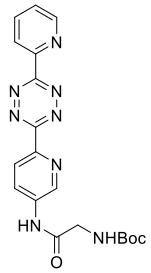

Dihydrotetrazine **S2** (300 mg, 0.73 mmol, 1.0 equiv.) was dissolved in acetic acid (15 mL). Sodium nitrite (93 mg, 1.10 mmol, 1.1 equiv.) was added and the solution was stirred for 10 min. The mixture was diluted with DCM, and washed 3 times with sat. $NaHCO_3$ (aq.). The organic layer was dried with Na_2SO_4 and the volatiles were removed under reduced pressure. The product was purified using column chromatography (0-8% MeOH in DCM) yielding tetrazine **S3** as a pink solid (151 mg, 51%). R_f = 0.45 (10% MeOH in DCM). ^{1}H NMR (400 MHz, DMSO-*d*$_6$) δ 10.62 (s, 1H), 9.05 (d, *J* = 2.5 Hz, 1H), 8.97-8.90 (m, 1H), 8.64 (d, *J* = 8.7 Hz, 1H), 8.59 (td, *J* = 8.0, 1.1 Hz, 1H), 8.43 (dd, *J* = 8.7, 2.5 Hz, 1H), 8.16 (dt, *J* = 7.7, 1.7 Hz, 1H), 7.73 (ddd, *J* = 7.7, 4.7, 1.2 Hz, 1H), 7.18 (t, *J* = 6.1 Hz, 1H), 3.84 (d, *J* = 6.1, 2H), 1.41 (s, 9H). ^{13}C NMR (100 MHz, DMSO-*d*$_6$) δ 169.5, 163.0, 162.8, 156.0, 150.6, 150.2, 144.0, 141.3, 138.2, 137.8, 126.6, 126.3, 124.9, 124.2, 78.2, 43.9, 28.2. LRMS (ESI+) *m*/*z* calcd for $C_{19}H_{21}N_8O_3^+$ $[M+H]^+$ 409.2, found: 409.1. The data agrees with the reported literature values. [28]

2-Amino-*N*-(6-(6-(pyridine-2-yl)-1,2,4,5-tetrazin-3-yl)pyridine-3-yl)acetamide hydrochloride (17). 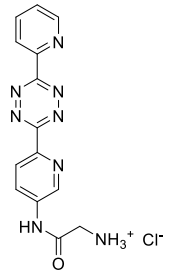

Boc-protected amine **S3** (40 mg, 98 µmol, 1.0 equiv.) was dissolved in dry DCM (2.2 mL) under nitrogen. 4M HCl in dioxane (735 µL, 2.94 mmol, 30 equiv.) was slowly added and the mixture was stirred for 30 min. The solvent was removed under reduced pressure, whereupon the pink solid was lyophilized yielding amine **17** (34 mg, quant.). ^{1}H NMR (400 MHz, DMSO-d_6) δ 11.57 (s, 1H), 9.16 (d, J = 2.4 Hz, 1H), 8.98-8.91 (m, 1H), 8.68 (d, J = 8.7 Hz, 1H), 8.61 (dt, J = 8.0, 1.1 Hz, 1H), 8.44 (dd, J = 8.7, 2.5 Hz, 1H), 8.35 (br. t, J = 5.6 Hz, 2H), 8.18 (dt, J = 7.7, 1.8 Hz, 1H), 7.75 (ddd, J = 7.7, 4.7, 1.2 Hz, 1H), 3.99-3.91 (m, 2H). ^{13}C NMR (100 MHz, DMSO-d_6) δ 166.1, 163.0, 162.7, 150.5, 150.0, 144.6, 141.3, 138.0, 137.6, 126.7, 126.6, 125.1, 124.3, 41.3. LRMS (ESI+) m/z calcd for $C_{14}H_{13}N_8O^+$ $[M+H]^+$ 309.1, found: 309.1. The data agrees with the reported literature values.[28]

^{1}H NMR study of the click-to-release reaction. The reactions between tetrazine **10** and the alkenes **6** and **9** in 3:1 CD_3OD/deuterated PBS were followed using ^{1}H NMR (500 MHz). Prior to the start of the tetrazine ligation, pinacol ester **6** (5 mM) was incubated in 3:1 MeOD-d_4/deuterated PBS. The hydrolysis of the pinacol ester was followed over time and showed full conversion to the free boronic acid within 2 h (Figure SI-1). Next, tetrazine **17** (5.0 mM) and the deprotected VBA **6** or the vinyl ether **9** (5.0 mM) were mixed 1:1 for a final concentration of 2.5 mM and the reactions were followed over time up to 14 days at room temperature.

Second order rate constant experiment. The reactions between the alkenes and dipyridyl tetrazine derivative **10** in 75% MeOH/PBS were followed on a plate reader (Spark M10 microplate reader (Tecan)) at a controlled temperature of 20 °C, by measuring the absorbance of the tetrazine at 540 nm. The tetrazine and alkene were both dissolved in methanol, and then diluted with PBS. After addition of the tetrazine to the alkene solution, the measurement was started directly. The final concentration of the tetrazine was 500 µM and of the excess of alkene was 5, 6.25, 7.50, 8.75 µM or 10mM. The time between the addition of the tetrazine and the start of the measurement was ± 20s. All reactions were performed in quadruplo. The kinetics were normalized and plotted in Figure SI-2A and 2B. The observed reactions were normalized by setting the absorbance at t = 0 s as 100%. Since the reactions did not end in a plateau after the set time, the plateau was set equal to the background absorbance of the dihydropyridazine absorption at the given wavelength. It was taken into account that the measurement was started after a certain time.

Pseudo-first-order rate constant determination. The pseudo first-order rate constants k_{obs} for the tetrazine reactions with an excess of alkene was determined. The decay of the absorbance of the tetrazine was plotted against time (min) for the 5 different concentrations of the alkene. The k_{obs} was determined by fitting an exponential 'one phase decay' (nonlinear regression) using PrismGraphPad Software whereby Y = (Y0 -plateau)*exp(-k_{obs}*time(s)) + plateau.

Second-order rate constant determination. To determine the second-order rate constant, the k_{obs} of the reactions was plotted against the concentration of the alkenes. The line was fitted using a linear regression and the slope gave k_2. The goodness of the fit is shown by the coefficient of determination (R^2). The data is shown in Figure SI-2A and 2B.

Click-to-release LCMS measurements. The reaction between tetrazine **17** and cladribine-VBA **16** in 1% DMSO/PBS was followed using LCMS. Prior to the start of the tetrazine ligation, pinacol ester **16** (0.2 mM) was incubated in 1% DMSO/PBS. The hydrolysis of the pinacol ester was followed over time and tetrazine **17** (0.2 mM or 2.0 mM) was subsequently added. The reaction was followed over 24 hours at 37 °C. The amount of cladribine was determined and was quantified by the area under the curve. The graph shows the relative amount compared to the amount of starting material.

Cell toxicity assays. ACPA-expressing B cell clones or HEK-TM cells were cultured with medium, and mIL21-Fc and soluble CD40L (from Biolegend) for the B cell clones. Stock solutions of tetrazine (500 mM), cladribine (10 μM) and cladribine-VBA (10 μM) were prepared in DMSO. Different concentrations were diluted in medium and cladribine-VBA was premixed with tetrazine in different amounts. All conditions were incubated overnight at 37 °C (except for the experiment in Figure SI-5, in there everything was mixed with the cells and directly incubated for 3 days) and added to $3x10^4$ ACPA-expressing B cell clones or 1×10^4 HEK-TM cells in a 96-well plate. The cells were incubated for 3 days, after which XTT labelling and electron-coupling reagents (Roche) were added to the culture according to the manufacturer's protocol and incubated for 4 hours. After the addition of a 5% Tween solution, cell viability was measured on a iMark TM Microplate Reader (from BioRad). Values measured at 630-690 nm were subtracted from 450-500 nm.

4.6 References

1. Oliveira, B. L.; Guo Z.; Bernardes, G. J. L.; Inverse electron demand Diels–Alder reactions in chemical biology. *Chem. Soc. Rev.* **2017,** *46* (16), 4895-4950.
2. Saxon, E.; Bertozzi, C. R., Cell surface engineering by a modified Staudinger reaction. *Science* **2000,** *287* (5460), 2007-2010.
3. Sletten, E. M.; Bertozzi, C. R., From mechanism to mouse: a tale of two bioorthogonal reactions. *Acc. Chem. Res.* **2011,** *44* (9), 666-676.
4. Debets, M. F.; van Berkel, S. S.; Dommerholt, J.; Dirks, A. J.; Rutjes, F. P. J. T.; van Delft, F. L.; Bioconjugation with strained alkenes and alkynes. *Acc. Chem. Res.* **2011,** *44* (9), 805-815.
5. Eising, S.; Lelivelt, F.; Bonger, K. M., Vinylboronic Acids as Fast Reacting, Synthetically Accessible, and Stable Bioorthogonal Reactants in the Carboni–Lindsey Reaction. *Angew. Chem. Int. Ed.* **2016,** *55*, 12243-12247.
6. Eising, S.; van der Linden, N. G. A.; Kleinpenning, F.; Bonger, K. M., Vinylboronic Acids as Efficient Bioorthogonal Reactants for Tetrazine Labeling in Living Cells. *Bioconjug. Chem.* **2018,** *29* (4), 982-986.
7. Eising, S.; Xin, B.-T.; Kleinpenning, F.; Heming, J. J. A.; Florea, B. I.; Overkleeft, H. S.; Bonger, K. M., Coordination-Assisted Bioorthogonal Chemistry: Orthogonal Tetrazine Ligation with Vinylboronic Acid and a Strained Alkene. *ChemBioChem* **2018,** *19* (15), 1648-1652.
8. Tornøe, C. W.; Christensen, C.; Meldal, M., Peptidotriazoles on solid phase:[1, 2, 3]-triazoles by regiospecific copper (I)-catalyzed 1, 3-dipolar cycloadditions of terminal alkynes to azides. *J. Org. Chem.* **2002,** *67* (9), 3057-3064.
9. Rostovtsev, V. V.; Green, L. G.; Fokin, V. V.; Sharpless, K. B., A stepwise huisgen cycloaddition process: copper (I)-catalyzed regioselective" ligation" of azides and terminal alkynes. *Angew. Chem. Int. Ed.* **2002,** *41* (14), 2596-2599.
10. Eising, S.; Engwerda, A. H. J.; Riedijk, X.; Bickelhaupt, F. M.; Bonger, K. M., Highly Stable and Selective Tetrazines for the Coordination-Assisted Bioorthogonal Ligation with Vinylboronic Acids. *Bioconjug. Chem.* **2018**.
11. Li, J.; Chen, P. R., Development and application of bond cleavage reactions in bioorthogonal chemistry. *Nat. Chem. Biol.* **2016,** *12*, 129-137.
12. Sauer, J.; Heldmann, D. K.; Hetzenegger, J.; Krauthan, J.; Sichert, H.; Schuster, J., 1,2,4,5-Tetrazine: Synthesis and Reactivity in [4+2] Cycloadditions. *Eur. J. Org. Chem.* **1998,** *12*, 2885-2896.
13. Thalhammer, F.; Wallfahrer, U.; Sauer, J., Reaktivität einfacher offenkettiger und cyclischer dienophile bei Diels-Alder-reactionen mit inversem elektronenbedarf. *Tetrahedron Lett.* **1990,** *31*, 6851-6854.
14. Versteegen, R. M.; Rossin, R.; Ten Hoeve, W.; Janssen, H. M.; Robillard, M. S., Click to release: Instantaneous doxorubicin elimination upon tetrazine ligation. *Angew. Chem. Int. Ed.* **2013,** *52*, 14112-14116.
15. Oneto, J. M. M.; Khan, I.; Seebald, L.; Royzen, M., In Vivo Bioorthogonal Chemistry Enables Local Hydrogel and Systemic Pro-Drug To Treat Soft Tissue Sarcoma. *ACS Cent. Sci.* **2016,** *2*, 476-482.
16. Rossin, R.; Van Duijnhoven, S. M. J.; Ten Hoeve, W.; Janssen, H. M.; Kleijn, L. H. J.; Hoeben, F. J. M.; Versteegen, R. M.; Robillard, M. S., Triggered Drug Release from an Antibody-Drug Conjugate Using Fast "Click-to-Release" Chemistry in Mice. *Bioconjug. Chem.* **2016,** *27*, 1697-1706.
17. Li, J.; Jia, S.; Chen, P. R., Diels-Alder reaction–triggered bioorthogonal protein decaging in living cells. *Nat. Chem. Biol.* **2014,** *10*, 1003-1005.
18. Zhang, G.; Li, J.; Xie, R.; Fan, X.; Liu, Y.; Zheng, S.; Ge, Y.; Chen, P. R., Bioorthogonal chemical activation of kinases in living systems. *ACS Cent. Sci.* **2016,** *2*, 325-331.
19. Carlson, J. C. T.; Mikula, H.; Weissleder, R., Unraveling Tetrazine-Triggered Bioorthogonal Elimination Enables Chemical Tools for Ultrafast Release and Universal Cleavage. *J. Am. Chem. Soc.* **2018,** *140*, 3603-3612.
20. Jiménez-Moreno, E.; Guo, Z.; Oliveira, B. L.; Albuquerque, I. S.; Kitowski, A.; Guerreiro, A.; Boutureira, O.; Rodrigues, T.; Jiménez-Osés, G.; Bernardes, G. J. L., Vinyl Ether/Tetrazine Pair for the Traceless Release of Alcohols in Cells. *Angew. Chem. Int. Ed.* **2017,** *56*, 243-247.
21. Wu, H.; Alexander, S. C.; Jin, S.; Devaraj, N. K., A Bioorthogonal Near-Infrared Fluorogenic Probe for mRNA Detection. *J. Am. Chem. Soc.* **2016,** *138*, 11429-11432.

22. Kipps, T. J., Chronic lymphocytic leukemia. *Curr. Opin. Hematol.* **2000,** *7* (4), 223-234.
23. Baker, D.; Herrod, S. S.; Alvarez-Gonzalez, C.; Zalewski, L.; Albor, C.; Schmierer, K., Both cladribine and alemtuzumab may effect MS via B-cell depletion. *Neurol. Neuroimmunol. Neuroinflamm.* **2017,** *4* (4), 1-13.
24. Leist, T. P.; Weissert, R., Cladribine: mode of action and implications for treatment of multiple sclerosis. *Clin. Neuropharmacol.* **2011,** *34* (1), 28-35.
25. Edwards, J. C. W.; Szczepański, L.; Szechiński, J.; Filipowicz-Sosnowska, A.; Emery, P.; Close, D. R.; Stevens, R. M.; Shaw, T., Efficacy of B-cell–targeted therapy with rituximab in patients with rheumatoid arthritis. *N. Engl. J. Med.* **2004,** *350* (25), 2572-2581.
26. Blencowe, C. A.; Russell, A. T.; Greco, F.; Hayes, W.; Thornthwaite, D. W., Self-immolative linkers in polymeric delivery systems. *Polym. Chem.* **2011,** *2* (4), 773-790.
27. Meijer, A.; Otto, S.; Engberts, J. B. F. N., Effects of the Hydrophobicity of the Reactants on Diels−Alder Reactions in Water. *J. Org. Chem* **1998,** *63* (24), 8989-8994.
28. Lang, K.; Davis, L.; Torres-Kolbus, J.; Chou, C.; Deiters, A.; Chin, J. W., Genetically encoded norbornene directs site-specific cellular protein labelling via a rapid bioorthogonal reaction. *Nat. Chem.* **2012,** *4* (4), 298-304.
29. Blackman, M. L.; Royzen, M.; Fox, J. M., The Tetrazine Ligation: Fast Bioconjugation based on Inverse-electron-demand Diels-Alder Reactivity. *J. Am. Chem. Soc.* **2008,** *130* (41), 13518-13519.

4.7 Supplementary Figures

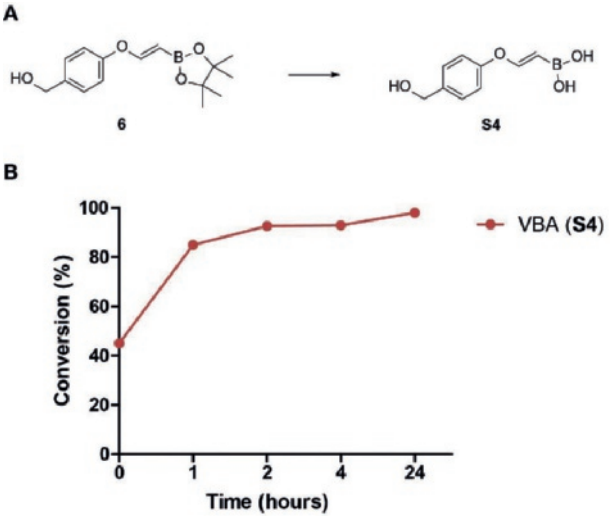

Figure SI-1. Pinacol hydrolysis in PBS. A) Schematic representation of the pinacol hydrolysis; B) Studies were performed with 5mM VBA **6** dissolved in 75% MeOD/deuteurated PBS at room temperature and analyzed at different time points by ^{1}H NMR.

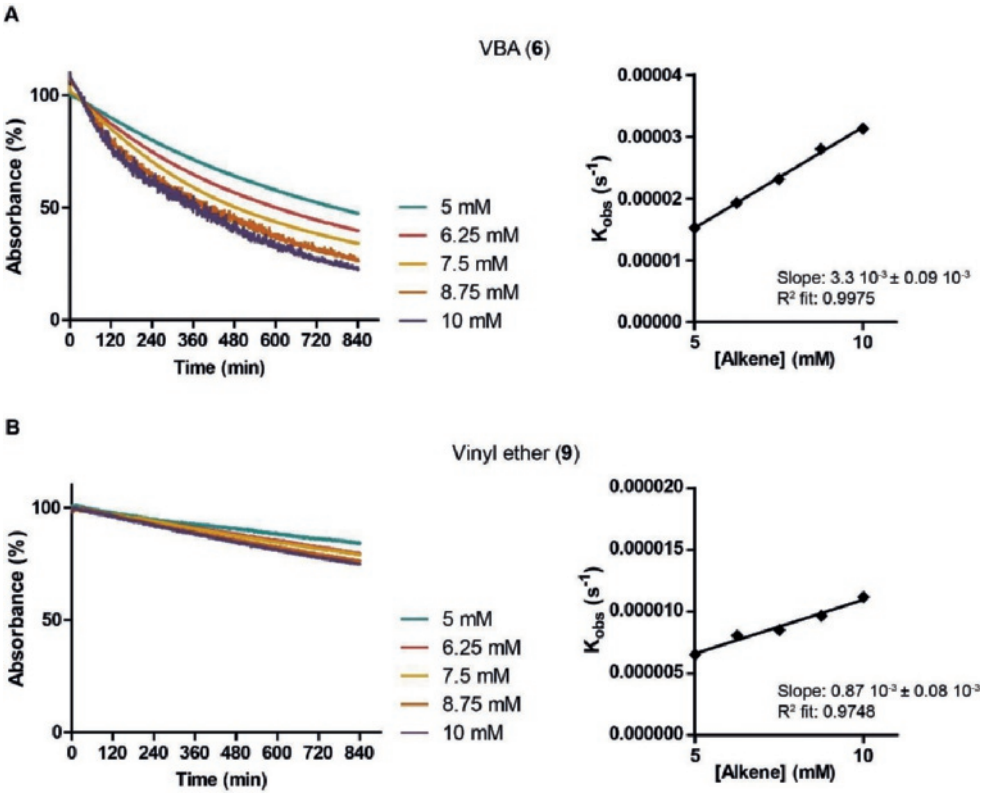

Figure SI-2. Kinetics of the click-to-release reaction with tetrazine **10** (500 μM) with 10 - 20 equiv. of the alkene in 75% MeOH/PBS. The left graph is the normalized absorbance at 540 nm of the reaction between tetrazine **10** and the alkene (A: VBA **6** and B: vinyl ether **9**) at different concentrations against time (min). The right graph shows the plot of the k_{obs} values against the alkene (A: VBA **6** and B: vinyl ether **9**) concentration. The slope of the linear fit is the second - order rate constant, the goodness of the fit is shown by R^2.

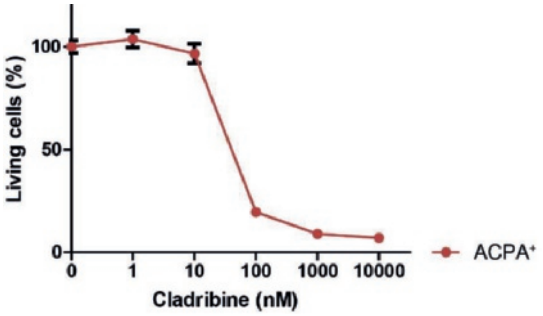

Figure SI-3. Dose dependency of ACPA-positive B cell clone for cladribine. Immortalized ACPA-positive B cells were incubated with cladribine for 3 days before an XTT assay was performed. Experiment was performed in triplo.

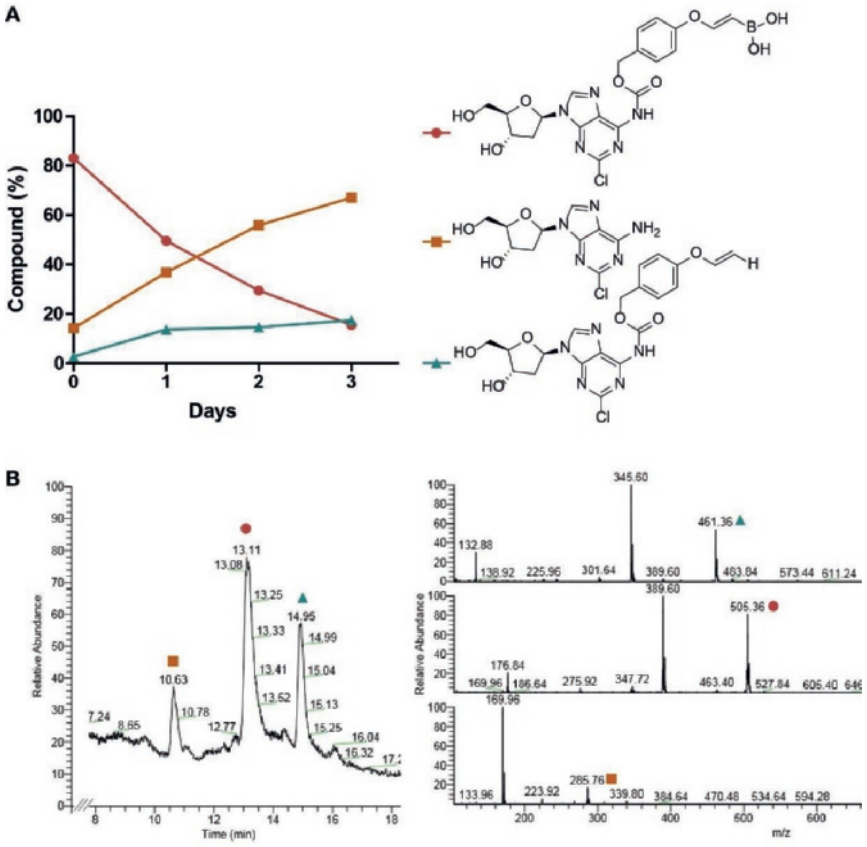

Figure SI-4. Stability of cladribine-VBA **16**. Studies were performed at 37 °C in PBS and analyzed at different time points by LCMS. A) Day 0 is not 100% since the stock solution (12mg/mL) in DMSO, was stored at -20 °C for approximately 10 weeks, and contained some unprotected cladribine; B) LCMS spectrum after 1 day of incubation.

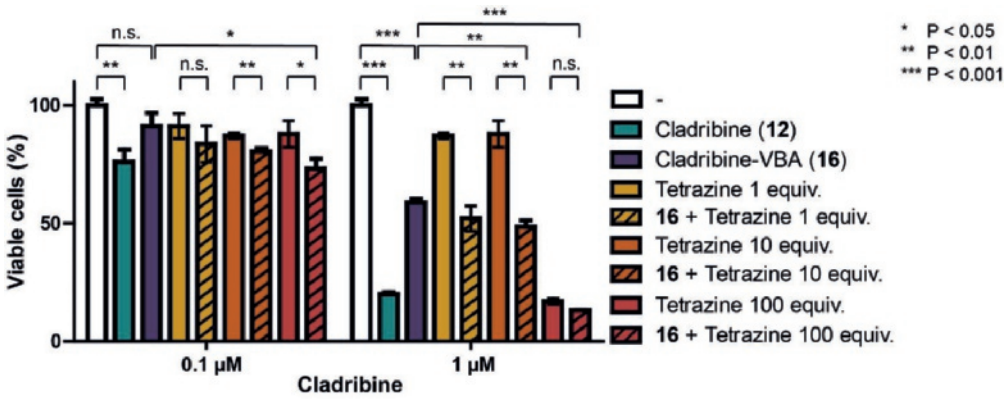

Figure SI-5. Incubation and click-to-release with ACPA-positive B cell clones (50.000 cells per well). For 0.1 µM cladribine significant deprotection was observed, however, the toxicity was only a small percentage of the control. For 1 µM cladribine, which showed clear cytotoxicity, the addition 1 and 10 equiv. tetrazine were not toxic, but 100 equiv. (100 µM) was as toxic as cladribine (1 µM). Click-to-release of cladribine-VBA **16** with 1 or 10 equiv. tetrazine showed a significant result to liberate cladribine, however, full deprotection was the goal. Statistics were calculated using a student t-Test using two-sample assuming unequal variances (confirmed by F-Test) and a two-tailed distribution.

Chapter 5

Multivalent Polymer Scaffolds for Targeting of ACPA-Selective B Cells

Lianne Lelieveldt*, Hendy Kristyanto*, Yvonne Bartels, Carl Figdor, Hans Ulrich Scherer, René Toes, Roel Hammink, Kimberly Bonger. *Manuscript in preparation.*
*authors contributed equally

Abstract

Rheumatoid arthritis (RA) is characterized by the production of anti-citrullinated protein antibodies (ACPA) in the majority of the patients. To obtain more knowledge about the origin and role of autoreactive B cells in RA, isolation of ACPA-producing B cells is required. Recently, a method was developed to target and isolate B cells using a tetravalent streptavidin (SA) protein conjugated to biotinylated antigens. Here we explore the possibility of using a higher multivalent scaffold for B cell targeting to increase binding avidity and the number of potential binding sites for cargo loading. The scaffold used for this purpose consists of poly(isocyanopeptides) (PIC). This polymer with a length of approximately 400 nm has more than 100 binding sites available compared to only 4 for SA. We synthesized this PIC scaffold containing a fluorophore and different antigen peptides. It was shown that both the citrullinated peptide-containing PIC and SA scaffold bound equally effective to ACPA-positive cells as evidenced by flow cytometry binding studies. However, a major difference between these two scaffolds was observed with respect to non-specific binding. For the antigens conjugated to the PIC scaffold hardly any non-specific binding was observed, whereas high background levels were detected for antigens conjugated to SA. It was also noted that the antigen used as negative control, CArgP, gave high background signals, whereas this was not observed for cyclic norleucine peptide (CNleP). Lastly, we indirectly showed that PICs were not internalized upon binding to the BCR, making them a suitable scaffold for carrying extracellular apoptotic signals.

5.1 Introduction

Rheumatoid arthritis (RA) is characterized by chronic inflammation causing cartilage and bone loss and occurs in ca. 1% of the western population. The inflammation results in deformed and painful joints and is sustained by antibody development of autoreactive B cells. These autoreactive antibodies are directed to citrullinated proteins and are present at the early onset of the disease.[1] Although anti-citrullinated protein antibodies (ACPA) have been extensively studied, much is unknown about the autoantibody-producing B cells. ACPA-positive B cells do display an activated and proliferative phenotype, however, they are present in low abundancy.[2] It has also been described that ACPA have low avidity compared to antibodies to 'recall' antigens.[3] These two features make it difficult to isolate ACPA-positive B cells for studies and to target these specific B cells for therapy.

A streptavidin (SA)-based method for enhanced isolation of these rare B cells was developed by Scherer *et al.*[4] They used fluorophore-containing SA tetramers conjugated to biotinylated citrulline-containing antigens to specifically detect ACPA-expressing B cells. However, it remains unclear whether they were able to isolate all ACPA-expressing B cells from circulation. Hence, we envision that a higher avidity for ACPA-positive B cells can be achieved by using a highly multivalent scaffold compared to the tetravalent SA system. In addition, while SA has only four possible binding sites, the use of a highly multivalent system provides more options for functionalization as for example multiple different antigens or a combination of antigens and drugs can be attached.

A good candidate for a multivalent system is the poly(isocyanopeptides) (PIC) scaffold. This polymer is semi-flexible and has already been shown to be effective in T cell activation because of proper arrangement and clustering of receptors by the attached components.[5] Mandal and coworkers showed that they could synthesize a filamentous synthetic dendritic cell (sDC) for T cell activation.[6] They were able to functionalize the isocyanopeptide polymer with anti-CD3 antibodies towards T-cell activation. In addition, they hypothesized and showed that, since the polymer is semi-flexible and contains multiple antibodies, the sDC was effective in T-cell binding and initiation of receptor clustering for T-cell activation. By comparing the sDCs to free anti-CD3 it was shown that the sDC increased T-cell activation by approximately 2.5 times and that these T-cells released 2-3 fold more IFNγ, a marker characterizing a late activation event.[7] This also underlines the benefit of multivalent scaffolds over monovalent compounds, in which the PICs mimic the protein mobility of natural plasma membranes.[8]

Due to low avidity of the citrullinated antigen targeting B cells we were curious to see whether enhanced binding to these B cells could be achieved using multivalent and flexible PICs to ACPA antigens. Moreover, in case successful binding is observed, this scaffold would be of great interest for future multivalent B cell targeting therapeutics.

5.2 Results and Discussion

Synthesis of multivalent antigen-containing SA and PIC scaffolds. To test the avidity for antigen-containing SA and PICs, we synthesized scaffolds containing the cyclic citrullinated peptide (CCP) antigen as well as a fluorophore for visualization. We used the cyclic citrullinated peptide 1 (CCP1) analogue, a well-known ACPA antigen,[9-10] as described in Chapter 2. The peptides CCP (**1**), CArgP (**2**) and CNleP (**3**, Figure 1), containing a biotin at the C-terminal lysine,

were conjugated to SA as described in Chapter 2 (Figure 1).[4] Prior to antigen conjugation, UV-Vis measurements were performed and the absorbance of SA and the absorbance of the respective fluorophore (AF647) were used to calculate the concentration of both (using the corresponding extinction coefficients and path length, see Section 5.5, Materials and Methods). The outcome of the calculations showed that on average every SA contained two fluorophores. Since SA can conjugate to four biotin molecules, the estimated fluorophore:antigen ratio was 1:2 (Note SI-1).

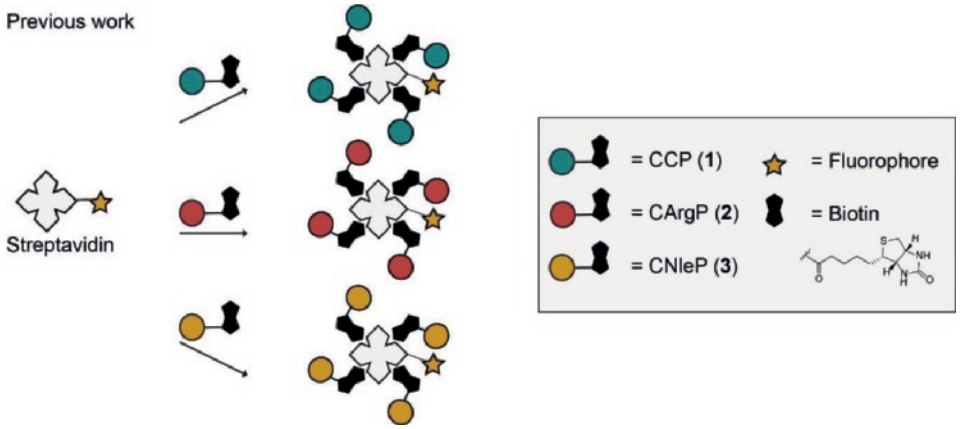

Figure 1. Overview of multivalent antigen-containing SA scaffolds. Three different conjugates were prepared, using NHS-AF647 and biotinylated peptides CCP, CArgP and CNleP.

The PIC scaffold is based on a water-soluble polyisocyano co-polymer bearing a non-functional methoxy and functional azide groups (Figure 2B). All PIC polymers were synthesized according to previously published methods.[5-6] The corresponding methoxy and azide isocyanide monomers were polymerized using a nickel catalyst to obtain azide-functionalized PICs with an average length of 383 nm. This resulted in a methoxy:azide ratio of 1:30, statistically yielding a polymer with a functional azide group every 3.5 nm. Considering the average polymer length, every scaffold contains approximately 110 available azides. Roughly half of the azides were utilized in a strain-promoted azide-alkyne cycloaddition by DBCO-PEG_4-biotin.[11-12] These polymers were further functionalized with a DIBO-AF647 (approximately 4% of the azides) prior to functionalization with an ACPA antigen peptide with the remaining azides.

For conjugation of CCP to PIC, we introduced a C-terminal lysine and reacted this peptide, after cyclization and purification, with NHS-PEG_4-DBCO (Figure 2A). This DBCO was subsequently used for the cycloaddition with the remaining azides on the PIC, in a final ratio of 1:10 fluorophore:CCP on the PICs (Figure 2B).

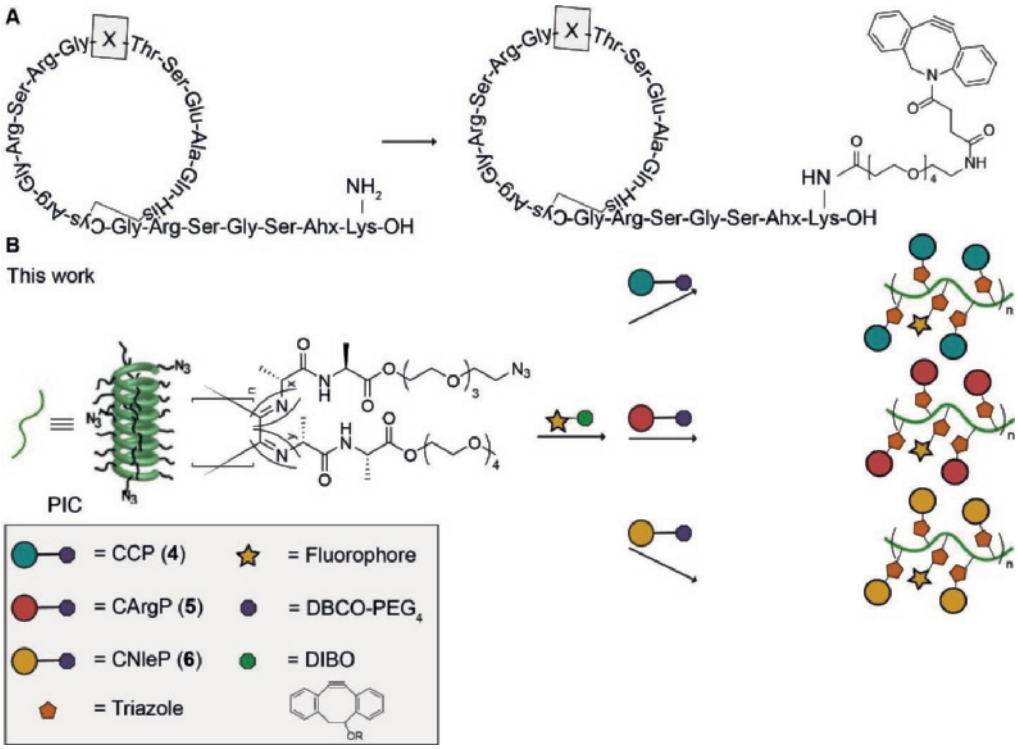

Figure 2. Overview of multivalent antigen-containing PIC scaffolds. A) The structure of CXP, with X being citrulline (CCP), arginine (CArgP) or norleucine (CNleP). CXP was synthesized with a lysine at the C-terminus which can be modified using a NHS-PEG_4-DBCO for cycloaddition purposes to the PIC polymers; B) Schematic overview of the synthesis approach of CXP loaded PICs. All PICs were first reacted with DBCO-biotin (not shown) and subsequently with DIBO-fluorophores and with one of the antigen peptides to form the multivalent antigen structure.

Flow cytometric binding studies of scaffold background. To evaluate the binding efficiencies of the different scaffolds to ACPA-expressing cells, we used $HEK^{ACPA\text{-}TM}$ as the antigen binding cells and non-transfected HEK cells as a negative control. These $HEK^{ACPA\text{-}TM}$ cells express transmembrane ACPA and GFP, and are known to bind to CCP.[4]

First, we examined the background signal of the unmodified scaffolds. For this, we used the SA and PIC scaffold conjugated to AF647, but without any antigen peptides. Scaffold concentrations were corrected to the amount of potentially bound antigens: while the PICs can contain 5 times more peptides than SA, 5 times lower scaffold concentrations were used to maintain the alleged peptide concentration throughout all experiments. This also means that the fluorophore concentration was lower for the PICs than for the SA scaffold. A starting concentration of around 1 μM was prepared for PIC and SA and serial dilutions were created from there. We next incubated the cell lines with the scaffolds at different concentrations for 30 minutes on ice, after which the cells were washed and fixed using 1% paraformaldehyde. The staining of cells was measured by flow cytometry. Since the ACPA-expressing cell line is GFP positive, double positive cells, stained for both GFP and AF647, were considered positive for scaffold binding. For the non-ACPA-

expressing cell line, no increased AF647 signal was expected, meaning that double negative cells were expected for the non-transfected HEK cells.

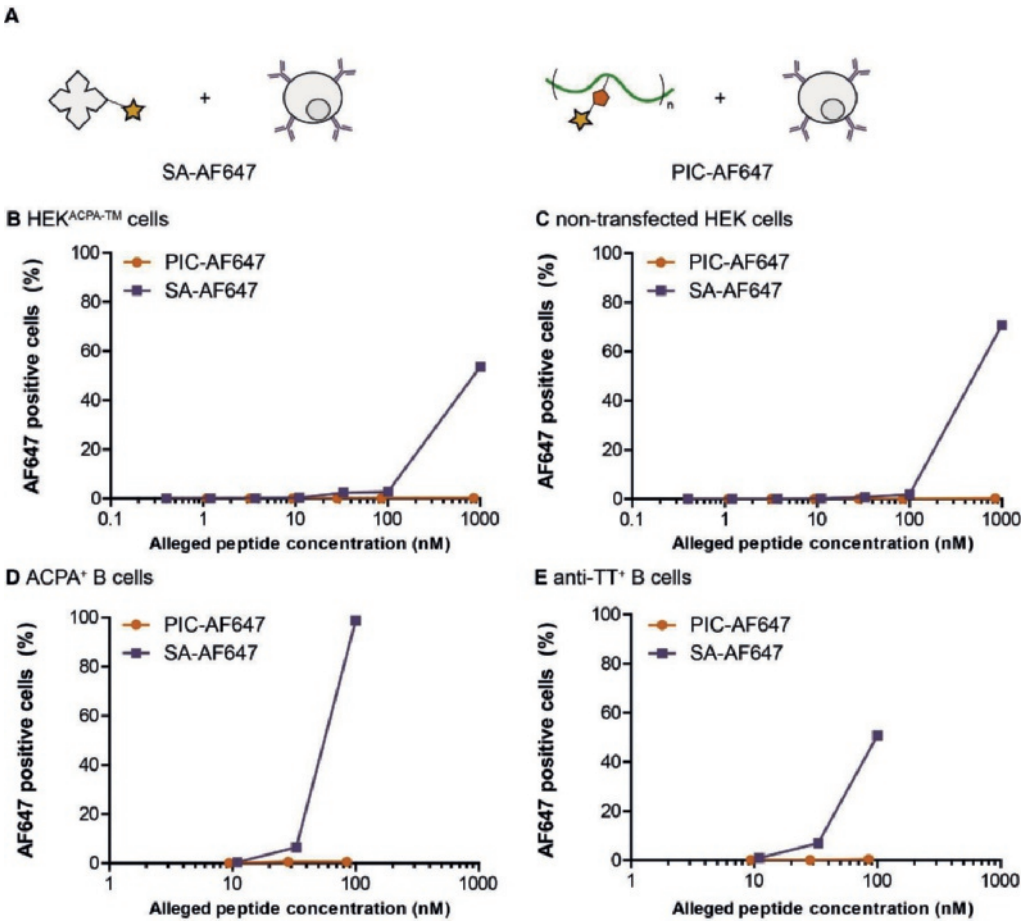

Figure 3. Flow cytometric binding studies of scaffold background for SA- and PIC-AF647. A) Schematic overview of experimental set-up; Percentage of positive cells was plotted against the alleged peptide antigen concentration for B) HEK$^{ACPA\text{-}TM}$ cells, C) non-transfected HEK cells, D) ACPA-positive B cells and E) anti-TT-positive B cells.

Figure 3A shows a schematic overview of the experimental set-up looking at background signal for both scaffolds. For both cell lines, no AF647 positive signal was expected due to the lack of antigen peptides. After measuring the fluorescence intensity for the different cell lines, we plotted the percentage of AF647 positive cells (see Figure SI-2 for HEK cell FACS plots) against the alleged peptide concentration on the scaffold. Figures 3B and C show that for both cell types high fluorescence signals were measured for SA-AF647, whereas hardly any signal was observed for PIC-AF647. This shows that the non-specific binding of SA for the different cell types was much higher than for the PIC scaffold. Although 5 times higher fluorophore concentrations were used in the SA samples to keep the peptide concentration constant, the observed background effect

was more than 5 times higher. This suggests that the non-specific binding is dependent on SA and not on the fluorophore itself.

In a follow-up experiment, we used immortalized B cells to evaluate binding. These B cells were previously isolated from an ACPA-positive RA patient and transduced with BCL-XL, BCL-6 and GFP genes resulting in an ACPA-secreting and -expressing, GFP-positive immortalized B cell line.[13] Similarly, immortalized B cells recognizing tetanus toxoid (TT) antigens were created. Both of these cells were used in experiments with both scaffolds with the ACPA-expressing B cells as target cells and the anti-TT-expressing B cells as the negative control cells. A similar experiment compared to both HEK cell lines was performed for the immortalized B cells. Since both cell lines are GFP positive, but no antigen is attached to the scaffold, GFP positive and AF647 negative signals were expected for both cell lines. Figures 3D and E (see Figure SI-3 for immortalized B cell FACS plots) show that indeed no AF647 positive cells were observed for the PIC scaffold. For the SA scaffold, however, increasing AF647 signals were observed with increasing scaffold concentrations. The background signal for SA was higher for the immortalized B cells compared to the HEK cell lines. So far, we do not have an explanation for this effect. Overall, the PICs do not show any background to all four cell types while increasing SA background with increasing concentrations was observed (Figure 3).

Flow cytometric binding studies of antigen loaded scaffolds. To see whether we could induce a higher binding avidity for the higher multivalent PIC scaffolds, we loaded the scaffolds with the peptide antigen CCP. The CCP antigens were synthesized with a C-terminal lysine and subsequently modified using NHS-PEG_4-DBCO (Figure 2A). The DBCO was reacted with the azides on the PICs, which were previously modified with the AF647 fluorophore (Figure 2B). The amounts of PIC-CCP and the SA-CCP for cell-binding experiments were based on equal peptide concentrations as described above. After incubation with the different cell types, we analyzed the data using flow cytometry (Figure 4A). Figure 4B depicts the increase in AF647 positive cells with the increase in peptide (and hence scaffold) concentration. Binding to non-transfected HEK cells was only observed at very high scaffold concentrations (Figure 4C). Since no ACPA receptor was present, this signal must be due to non-specific binding. Similar to what was observed for the non-loaded scaffolds (Figure 3), the SA scaffold gave a higher background signal than the PIC scaffold. For the ACPA-expressing B cells (Figure 4D) almost all cells were positive for AF647, even at the lowest concentration (1.2 nM), for both scaffolds. The difference between binding at the same concentration for ACPA-positive B cells and the $HEK^{ACPA\text{-}WT}$ cells is most likely due to the higher affinity for CCP of the immortalized B cells. Similarly, as observed for the non-transfected HEK cells, the anti-TT-positive B cells (Figure 4E) showed a background signal which was higher for SA than for the PIC scaffold. Figures SI-4 and SI-5 show the FACS plots corresponding to the HEK cells and the immortalized B cells, respectively.

Next, we evaluated the binding specificity for PIC and SA scaffolds loaded with control peptides CArgP and CNleP. High signals were observed for scaffolds containing CArgP. This peptide contains five positively charged arginine residues, which might explain the high binding to the negatively charged cell-membrane. Therefore, we evaluated whether a norleucine residue, an amino acid without a positive charge, at the variable position of CXP would diminish non-specific binding.

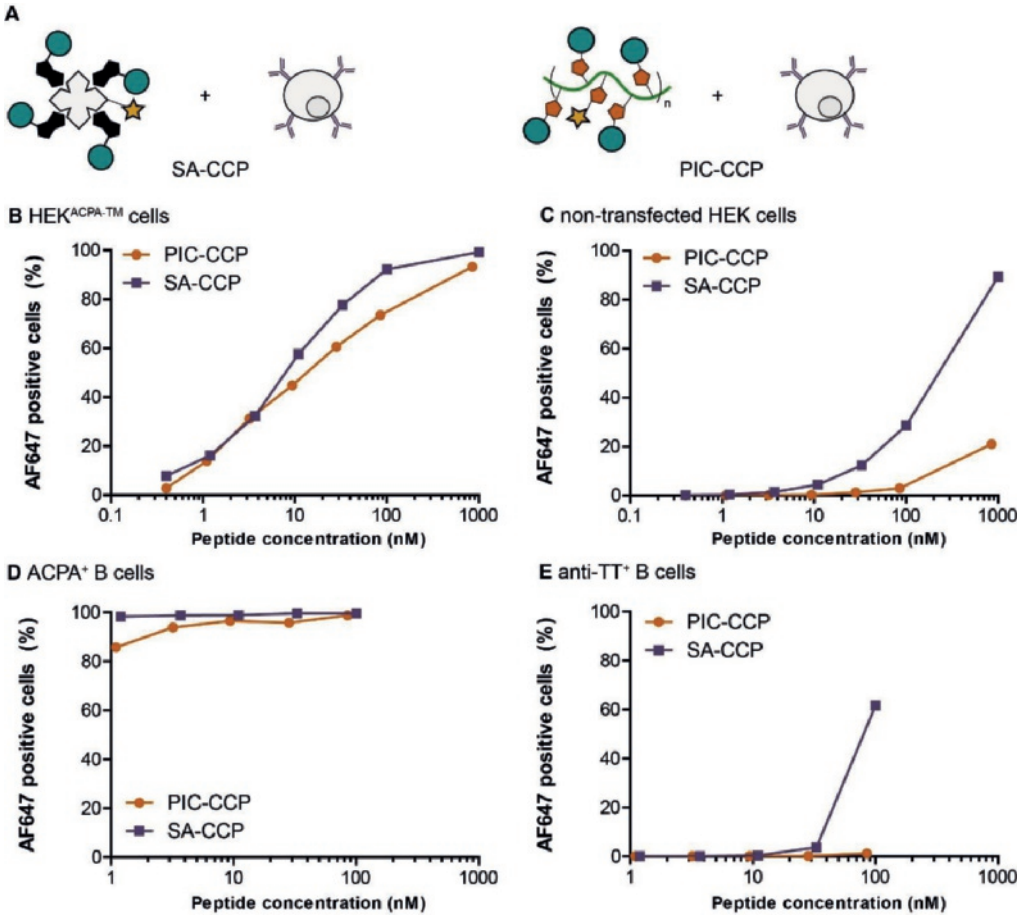

Figure 4. Flow cytometric binding titration of CCP loaded SA and PIC. A) Schematic overview of experimental set-up; Percentage of positive cells was plotted against the peptide antigen concentration for B) HEK$^{ACPA\text{-}TM}$ cells, C) non-transfected HEK cells, D) ACPA-positive B cells and E) anti-TT-positive B cells.

To test if the removal of one positive charge would indeed reduce the background signal, we used the PIC-scaffolds loaded with either CArgP or CNleP and incubated them with the different cell types for 30 minutes on ice (Figure 5A). After analyzing the data we observed that the CArgP gave high background levels for all cell lines, while CNleP hardly showed any binding (Figures 5 B-E, SI-6 and SI-7 for FACS plots). Therefore, we suggest to use CNleP as a proper negative control for future cell studies.

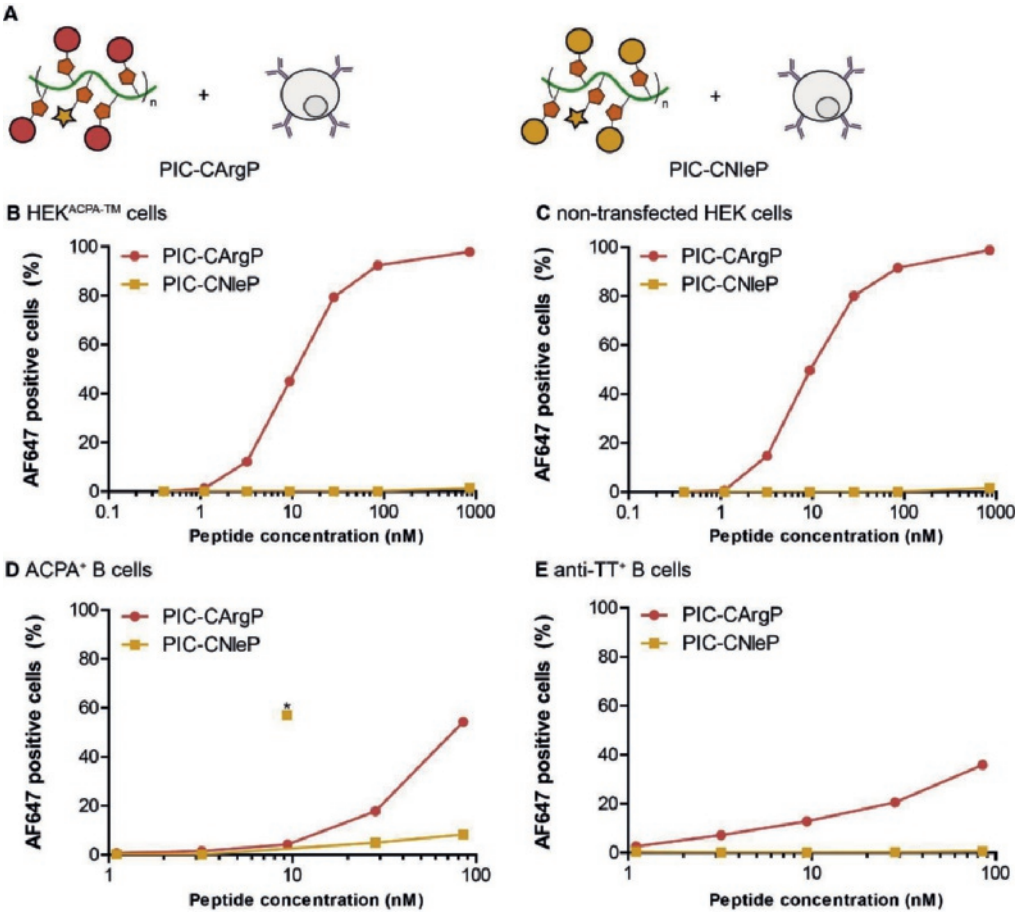

Figure 5. Flow cytometric binding studies and comparison of PIC loaded with either CNleP or CArgP. A) Schematic overview of experimental set-up; Percentage of positive cells was plotted against the peptide antigen concentration for B) HEK$^{ACPA\text{-}TM}$ cells, C) non-transfected HEK cells, D) ACPA-positive B cells and E) anti-TT-positive B cells. *data not representative

Internalization studies with the PIC scaffolds. The advantage of using the PIC scaffold is that there are multiple binding sites, which can be modified accordingly. Besides the addition of multiple (different) antigens, functional molecules can also be attached. One interesting example for the use of a multivalent scaffold is the possibility to target specific B cells using an autoantigen and simultaneously bind to regulatory molecules on the B cell membrane, to dampen B cell activation and proliferation.[14] Recently, PLGA particles have been used for the attachment of an autoantigen and a complement activating peptide to induce antigen-selective cytotoxicity.[15] More examples of multivalent structures used in the targeting of B cells have been described in Chapter 1.

Also, besides conjugation of a functional molecule interfering with processes on the outside of a B cell, the attachment of a toxin can induce antigen-selective cell death, *e.g.* when a toxin becomes activated after internalization into the B cell. The applicability of PICs for either of these purposes

is, however, dependent on the mode of binding and possibility of the PICs to enter the cells after binding to the BCR.

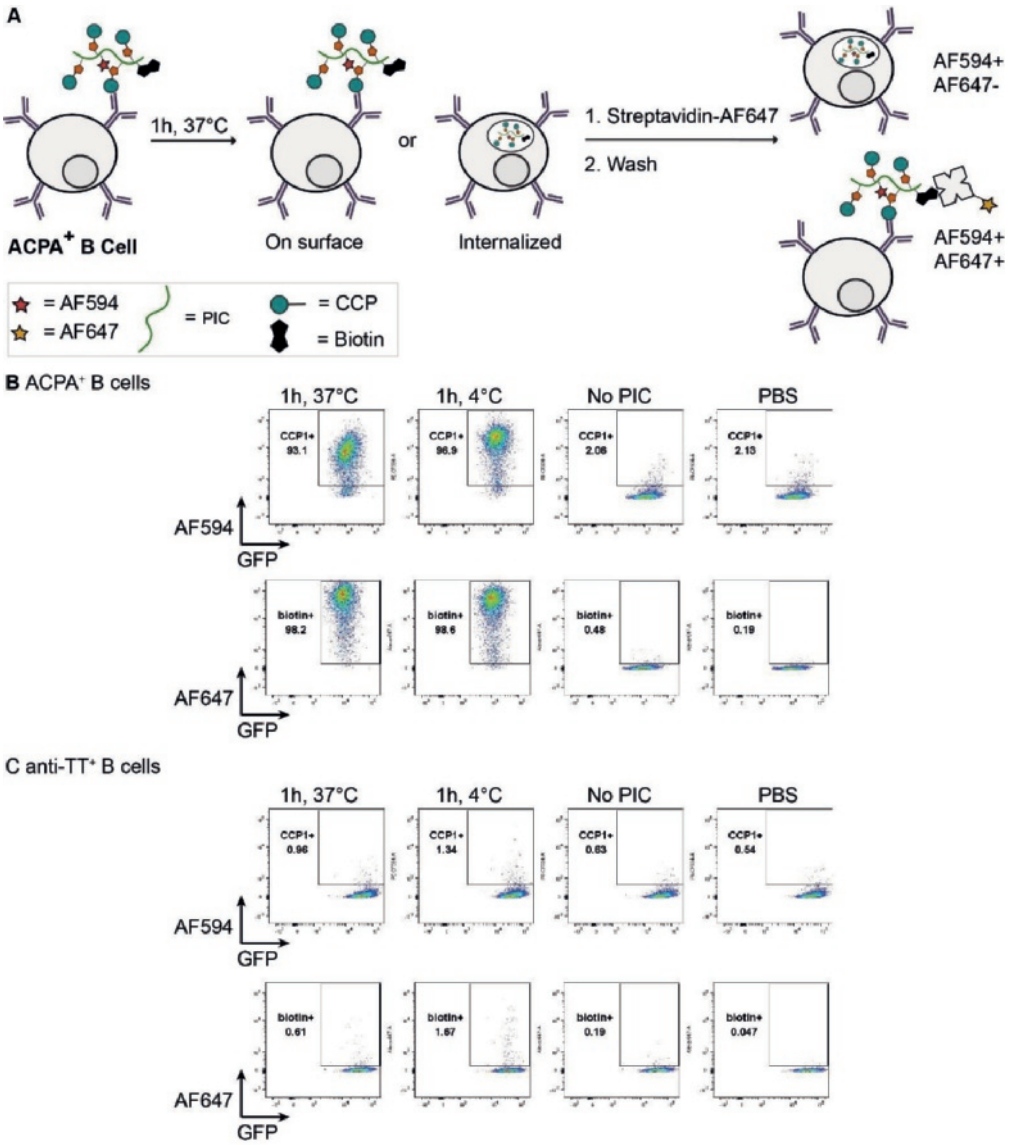

Figure 6. Internalization studies via indirect staining. A) Schematic representation of the experimental setup and expected outcome; B) Indirect internalization tested for ACPA-positive B cells. Staining for both AF647 and AF594 was measured; C) Indirect internalization tested for anti-TT-positive B cells. All signals were negative as expected due to the lack of the CCP binding to the BCR.

To test whether PICs were internalized into a B cell, we incubated the CCP loaded PICs with the immortalized B cells for 1 hour at 37 °C, after which the cells were washed thoroughly to remove

non-specific PIC binding. In case the all PICs were internalized, no PICs would be present on the surface of the cell, but when internalization is hampered the PICs will stay bound to the BCR on the cell surface. Since the PICs do also contain biotin molecules, we could indirectly stain the PICs with SA containing AF647. For this experiment, we synthesized PICs containing AF594, in order to detect both the PIC and SA in a different channel during flow cytometry measurements. After SA-AF647 was added and incubated for 30 minutes, the cell fluorescence was measured (Figure 6A).

Figure 6B (left-most panels) shows that the cells are positive for both AF594 and for AF647, meaning that SA was bound to the PIC scaffolds on the outside of the cell and that not all, if any, PICs were internalized. Since BCR internalization is an active process, we incubated the PIC scaffold with the cells also for 1 hour at 4 °C as a negative control. The second panel in Figure 6B shows that the cells were positive for both fluorophores, as expected, and that the fluorescent level was the same as observed at 37 °C. To show that the signal from AF647 was not a result of non-specific binding of SA, we omitted PIC in the first incubation step. Indeed, no fluorescent signal was observed indicating that SA could not bind to the cells without the PIC particles (panel 3, Figure 6B). It is still possible however, that a small amount of PICs is internalized, but we were not able to detect this. Microscopy studies will have to show this in the future. Finally, we evidenced in Figure 6C that the staining with PIC and SA was specific for the ACPA-expressing B cells, due to the antigen involved, as no fluorescent signal in both channels was observed for anti-TT-expressing B cells.

5.3 Conclusions

In this Chapter we have shown that PICs function as a promising multivalent scaffold for the binding to ACPA-positive cells. The data presented here shows that peptide loaded PIC and SA are comparable in binding avidity towards different B cell lines. The advantage of PIC over SA, however, is the low background observed for all cell types, with and without peptides loaded. We also showed that we could reduce the background signal caused by the CArgP peptide, which was used as a negative control. Most likely due to the high number of positive charges in CArgP high background signals were observed, which is probably related to electrostatic interactions with the cell membrane. Since PICs contain more CArgP peptides compared to SA, even more positive charges were combined on the polymers. A significant binding difference was observed when one arginine was replaced by norleucine, suggesting that the loss of one positive charge in the peptide was sufficient to dampen the background signal. We assume that the PICs decorated with the CNleP peptides benefit even more from this loss in positive charge, because of the higher loading of peptides on the polymer.

We indirectly showed that most or all PICs are still bound to the BCR, on the cell surface, within 1 h of incubation at 37 °C. Therefore, the PICs are of potential relevance to function as a scaffold to target B cells and to induce antigen selective toxicity by the additional conjugation of an inhibiting molecule. CD22 ligand is a good candidate, as it is already used to dampen the B cell activation by binding to Siglecs.[14] Alternatively, the attachment of a Fas ligand, which trimerizes the Fas receptor on the B cell membrane, can induce cell selective apoptosis. Further research into the influence of polymer length and spacing between peptides will complement our understanding for future application possibilities.

Summarizing, the work described in this Chapter represents a new polymer scaffold which can be readily functionalized and shows promising results in the targeting of ACPA positive cells compared to the often used SA scaffold. The PICs show a low background signal for all cell types, while this is significantly higher for SA. Functionalization with a variety of antigen peptides and the attachment of an apoptosis inducer may become an interesting application for this PIC scaffold in future research.

5.4 Acknowledgments

Dr. Roel Hammink is kindly acknowledged for providing us with the PIC polymers and for the fruitful collaboration. We thank Hendy Kristyanto (Leiden University Medical Center) for many of the flow cytometry experiments. Yvonne Bartels is acknowledged for the pioneering work on PICs as a multivalent scaffold for (CEP-1) antigens.

5.5 Materials and Methods

For general methods, see the materials and methods section of Chapter 2 (paragraph 2.4).

CCP-biotin (1). CCP-biotin was synthesized following the procedures described in the general peptide synthesis Section 2.4. Next, this peptide was cyclized and purified as described in the general cyclization method. HPLC: Rt. 12.753 min. LCMS (ESI+) m/z calcd for $C_{100}H_{171}N_{41}O_{34}S_2^{2+}$ $[M+2H]^{2+}$ 1277.61, found 1278.08. $C_{100}H_{172}N_{41}O_{34}S_2^{3+}$ $[M+3H]^{3+}$ 852.07, found 852.68. $C_{100}H_{173}N_{41}O_{34}S_2^{4+}$ $[M+4H]^{4+}$ 639.31, found 641.16

CArgP-biotin (2). CArgP-biotin was synthesized following the procedures described in the general peptide synthesis Section 2.4. Next, this peptide was cyclized and purified as described in the general cyclization method. HPLC: Rt. 12.731 min. LCMS (ESI+) m/z calcd for $C_{100}H_{172}N_{42}O_{33}S_2^{2+}$ $[M+2H]^{2+}$ 1277.13, found 1277.56. $C_{100}H_{172}N_{41}O_{34}S_2^{3+}$ $[M+3H]^{3+}$ 851.75, found 852.28. $C_{100}H_{173}N_{41}O_{34}S_2^{4+}$ $[M+4H]^{4+}$ 639.06, found 640.20.

CNleP-biotin (3). CNleP-biotin was synthesized following the procedures described in the general peptide synthesis Section 2.4. Next, this peptide was cyclized and purified as described in the general cyclization method. The biotin moiety was not attached on resin as described for CCP and CArgP, but functionalized using NHS-biotin (10 μL of a 100mM stock solution in DMSO) as described for the DBCO functionalization above. HPLC: Rt. 13.432 min. LCMS (ESI+) m/z calcd for $C_{100}H_{171}N_{39}O_{33}S_2^{2+}$ $[M+2H]^{2+}$ 1255.12, found 1255.88. $C_{100}H_{172}N_{39}O_{33}S_2^{3+}$ $[M+3H]^{3+}$ 837.08, found 837.64. $C_{100}H_{173}N_{39}O_{33}S_2^{4+}$ $[M+4H]^{4+}$ 628.06, found 628.60.

Lysine-peptides:

CCP-Lys (7). CCP-Lys was synthesized following the procedures described in the general peptide synthesis Section 2.4. Next, this peptide was cyclized and purified as described in the general cyclization method. HPLC: Rt. 10.209 min. LCMS (ESI+) m/z calcd for $C_{90}H_{157}N_{39}O_{32}S^{2+}$

$[M+2H]^{2+}$ 1164.08, found 1163.00. $C_{90}H_{158}N_{39}O_{32}S^{3+}$ $[M+3H]^{3+}$ 776.39, found 776.92. $C_{90}H_{159}N_{39}O_{32}S^{4+}$ $[M+4H]^{4+}$ 582.54, found 583.00.

CArgP-Lys (8). CArgP-Lys was synthesized following the procedures described in the general peptide synthesis Section 2.4. Next, this peptide was cyclized and purified as described in the general cyclization method. HPLC: Rt. 10.310 min. LCMS (ESI+) m/z calcd for $C_{90}H_{159}N_{40}O_{31}S^{3+}$ $[M+3H]^{3+}$ 776.06, found 776.64. $C_{90}H_{160}N_{40}O_{31}S^{4+}$ $[M+4H]^{4+}$ 582.30, found 582.68.

CNleP-Lys (9). CNleP-Lys was synthesized following the procedures described in the general peptide synthesis Section 2.4. Next, this peptide was cyclized and purified as described in the general cyclization method. HPLC: Rt. 12.054 min. LCMS (ESI+) m/z calcd for $C_{90}H_{157}N_{37}O_{31}S^{2+}$ $[M+2H]^{2+}$ 1142.08, found 1142.88. $C_{90}H_{158}N_{37}O_{31}S^{3+}$ $[M+3H]^{3+}$ 761.72, found 762.68. $C_{90}H_{159}N_{37}O_{31}S^{4+}$ $[M+4H]^{4+}$ 571.54, found 573.68.

DBCO-peptide functionalization. All peptides with a C-terminal lysine were functionalized with a NHS-PEG_4-DBCO after cleavage and cyclization. The lysine-containing peptides (2.0 μmol) were dissolved in DMF (2.0 mL) and DIPEA (204 μmol, 35.5 μL, 100 equiv.) was added. NHS-PEG_4-DBCO (16.2 mg, 25μmol) was dissolved in DMSO (100 μL, 250 mM) and 20 μL of the stock solution was added (resulting in a final concentration of 2.5 mM, 2.5 equiv.). The reaction was stirred for 5 hours at r.t. before the product was precipitated in Et_2O. The pellet was washed three times and dried afterwards.

CCP-DBCO (4). CCP-DBCO was synthesized following the procedures described in the general DBCO-peptide functionalization. CCP-Lys (**7**) was used as starting material. HPLC: Rt. 16.551 min. LCMS (ESI+) m/z calcd for $C_{120}H_{191}N_{41}O_{39}S^{2+}$ $[M+2H]^{2+}$ 1431.20, found 1432.08. $C_{120}H_{192}N_{41}O_{39}S^{3+}$ $[M+3H]^{3+}$ 954.47, found 955.36. $C_{120}H_{193}N_{41}O_{39}S^{4+}$ $[M+4H]^{4+}$ 716.10, found 718.36.

CArgP-DBCO (5). CArgP-DBCO was synthesized following the procedures described in the general DBCO-peptide functionalization. CArgP-Lys (**8**) was used as starting material. HPLC: Rt. 16.367 min. LCMS (ESI+) m/z calcd for $C_{120}H_{192}N_{42}O_{38}S^{2+}$ $[M+2H]^{2+}$ 1430.70, found 1431.52. $C_{120}H_{193}N_{42}O_{38}S^{3+}$ $[M+3H]^{3+}$ 954.14, found 955.08. $C_{120}H_{194}N_{42}O_{38}S^{4+}$ $[M+4H]^{4+}$ 715.86, found 717.48.

CNleP-DBCO (6). CNleP-DBCO was synthesized following the procedures described in the general DBCO-peptide functionalization. CNleP-Lys (**9**) was used as starting material. HPLC: Rt. 16.880 min. LCMS (ESI+) m/z calcd for $C_{120}H_{191}N_{39}O_{38}S^{2+}$ $[M+2H]^{2+}$ 1409.20, found 1410.08. $C_{120}H_{192}N_{39}O_{38}S^{3+}$ $[M+3H]^{3+}$ 939.80, found 940.88. $C_{120}H_{193}N_{39}O_{38}S^{4+}$ $[M+4H]^{4+}$ 705.10, found 707.28.

Modification of PICs. The PICs were kept at ice at all times and stored in nonstick microfuge tubes. DIBO-AF647 was dissolved in DMSO (1 mM). 4.90 μL of DIBO-AF647 stock solution was added to PICs (1.325 mL, 1 mg/mL), which were synthesized according to previously

published methods.[5-6] The reaction was kept at 4 °C overnight in a shaker. Afterwards, 50 μL was used for subsequent modification with a single antigen peptide. To this 50 μL, 8.50 μL of antigen peptide (2 mg/mL in PBS, 1.5 equiv. compared to available azides) was added. Next, PBS (8.50 μL) was added to have a final PIC concentration of 0.85 mg/mL. The reaction was again left overnight at 4°C.

Before using these scaffold in flow cytometry measurements, stock solutions of around 1 μM peptide concentration were prepared. Peptide concentrations were calculated starting with the initial concentration (mg/mL) and the molecular weight of a monomer (360 Da, weight of monomers stays the same after polymerization). From this 2.36 mM of monomer ($\frac{0.85\ mg/mL}{360} \times 1000$), one every 83 monomers contains an azide. Maximal peptide concentration on the PICs is therefore 28.44μM ($\frac{2.36\ mM}{83} \times 1000$). This mixture was then diluted to obtain the desired starting stock concentration for serial dilutions.

Peptide loading onto SA. SA fluorophore conjugates were purchased from Thermo Fisher. The proteins were dissolved in PBS (2 mg/mL) and 116 μL biotinylated peptides (5 mg/mL in PBS, 50 equiv.) were added to 125 μL of SA. The reaction was left overnight at 4 °C and the mixtures were purified afterwards using 40K Zeba spin desalting column to remove the excess of biotinylated peptide added. Protein concentrations were determined afterwards using UV-Vis measurements. Absorbance was measured at 280 nm and 654 nm. Using Lambert-Beers law (Abs = c * ε * d), fluorophore concentration was calculated, ε for AF647 is 270000 M^{-1} cm^{-1}, d is 0.1 cm. For SA the absorbance was first corrected for the fluorophore attached. The calculations were made using: $Abs_{SA} = Abs_{280} - Cf * Abs_{fluorophore}$ (in which Cf is the correction factor for AF647 and is 0.03). Using this corrected absorbance, the concentration was calculated according to the law of Lambert-Beer, using ε for SA is 167000 M^{-1} cm^{-1}. The correlation between the corrected SA concentration and the concentration at the wavelength of the fluorophore depicts the ratio of SA:fluorophore.

Flow cytometry measurements. The SA and PIC scaffolds were serial diluted and added to cell cultures containing either $HEK^{ACPA\text{-}TM}$, non-transfected HEK, ACPA-expressing or anti-TT-expressing immortalized B cells in a 96 well plate. Subsequently, the cells were kept on ice for 30 minutes unless described otherwise, washed, resuspended with 1% paraformaldehyde and measured by flow cytometry using BD LSRFortessa (BD Biosciences).

5.6 References

1. Willemze, A.; Trouw, L. A.; Toes, R. E. M.; Huizinga, T. W. J., Willemze, A.; Trouw, L. A.; Toes, R. E. M.; Huizinga, T. W. J.; The influence of ACPA status and characteristics on the course of RA. *Nat. Rev. Rheumatol.* **2012,** *8* (3), 144-152.
2. Kristyanto, H., personal communication.
3. Suwannalai, P.; Scherer, H. U.; Van Der Woude, D.; Ioan-Facsinay, A.; Jol-van Der Zijde, C. M.; Van Tol, M. J. D.; Drijfhout, J. W.; Huizinga, T. W. J.; Toes, R. E. M.; Trouw, L. A., Anti-citrullinated protein antibodies have a low avidity compared with antibodies against recall antigens. *Ann. Rheum. Dis.* **2011,** *70* (2), 373-379.
4. Kerkman, P. F.; Fabre, E.; van der Voort, E. I.; Zaldumbide, A.; Rombouts, Y.; Rispens, T.; Wolbink, G.; Hoeben, R. C.; Spits, H.; Baeten, D. L., Identification and characterisation of citrullinated antigen-specific B cells in peripheral blood of patients with rheumatoid arthritis. *Ann. Rheum. Dis.* **2016,** *75* (6), 1170-1176.
5. Mandal, S.; Hammink, R.; Tel, J.; Eksteen-Akeroyd, Z. H.; Rowan, A. E.; Blank, K.; Figdor, C. G., Polymer-based synthetic dendritic cells for tailoring robust and multifunctional T cell responses. *ACS Chem. Biol.* **2014,** *10* (2), 485-492.
6. Mandal, S.; Eksteen-Akeroyd, Z. H.; Jacobs, M. J.; Hammink, R.; Koepf, M.; Lambeck, A. J. A.; van Hest, J. C. M.; Wilson, C. J.; Blank, K.; Figdor, C. G., Therapeutic nanoworms: towards novel synthetic dendritic cells for immunotherapy. *Chem. Sci.* **2013,** *4* (11), 4168-4174.
7. Murphy, M.; Loudon, R.; Kobayashi, M.; Trinchieri, G., Gamma interferon and lymphotoxin, released by activated T cells, synergize to inhibit granulocyte/monocyte colony formation. *J. Exp. Med.* **1986,** *164* (1), 263-279.
8. Hammink, R.; Mandal, S.; Eggermont, L. J.; Nooteboom, M.; Willems, P. H. G. M.; Tel, J.; Rowan, A. E.; Figdor, C. G.; Blank, K. G., Controlling T-Cell Activation with Synthetic Dendritic Cells Using the Multivalency Effect. *ACS Omega* **2017,** *2* (3), 937-945.
9. Schellekens, G. A.; de Jong, B. A. W.; van den Hoogen, F. H. J.; van de Putte, L. B.; van Venrooij, W. J.; Citrulline is an essential constituent of antigenic determinants recognized by rheumatoid arthritis-specific autoantibodies. *J. Clin. Invest.* **1998,** *101* (1), 273-281.
10. Schellekens, G. A.; Visser, H.; de Jong, B. A. W.; van den Hoogen, F. H. J.; Hazes, J. M. W.; Breedveld, F. C.; van Venrooij, W. J.; The diagnostic properties of rheumatoid arthritis antibodies recognizing a cyclic citrullinated peptide. *Arthritis Rheum.* **2000,** *43* (1), 155-163.
11. Debets, M. F.; van Berkel, S. S.; Dommerholt, J.; Dirks, A. J.; Rutjes, F. P. J. T.; van Delft, F. L.; Bioconjugation with strained alkenes and alkynes. *Acc. Chem. Res.* **2011,** *44* (9), 805-815.
12. Sletten, E. M.; Bertozzi, C. R., From mechanism to mouse: a tale of two bioorthogonal reactions. *Acc. Chem. Res.* **2011,** *44* (9), 666-676.
13. Kwakkenbos, M. J.; van Helden, P. M.; Beaumont, T.; Spits, H., Stable long-term cultures of self-renewing B cells and their applications. *Immunol. Rev.* **2016,** *270* (1), 65-77.
14. Macauley, M. S.; Pfrengle, F.; Rademacher, C.; Nycholat, C. M.; Gale, A. J.; von Drygalski, A.; Paulson, J. C., Antigenic liposomes displaying CD22 ligands induce antigen-specific B cell apoptosis. *J. Clin. Invest.* **2013,** *123* (7), 3074-3083.
15. Pozsgay, J.; Babos, F.; Uray, K.; Magyar, A.; Gyulai, G.; Kiss, É.; Nagy, G.; Rojkovich, B.; Hudecz, F.; Sármay, G., In vitro eradication of citrullinated protein specific B-lymphocytes of rheumatoid arthritis patients by targeted bifunctional nanoparticles. *Arthritis Res. Ther.* **2016,** *18* (1), 1-12.
16. Molecular Probes, Alexa Fluor® 647 Protein Labeling Kit (A20173), Product information. Retrieved from https://www.thermofisher.com/order/catalog/product/A20173. **2004**, (accessed November 8, 2018).
17. Qureshi, M. H.; Yeung, J. C.; Wu, S.-C.; Wong, S.-L., Development and characterization of a series of soluble tetrameric and monomeric streptavidin muteins with differential biotin binding affinities. *J. Biol. Chem.* **2001,** *276* (49), 46422-46428.
18. AAT Bioquest. Extinction coefficient results. Retrieved from https://www.aatbio.com/resources/extinction-coefficient/Alexa_Fluor_647. **2018**, (accessed November 8, 2018).

5.7 Supplementary Information

Note SI-1.

Both the SA concentration and the fluorophore concentration were calculated using the equations and information below. Calculated values are used to determine the fluorophore:SA and fluorophore:peptide ratio.

Equations:

Absorbance correction for 280nm: $Abs_{280,corr} = Abs_{280} - C_f \times Abs_{654}$

Lambert-Beer Law: $C = \frac{Abs}{\varepsilon \times d}$

Fluorophore - protein ratio: $\frac{C_{654}}{C_{280}}$

With:
A = absorbance (average value)
C_f = correction factor (0.03 for AF647[16])
C = concentration (µM)
ε = extinction coefficient (M^{-1} cm^{-1}, 167000 for SA[17] and 270000 for AF647[18])
d = path length of the beam of light through the material sample (cm)

Calculations:

	Abs_{280}	Abs_{654}	$Abs_{280,\ corr}$	C_{280}	C_{654}	Ratio
SA-CArgP	0.266	0.795	0.242	14.5	29.4	2.03
SA-CCP	0.272	0.813	0.248	14.8	30.1	2.03

Both SA conjugates contain approximately 2 fluorophores per SA molecule. Since in theory 4 biotin peptides can be attached, the ratio of fluorophore to peptide is 2:4.

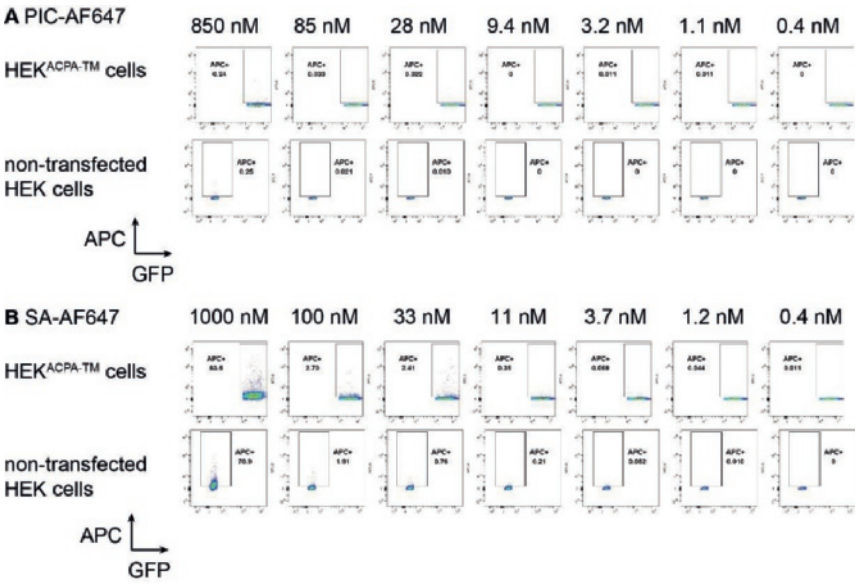

Figure SI-2. Flow cytometric binding studies of scaffold background for HEK$^{ACPA\text{-}TM}$ and non-transfected HEK cells for A) PIC-AF647 for B) SA-AF647.

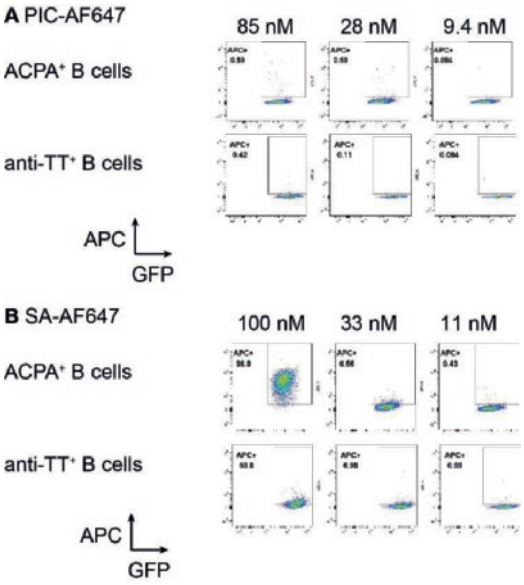

Figure SI-3. Flow cytometric binding studies of scaffold background for ACPA-positive and anti-TT-positive B cells for A) PIC-AF647 for B) SA-AF647.

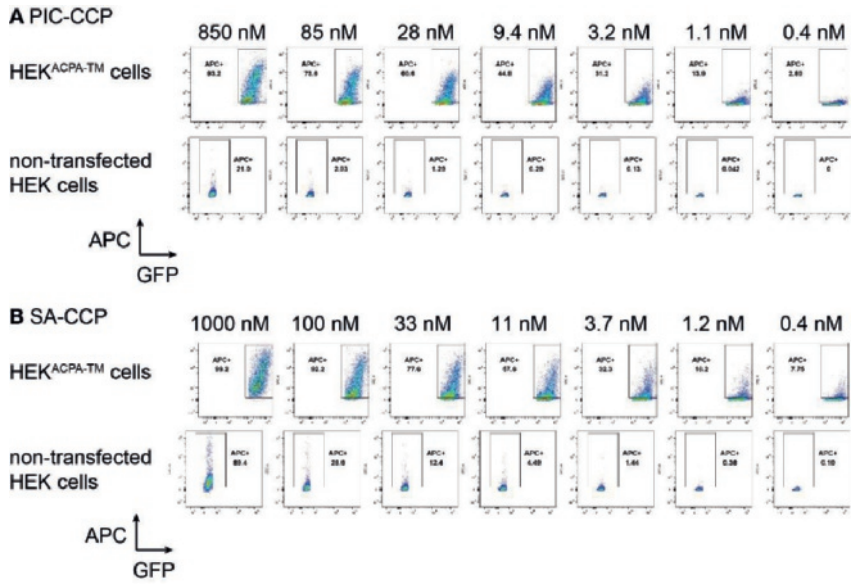

Figure SI-4. Flow cytometric binding titration of HEK$^{ACPA\text{-}TM}$ and non-transfected HEK cells for A) PIC-CCP and B) SA-CCP.

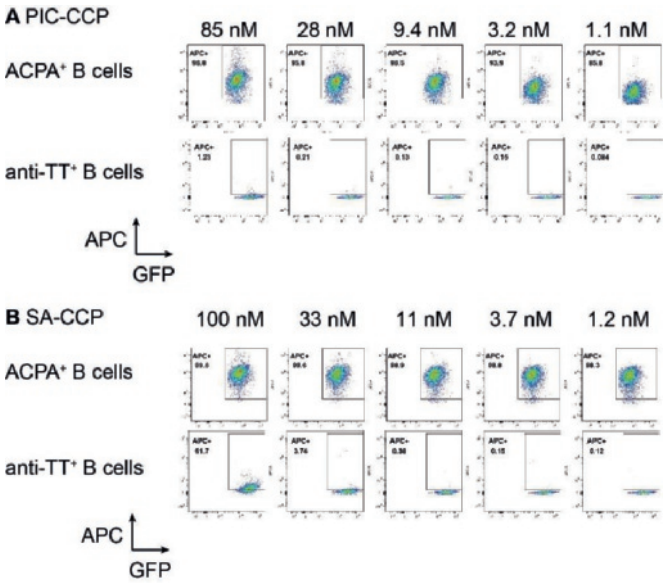

Figure SI-5. Flow cytometric binding titration of ACPA-positive and anti-TT-positive B cells for A) PIC-CCP and B) SA-CCP.

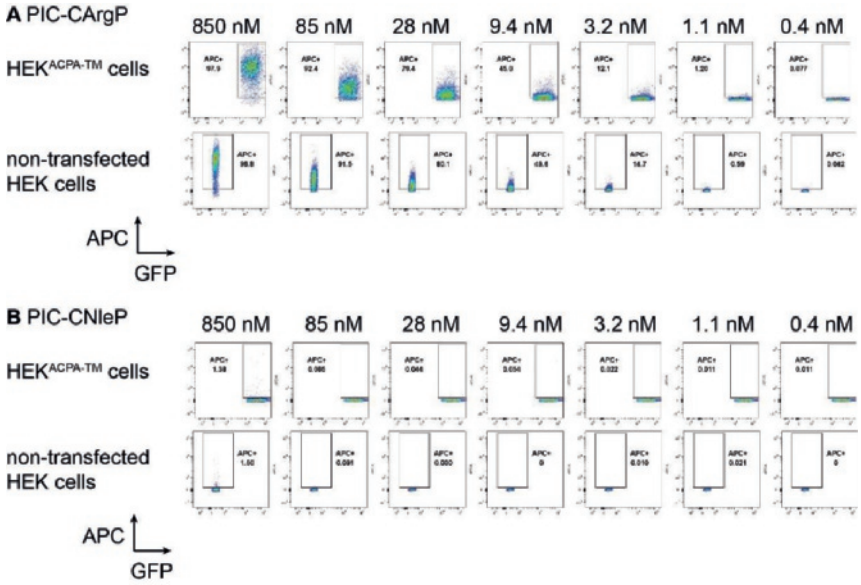

Figure SI-6. Flow cytometric binding studies with of HEK$^{ACPA\text{-}TM}$ and non-transfected HEK cells for comparison of PIC loaded with A) CArgP or B) CNleP.

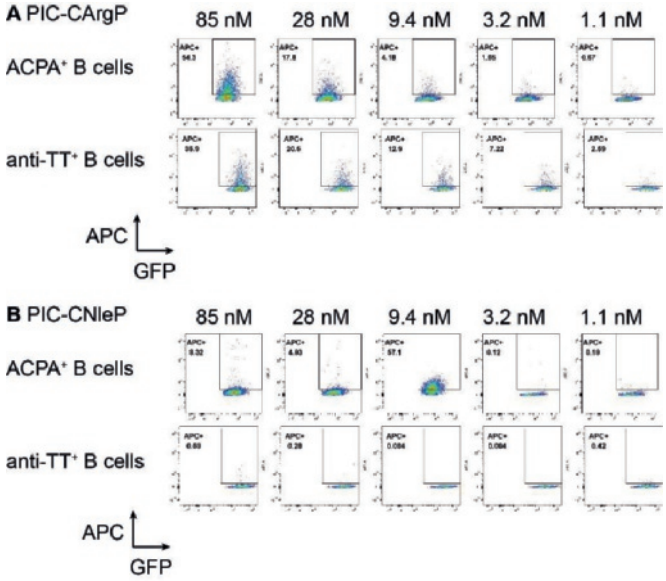

Figure SI-7. Flow cytometric binding studies with of ACPA-positive and anti-TT-positive B cells for comparison of PIC loaded with A) CArgP or B) CNleP.

Chapter 6

Synthesis of a Selective anti-CarP Peptide Antigen and its Application in the Antigen-Caging and Activation Strategy

Abstract

Antigen-specific targeting and elimination of autoreactive B cells can be beneficial for the treatment of autoimmune diseases, including rheumatoid arthritis (RA). Antibodies against citrullinated proteins are present in the majority of RA patients. However, other posttranslational modifications, such as carbamylation, are also involved in the development of autoantibodies in RA. Approximately 45% of RA patients is positive for antibodies against carbamylated proteins (anti-CarP antibodies), and most of these patients are also positive for anti-citrullinated protein antibodies (ACPA). However, 20-30% of RA patients is ACPA-negative, and these are not likely affected by strategies aimed at the elimination of ACPA-positive B cells. A fraction of these patients (10-20%) is positive for anti-CarP. A major limitation for anti-CarP-positive B cell targeting, however, is the lack of knowledge on small anti-CarP antigens. Only full-length proteins are considered as anti-CarP antigens, whereas peptide structures have not been identified to date. In this Chapter, we study the binding of a homocitrulline-containing peptide antigen against anti-CarP antibodies and we explore the translation of antigen-specific targeting of ACPA-positive B cells to anti-CarP-positive B cells. We show that the new homocitrulline-containing antigens, based on CCP, can be used as a targeting antigen for ACPA-negative but anti-CarP-positive sera. Anti-CarP antibodies were shown to be produced in mice with collagen-induced arthritis, a widely used model for RA pathology. Hence, we suggest that the change from citrullinated to carbamylated antigens can also be interesting to study B cell targeting in anti-CarP positive mice. Finally, we show that we can make the antigen-caging and activation strategy demonstrated for ACPA in Chapters 2 and 3 work on anti-CarP antibodies.

6.1 Introduction

In the past few years, it has become clear that the antibody response in RA was specific to multiple recognition elements. Besides ACPA, directed to citrullinated proteins, antibodies to carbamylated proteins were found in patient sera. Some of these posttranslational modifications are introduced by enzymes (*e.g.* citrulline to arginine, by PAD enzymes, see Chapter 2), others result from non-enzymatic conversions (*e.g.* carbamylation of lysines).[1]

Carbamylation is a posttranslational modification resulting from the interaction between isocyanic acid and amines residing in proteins (α-NH_2 or ε-NH_2). When isocyanic acid reacts with the ε-NH_2 group of the lysine side chain, the amino acid homocitrulline is formed (Figure 1).[2-3] Urea is a source of cyanate and is present in body fluids in equilibrium with ammonium cyanate at a suggested ratio of 1 to 500.000[4].

Increased protein carbamylation can be observed under certain conditions, for example in patients with enhanced levels of urea as a consequence of renal insufficiency.[2] Isocyanic acid can also be formed by myeloperoxidase (MPO)-mediated transformation of thiocyanate (Figure 1B), a component in cigarette smoke,[5] which is considered the most common environmental risk factor for RA.[6] MPO is mainly stored in granules of neutrophils[7] and is released during (chronic) inflammation. Chronic inflammation seen in RA patients can thus be a trigger to a higher level of cyanates and hence carbamylated proteins. Approximately 45% of RA patients have antibodies directed to carbamylated proteins and these anti-CarP antibodies were shown to display 96% specificity for RA patients compared to healthy controls.[8] Anti-CarP antibodies are mainly found in ACPA-positive patients, which include 70-80% of the RA patients,[9] but importantly also in 10-20% of ACPA-negative patients.[10-11] Similar to ACPA and rheumatoid factors, anti-CarP antibodies can be detected in the sera of RA patients many years before the onset of the disease.[12-14]

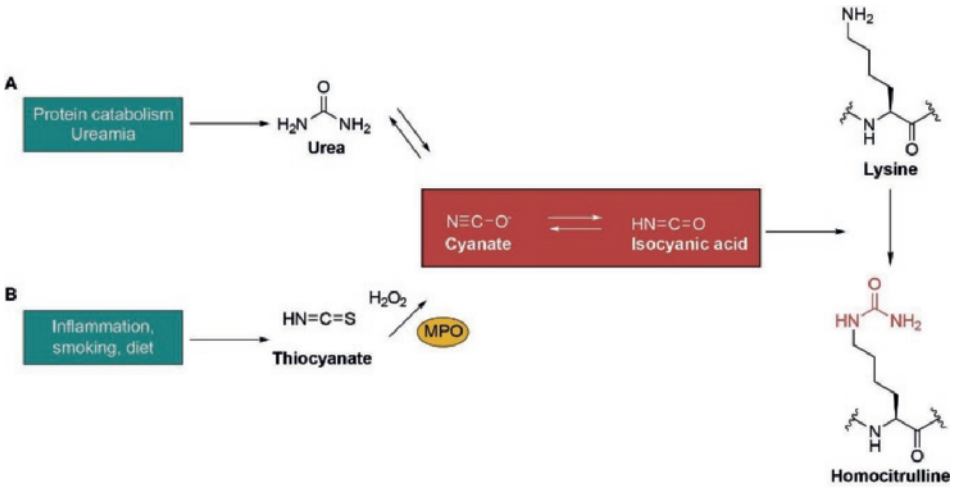

Figure 1. Protein carbamylation. Cyanate is formed from either urea (A) or thiocyanate (B). When isocyanic acid reacts with the lysine side chain, homocitrulline is formed.

To our knowledge, only carbamylated proteins and no peptide antigens are known for anti-CarP recognition.[10] To gain more information about anti-CarP antibodies, a peptide antigen (like CCP2 used for ACPA studies) and can be advantageous over using a full protein. In this Chapter we explore the possibility of using a homocitrulline analogue of the CCP peptide designed in Chapter 2, and test its binding capacity for anti-CarP antibodies. In Chapter 2 we also showed that we can selectively cage and activate citrulline-containing antigens to tune the binding to ACPA. We suggest that this strategy can interchangeably be used by carbamylated peptides, since the binding for both antibody types is dependent on the ureido group of citrulline and homocitrulline (HCit). If successful, this strategy might be of additional value for the 10-20% anti-CarP-positive and ACPA-negative RA patients.

Interestingly, an immune response against carbamylated antigens was also observed in collagen-induced arthritis (CIA) mice, the most frequently used animal model for arthritis.[15] Previous reports in literature showed that in CIA mice no ACPA were detected,[16] and that anti-CarP antibodies were already present prior to disease onset. The anti-CarP antibody response in these mice can be used as a model for immune responses to post-translationally modified proteins. Hence, we explore in this Chapter whether we can apply the caging and activation strategy, described in Chapter 2, on anti-CarP positive human sera and sera from an anti-CarP mouse model.

6.2 Results and Discussion

Anti-CarP antigen synthesis and recognition tests. To date, no specific carbamylated peptides have been identified that bind to anti-CarP antibodies. We were interested to see if we can modify the CCP antigen to bind to anti-CarP antibodies. Therefore, we synthesized the CCP peptide with homocitrulline instead of citrulline. Homocitrulline was protected with an Fmoc group (**1**) and subsequently used to synthesize the CHCitP peptide **2** using solid phase peptide synthesis (SPPS). All amino acids were coupled according to standard Fmoc SPPS procedures. The peptide was cyclized covalently, similar as in Chapter 2, and therefore the N-terminal cysteine was replaced by an alanine. The cyclization was achieved by reacting the N-terminus with chloroacetic anhydride and DIPEA. After deprotection of the full peptide, cyclization occurred in a basic buffer by nucleophilic addition of the cysteine onto the chloride.

In addition to CHCitP (**2**), we synthesized CLysP (**3**) containing a lysine at the homocitrulline position, functioning as the negative control, and CAcLysP (**4**) containing an acetylated lysine to look at specificity and cross-reactivity of the anti-CarP antibodies. CCP (**5**) and CArgP (**6**) were taken along for the same purpose and for comparison with ACPA (see Figure 2A).

To test these peptide antigens for anti-CarP recognition we used sera from mice immunized with carbamylated ovalbumin. Fibrinogen and carbamylated (Ca) fibrinogen were used as negative and positive controls, respectively, in an enzyme-linked immunosorbent assay (ELISA). In this ELISA, the different peptide antigens were attached to a streptavidin-coated well-plate and different concentrations of anti-CarP serum were added. After the incubation with a secondary antibody containing horseradish peroxidase and the addition of the substrate, a signal was measured corresponding to the binding of the primary antibody. Figure 2B shows that CHCitP (**2**) was indeed recognized by anti-CarP antibodies and resulted in signals of equal intensities as compared to carbamylated fibrinogen. This demonstrates that this peptide functions as a good antigen for

the anti-CarP antibodies in this serum. Hence, this carbamylated peptide antigen might be of interest to replace full protein antigens in the detection of anti-CarP antibodies in general.

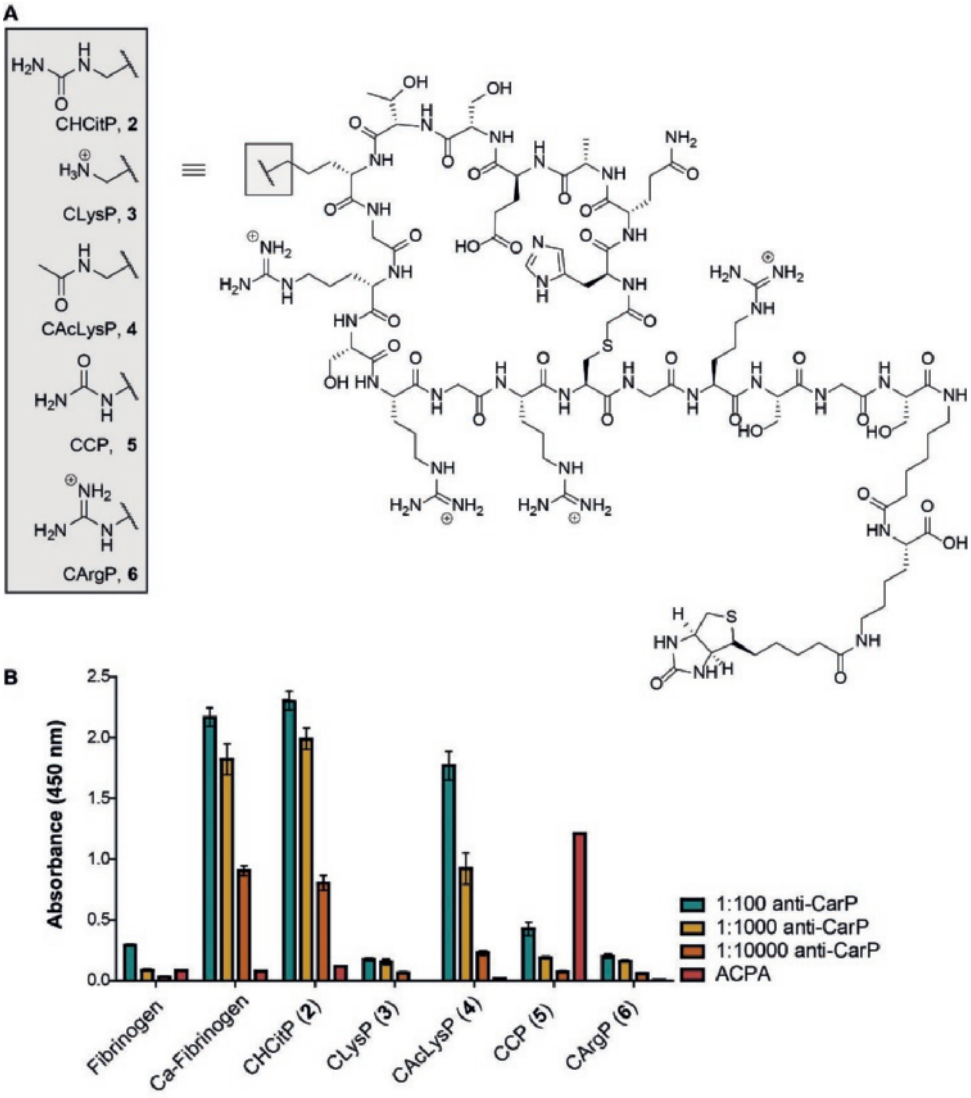

Figure 2. Binding of anti-CarP antibodies to homocitrulline-containing CCP-like peptide. A) Structures of all CXP peptides used in the ELISA; B) ELISA with CXP peptides against anti-CarP and monoclonal ACPA, using fibrinogen and carbamylated fibrinogen as negative and positive control. The anti-CarP serum was used at dilutions as indicated and the monoclonal ACPA, derived from immortalized B cell supernatant, was not diluted.

No anti-CarP binding was observed to fibrinogen, nor to the cyclic peptide containing a lysine residue, CLysP (**3**) (Figure 2B). The acetylated CLysP peptide (**4**), gave a significant signal, albeit with lower intensity as compared to carbamylated fibrinogen or CHCitP (**2**). This indicates that

the anti-CarP antibodies cross-react with CAcLysP (**4**). Furthermore, no binding of anti-CarP was observed for CCP (**5**) and CArgP (**6**), as expected. No cross-reactivity with any peptide was noted for the ACPA serum, as only CCP gave a positive signal. The cross-reactivity of the serum for carbamylated antigens might be due to the polyclonal nature of this serum; the ACPA used in this experiment are monoclonal antibodies derived from immortalized ACPA-expressing B cells.

To show that CHCitP (**2**) was not only recognized by one specific immunized mouse serum, ten additional sera were tested (Figure 3). The ELISA experiment was performed as described above and the data showed that all mice positive for carbamylated fibrinogen were also positive for CHCitP. In most sera, cross-reactivity with CAcLysP was also observed. For all mouse sera tested, no reactivity with CLysP (**3**), CCP (**5**) and CArgP (**6**) was detected.

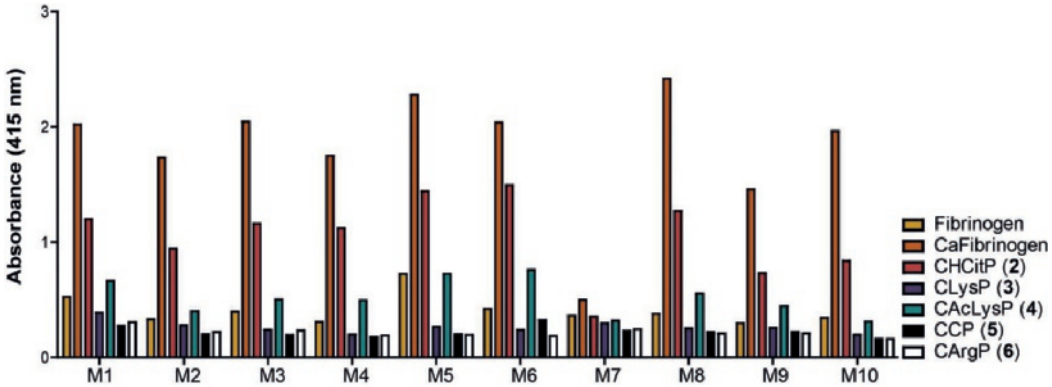

Figure 3. Reactivity of anti-CarP-positive mouse sera with synthetic (carbamylated) peptides. Sera from mice (M) immunized with carbamylated ovalbumin were tested for reactivity with the peptide antigens defined in Figure 2A.

These results strongly suggest that the carbamylated peptide is applicable for B cell targeting and isolation in this mouse model, but it may also be useful for targeting anti-CarP B cells in RA patients. To test whether CHCitP (**2**) is also recognized by anti-CarP antibodies in human serum, we analyzed a patient serum positive for both ACPA and anti-CarP antibodies by ELISA. Figure 4 shows that both CCP (**5**) and CHCitP (**2**) bind to antibodies in the serum and that the absorbance is much higher than for carbamylated fibrinogen. Although anti-CarP antibodies in mice and humans are developed according to different triggers and therefore might recognize different epitopes, these data indicate that CHCitP (**2**) is readily recognized by both human and mouse anti-CarP antibodies, while this is not the case for carbamylated fibrinogen. Since many patients do have anti-CarP antibodies, we next explored whether the antigen caging and activation strategy described in Chapter 2 can be applied to these carbamylated antigens.

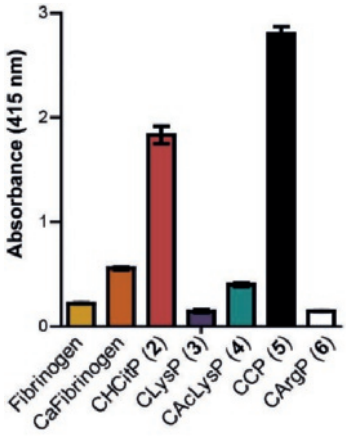

Figure 4. Reactivity of anti-CarP patient antibodies with CHCitP in ELISA. Microtiter plates were coated with (carbamylated) fibrinogen and peptide antigens **2**-**6** and incubated with an ACPA- and anti-CarP-positive patient serum. ELISA was performed in duplo.

CHCitP(CNBz) synthesis and activation. To examine whether we could apply the antigen caging and activation strategy as described in Chapter 2 on a carbamylated peptide, we synthesized Fmoc-HCit(CNBz)-OH (**7**) as shown in scheme 1 and used this amino acid in SPPS to synthesize CHCitP(CNBz) (**8**, Figure 5A).

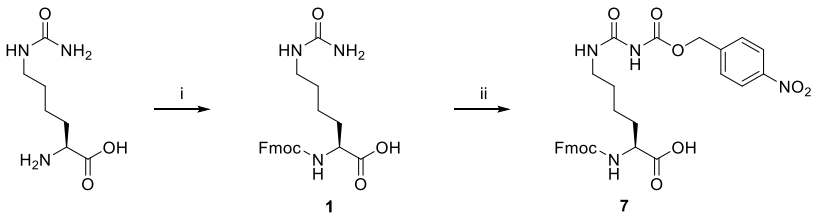

Scheme 1. Synthetic route to CNBz-caged Fmoc-HCit-OH (**7**). i) Fmoc-OSu, H_2O, dioxane, r.t., 16 h, quant. ii) *p*-Nitrobenzyl chloroformate, THF, overnight, 40 °C, 68% yield based on recovered starting material.

To test the antigen activation strategy, we used 0.3 equivalents of nitroreductase (NTR) for 1 h at 37 °C with NADH as cofactor as these conditions gave complete activation of the CCP antigen in Chapter 2. Upon reduction of the nitro group by NTR, 1,6-elimination of the CNBz group yielded activated CHCitP (**2**). The reactivity with anti-CarP patient sera was assessed using three sera, two of which were both anti-CarP- and ACPA-positive, whereas the third was neither reactive with carbamylated nor with citrullinated antigens. Figure 5B shows the binding of CHCitP (**2**) by anti-CarP antibodies, while CNBz-caged CHCitP (**8**) did not yield any signal, like the CLysP. This demonstrates that the caging group also masked recognition of the anti-CarP antigen and that binding was restored after the addition of NTR for both human RA sera reactive with CHCitP (**2**).

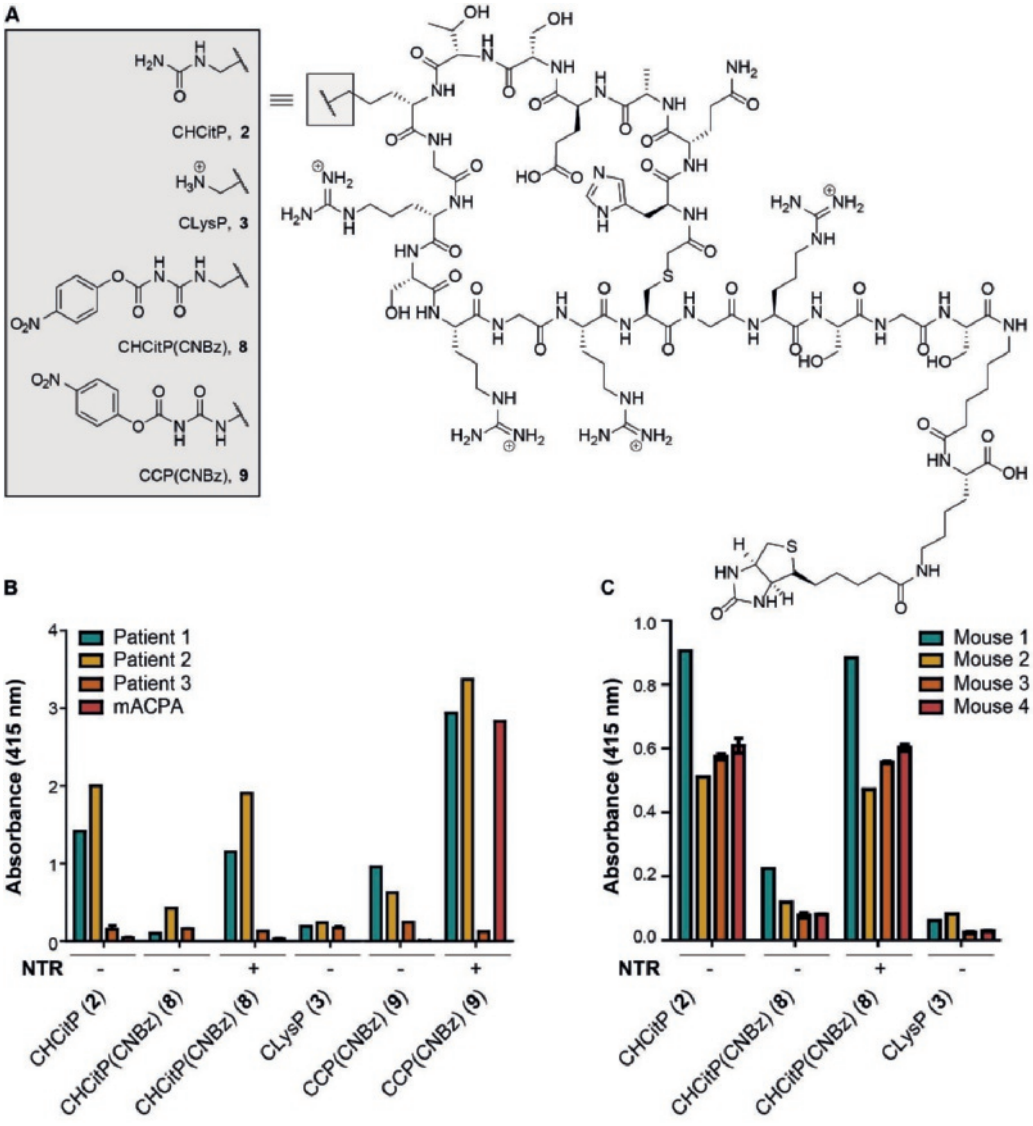

Figure 5. Reactivity of anti-CarP patient and mouse antibodies with CNBz-caged antigens peptides and after activation using NTR. A) Overview of the peptides used in this experiment. CHCitP and CLysP were used as positive and negative controls, respectively and CHCitP(CNBz) as the caged anti-CarP antigen; B) Three RA patient sera and monoclonal ACPA antibodies were used. A positive signal was seen for the CHCitP positive control, but also after the activation of CHCitP(CNBz) with NTR, using 0.3 equiv., for 1 h, at 37 °C and with NADH as a cofactor. The increasing signal was also observed after activation of CCP(CNBz); C) Four different mouse sera were tested against CHCitP and caged CHCitP(CNBz). All sera were positive for CHCitP, negative for the caged peptide antigen, and affinity was observed again after activation by NTR.

Since these sera are double positive for anti-CarP antibodies and ACPA, CCP(CNBz) with and without NTR treatment was tested as a control. While CCP(CNBz) showed only weak signals for

the two double positive human RA sera, no signal was seen for the monoclonal ACPA serum or the anti-CarP- and ACPA-negative serum (Patient 3). As soon as NTR was added, the signal increased showing the restored binding of ACPA, for the three ACPA-positive sera, to the free citrullinated peptide antigen.

To substantiate the activation of homocitrulline by NTR, reactivity with the same antigens was analyzed for the mice sera described above. As shown in Figure 5C, the addition of the CNBz-caging group to CHCitP completely masked anti-CarP antibody binding for all four mice sera tested. A similar negative signal was observed for the CLysP peptide. Treatment of CHCitP(CNBz) with NTR showed similar absorbance values as observed for the CHCitP positive control, demonstrating the successful restoration and recognition of the antigen by the mouse anti-CarP antibodies.

6.3 Conclusions

In this Chapter, we showed the design and synthesis of a carbamylated peptide, CHCitP (**2**), and its recognition by anti-CarP antibodies. We showed that CHCitP was recognized by both human and mice anti-CarP antibodies. Since no peptide antigens are known to date to detect anti-CarP antibodies, this finding can be advantageous for studies involving anti-CarP-producing B cells. Furthermore, we demonstrated that the antigen caging and activation strategy used for ACPA, as described in Chapter 2, can be applied to carbamylated peptides. Recognition of CHCitP (**2**) was proven to be selective to anti-CarP antibodies and dependent on the presence of the CNBz-caging group.

The antigen activation strategy for anti-CarP antibodies can now be tested in carbamylated ovalbumin-immunized mice as an *in vivo* animal model. For this, we envision to conjugate anti-mouse CD20 Fab fragments to an activating enzyme or chemical group to increase the local concentration of autoreactive antigens in close proximity to B cells. The carbamylated antigen can be further used as targeting antigen, for patients lacking ACPA but having anti-CarP antibodies. Finally, these anti-CarP antigens might be of use to isolate anti-CarP positive B cells, using streptavidin tetramers[17] or PICs (Chapter 6), from either mouse or human to study them in more detail.

6.4 Acknowledgements

Hendy Kristyanto (Leiden University Medical Centre) is kindly acknowledged for performing some of the ELISA experiments described in this Chapter.

6.5 Materials and Methods

For general methods, see the materials and methods section of Chapter 2 (paragraph 2.4).

2-(((9*H*-Fluoren-9-yl)methoxy)carbonylamino)-6-ureidohexanoic acid (1). H-HCit-OH

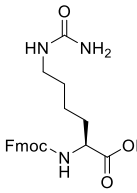

(1.00 g, 5.3 mmol, 1.0 equiv.) was suspended in dioxane (40 mL). $NaHCO_3$ (2.22 g, 26.4 mmol, 5 equiv.) was dissolved in H_2O (40 mL) and added to the suspension. Fmoc-OSu (1.78 g, 5.29 mmol, 1.0 equiv.) was dissolved in dioxane (20 mL) and was added dropwise to the suspension on ice. The mixture was stirred for 16 h at r.t. and the dioxane was removed under reduced pressure. 1M HCl was added until a pH of 4 and this was extracted with EtOAc (3 x 40 mL). The organic layer was dried over Na_2SO_4, filtered and concentrated *in vacuo*. The product, a white solid (2.17 g, 5.3 mmol, 100%), was used without further purification. R_f = 0.10 (10% MeOH in DCM). ^{1}H NMR (500 MHz, MeOH-d_4) δ 7.81 (d, J = 7.5 Hz, 2H), 7.69 (t, J = 8.3 Hz, 2H), 7.62 (s, 1H), 7.40 (t, J = 7.4 Hz, 2H), 7.33 (t, J = 7.9 Hz, 2H), 4.41 – 4.31 (m, 2H), 4.24 (t, J = 6.9 Hz, 1H), 4.17 – 4.14 (m, 1H), 3.12 (t, J = 6.8 Hz, 2H), 1.95 – 1.64 (m, 2H), 1.54 (ddt, J = 18.8, 11.9, 6.8 Hz, 2H), 1.49 – 1.39 (m, 2H). ^{13}C NMR (126 MHz, MeOH-d_4) δ 174.59, 173.46, 171.59, 160.88, 157.32, 143.77, 141.18, 127.38, 126.77, 124.84, 119.50, 66.53, 60.14, 53.91, 47.02, 31.00, 29.33, 24.88, 22.89, 19.46, 13.06. LRMS (ESI+) m/z calcd $C_{22}H_{26}N_3O_5^+$ $[M+H]^+$ 412.19, found: 411.92. $C_{44}H_{51}N_6O_{10}^+$ $[2M+H]^+$ 823.37, found 822.60.

15-(9*H*-Fluoren-9-yl)-1-(4-nitrophenyl)-3,5,13-trioxo-2,14-dioxa-4,6,12-triazapentadecane-11- carboxylic acid (7). Fmoc-HCit-OH (**1**) (2.18 g, 5.3 mmol, 1.0 equiv.) was dissolved in THF (122 mL) and heated to 40 °C. 4-nitrobenzyl chloroformate (1.71 g, 8.0 mmol, 1.5 equiv.) was dissolved in THF (5 mL) and added to Fmoc-HCit-OH. The reaction mixture was stirred overnight. The mixture was concentrated *in vacuo* and purified over silica (0-100% acetone in DCM), yielding a yellow solid product (**2**) (653 mg, 68% after regaining starting material). R_f = 0.14 (10% MeOH in DCM). ^{1}H NMR (500 MHz, DMSO-d_6) δ 10.24 (s, 1H), 8.24 (d, J = 8.5 Hz, 2H), 7.89 (d, J = 7.4 Hz, 2H), 7.72 (d, J = 7.3 Hz, 1H), 7.67 (s, 2H), 7.63 (d, J = 8.4 Hz, 2H), 7.41 (t, J = 7.2 Hz, 2H), 7.33 (t, J = 7.1 Hz, 2H), 5.34 (s, 1H), 5.26 (s, 2H), 4.34 – 4.20 (m, 3H), 3.87 (q, J = 7.7 Hz, 1H), 3.21 – 3.06 (m, 2H), 1.76 – 1.54 (m, 2H), 1.49 – 1.38 (m, 2H), 1.36 – 1.25 (m, 2H). ^{13}C NMR (101 MHz, DMSO-d_6) δ 156.02, 154.05, 152.50, 147.10, 143.86, 143.74, 140.68, 128.25, 127.59, 127.03, 125.28, 123.57, 120.07, 68.49, 65.52, 54.04, 46.68, 39.00, 30.73, 28.94, 22.97. HRMS (ESI+) m/z calcd for $C_{30}H_{30}N_4NaO_9^+$ $[M+Na]^+$ 613.19050, found: 613.19105

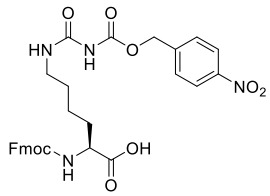

CHCitP (2). CHCitP was synthesized following the procedures described in the general peptide synthesis Section 2.4. Next, the peptides were cyclized as described in the general cyclization method. HPLC: Rt. 12.786 min. LCMS (ESI+) m/z calcd for $C_{101}H_{173}N_{41}O_{34}S_2^{2+}$ $[M+2H]^{2+}$ 1284.62, found 1285.12. $C_{101}H_{174}N_{41}O_{34}S_2^{3+}$ $[M+3H]^{3+}$ 856.75, found 857.40. $C_{101}H_{175}N_{41}O_{34}S_2^{4+}$ $[M+4H]^{4+}$ 642.81, found 644.84.

CLysP (3). CLysP was synthesized following the procedures described in the general peptide synthesis Section 2.4. Next, the peptides were cyclized as described in the general cyclization method. HPLC: Rt. 12.596 min. LCMS (ESI+) m/z calcd for $C_{100}H_{172}N_{40}O_{33}S_2^{2+}$ $[M+2H]^{2+}$ 1263.13, found 1263.56. $C_{100}H_{173}N_{40}O_{33}S_2^{3+}$ $[M+3H]^{3+}$ 842.42, found 843.12. $C_{100}H_{174}N_{40}O_{33}S_2^{4+}$ $[M+4H]^{4+}$ 632.07, found 634.52. $C_{100}H_{175}N_{40}O_{33}S_2^{5+}$ $[M+5H]^{5+}$ 505.85, found 507.00.

CAcLysP (4). CAcLysP was synthesized following the procedures described in the general peptide synthesis Section 2.4. Next, the peptides were cyclized as described in the general cyclization method. HPLC: Rt. 12.925 min. LCMS (ESI+) m/χ calcd for $C_{102}H_{174}N_{40}O_{34}S_2^{2+}$ $[M+2H]^{2+}$ 1284.13, found 1284.60. $C_{102}H_{175}N_{40}O_{34}S_2^{3+}$ $[M+3H]^{3+}$ 856.42, found 857.12. $C_{102}H_{176}N_{40}O_{34}S_2^{4+}$ $[M+4H]^{4+}$ 642.57, found 644.88.

CCP (5). CCP was synthesized following the procedures described in the general peptide synthesis Section 2.4. Next, this peptide was cyclized and purified as described in the general cyclization method. HPLC: Rt. 12.753 min. LCMS (ESI+) m/χ calcd for $C_{100}H_{171}N_{41}O_{34}S_2^{2+}$ $[M+2H]^{2+}$ 1277.61, found 1278.08. $C_{100}H_{172}N_{41}O_{34}S_2^{3+}$ $[M+3H]^{3+}$ 852.07, found 852.68. $C_{100}H_{173}N_{41}O_{34}S_2^{4+}$ $[M+4H]^{4+}$ 639.31, found 641.16.

CArgP (6). CArgP was synthesized following the procedures described in the general peptide synthesis Section 2.4. Next, this peptide was cyclized and purified as described in the general cyclization method. HPLC: Rt. 12.731 min. LCMS (ESI+) m/χ calcd for $C_{100}H_{172}N_{42}O_{33}S_2^{2+}$ $[M+2H]^{2+}$ 1277.13, found 1277.56. $C_{100}H_{172}N_{41}O_{34}S_2^{3+}$ $[M+3H]^{3+}$ 851.75, found 852.28. $C_{100}H_{173}N_{41}O_{34}S_2^{4+}$ $[M+4H]^{4+}$ 639.06, found 640.20.

CHCitP(CNBz) (8). CHCitP(CNBz) was synthesized following the procedures described in the general peptide synthesis Section 2.4. This peptide was cyclized as described in the general cyclization method. HPLC: Rt. 14.923 min. LCMS (ESI+) m/χ calcd for $C_{109}H_{178}N_{42}O_{38}S_2^{2+}$ $[M+2H]^{2+}$ 1374.14, found 1374.12 $C_{109}H_{179}N_{42}O_{38}S_2^{3+}$ $[M+3H]^{3+}$ 916.43, found 916.44. $C_{109}H_{180}N_{42}O_{38}S_2^{4+}$ $[M+4H]^{4+}$ 687.57, found 687.68.

CCP(CNBz) (9). CCP(CNBz) was synthesized following the procedures described in the general peptide synthesis Section 2.4. This peptide was cyclized and purified as described in the general cyclization method. HPLC: Rt. 14.854 min. LCMS (ESI+) m/z calcd for $C_{108}H_{176}N_{42}O_{38}S_2^{2+}$ $[M+2H]^{2+}$ 1367.12, found 1367.52. $C_{108}H_{177}N_{42}O_{38}S_2^{3+}$ $[M+3H]^{3+}$ 911.75, found 912.20. $C_{108}H_{178}N_{42}O_{38}S_2^{4+}$ $[M+4H]^{4+}$ 684.06, found 685.20.

Cell culture and monoclonal antibodies. See Section 2.4

Anti-CarP-positive mouse serum. Carbamylated ovalbumin and alum were used to induce and boost anti-CarP production as described in literature.[18]

RA plasma. Peripheral blood was obtained from ACPA- and anti-CarP-positive RA patients who visited the outpatient clinic of the Department of Rheumatology at Leiden University Medical Centre (LUMC). The patients met the 2010 ACR/EULAR criteria for RA at the time of diagnosis and gave written informed consent to participate in the study. Permission to conduct the study was obtained from the ethical review board of LUMC. Blood plasma was obtained by centrifuging heparin-treated peripheral blood.

ELISA experiments. See Section 2.4.

6.6 References

1. Shi, J.; van Veelen, P. A.; Mahler, M.; Janssen, G. M. C.; Drijfhout, J. W.; Huizinga, T. W. J.; Toes, R. E. M.; Trouw, L. A., Carbamylation and antibodies against carbamylated proteins in autoimmunity and other pathologies. *Autoimmun. Rev.* **2014,** *13* (3), 225-230.
2. Jaisson, S.; Kazes, I.; Desmons, A.; Fadel, F.; Oudart, J.-B.; Santos-Weiss, I. C. R. D.; Millart, H.; Touré, F.; Rieu, P.; Gillery, P., Homocitrulline as marker of protein carbamylation in hemodialyzed patients. *Clin. Chim. Acta* **2016,** *460*, 5-10.
3. Delanghe, S.; Delanghe, J. R.; Speeckaert, R.; Van Biesen, W.; Speeckaert, M. M., Mechanisms and consequences of carbamoylation. *Nat. Rev. Nephrol.* **2017,** *13*, 580-593.
4. Hagel, P.; Gerding, J. J. T.; Fieggen, W.; Bloemendal, H., Cyanate formation in solutions of urea: I. Calculation of cyanate concentrations at different temperature and pH. *Biochim. Biophys. Acta* **1971,** *243* (3), 366-373.
5. Wang, Z.; Nicholls, S. J.; Rodriguez, E. R.; Kummu, O.; Hörkkö, S.; Barnard, J.; Reynolds, W. F.; Topol, E. J.; DiDonato, J. A.; Hazen, S. L., Protein carbamylation links inflammation, smoking, uremia and atherogenesis. *Nat. Med.* **2007,** *13*, 1176-1184.
6. Silman, A., J.; Newman, J.; Macgregor, A., J., Cigarette smoking increases the risk of rheumatoid arthritis: Results from a nationwide study of disease-discordant twins. *Arthritis Rheum.* **1996,** *39* (5), 732-735.
7. Klebanoff, S. J., Myeloperoxidase: friend and foe. *J. Leukoc. Biol.* **2005,** *77* (5), 598-625.
8. Li, L.; Deng, C.; Chen, S.; Zhang, S.; Wu, Z.; Hu, C.; Zhang, F.; Li, Y., Meta-analysis: diagnostic accuracy of anti-carbamylated protein antibody for rheumatoid arthritis. *PloS one* **2016,** *11* (7), 1-14.
9. Vossenaar, E. R.; van Venrooij, W. J., Citrullinated proteins: sparks that may ignite the fire in rheumatoid arthritis. *Arthritis Res. Ther.* **2004,** *6* (3), 107-111.
10. Shi, J.; Knevel, R.; Suwannalai, P.; van der Linden, M. P.; Janssen, G. M. C.; van Veelen, P. A.; Levarht, N. E. W.; van der Helm-van Mil, A. H. M.; Cerami, A.; Huizinga, T. W. J.; Toes, R. E. M.; Trouw, L. A., Autoantibodies recognizing carbamylated proteins are present in sera of patients with rheumatoid arthritis and predict joint damage. *Proc. Natl. Acad. Sci.* **2011,** *108* (42), 17372.
11. Trouw, L. A.; Rispens, T.; Toes, R. E. M., Beyond citrullination: other post-translational protein modifications in rheumatoid arthritis. *Nat. Rev. Rheumatol.* **2017,** *13*, 331-339.
12. Brink, M.; Verheul, M. K.; Rönnelid, J.; Berglin, E.; Holmdahl, R.; Toes, R. E.; Klareskog, L.; Trouw, L. A.; Rantapää-Dahlqvist, S., Anti-carbamylated protein antibodies in the pre-symptomatic phase of rheumatoid arthritis, their relationship with multiple anti-citrulline peptide antibodies and association with radiological damage. *Arthritis Res. Ther.* **2015,** *17* (25), 1-8.
13. Gan, R. W.; Trouw, L. A.; Shi, J.; Toes, R. E. M.; Huizinga, T. W. J.; Demoruelle, M. K.; Kolfenbach, J. R.; Zerbe, G. O.; Deane, K. D.; Edison, J. D., Anti-carbamylated protein antibodies are present prior to rheumatoid arthritis and are associated with its future diagnosis. *J. Rheumatol.* **2015,** *42* (4), 572-579.
14. Shi, J.; van de Stadt, L. A.; Levarht, E. W. N.; Huizinga, T. W. J.; Hamann, D.; van Schaardenburg, D.; Toes, R. E. M.; Trouw, L. A., Anti-carbamylated protein (anti-CarP) antibodies precede the onset of rheumatoid arthritis. *Ann. Rheum. Dis.* **2014,** *73* (4), 780-783.
15. Stoop, J. N.; Liu, B.-S.; Shi, J.; Jansen, D. T. S. L.; Hegen, M.; Huizinga, T. W. J.; Trouw, L. A.; Toes, R. E. M., Antibodies specific for carbamylated proteins precede the onset of clinical symptoms in mice with collagen induced arthritis. *PLoS One* **2014,** *9* (7), 1-9.
16. Vossenaar, E.; Nijenhuis, S.; van Helsen, M. M.; van der Heijden, A.; van den Berg, W. B.; van Venrooij, W. J.; Joosten, L., Citrullination of synovial proteins in murine models of rheumatoid arthritis. *Arthritis Res. Ther.* **2003,** *5* (1), 30.
17. Kerkman, P. F.; Fabre, E.; van der Voort, E. I. H.; Zaldumbide, A.; Rombouts, Y.; Rispens, T.; Wolbink, G.; Hoeben, R. C.; Spits, H.; Baeten, D. L. P.; Huizinga, T. W. J.; Toes, R. E. M.; Scherer, H. U., Identification and characterisation of citrullinated antigen-specific B cells in peripheral blood of patients with rheumatoid arthritis. *Ann. Rheum. Dis.* **2016,** *75* (6), 1170-1176.
18. Dekkers, J. S.; Verheul, M. K.; Stoop, J. N.; Liu, B.; Ioan-Facsinay, A.; van Veelen, P. A.; de Ru, A. H.; Janssen, G. M. C.; Hegen, M.; Rapecki, S.; Huizinga, T. W. J.; Trouw, L. A.; Toes, R. E. M., Breach of autoreactive B cell tolerance by post-translationally modified proteins. *Ann. Rheum. Dis.* **2017,** *76* (8), 1449-1457.

Chapter 7

Summary, Future Perspectives and Concluding Remarks

7.1 Summary

Current B cell-directed therapies mainly induce generalized immune suppression by either inhibition or elimination of the complete B cell compartment, leaving patients at increased risk of infection.[1] Ideally, therapeutics only target autoreactive B cells involved in disease pathogenesis, while leaving healthy B cells intact. In this thesis, we describe research to explore and develop new approaches to target autoreactive B cells selectively, making use of epitopes targeting the unique B cell receptor. As free circulating autoantibodies recognize and bind the same autoreactive epitopes, the unique recognition element is likely to be quenched during administration. We envisioned that by physically caging the autoantigen we could circumvent binding to autoantibodies and by selective removal of the caging group in close proximity of a B cell we can improve binding to the autoreactive B cell.

In **Chapter 1**, we provided an overview of previously reported antigen-selective B cell targeting strategies in autoimmune diseases. We summarized the reported strategies to dampen a B cell response and we elaborated on the autoantigens used to target different diseases. Often, multivalent scaffolds were modified with an autoantigen combined with a functional molecule to induce anergy or apoptosis.

In **Chapter 2** we describe the caging of a cyclic citrullinated peptide (CCP) with a carboxynitrobenzyl (CNBz) group and the subsequent activation using the enzyme nitroreductase (NTR). We showed that we can fully retain the antigen from binding to both anti-citrullinated protein antibodies (ACPA) and ACPA-expressing B cells and that we can regain full binding only when removing CNBz using NTR. By conjugating the caged antigen peptide to a streptavidin-toxin, we induced selective cytotoxicity using this caging and activation strategy towards CCP recognizing B cells. We showed that this strategy is antigen-dependent, since B cells recognizing tetanus toxoid were not affected by the antigen-toxin conjugate.

In **Chapter 3** we showed that besides using an enzymatic cleavage strategy, we could also use a chemical click-to-release reaction to selectively activate an autoantigen. We synthesized citrulline linked to an iminosydnone at the ureido side chain and showed that we could incorporate this amino acid into CCP. We showed that the iminosydnone-caged CCP fully retained binding to both ACPA and ACPA-expressing B cells. The click-to-release reaction using DBCO yielded free CCP and regained binding to both ACPA and ACPA-expressing B cells. We also conjugated the CCP and iminosydnone-protected CCP to a MMAE toxin and observed no selective cytotoxicity. No antigen dependency was found, when comparing the caged with the uncaged CCP, and therefore we hypothesize that a multivalent system is needed to increase the selectivity for the BCR.

In **Chapter 4** we described the development of a new click-to-release reaction that is based on a tetrazine ligation with a phenoxyvinyl boronic acid. We showed that this reaction is faster than the ligation with the corresponding vinyl ether due to the attachment of the boronic acid moiety. By the conjugation of a lymphocyte specific toxin, cladribine, we showed that we can induce cell death mainly when the drug is activated after the click-to-release reaction with a dipyridyl tetrazine. Although the cladribine-VBA conjugate seemed to degrade over time, significant difference in cytotoxicity was obtained between the caged cladribine and the liberated toxin.

As we hypothesize that multivalency is important for BCR binding and we demonstrated this using tetravalent streptavidin (SA), in **Chapter 5** we studied another multivalent scaffold with increased valence. The use of a scaffold with increased valence allows the introduction of multiple functionalities which may be beneficial for imaging or therapeutic purposes. We used

poly(isocyanopeptides) (PICs) to attach both fluorophores and multiple antigen peptides to isolate CCP-recognizing B cells. We showed that the non-specific binding of this scaffold was lower compared to that of SA. In addition, we showed that the binding avidity of PIC and SA seemed comparable as demonstrated by a similar number of stained cells in a flow cytometric binding study. Furthermore, during our studies we found that the negative control peptide CArgP showed significant background binding to immortalized B cells. Replacing the positively charged arginine for a norleucine, however, diminished the background signal substantially. Lastly, we indirectly showed that it was not possible for the immortalized B cells to internalize the PIC scaffold. This is important information for future design of multivalent and multifunctional therapeutic structures based on the PIC scaffold.

In **Chapter 6** we show the discovery of a new synthetic antigen with affinity for anti-carbamylated protein antibodies (anti-CarP). We demonstrated that CHCitP, containing a homocitrulline, was efficiently bound by both human and mouse anti-CarP antibodies. We applied the carboxynitrobenzyl caging and activation mechanism, as described in Chapter 2, on CHCitP and established that similar results were obtained for both human and mouse sera. As mice cannot produce ACPA, this observation is an important step to allow the testing of the strategies described in this thesis in a mouse model, as well as in anti-CarP positive RA patient sera.

7.2 Future Perspectives

NTR modification and anti-CD20 Fab conjugation. To ensure that the activation of the caged antigen described in Chapter 2 occurs in close proximity of the B cell receptor (BCR), it is essential to target the nitroreductase (NTR) to the B cell membrane using a specific surface marker. Such a strategy, also described as antibody-directed enzyme prodrug therapy (ADEPT), has been explored extensively for local activation of cytotoxic prodrugs for tumor treatment.[2] The marker of interest here is CD20, a non-internalizing membrane protein specific for B cells, including memory B cells. The natural ligand for this protein is not known, but it is thought that CD20 functions as a calcium channel. Also, CD20 knockout mice display an almost normal phenotype.[1] CD20 is used as a therapeutic target for rituximab, which functions effectively as anti-cancer drug and has therapeutic benefit in RA. Here we specifically look at anti-CD20 Fab fragments, since they are known to be less immunogenic compared to a full antibody, since the Fc part is lacking.[3] In order to attach NTR to this Fab fragment, chemical modifications at the NTR and Fab fragment are needed.

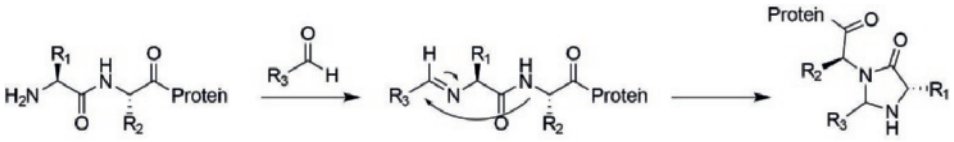

Figure 1. General reaction scheme for N-terminal imidazolidinone formation. The reaction with the aldehyde first results in the imine, after which the stable imidazolidinone is formed.[4]

As a first experiment, we tested a strategy using 2-pyridinecarboxyaldehyde (2-PCA) to modify NTR at the N-terminus only. This strategy was reported recently and allows the modification of the N-terminus of peptides and proteins without genetic engineering.[4] The selectivity is due to the required nucleophilic attack of the neighboring amide nitrogen of the protein backbone on the

initially formed N-terminal imine (Figure 1) providing a stable cycloadduct. Because of this mechanism, other lysines present in the protein are unaffected.

In order to attach an azide on the N-terminus, we synthesized two azide-containing 2-PCA analogues varying in linker length according to Scheme 1. We first synthesized the NHS-esters of both azidoacetic acid (**1**) and azido-PEG_4-acetic acid (**2**), which are needed to obtain 2-PCA azides **8** (without PEG tail) and **9** (with PEG tail, Scheme 1B). We started by oxidizing one of the alcohols of 2,6-pyridinedimethanol to the corresponding aldehyde **5**. The second alcohol was mesylated yielding compound **6**, and subsequently reacted with Boc-protected piperazine yielding the Boc-protected 2-PCA **7**. After Boc-deprotection using HCl in dioxane, NHS-esters **3** and **4** were used to yield 2-PCA azides **8** and **9**, respectively.

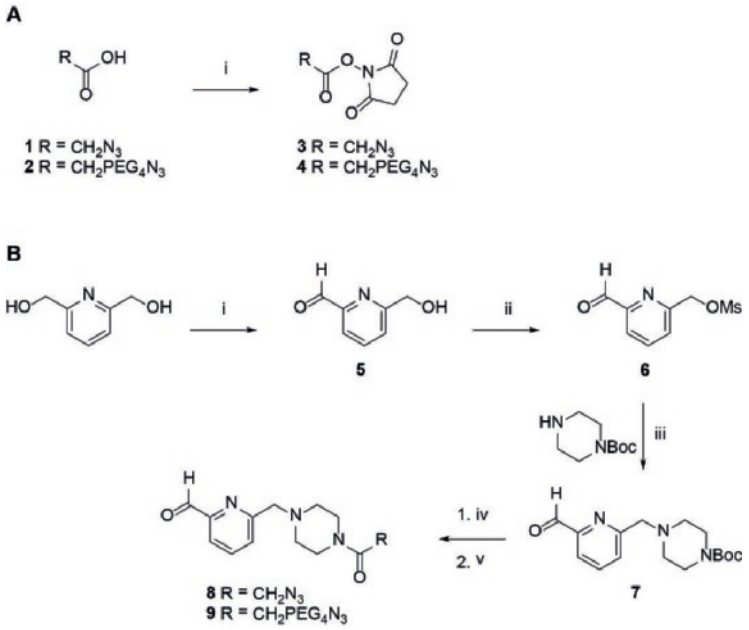

Scheme 1. Synthesis of azide-containing 2-PCA handles. A) Azide NHS synthesis without (**3**) and with PEG tail (**4**). i) EDC · HCl, NHS, DCM, r.t., 17 h, **3**: 70%, **4**: 65%; B) 2-PCA azide synthesis without (**8**) and with PEG tail (**9**). i) SeO_2, dioxane, 65 °C, 24 h, 92%; ii) MsCl, Et_3N, DCM, r.t., 30 min, 73%; iii) K_2CO_3, MeCN, 60 °C, 16 h, 87%; iv) 4M HCl in dioxane, DCM, r.t., 2 h; v) **3** or **4**, Et_3N, DMF, r.t., 2 h, **8**: 80%, **9**: 11%.

Next, we reacted NTR with 2-PCA azide **8** by incubating the reactants for 24 h in PBS buffer (Figure 2A). We performed the reaction at 4 °C, 21 °C and 37 °C to see if this affects the reaction efficiency of the conjugation. For two of the temperatures we used either no (only DMSO) or 100 equivalents of 2-PCA azide **8**. For the reaction at 4 °C we decided to also add 1000 equivalents as we expected the reaction to occur much slower at this temperature. After incubation, we tested the presence of the azide by reacting the alleged N_3-NTR with either DBCO-Cy5.5 or DBCO-PEG_{5000}. On SDS-PAGE gel (Figure 2B) we observed the fluorescent band of the click-reaction with DBCO-Cy5.5 in varying intensities. Although there was some background observed for the

NTR that was not functionalized with 2-PCA-azides, the intensity of the signal increased when azides were present. Especially at 21 °C and 37 °C a bright fluorescent signal was observed. We attempted to measure the efficiency of the modification conditions by reacting the NTR-azides with DBCO-PEG$_{5000}$. However, no cycloaddition with DBCO-PEG$_{5000}$ was observed for any of the conditions (Figure 2C). This might be due to steric hindrance of the enzyme, or to inefficient protein modification with the 2-PCA azide moiety.

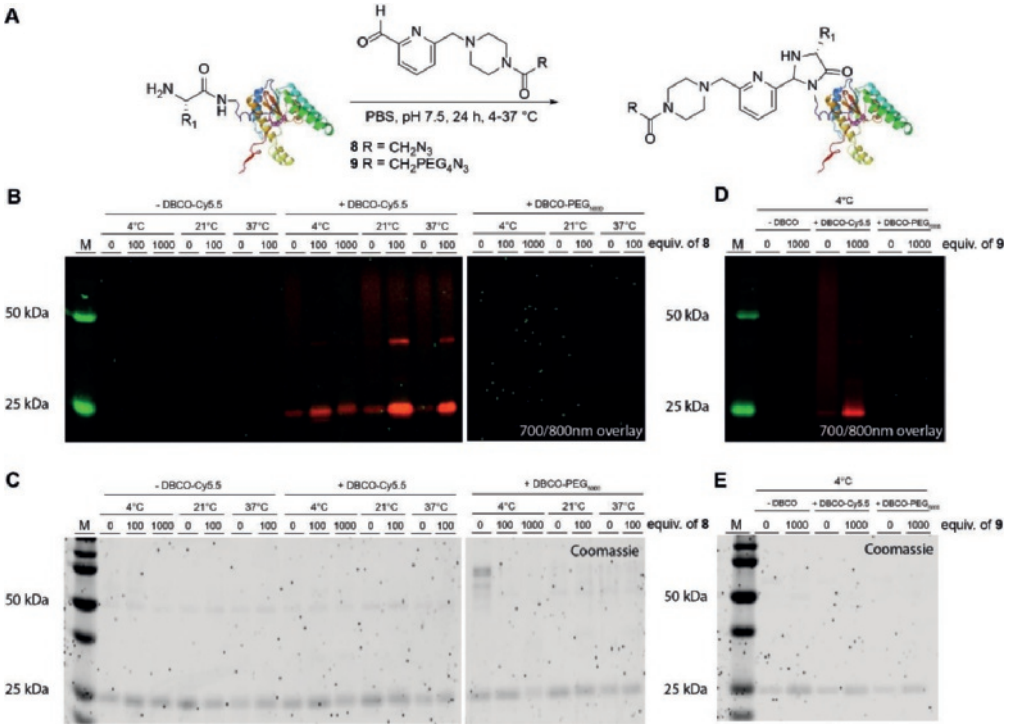

Figure 2. Strategy for the selective N-terminal modification of NTR. A) Reaction of 2-PCA-N_3 (**8**) or 2-PCA-PEG$_4$-N_3 (**9**) with NTR; B) The NTR modification using 0-1000 equiv. 2-PCA **8** was performed at 4 °C, 21 °C and 37 °C and subsequently reacted with DBCO-Cy5.5 or DBCO-PEG$_{5000}$, measured at 700 (red) and 800 nm (green); C) Coomassie Brilliant Blue staining of NTR reacted with 2-PCA **8**; D) The NTR modification using 0 or 1000 equiv. 2-PCA **9** was performed at 4 °C and subsequently reacted with DBCO-Cy5.5 or DBCO-PEG$_{5000}$, measured at 700 (red) and 800nm (green); E) Coomassie Brilliant Blue staining of NTR reacted with 2-PCA **9**.

Next, we evaluated if NTR functionalization could be improved using 2-PCA **9**, containing a short PEG tail. Incubating NTR with 2-PCA **9** at 4 °C followed by cycloaddition to DBCO-Cy5.5, provided a fluorescent signal for the modified NTR as expected (Figure 2D). Unfortunately, cycloaddition using DBCO-PEG$_{5000}$ (Figure 2E) did not result in a protein shift as evidenced by Coomassie Brilliant Blue staining of the SDS-PAGE gel. Hence, reaction efficiency could not be determined.

To test whether the reaction conditions of the N-terminal modification of NTR altered the enzyme activity, we tested the reaction efficiency of the 2-PCA-modified NTR. We used the

CCP(CNBz) and monoclonal ACPA in a similar ELISA assay as described in Chapter 2. Besides using unmodified NTR, we tested all conditions, such as different incubation temperatures and 2-PCA equivalents added, described earlier. The ELISA data showed that the enzyme was stable as there was no significant difference observed between the different incubation temperatures and 2-PCA concentrations (Figure 3).

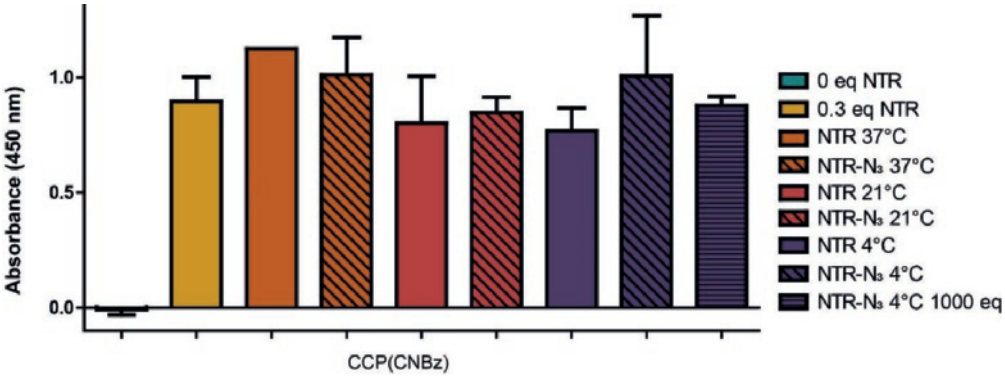

Figure 3. Activity of modified NTR. The activity was tested by studying the deprotection efficiency of NTR on the CCP(CNBz) in ELISA. Non-patterned bars are negative controls (no 2-PCA) of NTR for each condition, dashed bars depict NTR reacted with 100 equiv. of 2-PCA azide and the horizontal striped bars corresponds to 1000 equiv. of 2-PCA azide.

Next, we aimed to conjugate the anti-CD20 Fab fragment to one of the two different selectively modified NTR enzymes, with or without PEG chain. The Fab fragments with a LAETG and a histidine tag were produced using a hybridoma cell line. Fab fragments were excreted by cells and collected, after which they were purified by nickel affinity chromatography. The LAETG tag of the Fab fragments can be used in a sortase reaction. A sortase reaction using GGG-DBCO was performed at 4 °C for 24 h in sortase buffer (PBS + 50 mM Tris-HCl, pH 7.5, 150 mM NaCl, 10 mM $CaCl_2$). The strain promoted alkyne azide cycloaddition (SPAAC) between the Fab fragment and NTR was carried out overnight at 4 °C. The results were analyzed on SDS-PAGE gel (Figure 4).

We evaluated the results by non-reducing SDS-PAGE, so the heavy chain and the light chain of the Fab fragment remained connected. This simplifies the analysis as the molecular weight of both heavy and light chain is approximately 25.000 Da, similar to that of NTR. To test the reactivity of the DBCO on the Fab fragment, we reacted this with N_3-PEG_{5000}. In the third lane, a band shift was seen indicating the reaction between the Fab fragment and the PEG chain, meaning that the DBCO was active. Next, both modified NTRs were reacted and analyzed, but no reaction was observed.

Up to this point, the modification of NTR was inefficient and the following cycloaddition with the DBCO-modified Fab fragment was unsuccessful. As the described cycloadditions were performed at 4 °C overnight, it would be interesting to investigate other conditions such as an increased temperature or reaction time.

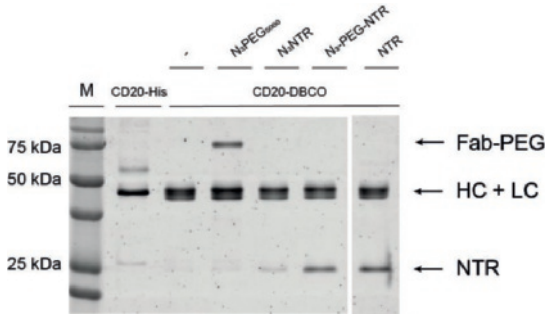

Figure 4. Analysis of SPAAC reactions with NTR and anti-CD20 Fab. Figure shows a SDS-PAGE gel under non-reducing conditions, to leave the heavy chain (HC) and light chain (LC) connected, of **8** or **9** modified NTR reacted with anti-CD20 Fab-DBCO. Anti-CD20-His is shown in the first lane. The Fab fragment conjugated to DBCO is shown in the other lanes. Third lane shows the cycloaddition with N_3PEG_{5000}, in the fourth lane N_3-NTR is added, in the fifth lane N_3-PEG-NTR is added and in the final lane unmodified NTR is added. Gel was stained with Coomassie Brilliant Blue.

Alternatively, another N-terminal modification strategy could be explored. Jensen *et al.* recently reported a general method for highly selective N-terminal acylation of proteins using 4-methoxyphenyl esters as acylating agents.[5] The authors showed that a N-terminal His tag, with the optimized sequence of $GHHH_n$, was useful for these reactions. As the His-purification tag is often used to purify recombinant proteins, this labeling method could be applied to these proteins. For our research, NTR expressed with a N-terminal His-tag may be modified using 4-methoxyphenyl 2-azidoacetate to yield the specific azide modification selectively on the N-terminus of NTR (Figure 5).

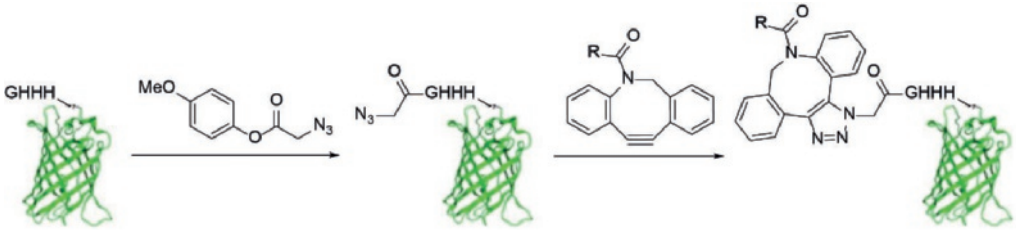

Figure 5. N-terminal His tag acylation of Gly-His_n-protein sequences. 4-Methoxyphenyl 2-azidoacetate acylation yields the N-terminal azide-labeled protein. This azide can subsequently be used in a SPAAC reaction. Protein depicted is enhanced green fluorescent protein.

Lastly, to circumvent a chemical N-terminal modification procedure, it would be interesting to clone NTR containing a GGG-sortase motif directly at the N-terminus. As such, the NTR and the Fab fragment can be conjugated in one step using Sortase. It has to been seen if ligating these two proteins using the sortase approach is feasible, although the results of previous studies indicate that this could be achieved.[6, 7]

Mono-functionalized iminosydnone caged antigen peptides. In Chapter 3 we described a strategy to retain antigen binding by introducing an iminosydnone at the citrulline side chain in CCP. We showed that activation of the antigen could be achieved via a click-to-release approach

using DBCO. After attachment of the MMAE toxin, with the aim to induce receptor-mediated cell death, we observed that the cytotoxicity was not dependent on the antigen. This result suggests that the use of a monovalent antigen-drug conjugate is insufficient to induce receptor internalization or that MMAE is unsuitable for inducing apoptosis in immortalized B cells.

In Chapter 1 we reviewed research describing an approach to eliminate plasma cells using an affinity matrix (AM, Figure 6). This AM is an antibody-mediated coating of the surface of plasma cells with an autoantigen of interest. The secreted antibodies by the plasma cells are in close proximity of the AM antigen thereby binding directly onto the AM surface. As a result, the complement system is activated and the plasma cells are terminated via complement-mediated lysis.[8] Anti-CD138 and anti-CD44 have already been used as antibody mediator for targeting the antigen of interest to the surface of plasma cells and it was shown that specific autoreactive long-lived plasma cells were successfully depleted *in vitro* using this strategy.[9]

A potential limitation of this approach *in vivo* is the presence of circulating autoantibodies. These antibodies may bind nonspecifically to the AM of protective plasma cells thereby inducing unwanted cytotoxicity.[10] The authors suggest that this can be circumvented by the removal of these autoantibodies using plasma exchange or immunoadsorption. As this will be unpleasant for patients, they suggest otherwise to carefully titrate the affinity matrix, since plasma cells are spread throughout the bone marrow, but separated in niches.[10] We suggest that by using our CCP-iminosydnone caging strategy, we have the ability to circumvent binding of circulating autoantibodies to CCP before binding to the ACPA-producing plasma cells. The caged CCP is first localized to the plasma cell membrane, using for example an anti-CD138 directing antibody (Figure 6A), before DBCO is added. The autoantigens are protected from circulating antibodies and are mainly captured by the autoantibodies secreted by the autoreactive plasma cell due to increased local concentration (Figure 6B).

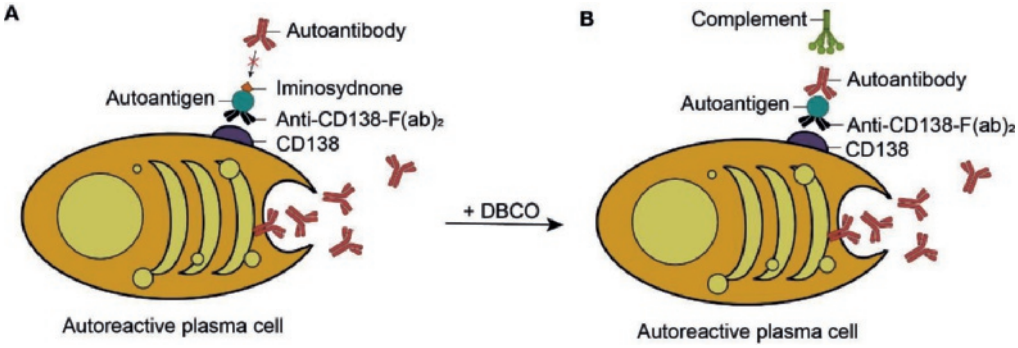

Figure 6. Targeting of autoreactive long-lived plasma cells. A) Anti-CD138 is targeted to the cell membrane of an autoreactive plasma cell together with the iminosydnone-caged autoantigen. This conjugate cannot be cleared in circulation by autoreactive antibodies, due to the iminosydnone-caging group. As soon as plasma cells are coated with the caged autoantigen, DBCO can react and release the activated autoantigen; B) The autoantibodies secreted by the plasma cells are available in high local concentrations and will bind to the plasma cells own membrane after which the complement is activated. Due to complement-mediated lysis, this autoreactive plasma cell will be depleted whereas protective plasma cells, which do not secrete autoantibodies, will not be coated and hence not be lysed.

Dual-functionalized iminosydnone caged antigen peptides. Recently, Bernard *et al.* reported the use of iminosydnones as a cleavable linker between an antibody and a fluorophore or a biotin moiety.[11] Hence, they showed that after adding a DBCO, the linkage between two compounds was broken.

To not only target the plasma cells, but also the memory B cells, a strategy in which a dual functionalized iminosydnone acts as a cleavable bridge between the CCP antigen peptide and an anti-CD20 Fab fragment was introduced in Chapter 3. Based on the strategy of Bernard *et al.*, we envisioned that we could link the anti-CD20 Fab fragment using this iminosydnone to the CCP peptide. However, as we suspect that monovalent antigen binding to the BCR is not sufficient to induce receptor internalization, we propose a strategy to attach a biotin to CCP(Im) and link this Fab-CCP to streptavidin-toxin (such as saporin, a ribosome inactivator) conjugate (Figure 7). We have shown in Chapter 2 that such a construct can successfully induce antigen-selective cell death.

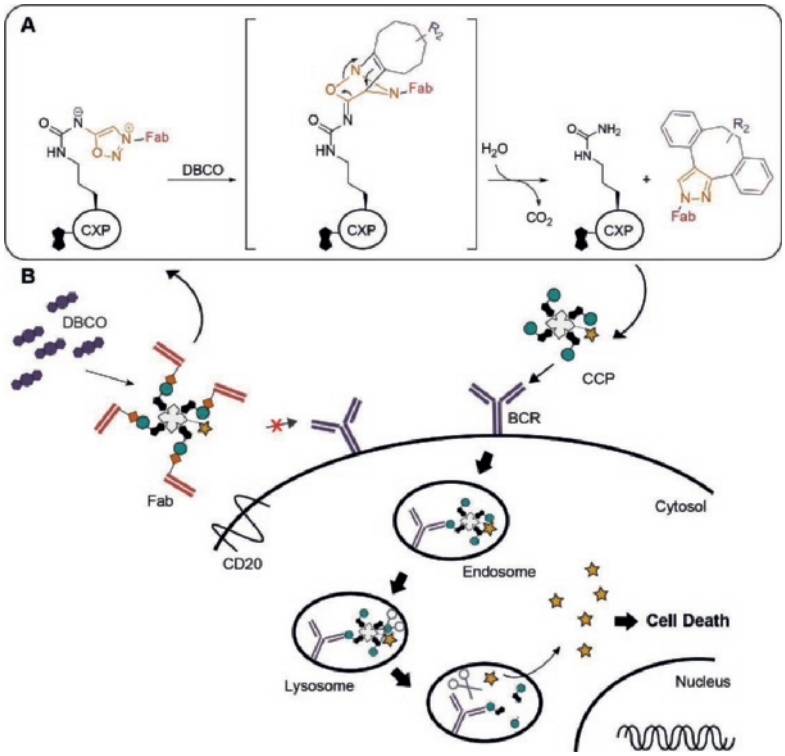

Figure 7. Schematic representation of B cell targeting using the Fab-iminosydnone-CCP-SA conjugate. A) Antigen activation mechanism. The cycloaddition of the iminosydnone with DBCO results in a retro-Diels Alder reaction creating an isocyanate in situ at the citrulline side chain. When water reacts with this isocyanate this results in an instable carbamoyl carbamate. Liberation of CO_2 restores the urea side chain of citrulline; B) Schematic representation of the targeting strategy. The Fab targets CD20 on the B cell membrane. Since the iminosydnone both binds and blocks the CCP peptide, this antigen is already localized to the B cell surface. If now DBCO is added, liberation of CCP-SA-ZAP can be bound to the neighboring BCR and be internalized, after which apoptosis is induced.

As described above, an anti-CD20 Fab fragment containing a LAETG sortase tag was produced. We envision that we can conjugate a triple-Gly peptide containing an azide to the Fab fragment using sortase. Using this azide, we can react the Fab fragment with an alkyne attached to the iminosydnone-CCP and hence conjugate the iminosydnone-CCP to the Fab fragment.

Our initial efforts to prepare a cleavable iminosydnone-containing linker are described. We aimed to introduce an alkyne handle for future conjugation as shown in Scheme 2, by following part of the synthetic route of the iodosydnone described by Bernard *et. al.*[11]

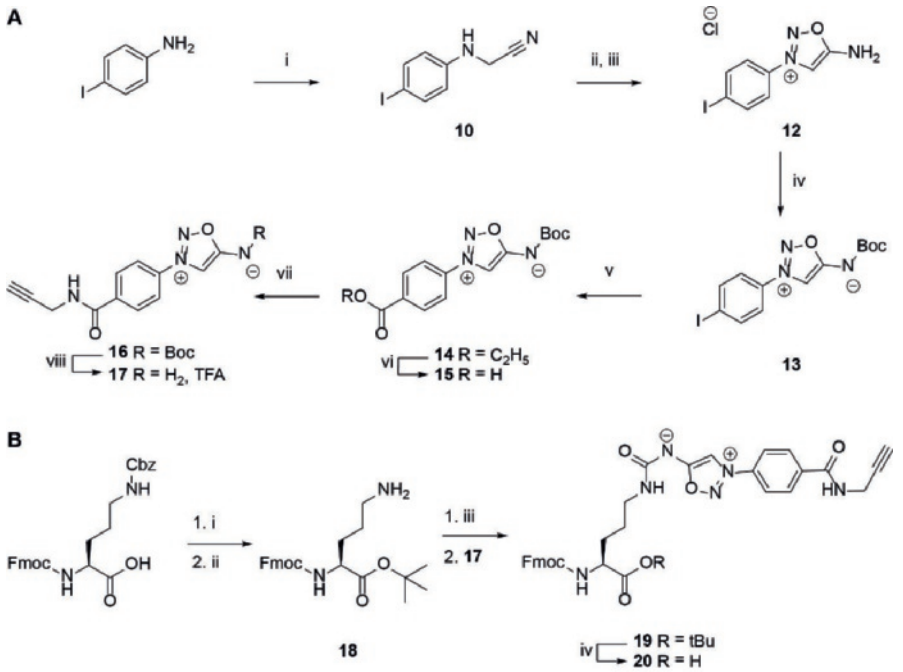

Scheme 2. Reaction scheme for the synthesis of Fmoc-Cit(ImAlk)-OH (**20**). A) Synthesis of iminosydnone (**17**). i) chloroacetonitrile, acetonitrile, NaI, K_2CO_3, under Ar, 3 days, reflux, 82%; ii) amyl nitrite, dry THF, 2 h, r.t.; ii) 4M HCl in dioxane, overnight, r.t., 95% over two steps; iv) Boc_2O, $NaHCO_3$, DMAP, dry THF, 70 h, 0 °C → r.t., 59%; v) $PdCl_2(PPh_3)_2$, EtOH, CO atmosphere, 2.5 h, 60 °C, 65%; vi) LiOH·H_2O, THF/H_2O, 2.5 h, r.t., 92%; vii) propargylamine, HATU, DIPEA, DMF, 2 h, r.t., 58%; viii) TFA/DCM (1:1), 4 h, r.t., 80%; B) Ornithine modification and Fmoc-Cit(ImAlk)-OH (**20**) synthesis. i) *tert*-butyl 2,2,2-trichloroacetimidate, BF_3 etherate, THF/hexane (1:1), overnight, 0 °C → r.t.; ii) Pd/C, H_2, MeOH, 2 h, r.t., 80% over two steps; iii) 1. triphosgene, sat. $NaHCO_3$/DCM (1:1), 10 min, 0 °C; 2. **17** was added, 3 h, 0 °C, 18% yield; iv). TFA/DCM (1:1), 2 h, r.t., quant.

First, iodoaniline was reacted with chloroacetonitrile to obtain the nitrile product **10** in good yield. Next, iodophenylacetonitrile (**10**) was reacted in two steps; first with isoamyl nitrite and next with 4M HCl in dioxane to induce ring closure to obtain iodosydnone **12**. The free amine was protected with a Boc group, after which the iodide was reacted with ethanol and $PdCl_2(PPh_3)_2$ under a CO atmosphere. The resulting ethyl ester (**14**) was hydrolyzed to the corresponding acid using LiOH. Next, propargylamine was reacted with the carboxylic acid (**15**) to form an amide bond and to attach a handle for a Cu-catalyzed Azide−Alkyne Cycloaddition (CuAAC). After Boc deprotection

using TFA, iminosydnone **17** could be attached to ornithine. First, Fmoc-Orn(Cbz)-OH was *tert*-butyl-protected on the free carboxylic acid. Then, Pd/C and H_2 were used to deprotect the Cbz group. This modified ornithine **18** was treated with triphosgene before iminosydnone **17** was added. After the reaction and purification, the *tert*-butyl group of the ornithine was removed to yield the citrulline-iminosydnone **20**.

We next used Fmoc-Cit(ImAlk)-OH (**20**) in solid phase peptide synthesis (SPPS) to prepare CCP(ImAlk). No difficulties were observed during the synthesis, although we were not able to isolate the desired peptide using preparative HPLC. The mass value corresponding to the desired caged peptide was observed, but in a very small amount. Since we confirmed the stability of the building block under several conditions, including those used for general SPPS, peptide cyclization and the cleavage mixture for SPPS, we cannot explain why the synthesis of the CCP(ImAlk) was not successful.

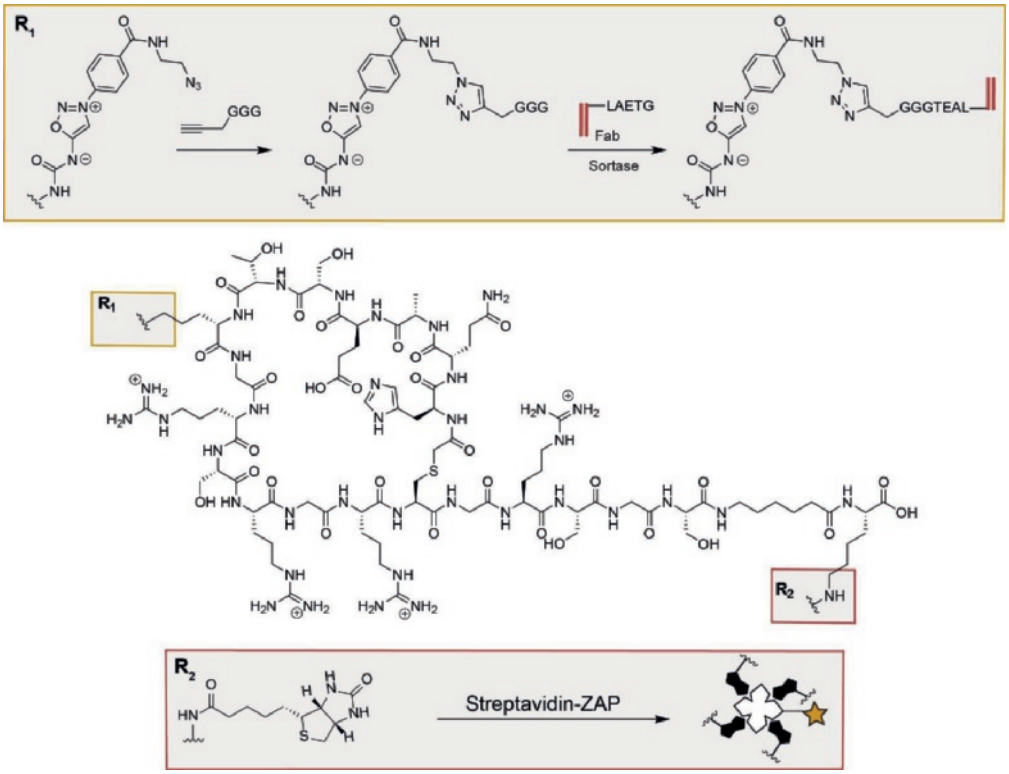

Figure 8. Overview of the targeting Fab-iminosydnone-CCP construct consisting of CCP conjugated to streptavidin-ZAP and caged by an iminosydnone linked anti-CD20 Fab fragment. R_1 shows the Fab conjugation by first reacting the azide functionalized iminosydnone with the GGG-alkyne, and finally the conjugation to the anti-CD20 Fab fragment using sortase. R_2 depicts the conjugation to streptavidin-ZAP.

Bernard and coworkers showed recently that they were able to synthesize an iminosydnone containing an azide and that this modified iminosydnone could be used in CuAAC for antibody conjugation.[11] Hence, future efforts should be directed to the synthesis of an azide-containing citrulline amino acid. Additionally, we aim to synthesize a triple-Gly peptide containing an alkyne

for conjugation to the CCP using CuAAC. Next, the GGG-modified CCP should be conjugated to the Fab fragment using sortase. Finally, to create a multivalent structure these Fab-antigen conjugates can be linked to streptavidin-ZAP as used in Chapter 2 (Figure 8).

A limitation of the proposed strategy above, is that the Fab fragment and the CCP antigen peptide are directly linked and hence dual binding of both the Fab fragment and the antigen to the B cell, which would create a multivalent binding interaction, is hampered. Thereby, at least two iminosydnones should be deprotected to create a multivalent interaction with the BCR. Finally, a stoichiometric amount of DBCO is needed for antigen activation. In order to activate the antigen locally, high concentrations of DBCO might have to be administered to achieve this. So far, the maximum non-toxic dose of DBCO is not known.

Use of DBCO-loaded cryogels for high local concentration of peptide antigens. Besides administering an excess of DBCO for local activation of caged antigens, we envision that DBCO can be localized to a specific inflamed region. One example is by using injectable hydrogels, for example using methacrylated (MA)-alginate cryogels,[12] which are filled with DBCO.

A cryogel is a hydrogel which is produced at subzero temperatures and used in many biomedical applications.[12] These cryogels have pores that are produced by growing ice crystals. By melting of these crystals, a macroporous network is formed with enhanced mechanic stability.[13] Cryogels used in cancer vaccination are made from alginate, which is a natural polymer that has been used in several applications, including drug delivery, cell delivery and tissue engineering.[12] By crosslinking alginate, combining covalent and ionic bonds, a tough network is created. Upon compression the weaker ionic crosslinks will reversibly break, hence the tough MA-alginate cryogels can be used for needle-injections without sustaining damage.[14] These cryogels loaded with tumor antigens are already in use and after implantation of these bio-based materials, dendritic cells are attracted and become activated after which they home to draining lymph nodes and present the antigen to T cells. This will subsequently lead to an anti-tumor response of the T cells. The release of large molecules, like proteins, from cryogels is often dependent on the diffusion rate, which is estimated to be between a few hours and a day.[15]

If a cryogel linked to DBCO is locally injected into inflamed tissue with a high number of effector cells, or to the lymph nodes, it can locally activate iminosydnone-caged antigens (Figure 9). This is different from a local injection of DBCO alone, which would diffuse from the site of interest. This difference was shown for vascular endothelial growth factor (VEGF), which has been locally delivered in ischemic murine hindlimbs over a time of 15 days using alginate hydrogels, whereas all VEGF was already deprived after 72 hours with a direct injection.[16]

The CCP antigens do not have to be administered locally, but will stay inactive until reaching the site of interest. The local induction of antigen-activation and thereby possible BCR binding for toxin uptake (Figure 9B) will decrease off-site activation of the antigen-drug conjugate. If small molecules are embedded in the gel and the release would be diffusion-dominated, all drugs would be released in a very short time period. Hence cleavable covalent linkages, including ester bonds or disulfide bonds, prolongs the drug release property.[15]

There is no enzyme in humans or animals than can degrade alginate.[12] Hence biodegradability may become an issue. Alternative to the MA-alginate, hyaluronic acid (HA) can be of interest. High molecular weight HA was used as a material for local regulation of wound healing and inflammatory response when conjugated to a cytokine-neutralizing antibody.[17]

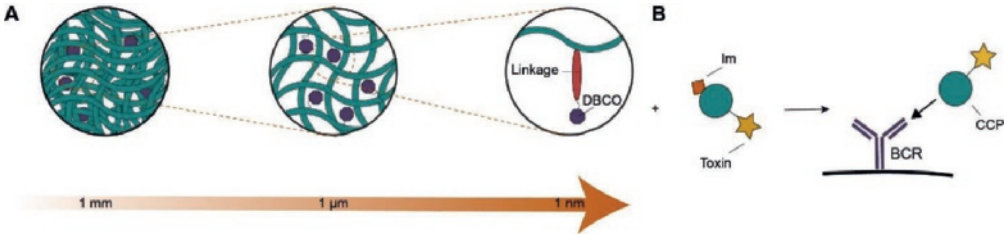

Figure 9. DBCO-containing hydrogel. A) DBCO (purple octagon) is linked to a hydrogel and can be injected locally; B) CCP(Im)-toxin (CCP - blue circle, Im – orange square, toxin – yellow star) is administered and only activated close to the hydrogel. Since the hydrogel will be injected in the inflamed tissue or lymph nodes, autoreactive B cells will be present and are targeted. A monovalent peptide is only depicted for clarity.

Functionalization possibilities of multivalent PICs. In Chapter 5 we showed that PIC polymers can be used successfully to bind ACPA-expressing B cells comparably to the SA control.[18] We further showed that not all, if any, PICs were internalized when incubated with the ACPA-expressing B cells at 37 °C for 1 hour.

An advantage of using PIC over SA is that there are multiple sites available for cargo conjugation. For example, besides adding an antigen, we may conjugate a fluorophore for imaging purposes and/or a toxin to induce cell death. In order to decide on the most optimal cargo to induce antigen-selective cell death, whether the cargo should either be effective inside the cell or on the cell surface, we should further characterize the binding and internalization behavior of PICs. We need to investigate at multiple time points and concentrations if PICs indeed remain on the cell surface, or are internalized under specific experimental conditions.

The PIC polymer that we tested in Chapter 5 is approximately 400 nm in length. Although this polymer seems not to be internalized by B cells, it is possible that polymers being shorter in length can be internalized. Hence, it is interesting to test different polymer lengths for this purpose. The PIC polymers have to be internalized in case a potent toxin, like monomethyl auristatin E (MMAE, Chapter 3), is used to induce antigen specific cell death. The advantage of PICs that are not internalized is that external signals may be attached to induce cell death. Similar to Siglec-engaging tolerance-inducing antigenic liposomes (STALs, see Chapter 1 and Figure 10A), a CD22 ligand, dampening the function of B cells by binding to glycoprotein CD22, can be attached adjacent to the autoantigen onto the PIC.[19] Previously, CD22 ligands with a 200-fold higher affinity than natural ligands were conjugated to STALs together with an autoantigen. Macauley *et al.* described that immunization of mice with these STALs showed a dramatically lower antibody response to the autoantigens than when immunogenic liposomes were used. They showed that tolerance induction was intrinsic to depletion of B cells, due to CD22-dependent apoptosis.[19] By introducing an autoantigen, antigen-selective B cell signaling was inhibited. Unilamellar liposomes, however, are spherical structures with a lower surface area to volume ratio and the number of recognition domains (like antigens or ligands) participating simultaneously in interaction with a surface is therefore limited.[20] Due to the higher surface to volume ratio and the semi-stiff characteristics of the PIC polymers, they may be more useful than liposomes because of the possibility of shaping around the cell surface to optimize receptor binding (Figure 10B). Indeed, it has been shown for the PICs that the combination of multivalency and an optimal flexible shape for interactions is beneficial.[21]

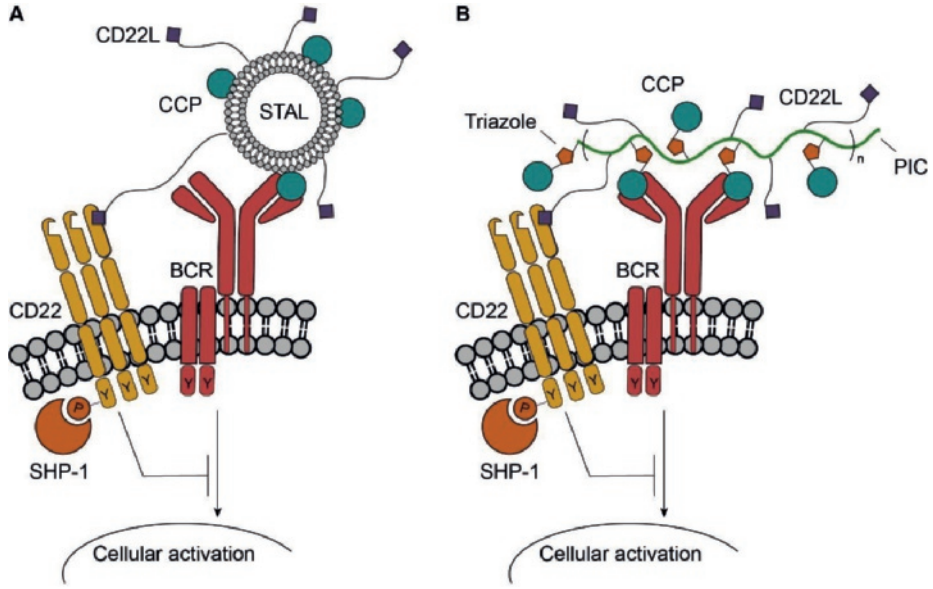

Figure 10. The influence of multivalent structures containing CD22 ligand and CCP on BCR-signaling in autoreactive B cells. A) Schematic representation of CCP-STALs; B) Schematic representation of PIC-containing CCP and CD22 ligand.

Since the PICs are known to be semi-flexible,[21] they might facilitate the clustering of receptors. A receptor of interest, is the Fas receptor (CD95). The Fas receptor is involved in the regulation of apoptosis. Apoptosis induced by the interaction between Fas and Fas ligand (FasL, a cell surface molecule belonging to the tumor necrosis factor family) is the main route by which unwanted lymphocytes are eliminated during lymphocyte development and in the course of an immune response.[22, 23] Also, cytotoxic T cells express FasL when activated to induce apoptosis of the target cell (for example, virus-infected cells or tumor cells).[24] Activation of mature B cells causes expression of Fas and the cells become sensitive to Fas-mediated killing.[25] It was shown before that an antibody to human Fas resulted in apoptosis of transformed mouse cells in 5 hours, indicating that this anti-Fas antibody works as an agonist.[24] This anti-Fas or FasL can be attached to PICs together with autoantigens to induce antigen-selective apoptosis (Figure 11).

Fas can also be activated by FasL, a protein with a molecular weight of 40 kDa, in solution (released from cell surfaces after cleavage by metalloproteinases).[24] Large proteins have already been attached to the PIC polymers and showed to be functional.[21] Hence we envision, that the conjugation of FasL to PIC together with the CCP antigen peptides allows for the antigen-selective induction of Fas trimerization on autoreactive B cells, followed by the initiation of apoptosis.

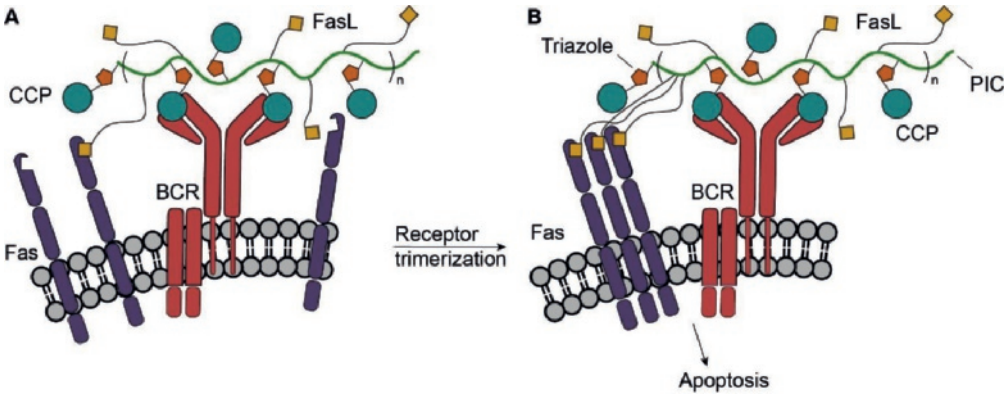

Figure 11. Fas activation using PIC loaded with CCP and FasL. A) PIC is targeted towards the BCR by multivalent CCP binding; B) The Fas receptor is trimerized due to multiple ligands in the close proximity of the B cell membrane. This activation leads to antigen specific cell death.

7.3 Concluding remarks

In this thesis, we introduced several autoreactive B cell targeting strategies making use of ACPA autoantigens. By caging and selective activation of autoantigens, we showed that we can direct binding to the BCR. By developing a peptide for anti-CarP antibodies, we showed that the activation strategy is adoptable to other (homo)citrulline containing antigens, a feature which is important in RA, since autoantibodies recognizing varying antigens are in play. We showed that besides an enzymatic approach, a chemical click-to-release strategy may be used for caging and activation purposes. It was evident that a monovalent structure was not sufficient to induce BCR internalization and subsequent cytotoxicity. We showed that PIC scaffolds bind comparably to a specific BCR as a SA scaffold, but that it shows less background binding and there are more handles to modify. We further developed a new click-to-release reaction based on VBA tetrazine ligation, which can be further developed for antigen activation applications.

The outlook and scope of the development of a new RA targeting strategy is promising. We showed that our caging and activation strategies can be applicable to several autoantigens for both human and mice serum *in vitro* and the next step will be to test this on B cells and finally in a mouse model. Using the anti-CarP antigen peptides, we observed that the caging and activation strategies can be used interchangeably between citrulline and homocitrulline. Although NTR is needed to activate the antigen in the strategy used for anti-CarP, which might be troublesome *in vivo*, we also expect that the click-to-release activation strategy will be possible for this antigen. We might, however, first need more information about the cytotoxicity of DBCO and the best way to achieve local antigen activation to continue this strategy. Doing so brings us another step closer to an effective and selective therapy towards autoreactive B cells in RA.

7.4 Acknowledgements

Camille Le Gall and dr. Martijn Verdoes (Radboud Institute for Molecular Life Sciences) are gratefully acknowledged for providing us with the anti-CD20 Fab fragments and their collaboration in this project. Mike Smeenk is thanked for the synthesis of iminosydnones **10**-**12**, **14**-**18**. We thank dr. Selma Eising for the synthesis of compound **5**-**7**.

7.5 Materials and methods

For general methods, see the materials and methods Section of Chapter 2 (paragraph 2.4).

2,5-Dioxopyrrolidin-1-yl 2-azidoacetate (3). 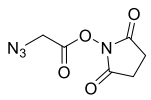 To a solution of 2-azido acetic acid (200 mg, 2.0 mmol, 1.0 equiv.) in dry DCM (10 mL), *N*-hydroxysuccinamide (273 mg, 2.4 mmol, 1.2 equiv.) and *N*-(3-dimethylaminopropyl)-*N*'-ethylcarbodiimide hydrochloride (455 mg, 2.4 mmol, 1.2 equiv.) were added and the reaction mixture was stirred at r.t. for 17 h. The reaction mixture was washed with H_2O and brine, and dried over Na_2SO_4. Volatiles were removed under reduced pressure. The residue was purified by silica gel column chromatography (0-25% EtOAc in heptane) to yield title compound **3** as a white solid (274 mg, 1.4 mmol, 70%). R_f = 0.25 (EtOAc/heptane 1:1); IR (film) 2113, 1818, 1786, 1736, 1426, 1366, 1283, 1202, 1095, 1066, 811, 647 cm^{-1}; ^1H NMR (400 MHz, chloroform-*d*) δ 4.24 (s, 2H), 2.88 (s, 4H). ^{13}C NMR (126 MHz, chloroform-*d*) δ 168.40, 164.14, 47.99, 25.56. Mass could not be found.

2,5-Dioxopyrrolidin-1-yl 14-azido-3,6,9,12-tetraoxatetradecanoate (4). 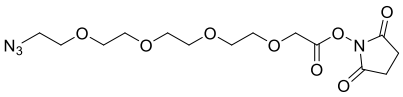 A solution of 14-Azido-3,6,9,12-tetraoxatetradecanoic acid (50 mg, 0.18 mmol, 361 µl, 1.0 equiv.) in *t*BME was added to dry DCM (2.5 mL). *N*-hydroxysuccinamide (25 mg, 0.22 mmol, 1.2 equiv.) and *N*-(3-dimethylaminopropyl)-N'-ethylcarbodiimide hydrochloride (42 mg, 0.22 mmol, 1.2 equiv.) were added and the reaction mixture was stirred at r.t. for 17 h. The reaction mixture was washed with H_2O and brine, and dried over Na_2SO_4. Volatiles were removed under reduced pressure. The residue was purified by silica gel column chromatography (50-60% EtOAc in heptane) to yield title compound **4** as a white solid (44 mg, 0.12 mmol, 65%). R_f = 0.29 (60% EtOAc in heptane); IR (film) 2873, 2103, 1819, 1786, 1736, 1431, 1352, 1301, 1203, 1070, 814, 648, 558 cm^{-1}; ^1H NMR (400 MHz, chloroform-*d*) δ 4.51 (s, 2H), 3.81 – 3.76 (m, 2H), 3.69 (dd, *J* = 4.0, 1.8 Hz, 2H), 3.68 – 3.66 (m, 2H), 3.65 (s, 8H), 3.40 – 3.35 (m, 2H), 2.84 (s, 4H). ^{13}C NMR (101 MHz, chloroform-*d*) δ 171.95, 168.96, 166.13, 71.42, 70.75, 70.71, 70.63, 70.10, 66.62, 50.78, 25.69, 25.48. Mass could not be found.

6-(Hydroxymethyl)picolinaldehyde (5). 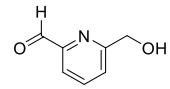 2,6-Pyridinedimethanol (500 mg, 3.6 mmol, 1.0 equiv.) and SeO_2 (200 mg, 1.8 mmol, 0.5 equiv.) were added to a Schlenk tube and put under N_2. 1,4-Dioxane (10 mL, not degassed or dried) was added, the mixture was sonicated for 2 min and then stirred at 65 °C for 24 h. After the mixture was cooled to r.t., it was diluted with DCM and filtered over celite. Then, the volatiles were removed under reduced pressure and the product was purified with column

chromatography (2.5% MeOH in DCM) yielding aldehyde **5** (405 mg, 82%) as a slightly yellow oil. R_f = 0.17 (2.5% MeOH in DCM). ^{1}H NMR (400 MHz, chloroform-*d*) δ 10.09 (s, 1H), 7.93 – 7.83 (m, 2H), 7.56 – 7.47 (m, 1H), 4.88 (s, 2H). ^{13}C NMR (100 MHz, chloroform-*d*) δ 193.2, 160.2, 151.8, 137.9, 124.9, 120.6, 64.2. LRMS (ESI+) *m/z* calcd. for $C_7H_7NNaO_2^+$ $[M+Na]^+$ 138.1, found: 138.0. The obtained data agrees with literature.[4]

(6-Formylpyridin-2-yl)methyl methanesulfonate (6). Alcohol **5** (350 mg 2.6 mmol, 1.0 equiv.) was dissolved in dry DCM, the solution was cooled to 0 °C and Et_3N (1.1 mL, 7.7 mmol, 3.0 equiv.) was added. Then, MsCl (237 µL, 3.1 mmol, 1.2 equiv.) was added dropwise and the mixture was stirred at r.t. for 30 min. The reaction was quenched with sat. $NaHCO_3$, the layers were separated and the aqueous layer was extracted with DCM (3 x). The combined organic layers were dried over Na_2SO_4 and the volatiles were removed under reduced pressure. The brown oil was purified with column chromatography (60% EtOAc in heptane) yielding methanesulfonate **6** (399 mg, 73%) as a slightly yellow solid. R_f = 0.35 (EtOAc/heptane, 3:2). ^{1}H NMR (400 MHz, chloroform-*d*) δ 10.05 (s, 1H), 7.98 – 7.92 (m, 2H), 7.74 – 7.69 (m, 1H), 5.42 (s, 2H), 3.14 (s, 3H). ^{13}C NMR (100 MHz, chloroform-*d*) δ 192.8, 154.8, 152.6, 138.5, 126.5, 121.7, 70.8, 38.2. LRMS (ESI+) *m/z* calcd. for $C_8H_{10}NO_4S^+$ $[M+H]^+$ 216.0, found: 216.1. The obtained data agrees with literature.[4]

***tert*-Butyl 4-((6-formylpyridin-2-yl)methyl)piperazine-1-carboxylate (7).** Methanesulfonate **6** (370 mg, 1.7 mmol, 1.0 equiv.) was dissolved in dry MeCN (10 mL) and 1-Boc-piperazine (384 mg, 2.0 mmol, 1.2 equiv.) and K_2CO_3 (475 mg, 3.4 mmol, 2.0 equiv.) were added. The mixture was stirred at 60 °C for 16 h, whereupon the solvent was evaporated. DCM and sat. $NaHCO_3$ were added, the layers were separated and the aqueous layer was extracted with DCM (3 x). The combined organic layers were dried over Na_2SO_4 and the volatiles were removed using a rotary evaporator. Then, the product was purified using column chromatography (80% EtOAc in heptane) yielding tertiary amine **7** (456 mg, 87%) as a white solid. R_f = 0.26 (EtOAc/heptane, 4:1). ^{1}H NMR (400 MHz, chloroform-*d*) δ 10.07 (s, 1H), 7.88 – 7.82 (m, 2H), 7.73 – 7.66 (m, 1H), 3.77 (s, 2H), 3.52 – 3.41 (m, 4H), 2.52 – 2.42 (m, 4H), 1.46 (s, 9H). ^{13}C NMR (100 MHz, chloroform-*d*) δ 193.7, 159.6, 154.9, 152.5, 137.6, 127.5, 120.4, 79.9, 64.3, 53.3, 28.6. LRMS (ESI+) *m/z* calcd. for $C_{16}H_{24}N_3O_3^+$ $[M+H]^+$ 306.2, found: 305.9. The obtained data agrees with literature.[4]

6-((4-(2-Azidoacetyl)piperazin-1-yl)methyl)picolinaldehyde (8). *tert*-Butyl 4-((6-formylpyridin-2-yl)methyl)piperazine-1-carboxylate **7** (25 mg, 82 µmol, 1.0 equiv.) was dissolved in dry DCM (1 mL) under N_2 and 4M HCl in dioxane (205 µL, 820 µmol, 10.0 equiv.) was added. The mixture was stirred for 2 h, whereupon the volatiles were evaporated. The solid was dissolved in DMF (1 mL) and 2,5-dioxopyrrolidin-1-yl 2-azidoacetate (**3**) (19 mg, 98 µmol, 1.2 equiv.) was added. Then, Et_3N (34 µL, 250 µmol, 3.0 equiv.) was added and the solution was stirred for 2 h. The volatiles were evaporated and the product was purified using column chromatography (50 to 100% EtOAc in heptane) yielding 2-PCA-N_3 **8** (19 mg, 80%) as a white solid. R_f = 0.49 (5% MeOH in EtOAc). IR (film) 2107, 1711, 1657, 1592, 1457, 1220, 1076, 1000, 788, 655 cm^{-1}. ^{1}H NMR (500 MHz, chloroform-*d*) δ 10.06 (s, 1H), 7.87 (d,

J = 3.9 Hz, 2H), 7.70 – 7.65 (m, 1H), 3.93 (s, 2H), 3.82 (s, 2H), 3.73 – 3.66 (m, 2H), 3.50 – 3.39 (m, 2H), 2.60 (q, *J* = 5.9 Hz, 4H). ^{13}C NMR (126 MHz, chloroform-*d*) δ 193.30, 172.07, 165.66, 158.46, 152.43, 137.69, 127.57, 120.65, 76.78, 63.60, 52.71, 50.68, 44.93, 41.88, 25.41. HRMS (ESI+) *m/z* calcd. for $C_{13}H_{17}N_6O_2$ $[M+H]^+$ 289.14075, found: 289.14130. *m/z* calcd. for $C_{13}H_{16}N_6NaO_2$ $[M+Na]^+$ 311.12269, found 311.12324

6-((4-(14-Azido-3,6,9,12-tetraoxatetradecanoyl)piperazin-1-yl)methyl)picolinaldehyde (9).

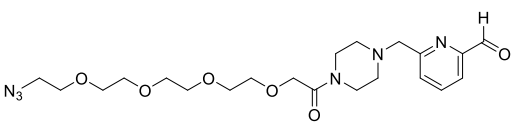

tert-Butyl 4-((6-formylpyridin-2-yl)methyl) piperazine-1-carboxylate **7** (50 mg, 0.16 mmol, 1.0 equiv.) was dissolved in dry DCM (2 mL) under N_2 and 4M HCl in dioxane (410 µL, 1.6 mmol, 10.0 equiv.) was added. The mixture was stirred for 2 h, whereupon the volatiles were evaporated. The solid was dissolved in DMF (1 mL) and 2,5-dioxopyrrolidin-1-yl 14-azido-3,6,9,12-tetraoxatetradecanoate (**4**) (74 mg, 0.20 mmol, 1.2 equiv.) was added. Then, Et_3N (69 µL, 0.49 mmol, 3.0 equiv.) was added and the solution was stirred for 2 h. The volatiles were evaporated and the product was purified using preparative HPLC (gradient: 5 to 100% MeCN in H_2O in 55 minutes) yielding 2-PCA-PEG$_4$-N$_3$ **9** (8 mg, 11%) as a yellow oil. R_f = 0.45 (75% EtOAc in heptane). IR (film) 2104, 1711, 1648, 1592, 1458, 1214, 1094, 799, 653 cm^{-1}. ^{1}H NMR (500 MHz, chloroform-*d*) δ 10.03 (s, 1H), 7.99 (d, *J* = 7.8 Hz, 2H), 7.83 (d, *J* = 6.4 Hz, 1H), 4.41 (s, 2H), 4.21 (s, 2H), 3.98 – 3.87 (m, 4H), 3.69 – 3.60 (m, 14H), 3.39 (q, *J* = 7.4, 4.9 Hz, 4H), 3.27 (s, 2H). ^{13}C NMR (126 MHz, chloroform-*d*) δ 192.28, 167.85, 152.74, 150.53, 138.94, 129.88, 122.27, 70.63, 70.53, 70.52, 70.38, 70.30, 70.28, 70.10, 69.94, 61.04, 52.29, 51.82, 50.59, 42.49, 39.05. HRMS (ESI+) *m/z* calcd. for $C_{21}H_{33}N_6O_6$ $[M+H]^+$ 465.24561, found: 465.24616 *m/z* calcd. $C_{21}H_{32}N_6NaO_6$ $[M+Na]^+$ 487.22755, found: 487.22607.

2-((4-Iodophenyl)amino)acetonitrile (10). Iodoaniline (5.00 g, 23 mmol, 1 equiv.) was dissolved in dry acetonitrile (60 mL). To this solution was subsequently added K_2CO_3 (3.80 g, 28 mmol, 1.2 equiv.) and NaI (3.40 g, 23 mmol, 1 equiv.). Chloroacetonitrile (2.89 mL, 46 mmol, 2 equiv.) was added dropwise and the mixture was then refluxed under argon for 3 days. Afterwards, the reaction was cooled down to room temperature and filtered over celite and rinsed with EtOAc. The organic layer was washed once with brine and dried over $MgSO_4$. The volatiles were evaporated and the product (4.82 g, 82% yield) was obtained after purifying on a dry loaded column (20-50% EtOAc in heptane). R_f = 0.52 (50% EtOAc in heptane). ^{1}H NMR (400 MHz, chloroform-*d*) δ 7.56 – 7.51 (m, 2H), 6.52 – 6.47 (m, 2H), 4.09 (d, *J* = 1.0 Hz, 1H), 4.07 (s, 2H). ^{13}C-NMR (100 MHz, chloroform-*d*): δ 144.76, 138.38 (2C), 116.55, 115.87 (2C), 81.76, 32.61. LRMS (ESI+): *m/z* calcd for $C_8H_7IN_2^+$ $[M+H]^+$ 258.8, found 258.9.

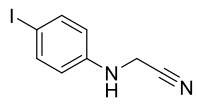

***N*-(Cyanomethyl)-N-(4-iodophenyl)nitrous amide (11).** Compound **10** (740 mg, 2.9 mmol, 1 equiv.) was dissolved in dry THF (3.8 mL) and isoamyl nitrite (1.19 mL, 8.6 mmol, 3 equiv.) was added dropwise to the mixture. This was left to stir for 2 hours at room temperature. Afterwards, the volatiles were removed yielding a crude product (821 mg, 2.9 mmol) with a high purity (>95%), so it was used in the next step without further purification. R_f = 0.62 (50% EtOAc in heptane). ^{1}H-

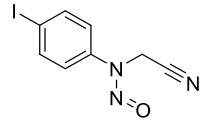

NMR (400 MHz, chloroform-*d*): δ 7.89 (d, 2H, *J* = 8.8 Hz), 7.33 (d, 2H, *J* = 8.8 Hz), 4.77 (s, 2H). ^{13}C-NMR (100 MHz, chloroform-*d*): δ 139.59, 139.20 (2C), 121.42, 112.12 (2C), 93.74, 30.34. LRMS (ESI+): *m*/*z* calcd for $C_8H_7IN_3O^+$ $[M+H]^+$ 288.0, found 288.1.

5-Amino-3-(4-iodophenyl)-1,2,3-oxadiazol-3-ium chloride (12). Compound **11** was dissolved in 6 mL 4M HCl in dioxane and was stirred at room temperature overnight. The product was obtained by trituration in diethyl ether (95% yield over two steps). ^{1}H-NMR (400 MHz, DMSO-*d*$_6$): δ 9.97 (s, 2H), 8.66 (s, 1H), 8.16 (d, 2H, *J* = 8.92 Hz), 7.84 (d, 2H, *J* = 8.93). ^{13}C-NMR (100 MHz, DMSO-*d*$_6$): δ 169.45, 139.19 (2C), 132.44, 124.36 (2C), 101.43 (1C missing). LRMS (ESI+): *m*/*z* calcd for $C_8H_7IN_3O^+$ $[M-Cl]^+$ 288.0, found 288.0

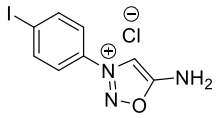

(*tert*-Butoxycarbonyl)(3-(4-iodophenyl)-1,2,3-oxadiazol-3-ium-5-yl)amide (13). Compound **12** (6.50 g, 20 mmol, 1 equiv.), $NaHCO_3$ (1.90 g, 34 mmol, 1.7 equiv.) and DMAP (276 mg, 2.3 mmol, 10 mol%) were dissolved in dry THF (100 mL). The mixture was cooled down to 0 °C. To this mixture, Boc_2O (7.40 g, 34 mmol, 1.7 equiv.) in THF (65 mL) was added dropwise and the reaction was stirred for 70 hours. The reaction was then quenched with 165 mL of aq. sat. NH_4Cl solution, THF was removed under reduced pressure and the product was extracted with EtOAC (3 x 80 mL). The organic layer was then dried and the product was obtained as an orange solid (4.79 g, 62% yield) after flash purification (0-50% EtOAc in heptane). R_f = 0.58 (50% EtOAc in heptane). ^{1}H-NMR (400 MHz, chloroform-*d*): δ 8.09 (s, 1H), 8.00 (d, 2H, *J* = 8.94), 7.54 (d, 2H, *J* = 8.94), 1.52 (s, 9H). ^{13}C-NMR (100 MHz, chloroform-*d*): δ 174.64, 160.72, 139.78, 139.75 (2C), 122.76, 122.74 (2C), 99.45, 79.24, 28.23 (3C). LRMS (ESI+): *m*/*z* calcd for $C_{13}H_{14}IN_3O_3^+$ $[M+H]^+$ 387.01, found 387.9

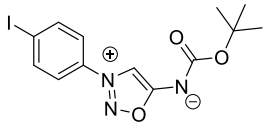

(*tert*-Butoxycarbonyl)(3-(4-(ethoxycarbonyl)phenyl)-1,2,3-oxadiazol-3-ium-5-yl)amide (14). Compound **13** (1.20 g, 3.1 mmol, 1 equiv.) was dissolved in dry ethanol (10 mL) and NEt_3 (10 mL). To this, $PdCl_2(PPh_3)_2$ (324 mg, 0.46 mmol, 15 mol%) was added. The compound was allowed to react in a CO atmosphere at 60 °C for 2.5 hours. The reaction mixture was then allowed to cool down and was filtered over celite. The mixture was then concentrated and purified using flash chromatography (0-50% EtOAc in heptane) to obtain an orange solid (668 mg, 65% yield). R_f = 0.35 (50% EtOAc in heptane). ^{1}H-NMR (400 MHz, chloroform-*d*): δ 8.32 (d, 2H, *J* = 8.87), 8.16 (s, 1H), 7.89 (d, 2H, *J* = 8.87), 4.45 (q, 2H, *J* = 7.14), 1.52 (s, 9H), 1.43 (t, 3H, *J* = 7.14). ^{13}C-NMR (100 MHz, chloroform-*d*): δ 174.88, 164.53, 160.95, 136.82, 134.93, 131.86 (2C), 121.63 (2C), 102.62, 79.36, 62.20, 28.36 (3C), 14.39. LRMS (ESI+): *m*/*z* calcd for $C_{16}H_{20}N_3O_5^+$ $[M+H]^+$ 334.1, found 334.4.

(*tert*-Butoxycarbonyl)(3-(4-carboxyphenyl)-1,2,3-oxadiazol-3-ium-5-yl)amide (15).

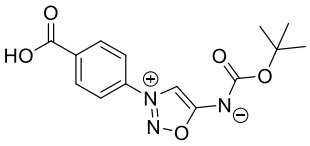

Compound **14** (650 mg, 2.0 mmol, 1 equiv.) was dissolved in THF (15 mL) and $LiOH \cdot H_2O$ (246 mg, 5.9 mmol, 3 equiv.) was added to water (15 mL). The two solutions were mixed for 2.5 hours at room temperature. The reaction mixture was then diluted with water and extracted with EtOAc (3 x 30 mL). The water layer was then acidified to pH 2 with 1M HCl and again extracted with EtOAc (3 x 30 mL). The organic layers were combined and dried with $MgSO_4$. The solvents were evaporated to yield a pure yellow compound (543 mg, 92% yield). R_f = 0.30 (10% MeOH, 0.5% AcOH in DCM). ^{1}H-NMR (400 MHz, MeOH-d_4): δ 8.46 (s, 1H), δ 8.32 (d, 2H, J = 8.92), 8.11 (d, 2H, J = 8.92), 1.51 (s, 9H). ^{13}C-NMR (100 MHz, MeOH-d_4): δ 166.32, 159.21, 136.65, 135.40, 131.29 (2C), 122.13 (2C), 108.99, 79.14, 27.11 (3C). HRMS (ESI+): m/z calcd for $C_{14}H_{15}N_3O_5^+$ $[M+H]^+$ 306.10900, found 306.10957

(*tert*-Butoxycarbonyl)(3-(4-(prop-2-yn-1-ylcarbamoyl)phenyl)-1,2,3-oxadiazol-3-ium-5-yl)amide (16).

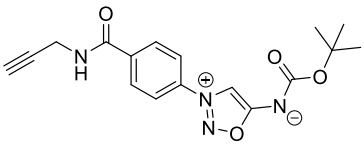

Compound **15** (540 mg, 1.8 mmol, 1 equiv.) was dissolved in DMF (20 mL). To this mixture was added HATU (738 mg, 2.2 mmol, 1.1 equiv.) and DiPEA (620 µL, 3.6 mmol, 2 equiv.) and was left to stir at room temperature for 5 minutes. Propargylamine (227 µL, 3.6 mmol, 2 equiv.) was added and stirred for 2 hours at room temperature. DMF was removed under reduced pressure and the product was obtained after flash chromatography (5% MeOH in DCM) to yield a yellow solid (349 mg, 58% yield). R_f = 0.24 (5% MeOH in DCM). ^{1}H-NMR (400 MHz, MeOH-d_4): δ 9.26 (t, 1H, J = 5.45), 8.60 (s, 1H), 8.21 (d, 2H, J = 8.82), 8.14 (d, 2H, J = 8.82), 4.11 (dd, 2H, J = 5.45, 2.49), 3.18 (t, 1H, J = 2.49), 1.44 (s, 9H). ^{13}C-NMR (100 MHz, MeOH-d_4): δ 174.72, 164.83, 160.13, 137.82, 136.01, 129.53 (2C), 122.90 (2C), 81.34, 77.81, 73.67, 29.19, 28.48 (3C) (1C missing). HRMS (ESI+): m/z calcd for $C_{17}H_{19}N_4O_4^+$ $[M+H]$ 343.14008, found 343.14078. $C_{17}H_{18}N_4NaO_4^+$ $[M+Na]^+$ 365.12203, found, 365.12403.

5-Amino-3-(4-(prop-2-yn-1-ylcarbamoyl)phenyl)-1,2,3-oxadiazol-3-ium 2,2,2-trifluoro acetate (17).

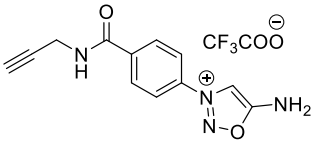

Compound **16** (349 mg, 1.1 mmol, 1 equiv.) was dissolved in DCM (20 mL). TFA (2 mL) was added dropwise. The mixture was left to stir for 4 hours at room temperature. The DCM was evaporated and the TFA was fully removed with co-evaporation with DCM (3 x) to yield a red/brown powder (259 mg, 80% yield, contaminated with a HATU remainder). ^{1}H-NMR (400 MHz, MeOH-d_4): δ 8.41 (s, 1H), 8.17 (d, 2H, J = 8.99), 8.12 (d, 2H, J = 8.99), 4.20 (d, 2H, J = 2.54), 2.65 (t, 1H, J = 2.54). ^{13}C-NMR (100 MHz, MeOH-d_4): δ 165.89, 140.19, 138.85, 129.28 (2C), 122.51 (2C), 78.91, 71.02, 37.48, 28.77 (1C missing). HRMS (ESI+): m/z calcd for $C_{12}H_{11}N_4O_2^+$ $[M\text{-}TFA]^+$ 243.08820, found 243.08871.

Fmoc-Orn(Cbz)-OtBu. Fmoc-Orn(Cbz)-OH (1.73 g, 3.7 mmol, 1.0 equiv.) was dissolved in THF/Hexane (30 mL, 1:1). This was cooled down to 0 °C and afterwards *tert*-butyl 2,2,2-trichloroacetimidate (1.32 mL, 7.4 mmol, 2.0 equiv.) was added. This was stirred for 15 min and then BF_3 etherate (228 uL, 1.8 mmol, 0.5 equiv.) was added to the mixture and the reaction was stirred overnight at room temperature. The product was obtained via column chromatography in a gradient of EtOAc in heptane (0% to 40%). R_f = 0.30 (30% EtOAc in heptane). ^{1}H NMR (500 MHz, MeOH-d_4) δ 7.79 (d, J = 7.5 Hz, 2H), 7.67 (t, J = 7.0 Hz, 2H), 7.39 (t, J = 7.4 Hz, 2H), 7.37 – 7.26 (m, 7H), 5.49 (s, 2H), 5.08 (s, 2H), 4.37 (qd, J = 10.6, 7.1 Hz, 2H), 4.22 (t, J = 6.8 Hz, 1H), 4.06 (dd, J = 8.6, 5.0 Hz, 1H), 3.15 (t, J = 6.7 Hz, 2H), 1.89 – 1.61 (m, 2H), 1.59 (d, J = 6.5 Hz, 2H), 1.46 (s, 9H). ^{13}C NMR (126 MHz, MeOH-d_4) δ 171.88, 157.50, 157.19, 143.92, 143.76, 141.18 (2C), 137.01, 128.06 (2C), 127.54 (2C), 127.38 (3C), 126.77 (2C), 124.86 (2C), 119.53 (2C), 81.36, 66.49, 65.96, 54.57, 47.04, 39.92, 28.55, 26.90 (3C), 26.00. HRMS (ESI+) m/z calcd for $C_{32}H_{36}N_2NaO_6^+$ $[M+Na]^+$ 567.24711, found 567.24580.

Fmoc-Orn-OtBu (18). Fmoc-Orn(Cbz)-OtBu was dissolved in methanol (40 mL). To this palladium on activated carbon (40 mg, 0.14 mmol) was added. The flask was then closed and H_2 was bubbled through while stirring till completion. The product was filtrated over celite and obtained via column chromatography in 10% methanol in DCM (1.20 g, 80% yield over two steps). R_f = 0.23 (10% MeOH in DCM). ^{1}H NMR (500 MHz, MeOH-d_4) δ 7.78 (d, J = 7.5 Hz, 2H), 7.66 (t, J = 7.8 Hz, 2H), 7.38 (t, J = 7.4 Hz, 2H), 7.30 (t, J = 7.4 Hz, 2H), 6.25 (s, 1H), 4.89 (s, 2H), 4.42 (dd, J = 10.6, 6.8 Hz, 1H), 4.31 (dd, J = 10.6, 6.8 Hz, 10H), 4.20 (t, J = 6.9 Hz, 1H), 4.06 (t, J = 8.8 Hz, 1H), 2.95 (t, J = 7.1 Hz, 1H), 1.95 – 1.83 (m, 1H), 1.74 (dt, J = 16.6, 8.9 Hz, 3H), 1.46 (s, 9H). ^{13}C NMR (126 MHz, MeOH-d_4) δ 171.36, 157.29, 143.75 (2C), 141.20 (2C), 127.42 (2C), 126.79 (2C), 124.80 (2C), 119.57 (2C), 81.66, 66.59, 54.28, 46.99, 38.92, 28.15, 26.89 (3C), 23.85. HRMS (ESI+) m/z calcd for $C_{24}H_{31}N_2O_4^+$ $[M+H]^+$ 411.228383, found 411.22757. $C_{24}H_{30}N_2NaO_4^+$ $[M+Na]^+$ 433.21033, found 433.20943.

Fmoc-Orn(Im-alkyne)-OtBu (19). Compound **18** (410 mg, 1.0 mmol, 1 equiv.) was dissolved in a mixture of DCM/sat. $NaHCO_3$ (1:1, 20 mL) and cooled down to 0 °C. While stirring vigorously, triphosgene (99 mg, 0.33 mmol, 0.3 equiv.) dissolved in DCM (1 mL) was added dropwise. This was left to react for 10 min. Afterwards, **17** (356 mg, 1.0 mmol, 1 equiv.) dissolved in DCM (1 mL) was added dropwise at 0 °C and stirred for 1 hour. The reaction was then quenched with brine (20 mL) and extracted with EtOAc (3 x 30 mL). The product was obtained after purification with flash chromatography (2.5-5% MeOH in DCM) to yield an orange solid (122 mg, 18% yield). R_f = 0.22 (5% MeOH in DCM). ^{1}H-NMR (400 MHz, DMSO-d_6): δ 8.26 (s, 1H), 8.12 (d, 2H, J = 8.88), 8.05 (d, 2H, J = 8.88), 7.78 (d, 2H, J = 7.53), 7.71 – 7.66 (m, 2H), 7.39 (t, 2H, J = 7.50), 7.32 (t, 2H, J = 7.39), 4.41 – 4.34 (m, 2H), 4.25 (d, J = 7.1 Hz, 1H), 4.22 (d, J = 2.5 Hz, 2H), 4.10 (dd, J = 8.7, 4.9 Hz, 1H), 3.25 (t, J = 6.2 Hz, 2H), 2.67 (t, J = 2.5 Hz, 1H), 1.93 – 1.81 (m, 1H), 1.78 – 1.69 (m, 1H), 1.68 – 1.60 (m, 2H), 1.48 (s, 9H). HRMS

(ESI+): *m/z* calcd for $C_{37}H_{39}N_6O_7^+$ $[M+H]^+$ 679.28802, found 679.28626. $C_{37}H_{38}N_6NaO_7^+$ $[M+Na]^+$ 701.26997, found 701.26923

Fmoc-Orn(Im-alkyne)-OH (**20**). Compound **19** (316 mg, 0.47 mmol, 1 equiv.), was dissolved in DCM (7 mL). TFA (7 mL) was slowly added to the mixture. This was stirred for 2.5 hours. The DCM was evaporated and the TFA removed by co-evaporation with DCM (3 x) to yield a yellow crystalline powder (280 mg, 96% yield). R_f = 0.27 (10% MeOH, 0.5% AcOH in DCM). ^{1}H-NMR (400 MHz, MeOH-d_4): δ 9.07 (s, 1H), 8.18 (s, 1H), 8.15 (d, 2H, *J* = 9.06), 8.12 (d, 2H, *J* = 9.06), 7.73 (d, 2H, *J* = 7.39), 7.64 (t, 2H, *J* = 6.41), 7.35 (t, 2H, *J* = 7.33), 7.28 (t, 2H, *J* = 7.34), 4.39 – 4.25 (m, 2H), 4.23 (d, *J* = 7.6 Hz, 1H), 4.20 (d, *J* = 2.4 Hz, 2H), 3.36 – 3.32 (m, 1H), 2.66 (t, 1H, *J* = 2.50), 2.00 – 1.89 (m, 1H), 1.81 – 1.75 (m, 1H), 1.75 – 1.65 (m, 2H).^{13}C-NMR (100 MHz, MeOH-d_4): δ 175.66, 167.16, 158.63, 145.20 (2C), 142.46 (2C), 140.45, 136.23, 130.75 (2C), 128.77 (2C), 128.25 (2C), 126.25 (2C), 124.03 (2C), 120.90 (2C), 111.37, 108.33, 80.32, 72.46, 67.96, 54.88, 40.82, 29.90, 29.41, 27.11, 24.20. HRMS (ESI+): *m/z* calcd for $C_{33}H_{31}N_6O_7^+$ $[M+H]^+$ 623.22487, found 623.22375. $C_{33}H_{30}N_6NaO_7^+$ $[M+Na]^+$ 645.20737, found 645.20802.

Protein modification with 2-PCA 8 or 9[4]. The protein (10 μM) and the indicated concentration of 2-PCA (500 mM stock in DMSO, 0 to 1000 equiv.) were combined in PBS buffer and incubated at 4, 21 or 37 °C for 24 h (400 rpm). The samples were purified by dialysis against PBS and were analyzed by SDS-PAGE (Figure 2).

Modified-NTR activity tested with ELISA. All reactants were dissolved in PBS pH 7.4. 10 μM (1 equiv.) of biotinylated CCP(CNBz) was treated with 3 μM (0.3 equiv.) NTR and 50 equiv. NADH (both from Sigma Aldrich) to test the NTR capacity for 1 hour at 37 °C. Next, biotinylated CCP(CNBz) and NTR-pretreated CCP(CNBz) were coupled to streptavidin-coated ELISA plates (C96 Maxisorp Nunc-immuno plate, Thermo-Scientific). Undiluted supernatants of the immortalized B cell clones were incubated with the respective antigens; antigen-bound IgG was detected by polyclonal rabbit anti-human IgG HRP (DAKO) and stained with TMB-UP (Biomerieux). The absorbance of the colorimetric signal was measured with iMark TM Microplate Reader (BioRad) at 450 nm.

Anti-CD20 Fab fragment isolation. The NKI-B20/1 hybridoma cell line, kindly provided by Ferenc A. Scheeren, was genetically engineered to secrete Fab fragments, with a heavy chain HC-LAETGG-Hisx6 and WT light chain. Cells were maintained at 37 °C with 5% CO2, and cultured in complete RPMI1640 medium, supplemented with 2 mM ultraglutamine, 50 μM Gibco 2-Mercaptoethanol, 1 x penicilin/streptomycin and 10% heat inactivated fetal bovine serum (FBS). Hybridoma supernatant containing antibodies was harvested and filtered through a 20 μm filter. Supernatant was run through a Ni-NTA column which was subsequently washed with 10 column volumes of PBS with 10 mM imidazole, and Fab fragments were eluted in PBS containing 500 mM imidazole. Buffer exchange to PBS was performed via ultracentrifugation with amicon Ultra-15 Centrifugal filter units.

Sortase reaction. eSrtA(2A-9) pET29b was a gift from David Liu (Addgene plasmid # 75145) and produced according to literature procedure.[26] The His-tag purified Fab fragments were transferred to sortase buffer (PBS + 50 mM Tris-HCl, pH 7.5, 150 mM NaCl, 100 mM $CaCl_2$). Sortase (1 equiv.) and the triple-Gly peptide (50 equiv.) was added. The reaction was incubated for 1 h at 37 °C and quenched afterwards using 0.5 M EDTA. Purification was performed using Fast Protein Liquid Chromatography on a NGC system 5BioRad using a SEC70 ENrich 10 x 300 column (Bio-Rad, 7801070), and 100 µL fractions collected in a 96 well plate. Fractions containing the sortagged protein were collected and run on 12% SDS gel to confirm purity, pooled and concentrated by ultracentrifugation with amicon Ultra-15 Centrifugal filter units (Sigma, 717185).

7.6 References

1. Stohl, W., A. N. Theofilipoulos, B Cell Trophic Factors and B Cell Antagonism in Autoimmune Disease. Karger Medical and Scientific Publishers: 2005; Vol. 8, p 140-174.
2. Prosser, G. A.; Copp, J. N.; Syddall, S. P.; Williams, E. M.; Smaill, J. B.; Wilson, W. R.; Patterson, A. V.; Ackerley, D. F. Discovery and evaluation of Escherichia coli nitroreductases that activate the anti-cancer prodrug CB1954. *Biochem. Pharmacol.* **2010,** *79*, (5), 678-687.
3. Nelson, A. L. Antibody fragments: Hope and hype. *mAbs* **2010,** *2*, (1), 77-83.
4. MacDonald, J. I.; Munch, H. K.; Moore, T.; Francis, M. B. One-step site-specific modification of native proteins with 2-pyridinecarboxyaldehydes. *Nat. Chem. Biol* **2015,** *11*, 326-331.
5. Martos-Maldonado, M. C.; Hjuler, C. T.; Sørensen, K. K.; Thygesen, M. B.; Rasmussen, J. E.; Villadsen, K.; Midtgaard, S. R.; Kol, S.; Schoffelen, S.; Jensen, K. J. Selective N-terminal acylation of peptides and proteins with a Gly-His tag sequence. *Nat. Commun.* **2018,** *9*, (1), 3307-3319.
6. Mao, H.; Hart, S. A.; Schink, A.; Pollok, B. A. Sortase-Mediated Protein Ligation: A New Method for Protein Engineering. *J. Am. Chem. Soc.* **2004,** *126*, (9), 2670-2671.
7. Popp, M. W.-L.; Ploegh, H. L. Making and Breaking Peptide Bonds: Protein Engineering Using Sortase. *Angew. Chem. Int. Ed.* **2011,** *50*, (22), 5024-5032.
8. Manz, R.; Assenmacher, M.; Pflüger, E.; Miltenyi, S.; Radbruch, A. Analysis and sorting of live cells according to secreted molecules, relocated to a cell-surface affinity matrix. *Proc. Natl. Acad. Sci.* **1995,** *92*, (6), 1921-1925.
9. Taddeo, A.; Gerl, V.; Hoyer, B. F.; Chang, H. D.; Kohler, S.; Schaffert, H.; Thiel, A.; Radbruch, A.; Hiepe, F. Selection and depletion of plasma cells based on the specificity of the secreted antibody. *Eur. J. Immunol.* **2015,** *45*, (1), 317-319.
10. Hiepe, F.; Radbruch, A. Plasma cells as an innovative target in autoimmune disease with renal manifestations. *Nat. Rev. Nephrol.* **2016,** *12*, 232-240.
11. Bernard, S.; Audisio, D.; Riomet, M.; Bregant, S.; Sallustrau, A.; Plougastel, L.; Decuypere, E.; Gabillet, S.; Kumar, R. A.; Elyian, J. Bioorthogonal Click and Release Reaction of Iminosydnones with Cycloalkynes. *Angew. Chem. Int. Ed.* **2017,** *56*, (49), 15612-15616.
12. Lee, K. Y.; Mooney, D. J. Alginate: properties and biomedical applications. *Prog. Polym. Sci.* **2012,** *37*, (1), 106-126.
13. Bencherif, S. A.; Sands, R. W.; Bhatta, D.; Arany, P.; Verbeke, C. S.; Edwards, D. A.; Mooney, D. J. Injectable preformed scaffolds with shape-memory properties. *Proc. Natl. Acad. Sci.* **2012,** *109*, (48), 19590.
14. Shih, T.-Y.; Blacklow, S. O.; Li, A. W.; Freedman, B. R.; Bencherif, S.; Koshy, S. T.; Darnell, M. C.; Mooney, D. J. Injectable, Tough Alginate Cryogels as Cancer Vaccines. *Adv. Healthc. Mater.* **2018,** *7*, (10), 1701469-1701481.
15. Li, J.; Mooney, D. J. Designing hydrogels for controlled drug delivery. *Nat. Rev. Mater.* **2016,** *1*, (12), 16071-16109.
16. Silva, E. A.; Mooney, D. J. Spatiotemporal control of vascular endothelial growth factor delivery from injectable hydrogels enhances angiogenesis. *Thromb. Haemost.* **2007,** *5*, (3), 590-598.
17. Sun, L. T.; Bencherif, S. A.; Gilbert, T. W.; Farkas, A. M.; Lotze, M. T.; Washburn, N. R. Biological activities of cytokine-neutralizing hyaluronic acid–antibody conjugates. *Wound Repair Regen.* **2010,** *18*, (3), 302-310.
18. Kerkman, P. F.; Fabre, E.; van der Voort, E. I. H.; Zaldumbide, A.; Rombouts, Y.; Rispens, T.; Wolbink, G.; Hoeben, R. C.; Spits, H.; Baeten, D. L. P.; Huizinga, T. W. J.; Toes, R. E. M.; Scherer, H. U. Identification and characterisation of citrullinated antigen-specific B cells in peripheral blood of patients with rheumatoid arthritis. *Ann. Rheum. Dis.* **2016,** *75*, (6), 1170.
19. Macauley, M. S.; Pfrengle, F.; Rademacher, C.; Nycholat, C. M.; Gale, A. J.; von Drygalski, A.; Paulson, J. C. Antigenic liposomes displaying CD22 ligands induce antigen-specific B cell apoptosis. *J. Clin. Invest.* **2013,** *123*, (7), 3074-3083.
20. Banerjee, R. Liposomes: Applications in Medicine. *J. Biomater. Appl.* **2001,** *16*, (1), 3-21.
21. Mandal, S.; Eksteen-Akeroyd, Z. H.; Jacobs, M. J.; Hammink, R.; Koepf, M.; Lambeck, A. J.; van Hest, J. C.; Wilson, C. J.; Blank, K.; Figdor, C. G. Therapeutic nanoworms: towards novel synthetic dendritic cells for immunotherapy. *Chem. Sci.* **2013,** *4*, (11), 4168-4174.
22. Parham, P., The immune system. 3 ed.; Garland Science: 2014.

23. Rathmell, J. C.; Cooke, M. P.; Ho, W. Y.; Grein, J.; Townsend, S. E.; Davis, M. M.; Goodnow, C. C. CD95 (Fas)-dependent elimination of self-reactive B cells upon interaction with CD4+ T cells. *Nature* **1995,** *376*, (6536), 181-184.
24. Nagata, S.; Golstein, P. The Fas death factor. *Science* **1995,** *267*, (5203), 1449-1456.
25. Daniel, P. T.; Krammer, P. H. Activation induces sensitivity toward APO-1 (CD95)-mediated apoptosis in human B cells. *J. Immunol.* **1994,** *152*, (12), 5624-5632.
26. Guimaraes, C. P.; Witte, M. D.; Theile, C. S.; Bozkurt, G.; Kundrat, L.; Blom, A. E. M.; Ploegh, H. L. Site-specific C-terminal and internal loop labeling of proteins using sortase-mediated reactions. *Nat. Protoc.* **2013,** *8*, (9), 1787-1799.

Chapter 8

Nederlandse Samenvatting

About the Author

List of Publications

Dankwoord

Nederlandse Samenvatting

Reumatoïde artritis (afgekort als RA) is een auto-immuunziekte die wordt gekenmerkt door chronische ontstekingen van gewrichten en slijmvliezen. Door deze ontstekingen kan kraakbeen en/of het onderliggende bot afgebroken worden. Ongeveer 1% van de wereldpopulatie lijdt aan RA, wat neerkomt op meer dan 17.6 miljoen mensen wereldwijd.

Een auto-immuunziekte wordt gekenmerkt doordat het immuunsysteem (het afweersysteem) lichaamseigen cellen en stoffen als lichaamsvreemd ziet. Deze stoffen worden dan herkend door antilichamen en afgebroken door immuuncellen, ondanks dat het lichaamseigen stoffen zijn en geen ziekteverwekkers. Bij RA is ook bekend dat ongeveer 80% van de patiënten specifieke antilichamen aanmaken voor gecitrullineerde eiwitten (gevormd door een post translationele modificatie). Deze antilichamen worden ook wel ACPA genoemd en zorgen er onder andere voor dat de ontsteking aanblijft. Gecitrullineerde eiwitten komen voor bij elke ontsteking en vormen op zich geen probleem. Het ontwikkelen van een antilichaam tegen deze eiwitten daarentegen, is specifiek voor de RA patiënten. Omdat deze antilichamen zo specifiek zijn voor het ziektebeeld, zijn ze tegelijkertijd interessant voor diagnostiek en uiteindelijk voor nieuwe therapieën.

ACPA worden geproduceerd door B-cellen, een type witte bloedcellen. Omdat de ACPA specifiek zijn voor RA patiënten, zijn deze ACPA-producerende B-cellen dit ook. Huidige therapieën zijn er op gericht om deze B-cellen op te sporen en te doden. Doordat alle B-cellen gedood worden, zijn de therapieën die nu op de markt zijn niet selectief en hebben zij veel bijwerkingen. De gezonde B-cellen zijn nodig voor het aanvechten van lichaamsvreemde stoffen, zoals bijvoorbeeld bacteriën en dus zal het doden van deze cellen zorgen voor een grotere kans op infecties.

Om die reden hebben wij onderzoek gedaan naar nieuwe mogelijkheden om selectief de ACPA-producerende B-cellen te doden, zonder daarbij de gezonde B-cellen aan te tasten. Op deze manier verwachten wij dat er een maximaal resultaat behaald kan worden met zo min mogelijk bijwerkingen.

In **Hoofdstuk 1** is een overzicht beschreven van de huidige mogelijkheden om B-cellen antigeen-specifiek te kunnen opsporen en eventueel doden. Een antigeen is de stof die bindt aan antilichamen of aan B-cel-receptoren. Verschillende antigenen zijn in de literatuur beschreven in combinatie met functionele moleculen die via verschillende processen B-cellen kunnen stilleggen of uitschakelen.

In **Hoofdstuk 2** beschrijven we eerst de selectie en synthese van een autoantigeen, genaamd cyclisch gecitrullineerd peptide (CCP), wat echter ook bindt aan ACPA. Omdat we specifiek B-cellen willen opsporen en niet gestoord willen worden door de circulerende ACPA (welke relatief veel meer aanwezig zijn dan B-cellen), wilden we CCP beschermen tegen binding aan circulerende ACPA. Daarom beschrijven we hoe we CCP hebben geblokkeerd met een carboxynitrobenzyl beschermgroep (CNBz) waardoor het niet meer kon binden aan ACPA. We hebben laten zien dat we met behulp van het enzym nitroreductase (NTR) de beschermgroep weer konden verwijderen en dat CCP weer kon binden aan ACPA. Het gebruik van deze selectieve binding werd gedemonstreerd door CCP ook te laten binden aan geïmmortaliseerde B-cellen. Er was geen binding te zien wanneer de CNBz groep werd geïntroduceerd en de binding werd hersteld zodra NTR was toegevoegd. Tot slot hebben we, door CCP vast te maken aan een streptavidine-toxine,

laten zien dat we selectief ACPA-producerende B-cellen konden doden en niet B-cellen die specifiek zijn voor een tetanus antigeen.

Omdat het gebruik van een enzym in een therapie moeilijkheden met zich mee zal brengen, hebben we ook onderzoek gedaan naar het gebruik van een beschermgroep die chemisch te verwijderen is. In **Hoofdstuk 3** hebben we gekeken naar de iminosydnone klik-en-verwijder reactie. We hebben laten zien dat de iminosydnone op CCP goed functioneerde als een blokkade, waardoor binding van CCP aan ACPA en ACPA-producerende B-cellen niet meer mogelijk was. Door de reactie met de stof DBCO werd de CCP ontschermd en kon binding weer plaatsvinden. Daarnaast hebben we CCP direct aan een potent toxine (monomethyl auristatin E) gezet om te onderzoeken of we ook met deze methode selectieve celdood konden induceren. Door binding van CCP aan de B-cel receptoren zou het toxine geïnternaliseerd worden, waarna het geactiveerd wordt en de cel kan doden. Het verkregen resultaat liet echter geen verschil zien tussen de verschillende beschermde en ontschermde antigenen, net zo min als een verschil met de negatieve controle. In alle gevallen was het toxine giftig en was er geen antigen selectiviteit. Onze hypothese hiervoor is dat een enkel CCP antigeen niet voldoende is om aan een B-cel receptor te binden en/of voor de internalisatie van het toxine te zorgen. In hoofdstuk 2 hebben we namelijk gezien dat een streptavidine conjugaat (een tetrameer) wel werkt.

In **Hoofdstuk 4** hebben we de ontwikkeling van een nieuw klik-en-verwijder reactie beschreven. Bij deze reactie hebben we gebruik gemaakt van een tetrazine en een phenoxy-vinylboorzuur (afgekort als VBA). We hebben deze moleculen gesynthetiseerd en laten zien dat deze reactie dankzij het boorzuur sneller verliep dan de vergelijkbare reactie tussen een tetrazine en een vinylether. We hebben de toepasbaarheid van deze VBA gedemonstreerd door het te koppelen aan een toxine (cladribine), specifiek voor witte bloedcellen (waaronder ook B-cellen vallen). We hebben cladribine beschermd met VBA en aangetoond dat de toxiciteit hierdoor was afgenomen en werd hersteld zodra de reactie met tetrazine had plaatsgevonden. Helaas zagen we ook dat het conjugaat niet volledig stabiel was, waardoor toxiciteit over tijd ook toenam. Tot slot hebben we, zoals verwacht, laten zien dat deze strategie met cladribine inderdaad meer effect had op B-cellen dan op niet-witte bloedcellen, zoals bijvoorbeeld niercellen.

Omdat wij verwachtten dat monovalentie niet genoeg zou zijn voor de binding van CCP aan B-cel receptoren en de internalisatie van het CCP-conjugaat, hebben we gekeken naar een nieuw multivalent systeem. In **Hoofdstuk 5** hebben we gebruik gemaakt van een langgerekt en semi-flexibel polymeer, poly(isocyanopeptides) (PICs), als basis. Aan dit polymeer hebben we vervolgens fluoroforen en CCP vastgezet, vergelijkbaar met een eerder gepubliceerd streptavidine systeem. Streptavidine heeft echter maar 4 mogelijkheden om iets aan vast te zetten, waar PICs er ruim 100 hebben. We vergeleken streptavidine met PICs en we zagen dat beide ongeveer even efficiënt waren in het binden van B-cellen. Het voordeel van de PICs, naast de meerdere binding plaatsen, bleek het lage achtergrond signaal in vergelijking met streptavidine. Tot slot hebben we nog gekeken naar de internalisatie van de PICs door de B-cellen, iets wat van belang is voor toekomstig gebruik van de PICs om B-cellen te lokaliseren en mogelijk te doden. Met behulp van een indirecte celkleuringsstudie hebben we gezien dat de PICs niet of nauwelijks internaliseren.

In **Hoofdstuk 6** hebben we gekeken naar anti-CarP antilichamen en een bijbehorend antigeen. Niet alle RA patiënten hebben ACPA en sommige van deze patiënten hebben wel anti-CarP antilichamen. Het onderzoek in dit proefschrift is gericht op antigenen specifiek voor ACPA, maar het zou een toevoeging zijn als deze methoden kunnen worden gebruikt voor andere RA specifieke antigenen, zoals voor anti-CarP antilichamen. Om deze reden modificeerden we het antigeen peptide CCP met een homocitrulline (resulterende in CHCitP) en dit bleek goed te binden aan zowel anti-CarP antilichamen geproduceerd door mensen als door muizen. Dit laatste is extra interessant omdat er geen muizen bestaan met ACPA en dus muisexperimenten niet gebruikt kunnen worden om strategieën ontworpen voor ACPA te testen voor de ontwikkeling van een nieuwe therapie. We hebben laten zien dat de CNBz beschermgroep, zoals gebruikt in Hoofdstuk 2, ook als beschermgroep kan dienen voor CHCitP en inderdaad zorgde voor de verminderde binding aan anti-CarP antilichamen. Tot slot demonstreren we dat we gebruik kunnen maken van NTR om deze bescherming ongedaan te maken en dus de binding aan anti-CarP antilichamen weer te kunnen herstellen. Hiermee hebben we laten zien dat we in staat zijn om een strategie ontworpen voor ACPA kunnen toepassen op anti-CarP antilichamen en dit biedt mogelijkheden voor dierstudies in de toekomst.

In **Hoofdstuk 7** worden, naast de Engelse samenvatting, de reikwijdte en de veelbelovende vooruitzichten van de specifieke B-cel lokalisatie strategieën beschreven, inclusief het gebruik van een dubbele lokalisatie techniek en andere antigeen activatie mogelijkheden.

Hopelijk zijn hiermee de grote lijnen van dit onderzoek duidelijk geworden. Houd er rekening mee dat deze samenvatting op een aantal punten gesimplificeerd is omwille van de begrijpelijkheid. Meer details zijn te vinden in de Engelstalige samenvatting in Hoofdstuk 7, en natuurlijk in de overige hoofdstukken van dit proefschrift.

About the Author

Lianne Lelieveldt was born on January 6, 1990 in Nijmegen, the Netherlands. She finished her secondary education at SSgN in Nijmegen, where she obtained her VWO degree. She then obtained her bachelor's (*bene meritum*) and master's degree (*cum laude*) in Molecular Life Sciences at the Radboud University Nijmegen. During her bachelor's she studied at W&J college in Washington, Pennsylvania, United States of America for one semester. During her master's she did a joint internship at the departments of Synthetic Organic Chemistry of prof. dr. Floris Rutjes and Bioorganic Chemistry of prof. dr. ir. Jan van Hest. She worked on the modification of tumor targeting antibodies using bioorthogonal chemistry under the supervision of dr. Marjoke Debets. Hereafter, she performed an internship at the Department of Chemistry, University of Copenhagen, Denmark. She worked on the synthesis of metallo-organozymes with specific proteolytic activity under the supervision of prof. dr. Morten Meldal. After obtaining her MSc degree in 2013, she moved back to Copenhagen University to work as a research assistant for 6 months. After travelling for 4 months, she started her doctoral research at the Chemical Biology group of dr. Kimberly Bonger at the Radboud University. Here, she worked in the field of Chemical Immunology and developed new caging and activation strategies for antigen-specific targeting of autoreactive B cells, of which the results are described in this thesis. After her PhD, she continued her work for 5 months as a postdoctoral researcher in the Chemical Biology group at the Radboud University Nijmegen. She is now looking forward to fulfill one of her dreams, a travel adventure around the world.

List of Publications

- **Antigen-Selective Cell-Targeting in Autoimmune Diseases**
  Lianne Lelieveldt*, Wilke Castelijns*, Kimberly Bonger. *Manuscript submitted*

- **Vinylboronic Acid Ligation for Efficient Click-to-release of a Lymphocyte-specific Cytotoxic Prodrug**
  Lianne Lelieveldt, Selma Eising, Abel Wijen, Hendy Kristyanto, Hans Ulrich Scherer, René Toes, Kimberly Bonger, *Manuscript in preparation*

- **Poly(isocyanopeptides) as Scaffold for Multivalent Targeting and Elimination of ACPA-Selective Autoreactive B cells**
  Lianne Lelieveldt*, Hendy Kristyanto*, Yvonne Bartels, Carl Figdor, Hans Ulrich Scherer, René Toes, Roel Hammink, Kimberly Bonger. *Manuscript in preparation.*

- **Sequential Prodrug Strategy to Target and Eliminate ACPA-Selective Autoreactive B cells.**
  Lianne Lelieveldt, Hendy Kristyanto, Ger Pruijn, Hans Ulrich Scherer, René Toes, Kimberly Bonger. *Molecular Pharmaceutics*, **2018**, *15*, (12), 5565-5573.

- **Metallo-Organozymes with Specific Proteolytic Activity**
  Ahmed Embaby*, Lianne Lelieveldt*, Frederik Diness, Morten Meldal. *Chemistry–A European Journal*, **2018**, 24, (66), 17424-17428.

  * Authors contributed equally

Dankwoord

Beste lezer,

Een hele prestatie dat je zover bent gekomen (tenzij je hier begonnen bent =D)! Graag zou ik van deze kans gebruik willen maken om iedereen te bedanken voor hun bijdrage, op welke manier dan ook, tijdens mijn PhD.

Allereerst wil ik **Kim** bedanken voor al het vertrouwen en enthousiasme over de laatste 4 jaar. Ik was zelf op zoek naar een PhD project binnen de chemische immunologie en ik had de hoop al bijna opgegeven toen ik jouw email ontving, ik weet nog precies waar; namelijk op een vliegveld in Patagonië. Toen ik eenmaal thuis kwam hebben we gelijk wat afgesproken en een maand later kon ik al aan de slag. Ik heb je altijd erg bewonderd om je onuitputtelijkheid aan ideeën en ik ben je dankbaar voor de mogelijkheid om ook met mijn eigen ideeën te komen en deze uit te voeren. Voor mij maakte het onze werkrelatie alleen nog maar makkelijker doordat we ook buiten de chemie veel interesses gemeen hebben/delen. Er zijn geen borrels, festivals of concerten genoeg en daar hebben we dan ook vaak samen van genoten (zelfs tot aan het zijn van buren op de DTRH camping aan toe). Kim, bedankt voor al je hulp (ook de laatste maanden), ideeën en enthousiasme. Ik ben heel erg blij voor je dat de toekomst er rooskleurig uitziet en dat de groep kan gaan groeien. Ik wens je veel plezier en succes bij het vervolg van de enige echte Bonger-groep.
Daarnaast wil ik graag **Floris Rutjes** en **Ger Pruijn** bedanken voor het vervullen van de rol als promotor. Ik wil jullie graag bedanken voor het nakijken van mijn thesis en voor de verschillende meetings en discussies over de inhoud ervan. Floris, jouw support in de laatste maanden is voor mij heel waardevol geweest, bedankt!
I would like to thank the doctoral thesis committee, consisting of **Daniela Wilson**, **Sander van Kasteren** and **Jan van Hest**, for critically reading the thesis manuscript. Jan jou wil ik graag ook nog bedanken voor het in contact brengen van Kim en mij ruim 4 jaar geleden!

Mijn eerste master stage is al een lange tijd terug, maar heel erg waardevol gebleken tijdens mijn carrière in de chemie. **Marjoke** ik wil jou nog heel graag bedanken voor die tijd. Ik heb echt veel geleerd en dat is mij later goed van pas gekomen, daar ben ik je erg dankbaar voor!

Dear **Hendy**, I am very grateful for having you as my partner in crime all this time! I think we did a great job combining chemistry and immunology. I wish you all the best! Ook **René Toes** en **Uli Scherer** wil ik graag bedanken voor deze vruchtbare samenwerking.

Dan wil ik graag Lise en Bastiaan bedanken dat jullie mijn paranimfen willen zijn! Met jullie beiden begon dit avontuur al ruim 10 jaar geleden. **Lise** we zaten al snel samen in een practicum groepje, maar nog belangrijker ook samen op Pinkpop. We hadden verschillende vriendengroepen en daardoor waren we altijd aan elkaar gewaagd tijdens de playbackshow borrels (althans, zo ziet onze groep dat graag ;)). Tijdens onze stages liepen we al rond (soms op hakken) op de derde verdieping en daardoor hebben we veel lief en leed in het onderzoek gedeeld, maar natuurlijk ook alle streepjesborrels. Waar ik zelf toch het meeste van heb genoten zijn alle concerten en festivals (knakworsten met goldstrike!!). Ik vind het heel bijzonder dat we deze traditie al zo lang hebben en dat de groep alleen maar groter is geworden. Dat we dit mogen blijven doen! Lieve **Bastiaan**,

of liever, Beebz, ook wij hebben elkaar (schijnbaar tijdens wiskunde..) in het eerste jaar al ontmoet. Het hoogtepunt uit onze bachelor moet toch wel W&J zijn! De Fratparties, het reizen langs de Eastcoast en uiteraard het harde studeren daar was echt een top tijd. Toen je na aandringen van veel mensen eindelijk je positie bij Jan aannam, werd je gelukkig ook nog mijn collega! Het was fijn om af en toe even te kunnen ouwehoeren tijdens lunch of even te kunnen zeuren tijdens een van onze 'frustratie' koffie pauzes ;) Ik vind het nog steeds heel erg jammer dat je halverwege moest verhuizen naar Eindhoven, ik heb je echt gemist! Heel veel succes met de afronding van jouw PhD en hopelijk zijn de frustratiekoffies daarna niet meer nodig en kunnen we allebei lekker genieten van biertjes, festivals en reizen!

Gelukkig heb ik ook erg leuk gezelschap gehad aan de Bonger groep. **Selma** jij was al voor mij begonnen en dat zorgde voor een warm welkom, ondanks dat ik al bekend was op de afdeling. We hebben al snel samen een student begeleid en een project opgestart. Ik heb je altijd bewondert om je chemische kennis en wil je graag bedanken voor het helpen bij het oplossen van synthetische vragen. Behalve dat je mijn collega was, heb ik ook genoten van de activiteiten buiten werk; weekendjes weg, een lekker biertje of de stapavonden aan het begin van onze samenwerking. **Fleur** jij werkte in het begin nog op het RIMLS, maar gelukkig heb je de oversteek gemaakt. Ik wil je erg bedanken dat ik bij je terecht kon met mijn bio-gerelateerde vragen! Vooral de laatste maanden hebben wij lief en leed gedeeld, dit was niet de leukste periode, maar ik was blij dat jij er was om me op de been te houden of om tegen te klagen ;) Gelukkig is er waardige opvolging gekomen. **Yvonne** jij was natuurlijk al bekend in onze groep vanwege stages, maar het was erg leuk dat je besloot om weer terug te komen. In het begin was je vooral in het RIMLS, maar ik ben blij dat je de laatste tijd steeds vaker aan onze kant van de weg te vinden was. Bedankt voor je gezelligheid en ik wens je heel veel succes met je PhD, maar dat komt vast goed want je kunt meer dan je zelf denkt! **Bob**, we hebben maar kort samen gewerkt maar je was een gezellige nieuwe aanwinst en je bracht een fijne nieuwe positieve energie met je mee. Bedankt voor je gezelligheid en ik wens je veel succes met je PhD!

Tijdens mijn promotie heb ik met veel studenten mogen samenwerken. Ik ben jullie erg dankbaar voor de gezelligheid op het lab en de inzet in jullie verschillende projecten. **Abel**, jij werkte onder de supervisie van Selma en mijzelf, wat vanwege onze stress van het laatste jaar niet altijd even makkelijk en leuk is geweest. Ik wil je graag bedanken voor de hoeveelheid synthese die je hebt gedaan en ook je geduld en precisie voor de optimalisatie hiervan. Dit zal resulteren in een mooie publicatie. **Angelina**, jij hebt gewerkt aan het PAD project, niet altijd makkelijk maar evengoed tot een leuk einde gebracht. Bedankt voor je inzet en zelfstandige werkhouding, jij komt er wel! **Kevin**, heel fijn dat jij me nog bent komen helpen om het iminosydnone project nog een stap verder te brengen! Naast je skills op het lab werd ook je bier brouwkunst zeer gewaardeerd. Veel succes met je PhD die geheid gaat volgen. **Laura**, ondanks dat jouw project niet de makkelijkste was heb je je er echt in vastgebeten en je best gedaan om het tot een goed einde te brengen. Ontzettend bedankt voor je doorzettingsvermogen, ik wens je het allerbeste voor de toekomst! **Lieke**, ondanks dat het snel duidelijk was dat onderzoek niet jouw interesse had, hebben we een gezellige tijd gehad! **Mike**, jou wil ik graag bedanken voor je hulp aan het iminosydnone project. Zoals je ziet is veel daarvan in dit proefschrift belandt en dat was nooit zover gekomen als jij in mijn laatste jaar niet was bijgesprongen. Succes met de laatste loodjes van je studie en alvast veel succes met je PhD. **Selina**, jij was de eerste student op het VBA click-to-release project van Selma

en mij. Ondanks dat de start van dit project soms wat moeizaam ging, heeft het toch een goede basis gelegd voor het hoofdstuk in dit proefschrift, bedankt! **Wilke**, jou wil ik graag bedanken voor een super literatuur scriptie die ervoor heeft gezorgd dat de introductie van dit proefschrift een volledig overzicht van de huidige literatuur beslaat. Echt super gedaan, dankjewel! **Yvonne**, jij hebt een mooi fundament gelegd voor het werk beschreven in hoofdstuk 5. Bedankt voor je motivatie en je kritische blik op het onderzoek!

Ik ben me ervan bewust dat het werk wat ik heb gedaan niet had gekund zonder de ondersteuning van de niet altijd zichtbare, maar zeker erg belangrijke krachten achter de schermen. **Marieke**, jou wil ik graag vooral bedanken voor alle gezelligheid! Voor officiële regel dingen kwam ik natuurlijk niet zo vaak bij jou, op de laatste maanden na, maar al die kerstborrels over de jaren heen hebben we maar mooi voor elkaar gekregen. Ik heb je interesse altijd erg gewaardeerd en ik zal je missen! **Els**, hartelijk dank voor alle hulp bij administratieve zaken. Ook was ik altijd blij verrast als ik een dag voor mijn vakantie een email van je kreeg om me veel plezier te wensen. Heel attent en het zijn vaak de kleine dingen die het 'm doen, bedankt! **Peter** van Dijk, hartelijk bedankt voor alle hulp op veel verschillende vlakken. Naast allerlei praktische dingen, wil ik je ook bedanken voor je positiviteit en interesse over de jaren. Heb je het toch nog van me gewonnen en zit een gezamenlijk afscheidsfeestje er niet in. Voor nu wens ik je nog veel plezier op de werkvloer en voor erna alle geluk en gezondheid met je pensioen. Behalve voor alle hulp bij bestellingen en het vinden van epjes en puntjes, wil ik graag **Jan** Dommerholt bedanken voor de gezellige praatjes en alle fijne F1 analyses op de maandag ochtend na een race weekend. Deze nabeschouwing was uiteraard leuker als Max een race op zijn naam wist te schrijven of als de Duitse zender zelf Vettel had uitgescholden. **Peter** van Galen bedankt voor het draaiende houden van de mass-spec faciliteiten, ook als de apparatuur al van streek was zodra ik de massa kamer binnen kwam (volgens jou dan ;)). **Helene**, bedankt voor jouw hulp met de verschillende HPLCs. **Paul** White many thanks for the increased possibilities concerning NMR, I have greatly enjoyed your enthusiasm (and of course your BBQ skills)! **Hans** Adams, altijd gezellig als jij op een gegeven moment even een praatje kwam maken. Dan wel over peptide chemie of over alles wat er mis was ;) Ik ben je erg dankbaar voor de goede achtergrond die ik heb gekregen over peptide chemie (al tijdens mijn master stage 7 jaar geleden!).

Het leuke van werken in een interdisciplinair veld is dat je veel mensen uit verschillende groepen leert kennen. Natuurlijk BMC, ondanks dat ik voornamelijk in het Huygens heb gewerkt, wil ik jullie allemaal, **Ger**, **Amrah**, **Annemarie**, **Bas**, **Carla**, **Cynthia**, **Els**, **Fleur**, **Ilmar**, **Marina**, **Mathijs**, **Merel**, **Selma**, **Wilbert**, en **Wilma** bedanken dat ik altijd mocht komen voor een ELISA en voor het welkome gevoel als ik er was. Ook voor de gezelligheid en hulp wil graag de BOC groep: **Jan** van Hest, **Annika** (erg leuk dat wij nog u-tje buren zijn geweest!), **Anika**, **Bastiaan**, **Britta**, **Dave**, **David**, **Dennis**, **Emilia**, **Hans**, **Henan**, **Imke** & **Pascal** (beide zeer gewaardeerde leden van de pineapple bende, jullie zijn schatten!), **Jan** Pille (bedankt voor de ELP samenwerking, wie weet krijgt dit nog een vervolg in de toekomst), **Joep**, **Lise**, **Loai**, **Marcel**, **Mark**, **Marlies**, **Mathijs**, **Morten**, **Nanda**, **Ruud**, **Sanne** (vi ses i København!), **Saskia**, **Stijn**, **Zhipeng**, en SOC groep: **Floris** Rutjes, **Abbas** (thanks for your enthusiasm and of course the linzensoep!), **Alejandra** (you deserved how everything came together!), **Bram**, **Claudia**, **Dani**, **Danny** (we zien mekaar nog op feestjes en etentjes!), **Emiel**, **Freek**, **Henri**, **Hidde** (mede bierfanaat, of beter nog specifiek Mikkellers!), **Ivan**, **Johan**, **Jona**, **Jorgen**, **Marjoke**, **Rens**, **Sam**, **Stefan** (het is weer eens

tijd voor een motor tourtochtje!), **Thomas**, **Toni**, **Torben** en **Victor** (de goedzak van de afdeling, bedankt voor je gezelligheid tijdens de vele lunches, borrels en etentjes!) bedanken! Andere mensen die ik graag nog in het zonnetje wil zetten voor gezelligheid en samenwerkingen komen van de TIL groep: **Bas**, **Camille** (many thanks for help with the Fab fragments and our collaboration), **Floris** van Dalen (bedankt voor je goede en soms interessante muzikale contributie aan ons lab. Ik ben blij dat je ons team kwam versterken!), **Iris**, **Jorieke**, **Loek**, **Martijn** en **Roel** (bedankt voor je hulp met de PICs en onze samenwerking. Ik heb je kritische blik altijd erg gewaardeerd en het blijft me verbazen dat ik je vaak 'even' iets wilde komen vragen en pas een uur later op mijn plek terug kwam ;)). Ook wil ik graag **Sjoerd** Postma bedanken voor je positiviteit en gekke uitspattingen, dit heeft voor veel slappe lach gezorgd tijdens mijn PhD maar ook al tijdens mijn studie. **Britta** Helwig, ook jou wil ik bedanken voor de gezellige praatjes op de gang en de organisatie van verschillende borrels! Veel succes nog met je PhD!

Morten Meldal, tak for sjov tiden og for vores samarbejde, den sidste resulterede i en god artikel.

I would like to thank **dr.** Anupama **Shanmug**anathan for your great drill in immunology at W&J. Ever since your lectures I have been motivated to work in the field of immunology.

Tijdens de afgelopen vier jaar heb ik samen met de piketploeg en BHVers ervoor mogen zorgen dat de werkplek veilig bleef. Naast serieuze incidenten werd er altijd veel gelachen en waren we een goed team. Allereerst, **Ricardo** de meest verstandige van het hele stel (…), bedankt voor veel leerzame momenten en de organisatie van het realistisch oefenen. Daarnaast wil ik graag **Christel**, **Danny**, **Geert-jan**, **Gerben**, **Lars**, **Michel**, **Mirjam**, **Rene**, **Serge**, **Stefan** en **Victor** bedanken voor de goede samenwerking.

Ik ben dankbaar voor het feit dat ik bij de groep van het ICI mocht horen. Ik heb zo veel leuke mensen leren kennen en we hebben met zijn allen zeker een (persoonlijke) groei doorstaan. Bedankt **Hendy**, **Berend**, **Dennis**, **Dion**, **Elko**, **Eveline**, **Jorieke**, **Joost**, **Jorick**, **Laurent**, **Loek**, **Martje**, **Sebastiaan**, **Tim** en alle anderen voor alle diepgaande gesprekken en eerlijkheid, maar ook voor alle gezellige etentjes en avonden!

Buiten het werk om was er gelukkig ook tijd om te ontspannen en met wie kan je dit beter doen dan met je lieve vrienden? Ook al heb ik misschien niet altijd evenveel tijd voor jullie gehad als ik zou willen, ik ben blij dat we elkaar met enige regelmaat nog zien! Vooral mijn oude studiegenoten, **Anneloes**, **Bastiaan** (Basti buddy!), dr. **Daniël** (en gelukkig ook mijn collega gedurende deze 4 jaren), **Ian**, **Leoni**, **Peter** (Heenbam! Gezellig dat je me in de laatste maanden kwam vergezellen met schrijven!), **Pjotr** en **Shane** bedankt voor jullie regelmatige interesse in mijn onderzoek en juist voor de ontspanning daaromheen! In het speciaal wil ik jou graag bedanken, **Frank**, dat je me altijd gesteund hebt en me maar vaak genoeg verteld hebt dat stress niet helpt (dit geldt natuurlijk ook voor jou ;)). Ik koester onze waardevolle vriendschap en ik weet zeker dat er nog veel biertjes en reisverhalen uitgewisseld zullen worden!

Martijn jou wil ik ook graag bedanken voor de gezellige avonden onder het genot van een biertje en ook voor je nuchtere kijk. **Mats** bedankt voor de ontspannende tour tochten op de motor, dat we nog maar op veel zonnige dagen en gas mogen opentrekken!

Mange tak til min kære ven **Daniel**! Jeg er glad for, at vi kan dele vores passion for øl med hinanden. Jeg vil gerne takke dig for den store tid i København og for lytte til min klage over 'The machine'. Jeg er meget glad for at du bor nu i Holland. **Rob** ook wij hebben veel tijd doorgebracht in het mooie Kopenhagen en de nodige dansjes gedaan op een van onze vele stapavonden (en Distortion!). Bedankt voor je gezelligheid en vrolijkheid! **Sanne** en **Morten**, ook jullie wil ik graag bedanken voor de gezelligheid in Kopenhagen en natuurlijk ook in Nijmegen!

Graag wil ik ook **Evie**, mijn kleine zusje en grote vriendin bedanken. Ik ben ontzettend blij met het mooie ontwerp van mijn kaft en vind het heel speciaal dat jij deze voor mij wilde maken. Ik vind het ook erg bijzonder dat wij zoveel interesses met elkaar delen en veel leuke dingen samen doen, een beter zusje had ik me niet kunnen wensen!

Lieve **pap** en **mam**, ik ben jullie heel dankbaar voor alle steun de afgelopen jaren. Het was niet altijd rozengeur en maneschijn, maar jullie stonden altijd voor me klaar. Ik ben heel blij dat ik mijn verdriet maar vooral ook mijn geluk met jullie kan delen. Laten we blijven genieten van alle leuke dingen die we samen doen. Of het nou een bierfestival, een concert of een avondje stappen met de vierdaagse is, ik ben trots dat wij ook deze dingen allemaal samen kunnen doen!

Ik wil ook graag mijn lieve oma's bedanken voor hun interesse en warmte. Het is niet voor niks dat ik dit werk aan jullie heb opgedragen. Een hele dikke knuffel voor jullie **oma Beestjes** en **oma Klok**!

Tot slot wil ik graag dr. **Rens** bedanken. Mijn PhD heeft dit proefschrift als resultaat, maar nog belangrijker ons samenzijn! Ik wil je heel erg bedanken voor je hulp tijdens mijn PhD en ook je geduld in de laatste maanden. Ik vind het bijzonder dat we dit allebei van mekaar hebben mogen meemaken! Nog veel belangrijker, ik wil je graag bedanken voor de fijne tijd die we samen hebben. Het is super om de passie voor bier, Formule 1 en reizen met jou te kunnen delen. Ons grote avontuur gaat nu echt bijna beginnen, samen de grote wereld in. Ik kan niet wachten! Ik hou van jou!